UNIVERSITY OF SOUTHAMPTON

Performance Analysis of Wireless Communications Systems in Fading Channels

by

Xiang Liu

Supervisor: Prof. Lajos Hanzo

A thesis submitted in fulfillment for the
degree of Doctor of Philosophy

in the
Faculty of Engineering, Science and Mathematics
School of Electronics and Computer Science

December 2006

Dedicated to my parents.

UNIVERSITY OF SOUTHAMPTON

ABSTRACT

FACULTY OF ENGINEERING, SCIENCE AND MATHEMATICS
SCHOOL OF ELECTRONICS AND COMPUTER SCIENCE

Doctor of Philosophy

by Xiang Liu

In this thesis we investigate a range of performance evaluation problems encountered in wireless networks. The first part of the thesis covers the performance analysis of ad hoc networks based on Gaussian approximations. More specifically, Chapter 3 quantifies the benefits of perfect rate adaptation on the achievable throughput of random ad hoc networks. The advantages of Large Area Synchronous (LAS) spreading codes in ad hoc networks obeying an infinite rectilinear node topology are outlined in Chapter 4. The second part of the research covers the performance analysis of wireless systems based on characteristic functions. Specifically, the exact average Bit Error Ratio (BER) calculation of an asynchronous DS-CDMA system using random spreading sequences and BPSK modulation for communicating over various fading channels is discussed in Chapter 5. The exact average BER calculation of general Rectangular Adaptive Quadrature Amplitude Modulation (R-QAM) systems subjected to asynchronous Co-Channel Interference (CCI) and Nakagami-m fading is the topic of Chapter 6. The exact average BER calculation of a BPSK- or QPSK-modulated Orthogonal Frequency Division Multiplexing (OFDM) system subjected to Carrier Frequency Offset (CFO), Phase Estimation Error (PER) and Nakagami-m fading is the subject of Chapter 7.

Attaining the highest possible capacity is the key design objective in ad hoc networks. In this context it was concluded in Chapter 3 that perfect rate adaptation has the potential of considerably improving the achievable throughput of random ad hoc networks in comparison to fixed rate transmissions, since rate adaptation is capable of mitigating the effects of link quality fluctuations. This conclusion is confirmed in practical terms in the context of our Adaptive Quadrature Amplitude Modulation (AQAM) examples. For a low normalized minimum distance between the ad hoc nodes, $32\% \sim 162\%$ throughput improvement is achieved in the absence of fading. By contrast, in the presence of shadowing, the corresponding throughput improvement is $54\% \sim 287\%$, although these gains gradually eroded as the distance between the nodes was increased.

In Chapter 4 it was exploited that both the auto-correlation and cross-correlation function of LAS codes exhibits an Interference Free Window (IFW) over a limited duration, which renders them potentially applicable in DS-CDMA ad hoc networks. The BER performance of an ad hoc network obeying an infinite rectilinear node topology is investigated. Our results show that the LAS code aided ad hoc system exhibits a significantly better performance than the family of traditional spreading sequences used in a quasi-synchronous DS-CDMA scenario having a low number of resolvable multipath components and a sufficiently high number of RAKE receiver branches. The asynchronous LAS DS-CDMA system achieves a BER below 10^{-6} in conjunction with high per-bit SNR values and small maximum propagation delays.

Random signature sequences have often been employed by the benchmark schemes used for the performance evaluation of DS-CDMA systems. Hence in Chapter 5 a unified approach is proposed for the exact average BER analysis of an asynchronous DS-CDMA system using random spreading sequences and BPSK modulation for communicating over various fading channels. Several closed-form expressions are derived for the conditional CFs of the interfering signals in various fading channels. A unified exact BER expression is provided, which requires only a single numerical integration. Our simulation results verify the accuracy of our exact BER analysis for various combinations of the spreading sequence length and fading parameters. The Standard Gaussian Approximation (SGA) also shows a reasonable accuracy compared to our simulation results, albeit it slightly over-estimates the average BER when the fading severe, while it underestimates it, when the fading is benign, especially when either there is a low number of interferers or the SNR is high and short spreading sequences are used.

In Chapter 6 it was argued that the family of QAM schemes constitutes a bandwidth-efficient transmission technique and hence has found its way into virtually all recent wireless standards. An exact and general BER expression is derived for R-QAM systems subjected to asynchronous CCI and Nakagami-m fading, which requires only two single numerical integrations. A new closed-form formula is provided for the Characteristic Function (CF) of the CCI. Our simulation results verify the accuracy of our exact BER analysis in the context of different QAM constellation sizes and for various channel statistics. By contrast, the Gaussian model of CCI fails to equally accurately predict the BER performance of QAM.

The focus of Chapter 7 is on Orthogonal Frequency Division Multiplexing (OFDM) which has been employed in numerous wireless standards and has emerged as one of the

promising candidates for employment in next-generation communication systems. However, the performance of the OFDM system is degraded by the Carrier Frequency Offset (CFO) and the Phase Estimation Error (PER). Several new exact close-form expressions are derived for calculating the average BER of OFDM systems in the presence of both CFO and PER in the context of frequency-selective Nakagami-m fading channels. Our simulation results verify the accuracy of our exact BER analysis for various combinations of the normalized CFO values, the PER value, the number of OFDM subcarriers and the Nakagami-m fading parameter. By contrast, the Gaussian approximation slightly overestimates the average BER, especially when the normalized CFO is small, the number of OFDM subcarriers is low and when the fading is less severe.

Acknowledgements

First of all, I would like to sincerely thank Prof. Lajos Hanzo for his admirable supervision and persistent encouragement. During the last three years, I have learned a lot from his enthusiasm, attitude and inspirational insight in research, which will be of great benefit to my future career and life. I would also like to express my appreciation for his financial support in the framework of the NEWCOM, NEXWAY and PHOENIX projects. Furthermore, I could not have finished my research without the aid of a number of my colleagues. I would also like to thank Dr. Lie-Liang Yang for his numerous suggestions in improving my research. My sincere thanks are also due to Dr. Bee Leong Yeap, Dr. Song Ni, Dr. Feng Guo, Dr. Wei Liu, Mr. Wei Liu, Dr. Bin Hu, Mr. Jin Wang, Dr. Ming Jiang, Mr. Yosef Akhtman, Mr. Sohail Ahmed, Dr. Mohamad Yusoff Alias, Dr. Soon Xin Ng, Mr. Ronald Tee, Mr. Choo L Koh, Mr. Chun-Yi Wei, Ms. Noor Othman, Dr. Wei Hua, Dr. Jianmin Zhang, Mrs. Denise Harvey and Ms. Fang-Chun Kuo for their wonderful help both in my work and in my life. Finally, I would like to thank my family for their invaluable support.

List of Publications

1. Xiang Liu and Lajos Hanzo, "Exact BER of Rectangular-Constellation Quadrature Amplitude Modulation Subjected to Asynchronous Co-Channel Interference and Nakagami-m Fading," to be submitted to *IEEE Vehicular Technology Conference*, (Dublin, Ireland), 23-25 April 2007.

2. Xiang Liu and Lajos Hanzo, "Exact BER Analysis of OFDM Systems Communicating over Frequency-Selective Fading Channels in the Presence of Both Carrier Frequency Offset and Channel Estimation Errors," to be submitted to *IEEE Vehicular Technology Conference*, (Dublin, Ireland), 23-25 April 2007.

3. Xiang Liu and Lajos Hanzo, "Exact BER of Rectangular-Constellation Quadrature Amplitude Modulation Subjected to Asynchronous Co-Channel Interference and Nakagami-m Fading," to appear in *Electronics Letters*, July 2006.

4. Xiang Liu and Lajos Hanzo, "A Unified Exact BER Performance Analysis of Asynchronous DS-CDMA Systems Using BPSK Modulation over Fading Channels," accepted subjected to revision for publication in *IEEE Transactions on Vehicular Technology*, May 2006.

5. Xiang Liu and Lajos Hanzo, "Precise BER Formulae for Asynchronous QPSK Modulated DS-CDMA Systems Using Random Quaternary Spreading over Rayleigh Channels," submitted to *IEEE Transactions on Vehicular Technology*, October 2005.

6. Xiang Liu, Hua Wei and Lajos Hanzo, "Analytical BER Performance of LAS DS-CDMA Ad Hoc Networks," submitted to *IEE Proceedings Communications*, October 2005.

7. Xiang Liu and Lajos Hanzo, "Accurate BER Analysis of Asynchronous DS-CDMA Systems in Ricean Channels", to appear in *Proceedings of the IEEE Vehicular Technology Conference*, (Montreal, Quebec, Canada), 25-28 September 2006.

8. Xiang Liu and Lajos Hanzo, "Exact BER Calculation of Asynchronous DS-CDMA Systems Communicating over Hoyt Channels", to appear in *Proceedings of the Ninth International Symposium on Spread Spectrum Techniques and Applications*, (Manaus, Brazil), 28-31 August 2006.

9. Jianmin Zhang, Lie-Liang Yang, Xiang Liu and Lajos Hanzo, "BER Analysis of Inter-Carrier Interference Contaminated OFDM Systems Communicating Over Rapidly-Fading Nakagami-m Channels", to appear in *Proceedings of the Ninth International Symposium on Spread Spectrum Techniques and Applications*, (Manaus, Brazil), 28-31 August 2006.

10. Xiang Liu and Lajos Hanzo, "Accurate BER Analysis of QPSK Modulated Asynchronous DS-CDMA Systems Communicating over Rayleigh Channels," in *Proceedings of the IEEE Vehicular Technology Conference*, (Melbourne, Australia), 7-10 May 2006. (CD-ROM)

11. Xiang Liu and Lajos Hanzo, "Exact BER Performance of Asynchronous DS-CDMA Systems Using Quadriphase Spreading and QPSK Modulation over Rayleigh Channels," in *Proceedings of the IEEE Wireless Communications and Networking Conference*, (Las Vegas, NV, USA), 3-6 April 2006. (CD-ROM)

12. Xiang Liu and Lajos Hanzo, "Effects of Rate Adaptation on the Throughput of Random Ad Hoc Networks," in *Proceedings of the IEEE Vehicular Technology Conference*, vol. 3, (Dallas, TX, USA), pp. 1887-1891, 25-28 September 2005.

13. Xiang Liu, Hua Wei and Lajos Hanzo, "Analytical BER Performance of DS-CDMA Ad Hoc Networks Using Large Area Synchronized Spreading Codes," in *Proceedings of the Sixth International Conference on 3G and Beyond - 3G 2005*, (London, UK), pp. 249-253, 07-09 November 2005.

Contents

List of Symbols

α	The power decay pathloss exponent.
β	The minimum SINR required for successful reception.
η_i	The background noise encountered at node i.
γ	The signal-to-interference-plus-noise ratio.
$\Gamma(\cdot)$	The gamma function [1].
γ_b	The SINR per bit.
γ_s	The SINR per symbol.
γ_{ji}	The SINR at node i experienced by the signal arriving from node j.
$\hat{R}_\psi(\tau)$	The normalized partial auto-correlation function of the chip waveform $\psi_{T_c}(t)$, $\hat{R}_\psi(\tau) = \frac{1}{T_c}\int_\tau^{T_c} \psi_{T_c}(t)\psi_{T_c}(t-\tau)\mathrm{d}t$.
ι	The width of the Interference Free Window.
$\mathcal{N}_t$	The subset of nodes simultaneously transmitting at some time instant.
$\Psi(t)$	The chip waveform.
$\Psi_2(\alpha;\gamma,\gamma';x,y)$	One of Horn's confluent hypergeometric functions of two variables.
σ	The standard deviation of the lognormal shadowing.
τ_k	The propagation delay of the kth user.
τ_{max}	The maximum propagation delay
$\Theta(f(n))$	The big-Theta notation. A function is in $\Theta(f(n))$ if it is not much worse, but also not much better than $f(n)$, i.e. there exist two positive real constants, c_1 and c_2, and a positive integer, n_0, such that $c_1 n \leq \Theta(f(n)) \leq c_2 n$ for $\forall n \geq n_0$ [2].

$a_k(t)$	The binary spreading signal of the kth user.
a_{kj}	The jth chip in the binary spreading sequence of the kth user.
$b_k(t)$	The binary data signal of the kth user.
b_{kj}	The jth data bit of the kth user.
c	The throughput capacity.
c_a	The average achievable throughput with rate adaptation.
c_g	The achievable throughput without rate adaptation.
c_i	The achievable normalized per-node throughput improvement attained with the advent of perfect rate adaptation, $c_i = \frac{c_a}{c_g}$.
c_i^0	The maximum achievable normalized throughput improvement c_i attained when we have $r_{min} = 0$.
c_{xx}	The discrete aperiodic auto-correlation function of the sequence x.
c_{xy}	The discrete aperiodic cross-correlation function between the sequences x and y.
G	The power gain between two nodes.
G_{ji}	The power gain between nodes j and i.
L	The length of a spreading sequence.
L_p	The total number of resolvable paths.
L_r	The total number of RAKE branches.
N_0	The double-sided spectral density of the background noise.
$O(f(n))$	The big-O notation. A function is in $O(f(n))$ if it is less than some constant multiple of $f(n)$, i.e. there exist a positive real constant, c, and a positive integer, n_0, such that $O(f(n)) \leq cf(n)$ for $\forall n \geq n_0$ [3].
P_t	The transmit power.
$Q(x)$	The Gaussian Q-function
r	The distance between two nodes.
r_n	The common reliable transmission range.

$R_\psi(\tau)$ The normalized partial auto-correlation function of the chip waveform $\psi_{T_c}(t)$, $R_\psi(\tau) = \frac{1}{T_c}\int_0^\tau \psi_{T_c}(t)\psi_{T_c}(t+T_c-\tau)\mathrm{d}t$.

r_{ji} The distance between nodes j and i.

r_{min} The minimum distance between nodes.

T_c The chip duration.

T_s The symbol duration.

${}_1\mathbb{F}_1(\alpha;\beta;x)$ The confluent hypergeometric function.

$\mathbb{F}^{A:B^{(1)};...;B^{(n)}}_{C:D^{(1)};...;D^{(n)}}\left(\begin{matrix}\left[(a):\theta^{(1)},...,\theta^{(n)}\right]:\left[(b^{(1)}):\phi^{(1)}\right];...;\left[(b^{(n)}):\phi^{(n)}\right];\\ \left[(c):\psi^{(1)},...,\psi^{(n)}\right]:\left[(d^{(1)}):\delta^{(1)}\right];...;\left[(d^{(n)}):\delta^{(n)}\right];\end{matrix} x_1,...,x_n\right)$ The generalized Lauricella function of n variables.

$\mathbb{F}^{A:B;B'}_{C:D;D'}\left[\begin{matrix}(a):(b)\,;(b')\,;\\ (c):(d)\,;(d')\,;\end{matrix} x,y\right]$ The Kampé de Fériet function.

$\mathbb{F}^{(n)}_A(\alpha;\beta_1,...,\beta_n;\gamma_1,...,\gamma_n;x_1,...,x_n)$ is The Lauricella function of n variables

${}_p\mathbb{F}_q(\alpha_1,\alpha_2,...,\alpha_p;\beta_1,\beta_2,...,\beta_q;x)$ The generalized hypergeometric function.

$\mathbb{H}_7(\alpha;\gamma,\delta;x,y)$ One of Horn's confluent hypergeometric functions of two variables.

$\mathbb{I}_0(x)$ The zeroth-order modified Bessel function of the first kind.

$\mathbb{J}_0(x)$ The zeroth-order Bessel function of the first kind.

$\widetilde{x}$ The complex variable.

$\widetilde{x}^*$ The complex conjugate of the complex variable $\widetilde{x}$.

$\Im\{\widetilde{x}\}$ The imaginary part of the complex variable $\widetilde{x}$.

$\Re\{\widetilde{x}\}$ The real part of the complex variable $\widetilde{x}$.

Chapter 1

Introduction

Wireless communication techniques have experienced an exponential growth during the past decade. At the time of writing cellular wireless networks might be viewed as the most successful means of person to person communications, considering that the cell phone has become an important part of our everyday life. It has evolved from the analogue first generation era (1G) to the digital second generation era (2G), and to the third generation (3G) broadband communications era. Research is now under way towards the fourth generation (4G) systems of the near future, seamlessly integrating different types of wireless networks with wired backbone networks and supporting heterogeneous services over a single all-IP-based core network [4]. Most operational wireless networks are infrastructure-based, which require careful network planning. As a design alternative, ad hoc networks may be expected to play an important role in future communication systems [4].

The rest of the chapters in this thesis cover mainly two areas related to the performance analysis of wireless communications systems in fading channels, namely that of ad hoc networks based on Gaussian approximations and that of wireless systems based on Characteristic functions. The subsequent chapters are organized as follows:

- **Chapter 2:** The basic concepts of ad hoc networks is introduced. This is followed by an outline of the evolution of ad hoc networks. Then a number of research efforts focussed on the design challenges of ad hoc networks, such as capacity, routing, broadcast/multicast/geocast, medium access control, security, Quality of Service (QoS), energy efficiency, modeling/simulation, etc., are briefly reviewed.

- **Chapter 3:** Capacity is one of the most important design issues in ad hoc networks. A brief overview of related work on the capacity of ad hoc networks is provided. Then we focus our attention on the effects of perfect rate adaptation on the achievable throughput of random ad hoc networks, which is discussed in the context of both pathloss and shadow fading. We conclude that perfect rate adaptation has the potential of considerably improving the achievable throughput of random ad hoc networks compared to fixed rate transmissions, since rate adaptation is capable of mitigating the effects of link quality fluctuations. This conclusion is further confirmed by simulations carried out in the context of our Adaptive Quadrature Amplitude Modulation (AQAM) examples.

- **Chapter 4:** The family of Large Area Synchronous (LAS) codes exhibits an Interference Free Window (IFW) over a limited duration, which renders them potentially applicable in DS-CDMA ad hoc networks. The related prior research on LAS codes is reviewed. Then the BER performance of an ad hoc network obeying an infinite rectilinear mesh topology is investigated. Our results show that the LAS ad hoc system exhibits a significantly better performance than the family of traditional spreading sequences used in a quasi-synchronous DS-CDMA scenario having a low number of resolvable multipath components and a sufficiently high number of RAKE receiver branches.

- **Chapter 5:** Random signature sequences have often been employed in benchmark systems in the performance evaluation of DS-CDMA systems. The related research on the average BER calculation of asynchronous DS-CDMA systems is reviewed and the statistical properties of various fading channels are summarized. Then a unified exact BER expression is derived for asynchronous DS-CDMA systems using BPSK modulation and random spreading sequences subjected to various fading channels. Furthermore, several closed-form expressions are derived for the conditional Characteristic Functions (CF) of the interfering signals in various fading channels. Our numerical results verify the accuracy of our exact BER analysis for various combinations of the spreading sequence length and the fading parameters, and they also demonstrate the reasonably high accuracy of the Standard Gaussian Approximation (SGA) of the Multiple Access Interference (MAI).

- **Chapter 6:** The family of QAM schemes constitutes a bandwidth-efficient transmission technique and hence has found its way into virtually all recent wireless standards. A brief overview of related work is provided on the average BER calculation of QAM systems communicating over AWGN or fading channels. Then a

general Rectangular QAM (R-QAM) system subject to asynchronous Co-Channel Interference (CCI) and Nakagami-m fading is investigated. An exact and general BER expression is derived, which requires only two single numerical integrations and a new closed-form formula is provided for the CF of the CCI. Our simulations verify the accuracy of our exact BER expression for different constellation sizes and for various channel statistics. As expected, they also demonstrate a good accuracy for the Gaussian Approximation of the CCI, although the accuracy becomes lower when the per-bit SIR is high, the fading is less severe, the constellation size is small and hence the number of bits/symbol is low.

- **Chapter 7:** OFDM has been employed in numerous wireless standards and has emerged as one of the promising candidates to be employed in next-generation communication systems. However, the performance of the OFDM system is sensitive to the Carrier Frequency Offset (CFO), which destroys the orthogonality of the OFDM subcarriers and inflicts Inter-Carrier Interference (ICI). An overview of the related work on the BER degradation induced by CFO in OFDM systems is provided. Then an OFDM system using BPSK/QPSK modulation communicating over frequency-selective Nakagami-m channels in the presence of both the CFO and the Phase Estimation Error (PER) is presented. Several new closed-form expressions are provided for calculating the average BER of a BPSK- or QPSK-modulated OFDM system. Our simulation results verify the accuracy of our exact BER analysis for various combinations of the normalized CFO values, the PER value, the number of OFDM subcarriers and the Nakagami-m fading parameter. By contrast, the Gaussian approximation slightly over-estimates the average BER, especially when the normalized CFO is small, the number of OFDM subcarriers is low and when the fading is less severe.

The novel contributions of the thesis are as follows:

- Study the effects of perfect rate adaptation on the achievable throughput of random ad hoc networks, which are discussed in the context wireless channels subjected to both pathloss and shadow fading [5].
- Comparative study of the BER performance of a DS-CDMA ad hoc network using LAS codes as well as traditional spreading sequences and obeying an infinite rectilinear mesh topology both in quasi-synchronous and asynchronous scenarios [6, 7].

- A unified exact BER expression is derived for asynchronous DS-CDMA systems using BPSK modulation and random spreading sequences subjected to various fading channels. Furthermore, several closed-form expressions are derived for the conditional CF of the interfering signals in various fading channels [8–10].

- A general Rectangular QAM (R-QAM) system subject to asynchronous Co-Channel Interference (CCI) and Nakagami-m fading is investigated. An exact and general BER expression is derived and a new closed-form formula is provided for the CF of the CCI [11, 12].

- An OFDM system using BPSK/QPSK modulation schemes for communicating over frequency-selective Nakagami-m channels in the presence of both the CFO and the Phase Estimation Error (PER) is studied. Several new closed-form expressions are provided for calculating the average BER of an BPSK- or QPSK-modulated OFDM system [13].

Chapter 2

Overview of Wireless Ad Hoc Networks

2.1 Concepts

The adjective "ad hoc" is originated from the Latin language, implying the quality of being irregular or unplanned, taking place when necessary [14]. The IEEE 802.11 subcommittee defines an ad hoc network as "a network composed solely of stations within mutual communication range of each other via the wireless medium. An ad hoc network is typically created in a spontaneous manner. The principal distinguishing characteristic of an ad hoc network is its limited temporal and spatial extent. These limitations allow the act of creating and dissolving the ad hoc network to be sufficiently straightforward and convenient so as to be achievable by non-technical users of the network facilities; i.e. no specialized 'technical skills' are required and little or no investment of time or additional resources is required beyond the stations that are to participate in the ad hoc network. The term ad hoc is often used as slang to refer to an independent basic service set." [15] The Internet Engineering Task Force (IETF) also refers to "ad hoc networks" as "Mobile Ad hoc NETworks (MANET)" and deems it somewhat synonymous with mobile packet radio networks, mobile mesh networks and mobile, multihop, wireless networks [16]. In addition, the term "ad hoc mode" usually refers to the ability of nodes to directly communicate with one another.

An ad hoc network is an autonomous system of nodes. These nodes may be constituted by any wireless device equipped with wireless transceivers using antennae, for example,

Personal Digital Assistants (PDAs), laptops, mobile phones, etc. They may be stationary, but more likely to be mobile. They may join or exit the network arbitrarily. The ad hoc network may operate in isolation or may be connected to infrastructure-based networks via gateways.

In addition to a range of characteristics inherited from classic cellular wireless networks, ad hoc networks have their own specific features [4, 16, 17]:

- *Require no Infrastructure* — Unlike the classic base-station-aided cellular networks, an ad hoc network does not rely on any infrastructure, hence it may be temporarily formed, when needed. Hence ad hoc networks may be established anywhere and anytime.

- *Distributed* — There is no centralized administration in an ad hoc network. All nodes in the network have equal rights, and cooperate in a distributed manner. Each node acts as an independent router and generates data independently. Hence even if some of the nodes in the network malfunction or roam out of reach, the other nodes can continue operating. Accordingly, an ad hoc network is self-organized and self-healing.

- *Mobile* — In a cellular network, each user communicates with a fixed base station, sometimes with several fixed base stations for the sake of achieving marco-diversity, and hands over to another serving base station(s), when moving from one cell to another. In an ad hoc network all nodes may be free to move, while communicating with others.

- *Dynamic Topology* — The topology of a cellular network is star-like, as illustrated in Figure 2.1(a). On the other hand, the topology of an ad hoc network may be arbitrary, as illustrated in Figure 2.1(b). Furthermore, in an ad hoc network the movement of nodes, the received signal level variation incurred by imperfect power control, by joining and leaving the network, etc. may result in the link's disconnection between nodes. As a consequence, the topology and routing of an ad hoc network may be constantly changing and hence it is fairly unpredictable.

- *Multihop Routing* — In traditional cellular networks there is only a single wireless hop between the user and its base station. In an ad hoc network, two nodes may communicate directly when both are within the other's wireless coverage. Since the coverage of a node is limited by its maximum transmit power, they have to communicate via intermediate nodes roaming between them, when they are far

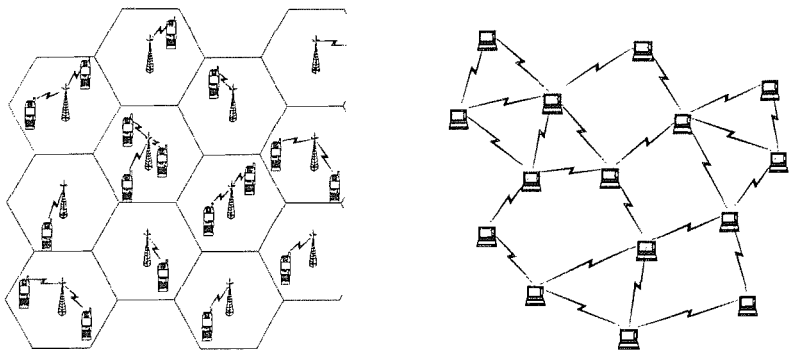

(a) The cellular network (b) The ad hoc network

FIGURE 2.1: The topologies of the cellular network and the ad hoc network.

apart. Hence, the active routes in an ad hoc network generally consist of multiple hops and the data have to be stored and forwarded via several intermediate nodes, before arriving at their destination.

- *Bandwidth-Constrained* — Since there is no wired infrastructure support in an ad hoc network, all nodes communicate with each other wirelessly. The capacity of the wireless channel is typically lower than its wired counterpart due to its physical properties. Additionally, multiple access, fading, noise, interference, traffic congestion, etc. degrade the capacity of wireless links.

- *Energy-Constrained* — In an ad hoc network some or most of the nodes may be mobile devices, such as PDAs, laptops, etc. Since these devices may be constantly moving, their energy is exclusively supplied by batteries. Hence for these nodes energy conservation is important.

- *Limited Security* — Generally speaking, the use of open and shared broadcast-type wireless channels renders mobile wireless networks more prone to information security threats than fixed wired networks. However, as a benefit of its self-organizing and self-healing capability, the decentralized nature of the ad hoc network enables it to become more robust than centralized networks.

The attractive features of ad hoc networks render them suitable for use in situations where the infrastructure is either unavailable, untrustable or unreliable. A few typical applications are in the field of military communications between soldiers in the battle field, the rescue communications in emergency or disaster operations, or in accidents, in the wireless network connecting all equipment in the home, in temporary meetings both indoors and outdoors, etc.

Feature	Cellular Network	Ad Hoc Network
infrastructure	base-station-based	infrastructureless
deployment	pre-installed	when necessary
backbone network	wired	wireless
control	centralized	distributed
mobility	fixed base stations	possibly free to move
topology	star-like	arbitrary
connectivity	stable	dynamic
routing	single hop	multiple hop

TABLE 2.1: Comparison between cellular and ad hoc networks.

In Section 2.2 the historic evolution of ad hoc networks is outlined. A number of challenges faced by the designer of ad hoc networks are summarized in Section 2.3. Finally, we conclude this chapter in Section 2.4.

2.2 History

The predecessor of the ad hoc network is considered to be the Packet Radio Network (PRNET) [4, 18, 38], which dates from the 1970s. In 1972 the Defense Advanced Research Projects Agency (DARPA) in the USA initiated the PRNET project for the sake of improving battlefield communications [4], which cannot rely on a fixed pre-deployed infrastructure. PRNET featured a distributed wireless network consisting of a collection of mobile nodes, which were formed by soldiers, tanks, aircrafts, etc. which invoked a combination of the ALOHA[1] [39] and the Carrier Sense Multiple Access (CSMA)[2] [40] approaches for medium access and multihop store-and-forward routing.

The DARPA PRNET project pioneered the research of such autonomous networks. Several related projects developed these ideas further as the evolution of autonomous networks. The SURvivable Adaptive Networks (SURANs) [19] programme was established by DARPA in 1983 to deal with open problems in PRNET, which focused on the design of algorithms capable of supporting large, adaptive, robust and secure networks. Amongst other achievements, this programme proposed the Low-cost Packet Radio (LPR) concepts of [20] in 1987, which intended to develop light-weight, low-cost, low-power radios designed for large, sophisticated packet networks. From the early

[1] ALOHA is a distributed protocol which dynamically allocates the sharing channel among multiple communicating terminals.

[2] CSMA is a distributed MAC protocol in which a node verifies the absence of other traffic before transmitting on a shared broadcast-type medium. If a carrier is detected, the node postpones its transmission.

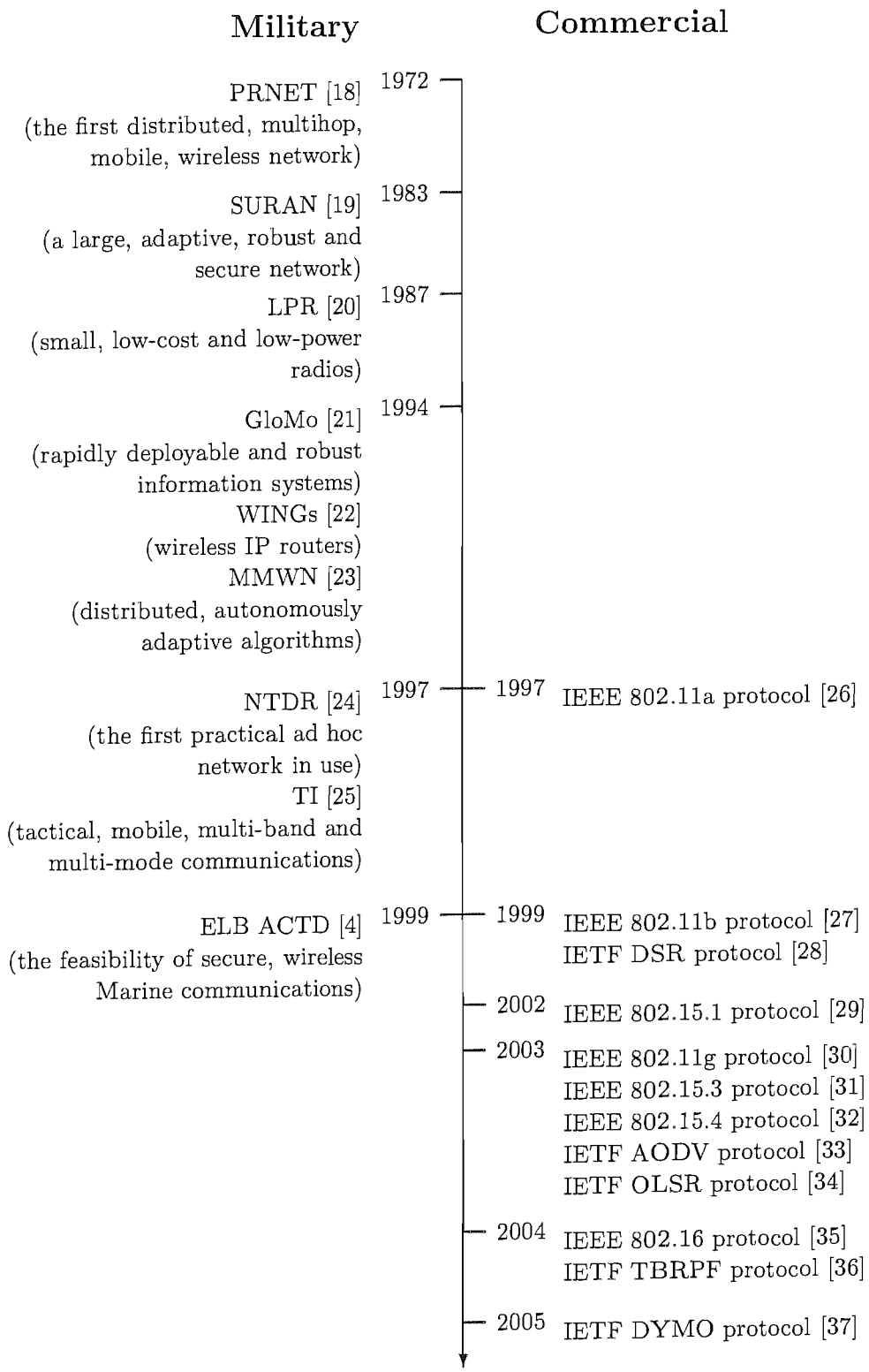

FIGURE 2.2: The evolution of ad hoc networks.

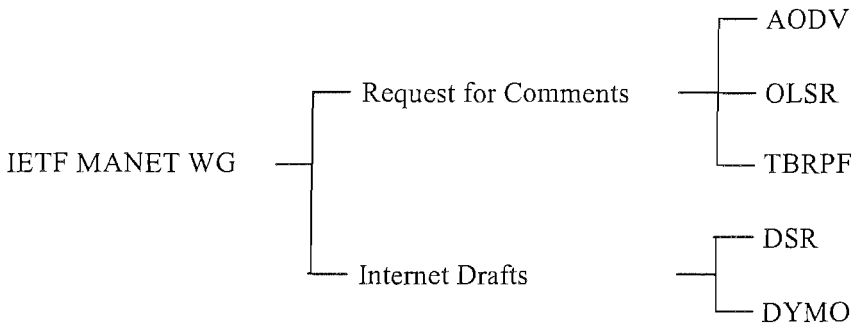

FIGURE 2.3: The IETF MANET routing protocols.

1990s onwards, the evolution of the Internet and cost-efficient personal computers further fuelled the implementation of packet radio networks. In 1994 the Department of Defense in USA initiated the Global Mobile (GloMo) Information Systems [21] programme, which aimed at the development of rapidly deployable and robust information systems in mobile environments. As part of the GloMo programme, Wireless Internet Gateways (WINGs) [22] were designed to seamlessly extend the global IP-based Internet to distributed, dynamic, self-organizing, multihop wireless networks. The Multimedia Mobile Wireless Network (MMWN) featured in [23] constituted a modular system of distributed, autonomous adaptive algorithms cooperating in the interest of supporting real-time multimedia applications in large, multihop mobile wireless networks. The Near-Term Digital Radio (NTDR) system [24] became the first practical ad hoc network used by the US Army [17] and it featured a hierarchical cluster-based network architecture and link-state routing. The Tactical Internet (TI) [25], implemented by the US Army in 1997, applied modified commercial Internet protocols for the sake of supporting integrated battlefield communications and provided tactical, mobile, simultaneous multi-band, multi-mode communications. Extending the Littoral Battle-space Advanced Concept Technology Demonstration (ELB ACTD) [4] in 1999 was explored in order to demonstrate the feasibility of establishing a secure, wireless wide-area TI between ships at sea and marines on land via an aerial relay. But again, most of the early research was sponsored by the military and hence has not been published until the mid-1990s in the open literature.

Nonetheless, ad hoc networks have become one of the hottest research field during the past decade, although at the time of writing ad hoc networks have not been employed in commercial applications, and most of the research is still in the speculative or experimental stages. Based on the recent research advances in the field of ad hoc networks, a number of standardization activities began to emerge during the mid-1990s.

Family	Protocol	Distance (m)	Rate (Mbps)	Band (GHz)
IEEE 802.15 (WPAN)	IEEE 802.15.1	< 10	1	2.4
	IEEE 802.15.3	< 10	> 20	2.4
	IEEE 802.15.4	< 10	0.02-0.2	2.4
IEEE 802.11 (WLAN)	IEEE 802.11a	50-100	< 54	5
	IEEE 802.11b	50-100	< 11	5
	IEEE 802.11g	50-100	< 54	5
IEEE 802.16 (WMAN)	IEEE 802.16	2k-50k	30-120	2-66
IEEE 802.20 (MWMAN)	N/A	N/A	< 1	< 3.5

TABLE 2.2: IEEE 802 standard family of wireless network protocols.

The MANET Working Group (WG) within the IETF was formed for the sake of standardizing IP routing protocols for ad hoc networks [16]. The MANET WG is dedicated to designing unicast routing protocols as well as to their performance evaluation and has published several Internet Drafts and Requests For Comments (RFC) on Dynamic Source Routing (DSR) [28], Dynamic MANET On-demand (DYMO) Routing [37], Ad hoc On-Demand Distance Vector (AODV) Routing [33], Optimized Link State Routing (OLSR) [34] and Topology Dissemination Based on Reverse-Path Forwarding (TBRPF) [36] protocols. In the future the MANET WG will also investigate both multicast and Quality of Service (QoS) problems in MANET environments.

The IEEE 802 LAN/MAN Standards Committee develops Local Area Network (LAN) and Metropolitan Area Network (MAN) standards. There are four main families of wireless network protocols. The most well-known IEEE 802.11 [15, 27, 30] family defines access techniques for wireless LANs utilizing Carrier Sense Multiple Access with Collision Avoidance (CSMA/CA)[3]. The IEEE 802.15 [29, 31, 32] family defines access techniques for Wireless Personal Area Networks (WPANs), which are mainly used for automatically connecting personal computers to personal electronic devices, such as mobile phones, mp3 players, portable media players, digital cameras, PDAs, etc. within a short distance. The IEEE 802.16 [35] family defines the air interface for fixed Broadband Wireless Access (BWA) systems, which are mainly used for wireless MANs (WMANs) operating at a high transmission rate over a long distance. The new IEEE 802.20 [41, 42] family is still under development, and is quite similar to the IEEE 802.16 family designed for high-speed and long-distance transmission, but will intend to focus on Mobile Broadband Wireless Access (MBWR) techniques, which are mainly used for Mobile WMANs (MWMANs).

[3]CSMA/CA is a modification of pure CSMA. In CSMA/CA, a node broadcast its intent to transmit before any actual transmission, and it transmits information if there is no intent collision happened.

2.3 Design Challenges

Although the family of ad hoc networks has the above-mentioned advantages, such as being capable of self-organizing, self-healing, coupled with ease of deployment, etc. its flexibility imposes a number of design challenges [4, 17, 41], which are outlined below.

2.3.1 Capacity

The achievable network capacity is one of the most important performance metrics in the evaluation of an ad hoc network. However, its multihop and mobile nature renders the related capacity investigations a challenging task [5, 43–52].

It has been shown in [43] that the per-node throughput of an ad hoc network is not scalable[4], a parlance indicating that the attainable per-node capacity decreases as the network size tends to infinity.

There are a number of techniques, which may be used for improving the capacity of wireless networks, such as directional antennae [44, 45] and rate adaptation [5, 46]. However, none of them are capable of changing the capacity scaling law[5] of ad hoc networks due to the limitations of realistic systems [45] or the Shannon limits [5].

The exploitation of the network's dynamically fluctuating channel quality also improves the achievable capacity, for example by deferring transmissions, when they impose a high "cost" in terms of the transmit power or the number of hops, to the instant when they impose a low cost [5, 46–48]. The main reasons for the channel quality fluctuations are co-channel interference, fading [5, 46] and mobility [47, 48]. However, it was demonstrated in [5] that even perfect channel-quality-dependent rate adaptation fails to change the capacity scaling law of ad hoc networks, regardless of the absence or presence of shadow fading. Mobility may be exploited for rendering the capacity of ad hoc networks scalable, even when the number of communicating nodes n is high, provided that the inevitable transmission delay is ignored [47]. A two-hop strategy was adopted in [47], where the source distributed its packets to a large number of relay nodes, and each relay node temporarily stored the packets, then roamed and only delivered them to the destination when they were nearby. However, the expected end-to-end delay per data packet imposed

[4] A network is scalable if it can provide acceptable service even when the network size tends to infinity.

[5] The scaling law in ad hoc networks characterizes how the network performance varies, as the number of nodes in the network tends to infinity. In this chapter the network performance is quantified in terms of the achievable per-node throughput.

by the above strategy might be a logarithmic function of the network size [48], which suggests that mobile ad hoc networks constituted by many nodes may not be scalable in real-time applications.

The capacity of an ad hoc network may also be improved with the aid of additional infrastructure[6] support, which implies that the network is no longer a stand-alone ad hoc network, but a hybrid wireless network. The per-node throughput may be improved with the assistance of both regular base stations [49] and random distributed access points [50]. However, they still fail to change the capacity scaling law of ad hoc networks.

Most research on network capacity was carried out under the assumption of irrealistic simplifying conditions and highly mathematical abstractions [5, 43–45, 47–50], which have limited applicability for realistic networks. A mathematical framework was defined for studying the capacity of wireless ad hoc networks in [46], which was suitable for investigating the effects of multihop routing, spatial reuse[7], successive interference cancellation (SIC), power control, variable-rate transmissions, node mobility and fading. However, the associated computational complexity of scheduling would increase exponentially, as the network size increases. Various capacity studies based on simulations have been performed in [51, 52].

2.3.2 Routing

Table 2.3: Routing protocols categorized according to the diverse approaches of obtaining routing information.

Proactive Routing Protocols	
DSDV	*Destination-Sequenced Distance Vector protocol* In DSDV, each node maintains a routing table, which records all possible destinations within the network and the number of hops required for reaching each destination from it. Each entry in the routing table has a unique number indicating how old the route is [53].
WRP	*Wireless Routing Protocol* In WRP, each node maintains four routing tables, and periodically sends a *hello* message for maintaining connectivity [54].

[6]The infrastructure may be either regularly allocated base stations [49] or randomly distributed access points [50].

[7]Spatial reuse implies that more than one nodes are allowed to transmit at a given time.

GSR	*Global State Routing protocol* In GSR, instead of broadcasting information throughout the network, each node maintains a topology (link state) table based on up-to-date information received from the neighbouring nodes and periodically exchanges its link state information with its neighbours only [55].
FSR	*Fisheye State Routing protocol* FSR improves GSR by exchanging information about neighbours more frequently than it does about more distant node. Hence the routing overhead traffic is reduced throughout the network at the cost that each node has inaccurate information about distant nodes [56].
STAR	*Source-Tree Adaptive Routing protocol* In STAR, each node maintains a source tree which is a set of links containing the preferred paths to specific destinations, updates its source tree based on both the information about adjacent links and on the source trees reported by its neighbours, and in exchange it reports changes in its own source tree to all of its neighbours [57].
DREAM	*Distance Routing Effect Algorithm for Mobility* In DREAM, each node maintains a routing table storing the geographical coordinates of all other nodes. These coordinates can be obtained with the aid of a Global Position System (GPS) and they are periodically exchanged between nodes [58].
MMWN	*Multimedia support in Mobile Wireless Networks protocol* In MMWN, the network is clustered as a hierarchical architecture of *endpoints* and *switches*. Each endpoint has single-hop wireless connectivity to a switch, and all switches have multihop wireless connectivity to one another [59].
CGSR	*Cluster-head Gateway Switch Routing protocol* In CGSR, the nodes in the network are also aggregated into clusters and all intra- as well as inter-cluster communications are controlled by a cluster-head elected by nodes [60].

HSR	*Hierarchical State Routing protocol* HSR maintains a multi-level hierarchical topology, where elected cluster-heads at a lower level become members of the next higher level. In addition to multi-level clustering based on a geographical relationship between nodes, HSR also provides multi-level logical partitioning based on functional affinity between nodes [56].
OLSR	*Optimised Link State Routing protocol* OLSR minimizes both size of each control message and the number of rebroadcasting nodes during each route update by selecting a set of neighbouring nodes for the source to retransmit its packets. Any node not in the set can read and process the packets but cannot retransmit it [34].
TBRPF	*Topology Broadcast Reverse Path Forwarding protocol* In TBRPF, each node calculates the shortest paths to all reachable destinations and creates a source tree, based on partial topology information stored in its topology table and minimizes the control overhead by reporting only part of its source tree to neighbours [36].
Reactive Routing Protocols	
AODV	*Ad hoc On-demand Distance Vector protocol* In AODV, when a route to a new destination is needed, the source broadcasts a routing request. Once the routing request reaches either the destination or an intermediate node, which has a recent route information to the destination, the route reply follows the reverse path of the route request back to the source [33].
DSR	*Dynamic Source Routing protocol* In DSR, intermediate nodes do not have to have a routing table. Instead, each packet carries a complete list of nodes it traversed through from the source to the destination, and each node may overhear any packet's routing information for its own use [28].

ROAM	*Routing On-demand Acyclic Multipath protocol* ROAM is an on-demand routing algorithm maintaining multiple loop-free paths based solely on distances to destinations. Each node maintains entries only for those destinations for which data flows through the node. A node does not send updates for active destinations, unless its distance to them increases beyond a given threshold [61].
LMR	*Light-weight Mobile Routing protocol* In LMR, a node initiates a new route by broadcasting its request throughout the network and each node maintains multiple routes to its destinations for the sake of adapting to topological changes with a minimal amount of overhead [62].
TORA	*Temporally Ordered Routing Algorithm* Similar to LMR, TORA also provides multiple routes for any source-destination pair. Furthermore, in TORA each node uses a *height* metric for establishing and maintaining a directed acyclic graph rooted from each destination, which renders TORA loop-free [63].
ABR	*Associativity-Based Routing protocol* The principle of ABR lies on the fact that a mobile node's association with its neighbour changes as it is moving and its transition period is characterized by an associativity "tick". A mobile node exhibits high state of mobility when it has low associativity ticks with its neighbours, while it is in the stability state if high associativity ticks are observed[64].
SSA	*Signal Stability Adaptive protocol* SSA selects sustained routes based on signal strength and location stability, rather than by using an associativity tick as in ABR [65].
RDMAR	*Relative Distance Micro-discovery Ad hoc Routing protocol* When a new route has to be established, RDMAR estimates the distance between the source and the destination and then limits the routing setup query flood to the neighbouring region of the source [66].
LAR	*Location-Aided Routing protocol* LAR utilizes location information obtained from a Global Position System (GPS) for limiting the search for a new route to a smaller region rather than exploring the entire network, hence it reduces the routing overheads [67].

ARA	*Ant-colony-based Routing Algorithm protocol* ARA attempts to map the food searching intelligence of ants to the routing algorithm. When ants seek food, they start from their nest and walk towards the food, while leaving behind a transient trail, which indicates the path taken by the ant and allows other to follow unless the trail disappears [68].
FORP	*Flow Oriented Routing Protocol* FORP exploits the mobility information collected from the nodes for predicting the forthcoming topology changes in order to use an alternative route for the flow before a route failure occurs [69].
CBRP	*Cluster-Based Routing Protocol* In CBRP the nodes are grouped into clusters. Each cluster has a cluster head, which coordinates the communications within the cluster and with other clusters. The routing information is exchanged only between cluster heads [70].
Hybrid Routing Protocols	
ZRP	*Zone Routing Protocol* In ZRP, each node defines a routing zone. Hence, for nodes within the routing zone, routes are immediately available, while for those outside the routing zone the routes are determined on-demand [71].
ZHLS	*Zone-based Hierarchical Link State routing protocol* ZHLS divides the network into non-overlapping zones, but there is no "head" node. Each node has a node ID and a zone ID, which is obtained from a GPS and is required for inter-zone routing [72].
SLURP	*Scalable Location Update Routing Protocol* SLURP relies on a location update mechanism, which maintains approximate location information for all nodes. Each node is mapped to a geographic sub-region of the network, and is responsible for storing the current locations of all nodes mapped to this sub-region [73].
DST	*Distributed Spanning Trees-based routing protocol* DST groups the nodes into a number of trees and the root node of each tree controls the structure of the tree. Packets are either sent to all possible neighbours in the tree and adjoining connections between it and other trees, or sent along the tree edges from the source [74].

DDR	*Distributed Dynamic Routing protocol* DDR is also a tree-based routing algorithm, but in DDR the trees do not require a root node. The trees in the network form a forest. Each tree of the forest constructed forms a zone, which is assigned a zone ID by running a zone naming algorithm [75].

In traditional cellular networks each mobile user communicates with his/her home base station via the wireless interface and each base station subsystem (BSS) is connected to a mobile switching centre (MSC) via a fixed point-to-point line. The MSC is responsible for the switching of calls to and from the mobile users. Hence the routing in cellular networks is simple. In the operational wired Internet it is the routers that take the responsibility for routing data from one node to another according to their routing tables. Since the topology of the Internet is typically slowly changing, the routing tables are also relatively stable. However, the situation in ad hoc networks is entirely different from the former owing to its highly dynamic nature. Hence traditional link-state- [8] [76] and distance-vector-based[9] [77] routing algorithms designed for the infrastructure-based Internet are not directly applicable to ad hoc networks, since they would impose an excessive control traffic load. Therefore efficient wireless routing has been the most intensive research area in ad hoc networks [78, 79].

Since the launch of the DARPA PRNET project [18], numerous routing protocols and algorithms have been developed for ad hoc networks, which may be categorized [78, 79] as proactive, reactive and hybrid routing protocols.

- *Proactive Routing Protocols* — Proactive routing is also often referred to as table-driven routing, since it attempts to maintain consistent, up-to-date routing information from each node to every other node or nodes located in a specific area of the network, regardless, whether any nodes are engaged in communications. This requires that each node maintains one or more routing tables for storing routing information, periodically updates these tables and propagates the required updates through the network, if the network topology changes. A few examples are

[8] In link-state routing, each node broadcasts a short message, i.e. the so-called link-state advertisement (LSA), throughout the network. The LSA carries the link-state information of the node, which includes the identity of the node and all other nodes it is connected to as well as includes a sequence number indicating how old the link-state message is. Hence each node may form a connectivity graph of the network and accordingly independently calculate the best next hop from it to any possible destination in the network.

[9] In distance-vector-based routing, each node periodically exchanges routing updates with a limited subset of the nodes in the network, which roam in its vicinity, i.e. with its neighbouring nodes.

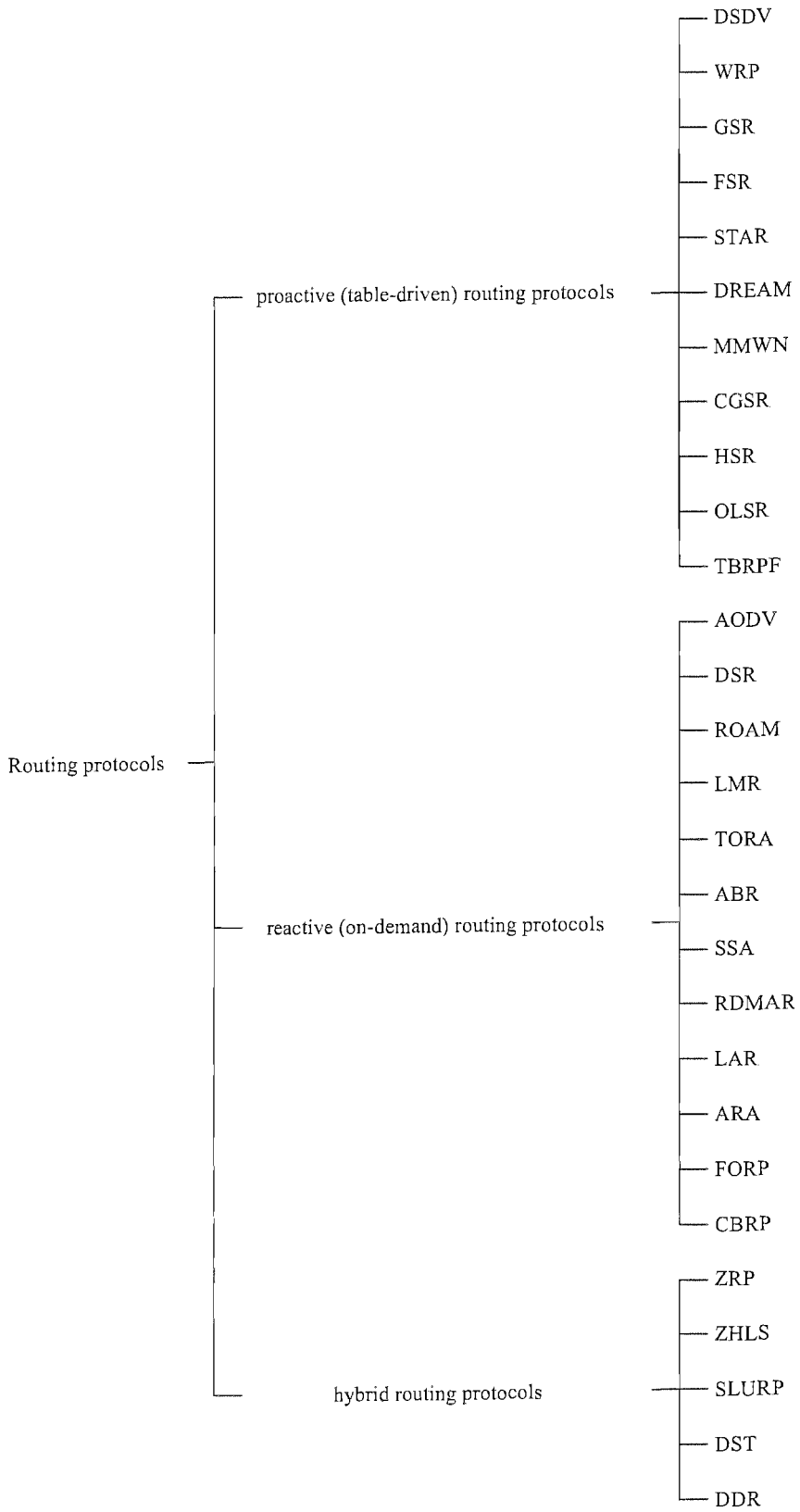

FIGURE 2.4: Routing protocols categorized according to the diverse approaches of obtaining routing information.

the so-called Destination-Sequenced Distance Vector (DSDV) protocol [53], the Wireless Routing Protocol (WRP) [54], the Global State Routing (GSR) protocol [55], the Fisheye State Routing (FSR) protocol [56], the Source-Tree Adaptive Routing (STAR) protocol [57], the Distance Routing Effect Algorithm for Mobility (DREAM) [58], the Multimedia support in Mobile Wireless Networks (MMWN) protocol [59], the Cluster-head Gateway Switch Routing (CGSR) protocol [60], the Hierarchical State Routing (HSR) protocol [56], the Optimised Link State Routing (OLSR) protocol [34] and the Topology Broadcast Reverse Path Forwarding (TBRPF) protocol [36].

- *Reactive Routing Protocols* — Reactive routing is also referred to as demand-driven or on-demand routing [78, 79], which creates routes using a route discovery process only when requested by nodes for sending data to a particular destination. Each node only saves the specific routes leading to the destinations, when the node concerned serves as a source or intermediate node within this particular route, which reduces the control overheads imposed on the network. A few examples are the Ad hoc On-demand Distance Vector (AODV) protocol [33], the Dynamic Source Routing (DSR) protocol [28], the Routing On-demand Acyclic Multipath (ROAM) protocol [61], the Light-weight Mobile Routing (LMR) protocol [62], the Temporally Ordered Routing Algorithm (TORA) [63], the Associativity-Based Routing (ABR) protocol [64], the Signal Stability Adaptive (SSA) protocol [65], the Relative Distance Micro-discovery Ad hoc Routing (RDMAR) protocol [66], the Location-Aided Routing (LAR) protocol [67], the Ant-colony-based Routing Algorithm (ARA) protocol [68], the Flow Oriented Routing Protocol (FORP) [69] and the Cluster-Based Routing Protocol (CBRP) [70].

- *Hybrid Routing Protocols* — As the terminology implies, hybrid routing intends to combine the advantages of both proactive routing and reactive routing. They usually group nodes into zones, trees or clusters and employ proactive algorithms within these areas in contrast to the reactive algorithms outside these areas. A few examples are the Zone Routing Protocol (ZRP) [71], the Zone-based Hierarchical Link State (ZHLS) [72], the Scalable Location Update Routing Protocol (SLURP) [73], the Distributed Spanning Trees-based (DST) routing protocol [74] and the Distributed Dynamic Routing (DDR) [75].

Simple Flooding Methods The simple flooding algorithm is initiated by a source node broadcasting a packet to all neighbours. Each of those neighbours in turn rebroadcasts the packet. This continues until all reachable nodes in the network have received the packet [84].
Probability-Based Methods The probability-based methods use some basic understanding of the network topology for assigning a probability to a node to rebroadcast [85].
Area-Based Methods The area-based methods assume that nodes have common transmission distances. A node will rebroadcast only if the rebroadcast will reach sufficient additional coverage area. On the maximum extreme, if a node is located at the boundary of the sender node's transmission distance, then a rebroadcast would reach 61% additional area [85].
Neighbour-Knowledge-Based Methods The neighbour-knowledge-based methods maintain neighbour information obtained from periodic *hello* packets, and accordingly decide whether to rebroadcast [86, 87].

TABLE 2.4: Broadcast routing protocols.

2.3.3 Broadcast, Multicast and Geocast

Routing protocols may also be categorized based on the type of transmissions invoked [4] rather than on the criteria used in Subsection 2.3.2, which leads to the philosophy of Unicast [80], Broadcast [81], Multicast [82] and Geocast [83] type regimes.

Unicasting [80] is also referred to as peer-to-peer communication, which is the service taking place between a single source and a single destination. Unicasting is the main transmission type in the operation of the Internet and serves as the foundation of other types of protocols.

Broadcasting [81] is the communication service, in which a source sends the same message to all nodes or all its neighbours in the network. It is also often referred to as *flooding* and it is typically used for, but not limited to, route discovery and neighbour discovery. Existing broadcast protocols may be categorized [81] into simple flooding methods (also termed as blind flooding) [84], probability-based methods [85], area-based methods [85] and neighbour-knowledge-based methods [86, 87].

Multicasting [82] is an efficient communication service taking place between a single source and multiple selected destinations. It reduces the unnecessary traffic in the network compared to unicasting, and alleviates the work load of the nodes that are uninterested in the data packets compared to broadcasting [82]. According to the techniques

of how routes are created for specific members of the multicast group, the multicast routing protocols used in ad hoc networks may be categorized into four groups [4, 82]:

- *Tree-Based Multicast* — These multicast protocols have been adopted from wired networks. As in fixed multicast routing, tree-based multicast routing protocols create a tree over which the multicast data is forwarded, where there is only one path between any source and destination pair. Representatives of the route-tree-based multicast protocol family include the Distance Vector Multicast Routing Protocol (DVMRP) [88], the Ad hoc Multicast Routing protocol utilizing Increasing id numberS (AMRIS) [89], the Multicast Ad hoc On-demand Distance Vector (MAODV) protocol [90], the Lightweight Adaptive Multicast (LAM) protocol [91] and the Location Guided Tree (LGT) construction algorithm [92] designed for small group multicast.

- *Mesh-Based Multicast* — Multicast meshes outperform multicast trees in mobile networks, since they have multiple paths between any source and destination pair, which enables multicast datagrams to be delivered to the destinations, even if some links fail. Representative mesh-based multicast protocols include the On-Demand Multicast Routing Protocol (ODMRP) [93], the Core-Assisted Mesh Protocol (CAMP) [94] and the Forwarding Group Multicast Protocol (FGMP) [95].

- *Stateless Multicast* — In order to reduce the considerable overheads imposed by maintaining routing trees or meshes in the case of frequently moving or high-speed nodes, the source specifies the multicast destination list in its multicast data packets and an intermediate node only looks at the packet header for the sake of forwarding, hence there is no need to maintain the multicast paths. A representative of the stateless multicast protocol family is the so-called Differential Destination Multicast (DDM) [96].

- *Hybrid Multicast* — It is possible to combine tree-based routing and mesh-based routing for the sake of striking a tradeoff between the data forwarding efficiency and robustness. Representative hybrid multicast protocols are the Ad hoc Multicast Routing (AMRoute) [97] and the Multicast Core Extraction Distributed Ad hoc Rouging (MCEDAR) [98].

Table 2.5: Multicast routing protocols.

Tree-Based Multicast

DVMRP	*Distance Vector Multicast Routing Protocol* DVMRP is used when a node receives a multicast packet and it wants to find out if other multicast nodes it is connected to need to receive the packet. Initially every node in the network is assumed to be part of the multicast group. The source node sends a multicast message to all adjacent nodes, each of which then selectively forward the message to downstream nodes, until the message eventually passes to all multicast group members [88].
AMRIS	*Ad hoc Multicast Routing protocol utilizing Increasing id numberS* AMRIS constructs a shared tree for supporting multiple sources and destinations in a multicast session. AMRIS dynamically assigns an ID number to each node in each multicast session and generally the ID number increases as the tree expands from the source [89].
MAODV	*Multicast Ad hoc On-demand Distance Vector protocol* MAODV is derived directly from unicast AODV in Table 2.3. The multicast route request is broadcast similar to the unicast route request, and the route reply propagates back from the nodes that are members of the multicast group [90].
LAM	*Lightweight Adaptive Multicast protocol* LAM builds a group shared multicast routing tree for each multicast group. Each node needs to store its parent node and a list of its one-hop children nodes when it is in a multicast group, or store its potential parent and children nodes when it is waiting for joining a multicast group [91].
LGT	*Location Guided Tree construction algorithm* LGT is a small group multicast algorithm based on packet encapsulation. It builds an overlay multicast packet distribution tree on top of the underlying unicast routing protocol. Multicast data is encapsulated in a unicast packet and transmitted only among the group nodes [92].
Mesh-Based Multicast	

ODMRP	*On-Demand Multicast Routing Protocol* ODMRP applies on-demand routing techniques to avoid channel overhead and improve scalability. It uses a concept of forwarding group, a set of nodes responsible for forwarding multicast data on shortest path between any member pairs, to build a forwarding mesh for each multicast group [93].
CAMP	*Core-Assisted Mesh Protocol* CAMP defines a shared multicast mesh for each multicast group for maintaining the connectivity of multicast groups. CAMP consists of the maintenance of multicast meshes and loop-free packet forwarding over such meshes. [94].
FGMP	*Forwarding Group Multicast Protocol* FGMP makes a decision to forward multicast packets depending on a forwarding flag, which is associated with a timer. When a node in the forwarding group learns of a receiver member, it resets its forwarding timer. A node with enabled forwarding flag (i.e., timer has not expired) is responsible for forwarding the multicast packets for that group [95].
Stateless Multicast	
DDM	*Differential Destination Multicast protocol* In DDM, the source node controls multicast group membership. The source places a differentially-encoded and variable-length list of destination addresses in multicast data packet headers, resulting in packets capable of self-routing towards their destinations [96].
Hybrid Multicast	
AMRoute	*Ad hoc Multicast Routing protocol* AMRoute creates a bidirectional, shared tree using only group senders and receivers as tree nodes for data distribution. AMRoute assumes the existence of an underlying unicast routing protocol that can be used for taking care of network dynamics [97].

MCEDAR	*Multicast Core Extraction Distributed Ad hoc Rouging protocol* MCEDAR uses a mesh as the underlying infrastructure, so it can tolerate a few link breakages without reconfiguration of the infrastructure. The efficiency is achieved by using a forwarding mechanism on the mesh that creates an implicit forwarding tree. This ensures that the packets need to travel only the minimum distance in the tree [98].

Geocasting [83] may be regarded as a variant of conventional multicasting, where data packets are delivered to nodes located in a specific geographic area, which is called *geocast region*. Typically, geocasting requires the assistance of a Global Position System (GPS) or similar positioning systems for the sake of obtaining node location information.

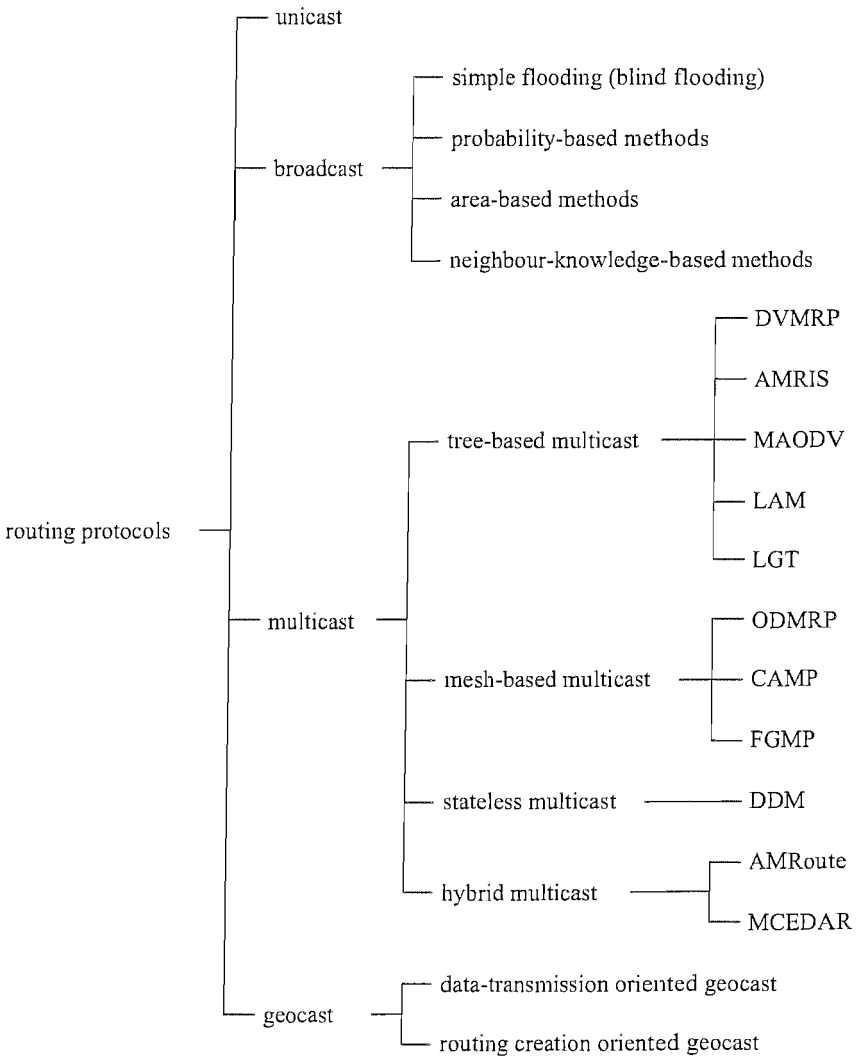

FIGURE 2.5: Routing protocols categorized based on the type of transmissions invoked.

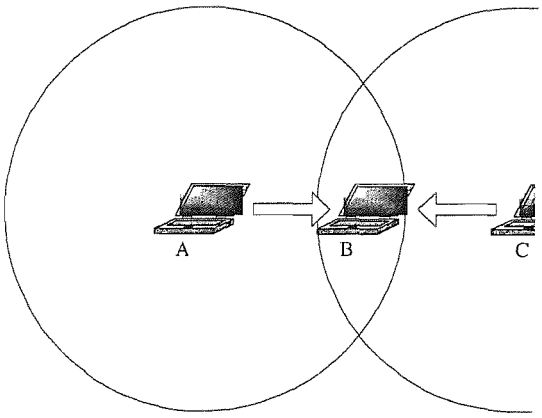

FIGURE 2.6: The hidden node problem.

According to how the data is forwarded from the source to the geocast region, geocast protocols may be categorized into two groups, namely data-transmission oriented[10] [99–101] and routing-creation oriented[11] [102, 103].

2.3.4 Medium Access Control

Medium Access Control (MAC) protocols define how the nodes may access their shared channel. In an ad hoc network the so-called hidden node problem and exposed node problem [104] are important issues affecting the design of MAC protocols.

- *Hidden Node Problem* [104] — This problem is illustrated in Figure 2.6, where the nodes A and C are hidden from each other, which implies that one cannot detect the other's transmission, since they are outside each other's transmission range limited by their transmit powers. However, their transmission range is sufficiently high for reaching node B, which is capable of communicating with both of them. Hence it would result in transmission collision, when both node A and node C are trying to transmit data to node B at the same time.
- *Exposed Node Problem* [104] — This problem is characterized by Figure 2.7. The nodes B and C are said to be exposed to each other, which implies that one's transmission would block the other's transmission, even though there is no interference between their transmissions because they are within the transmission range

[10]Data-transmission oriented protocols use flooding or a variant of flooding to forward geocast packets from the source to the geocast region.

[11]Routing-creation oriented protocols create routes from the source to the geocast region via control packets.

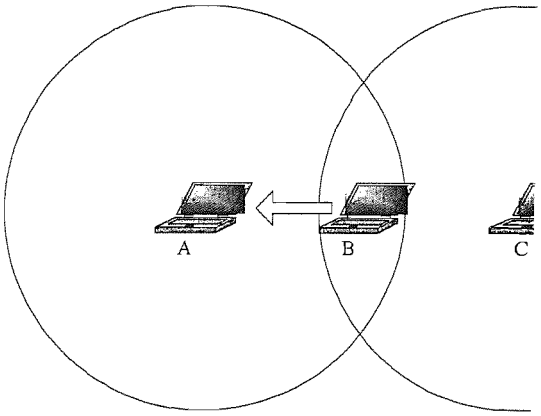

FIGURE 2.7: The exposed node problem.

of each other. Node A is within the transmission range of node B, but out of the range of node C. When node B is transmitting to node A, node C has to defer its transmission to node D even though this transmission would not interfere with the reception of node A, since node C is within the transmission range of node B and senses that the channel is used by node B.

According to the specific design aims, MAC protocols may be categorized into seven groups [104], which are highlighted below with reference to Figure 2.8.

- *Handshaking Signaling Approach* [104] — The handshake protocols employ Request To Send (RTS), Clear To Send (CTS) and Acknowledgement (ACK) frames for managing the flow of long data transmission sessions for the sake of reducing the impact of hidden nodes. These techniques include CSMA/CA^3 [26], Multiple Access with Collision Avoidance (MACA) [105], Floor Acquisition Multiple Access (FAMA) [106], MACA for Wireless LANs (MACAW) [107], Common-Transmitter-based MACA (MACA-CT) [108], Receiver-Transmitter-based MACA (MACA-RT) [108] and Receiver Intiated Channel Hopping with Dual Polling (RICH-DP) [109].

- *Common Control Channel Signaling Approach* [104] — Unlike in the traditional CSMA/CA technique and its derivatives, a dedicated control channel is used in this approach, which facilitates a substantial increase of simultaneous data transmissions, since the channel holding time of the control traffic is very short. A specific example of such a protocol is the Busy Tone Multiple Access (BTMA) [110] scheme, which transmits the busy tone signal in a dedicated signalling channel.

CSMA/CA	*Carrier Sense Multiple Access with Collision Avoidance* CSMA/CA is a modification of pure CSMA[2]. In CSMA/CA, a node broadcast its intent to transmit before any actual transmission, and it transmits information if there is no intent collision happened [26].
MACA	*Multiple Access with Collision Avoidance* MACA does not use carrier sensing. There is no ACK in MACA, and a three-way communications regime adopting the RTS-CTS-data modes is adopted. It is assumed that the MAC layer's frame loss is handled by the higher layer protocols, requesting retransmissions [105].
FAMA	*Floor Acquisition Multiple Access* FAMA also employs RTS-CTS-data handshake signalling. However, in FAMA a source is capable of multiple frame transmission by setting a specific flag in its data header if it has more data frames to send, rather than invoking the RTS/CTS mechanism for each individual frame [106].
MACAW	*MACA for Wireless LANs* In MACAW before a data frame is transmitted, a *data sending* (DS) control frame containing the duration of data and ACK frames is sent by the source node to notify the other nodes in its range not to transmit. A RTS-CTS-DS-data-ACK handshake signalling is adopted in MACAW [107].
MACA-CT	*Common-Transmitter-based MACA* MACA-CT is a multi-channel CSMA applied to direct-sequence spread-spectrum systems. In MACA-CT, each node uses a shared control channel for initiating its transmission and then turns to a dedicated data channel for data transmission [108].
MACA-RT	*Receiver-Transmitter-based MACA* MACA-RT is another multi-channel CSMA applied to direct-sequence spread-spectrum ad hoc networks, where each node has two spreading nodes, namely a code for transmitting and another for receiving [108].
RICH-DP	*Receiver Intiated Channel Hopping with Dual Polling* RICH-DP is a multi-channel CSMA technique applied to frequency-hopping spread-spectrum ad hoc networks. RICH-DP does not require carrier sensing or the assignment of unique transmit/receive spreading codes to nodes. Instead, all nodes employ a shared frequency-hopping sequence [109].

TABLE 2.6: MAC protocols using the handshaking signaling approach.

- *Adaptive Transmission Range/Power Control Approach* [104] — The employment of a high transmit power may increase the likelihood of reaching the destination node in a single hop or within a reduced number of hops. However, this might also increase the interference imposed on other nodes and may result in creating more exposed nodes. A particular example of the family of these protocols is Power Controlled Multiple Access (PCMA) [111], where the nodes transmit data at the power level suggested by the receiver superimposed on the dedicated signalling channel's busy tone.

- *Directional/Adaptive Antennas Approach* [104] — The employment of directional antennae may alleviate the impact of the hidden node problem to some extent compared to omnidirectional antennas [112]. Traditional protocols designed for supporting omnidirectional antennae, namely CSMA/CA and its derivatives for example, can also be applied in a directional MAC protocol based on each antenna.

- *Fairness-Based Approach* [104] — A fair MAC protocol ensures fair competition for the wireless channel bandwidth among nodes. In the heterogeneous networks supporting different service levels, resource allocation is usually based on the *weight* of each node. There are three specific fairness-based approaches. Utility-based approaches [113] attempt to maximize the total *utility*, which is determined by the specific design objective. Link-state [8] (i.e. network topology) dependent approaches [114] attempt to achieve fairness with the aid of intelligent transmit scheduling based on the channel-quality information estimated. Back-off-based approaches [115] achieve fairness by decreasing the variance among the back-off[12] values of different nodes.

- *Energy-Efficiency-Based Approach* [104] — Power consumption is one of the main concerns in the MAC design and the efficient energy usage has the potential of increasing the battery recharge period of the network. A number of energy-efficient MAC design approaches are capable of adjusting the transmit power level [111, 116, 117], hibernating when the node neither transmits nor receives [15, 118, 119], or of activating batch transmissions of a number of packets without extra control signalling [15, 120], etc.

- *Multimedia/QoS Based Approach* [104] — Ad hoc networks are expected to support heterogeneous services, while satisfying different QoS requirements, such as

[12]Back-off is a mechanism which ensures that a node retransmits its packets after some time, when it detects collision or the channel is busy. This is implemented by a back-off timer counting down from a random or deterministic value.

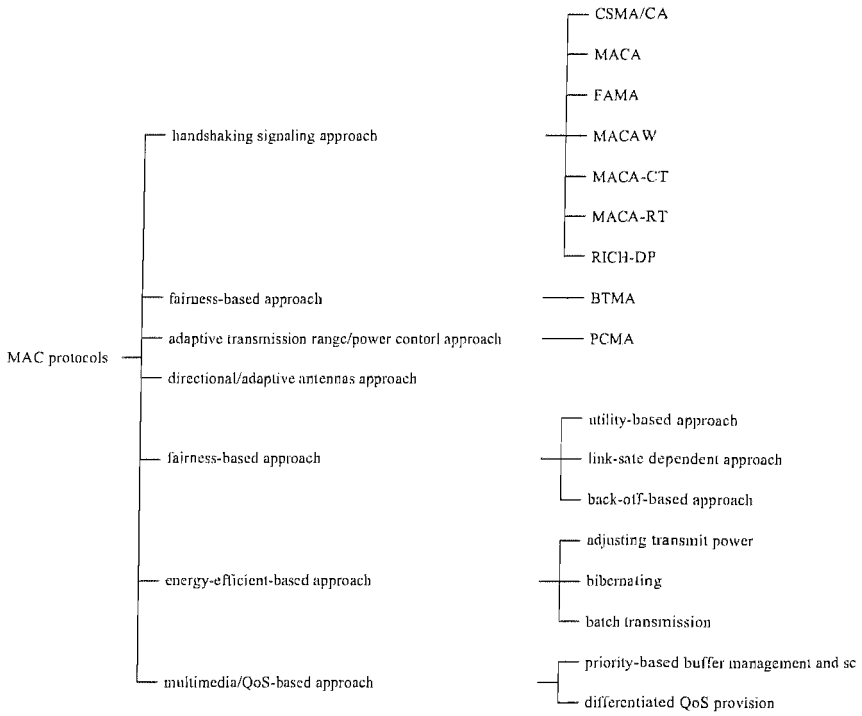

FIGURE 2.8: MAC protocols categorized according to the specific design aims.

maintaining the requested throughput, the maximum tolerable delay, the highest affordable packet loss rate, etc., which should be taken into account during the MAC design. A few different mechanisms adopted for supporting multimedia traffic are priority-based buffer management and scheduling [121] as well as differentiated QoS provision instead of guaranteed QoS [122–125].

2.3.5 Security

Owing to their inherently open and shared broadcast radio channels, ad hoc networks are more vulnerable against security attacks, such as passive eavesdropping, denial of service, flow disruption, resource depletion, data integrity, stolen device, etc [4]. Security in ad hoc networks is expected to support availability, provide confidentiality, integrity, authentication and nonrepudiation [126].

The security issue in ad hoc networks pervades all layers of the protocol stack, although the network-layer security and the link-layer security are of main concern in the open literature.

Ariadne	Ariadne is a secure extension of DSR that prevents attacker or compromised nodes from tempering with uncompromised route consisting of uncompromised nodes and also prevents a large number of types of denial-of-service attacks [128].
hop count hash chains	A hop count hash chain is devised so that an intermediate node cannot decrease the hop count in a routing update, hence provides authentication for the lower bound of the hop count [129, 130].
hash tree chains	A hash tree train is proposed to ensure a monotonically increasing hop count as the routing update traverses the network [131].
SLSP	*Secure Link State routing Protocols* SLSP adopts a digital signature approach in authentication for verifying a message's veracity and various rate control mechanisms for protecting denial-of-service attacks [132].
ARAN	*Authenticated Routing for Ad-hoc Networks* ARAN uses a preliminary certification process followed by a route instantiation that ensures end-to-end authentication. In ARAN the routing messages are authenticated at each hop from source to destination as well as on the reverse path [133].

TABLE 2.7: Security solutions in the network layer.

Security solutions found in the network layer aim for guaranteeing successful routing and forwarding even in the presence of attacks. Accordingly, existing solutions may be categorized into two group: secure ad hoc routing protocols and secure packet forwarding protocols [127]. The former includes techniques such as Ariadne [128], hop count hash chains [129, 130], hash tree chains [131], the Secure Link State routing Protocols (SLSP) [132], Authenticated Routing for Ad-hoc Networks (ARAN) [133], etc. The latter typically consists of detecting malicious nodes and then triggering certain actions to protect the network from future attacks launched by this node [134–136].

The most prevalent security solutions in the link layer are those integrated into the IEEE 802.11 and Bluetooth standards [4]. The first security scheme used in the family of IEEE 802.11 standards is Wired Equivalent Privacy (WEP), which aims for preventing eavesdropping and unauthorized access based on cryptography. Unfortunately, WEP is prone to message privacy and message integrity attacks as well as to probabilistic cipher key recovery attacks [127]. The cryptographic security mechanisms in the link layer of the Bluetooth specifications implement key management, authentication and confidentiality services [137]. Moreover, the Bluetooth security architecture suffers from the weaknesses of the initialization key-generation process.

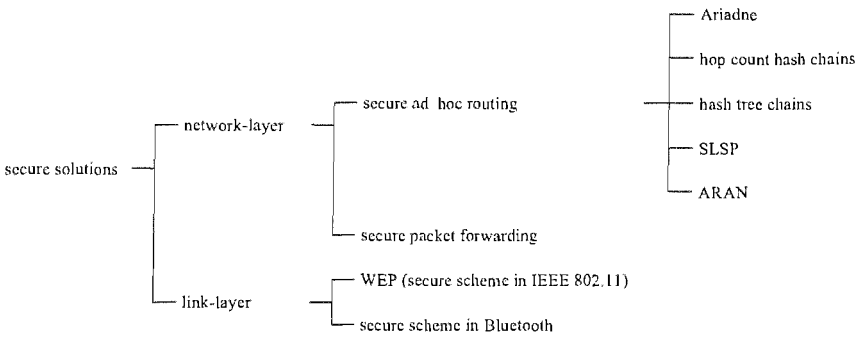

FIGURE 2.9: Security solutions in the network layer-and the link-layer.

In a managed environment, where there is a common, trusted authority guaranteeing the correct operation of the ad hoc network, authentication is sufficient for the provision of the critical network functions. However, a managed environment only exists in a few special cases, such as military networks and corporate networks. When there is no such authority, conventional authentication and access control cannot solve the *selfishness* problem, where a selfish node may purposely refuse to relay packets for others for the sake of extending its battery life for its own use. Even a small fraction of selfish nodes would severely degrade the achievable network performance. Recently a number of research efforts aimed for stimulating node cooperation in ad hoc networks, which may be categorized into two groups [137], namely the so-called currency-based[13] [138] and local monitoring-based[14] [139–142] techniques.

2.3.6 Quality of Service

Quality-of-Service (QoS) is defined as "a set of service requirements to be met by the network, while transporting a flow" [143], and is typically measured by the achievable bit-rate, delay, jitter, packet loss and so on. Due to the distributed and mobile nature of ad hoc networks, most existing QoS solutions provided for the Internet may not be directly applied to ad hoc networks.

Generally speaking, maintaining a certain QoS is also a multi-layer task, which requires the cooperation between QoS models, QoS routing, QoS signaling and QoS MAC protocols [144].

[13]A currency-based scheme introduces a virtual money and mechanisms for charging service usage and rewarding service provision, which encourages the nodes to provide services for other nodes and to moderately use the network resource.

[14]In the local monitoring-based scheme each node monitors its local neighbours and evaluates their behaviors. This scheme gradually isolates selfish nodes from the network.

CEDAR (Core-Extraction Distributed Ad hoc Routing)
CEDAR dynamically establishes the core of the network, which is a subset of the nodes in the network and then incrementally propagates the link state of stable high bandwidth links to the nodes of the core [148].
Ticket-Based Probing
The ticket-based probing is a multipath distributed routing scheme, where a *ticket* represents the permission to search a path. The source node sends a routing message, referred to as a *probe*, carrying one or more tickets to the destination. The ticket-based probing scheme utilizes tickets to limit the number of paths searched during route discovery rather than broadcasting [149].
Bandwidth-Based Routing
In the bandwidth-based routing protocol the source is informed of the bandwidth and of the QoS available to any destination in the mobile network. This knowledge enables the establishment of QoS connections within the mobile network and manages the efficient support of real-time applications [150].

TABLE 2.8: QoS routing protocols.

- *QoS Models* [145] — A QoS model defines the methodology and architecture invoked for implementing a certain type of services. The first attempt in QoS modeling is relies on the Flexible QoS Model designed for MANETs (FQMM) [145] based on two well-known QoS models devised for the Internet, namely the Integrated Services (IntServ)[15] [146] and Differentiated Services (DiffServ)[16] [147]. FQMM features dynamic node roles, hybrid provisioning of InServ-based per-flow and DiffServ-based per-class granularities, as well as adaptive traffic conditioning.

- *QoS routing* [148–150] — QoS routing finds appropriate routes for the diverse traffic flows in order to meet their specific QoS requirements on the basis of an incomplete knowledge of all the resources in the network. However, maintaining a certain QoS is still guaranteed even some of the resources have been reserved owing to the frequent changes of the network topology caused by node mobility. A few examples of QoS routing algorithms include Core-Extraction Distributed Ad hoc Routing (CEDAR) [148], ticket-based probing [149], bandwidth-based routing [150], etc.

- *QoS Signaling* [151, 152] — QoS signaling is responsible for both reserving and releasing the network resources, as well as setting up, maintaining and removing connections along the route determined by the routing protocols used. The

[15]IntServ specifies a fine-grained QoS support system, where each application flow requiring some QoS guarantees has to make an individual reservation.

[16]DiffServ specifies a relatively coarse-grained QoS support system, which deals with classes of flows rather than with single flows.

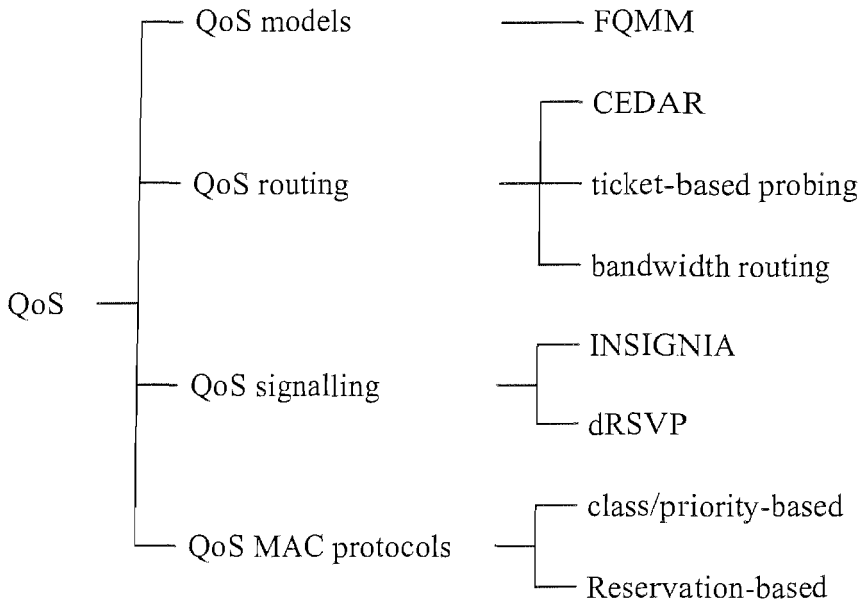

FIGURE 2.10: QoS solutions in ad hoc networks.

conventional Resource ReSerVation Protocol (RSVP) [153] designed for the Internet cannot be applied in ad hoc networks due to the high associated signaling overheads imposed by node mobility, hence new signaling algorithms are required. Two important efforts in signaling protocols designed for ad hoc networks are the so-called INSIGNIA[17] [151] and dynamic RSVP (dRSVP)[18] [152] techniques.

- *QoS MAC protocols* [154–156] — While solving the well-known hidden node problem portrayed in Figure 2.6, a QoS MAC protocol is expected to support real-time traffic, while satisfying the required QoS requirements in ad hoc networks. The existing numerous QoS-based MAC protocols may be categorized into two groups: class/priority-based [154, 155] and reservation-based [156]. The former family provides differentiated services by classifying them into several categories, mostly using backoff algorithms. The latter category reserves resources for real-time flows for the sake of maintaining the required end-to-end QoS in ad hoc networks.

[17]INSIGNIA utilizes in-band signaling, which prevents QoS-related control packets from having to compete with the data packets for access to the channel and can potentially facilitate rapid restoration of QoS requirements along a new path during topology changes.

[18]In dRSVP, an application states its QoS requirements by specifying the minimum and maximum level of acceptable service and the network provides service at a point in this range.

2.3.7 Energy Efficiency

In traditional cellular networks mobile users operate independently and communicate with each other via base stations. There is no battery-power-related energy limitation for base stations. By contrast, the nodes in ad hoc networks cooperate with each other and most of them are small, battery-powered devices. Hence energy efficient communications is one of the critical issues in an ad hoc network. Typically two energy-related metrics are used, namely *the energy consumed per packet* and *the network lifetime* [157], rather than the most commonly used shortest path metric between the source-destination pair, as in DSR[19], DSDV[19], TORA[19], WRP[19], etc [158]. Networks using the former metric attempt to find the optimal path, which minimizes the total energy consumption as a packet is sent from the source to the destination. However, in a routing protocol using this metric, a node may exhaust its own energy source because of the excessive number of forwarding operations carried out on behalf of other nodes. Therefore, it is necessary for routing protocols to take into account the total achievable network lifetime.

Current research aiming for optimizing the above two metrics, i.e. for minimizing a node's power consumption both when it actively sends and receives packets as well as when it is in dormant mode [157]. Both the transmission power control approach and the load distribution approach attempt to minimize the energy used for active communication, while the power-save approach attempts to minimize the energy consumed in the dormant mode.

- *Transmission Power Control Approach* [159–161] — If a node's transmission power is controllable, the higher its transmit power, the larger its direct communication range as well as the higher the number of its immediate neighbours. Hence increasing the transmit power may reduce the number of hops from the source to the destination. The Flow Augmentation Routing (FAR)[20] [159] protocol, the Online MaxMin Routing (OMM)[21] [160] protocol and the Power aware Localized Routing (PLR)[22] [161] protocol fall into this category.

[19] Please refer to Table 2.3.

[20] The FAR protocol assumes a static network and the data-generation rate is known. It attempts to find the optimal routing path for a given source-destination pair that minimizes the sum of link costs along the path.

[21] The OMM protocol attempts to minimize power consumption and maximize the network lifetime at the same time without knowing the data-generation rate.

[22] The PLR protocol assumes that a source node has the local information of both its neighbours and of the destination. Based on this information, the PLR routing algorithm attempts to minimize the total power needed to route a message between a source and a destination.

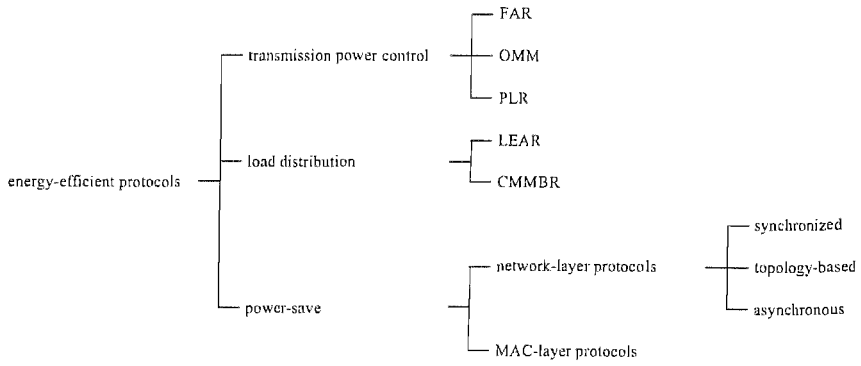

FIGURE 2.11: Energy-efficient protocols in ad hoc networks.

- *Load Distribution Approach* [162, 163] — The load distribution approach attempts to balance the energy consumption among all nodes by selecting a route consisting of energy-rich intermediate nodes rather than the shortest route. This approach does not necessarily provide the lowest-energy route, but avoids overloaded nodes hence extends the network lifetime. The Localized Energy-Aware Routing (LEAR)[23] [162] protocol and the Conditional Max-Min Battery Capacity Routing (CMMBR)[24] [163] protocol fall into this category.

- *Power-Save Approach* [15, 118, 164–166] — At the time of writing most hardware devices are designed to support a number of low-power-consumption modes, which configure one or several subsystems in the idle, sleep or power-down states for the sake of saving energy. Both the network layer and the MAC layer protocols may support power-saving. The former is driven by the real traffic and uses synchronized [15], topology-based [164, 165] or asynchronous [166] strategies to schedule the activation of the power-save modes. By contrast, the latter is driven by the medium access process for the sake of keeping nodes silent, which are not in active transmission mode [118].

[23]LEAR modifies the route discovery procedure in DSR for balancing energy consumption. In LEAR a node determines whether to forward the route-request message or not, depending on its remaining batter power.

[24]In CMMBR, when all nodes in a legitimate route between a source and a destination have sufficient remaining battery capacity, a route with minimum total transmission power among these routes is selected. However, if all routes have nodes with low battery charge, a route which maximizes the minimum remaining energy is selected.

2.3.8 Modeling and Simulation

Investigating an ad hoc network in the context of a test bed is expensive and the results are limited to the specific scenarios related to the test bed, therefore they cannot be repeated by other researchers [167]. Hence modeling and simulation play an important role in the performance evaluation of ad hoc networks, since they are capable of studying the system's behaviour by appropriately varying its parameters.

There are at least two innovative concepts in simulations, which distinguish the ad hoc network model from traditional wired network models, namely the associated mobility and the open wireless medium [167]. Accordingly, there are several high-significance issues, when modeling ad hoc networks:

- *Simulation Area* [167] — This area is a virtual range in which the behaviour of nodes is investigated. The most popular models considered are two-dimensional areas, which may be used for many realistic scenarios. Two-dimensional models may be extended to three-dimensional models, which may be used for nodes roaming inside multi-storey buildings. Occasionally one-dimensional models are also used for scenarios such as highways.

- *Boundary Policy* [168–170] — Usually the simulation area is bounded, which influences how a mobile node behaves, when it reaches the area boundaries when roaming. There are three main boundary handling policies in ad hoc network simulation, namely the bouncing boundary, the leave and replace boundary, and the torus boundary. The first solution assumes that a mobile node is bounced back toward the simulation area, when reaching the boundaries [168–170]. The second solution clones a node somewhere randomly in the simulation area, which obeying a certain geographic distribution, instead of bouncing back a node [168–170]. The last solution is the most useful one in ad hoc networks, which allows the node about to leave to be reflected back and reenter the simulation area from the opposite side at the same speed and direction [168, 170].

- *Propagation Model* [167, 171] — The choice of the appropriate propagation model has been extensively investigated in wireless communications. Just to mention a few, the following factors could be considered in wireless propagation modeling [171]: pathloss, fading, reflection, refraction, scattering, diffraction, and so on. An alternative choice to the employment of various power laws for modeling the pathloss is to use receiver and carrier-sense thresholds for defining the coverage,

detection and interference areas [167]. The coverage or transmission area refers to the area, where the transmitted signal can be correctly detected and decoded. The detection area denotes the area, where the transmitted signal can be detected by a carrier sensing mechanism without being necessarily decoded. The interference area denotes the area in which the transmitted signal interferes with other transmissions without being decoded or detected.

- *Mobility Model* [167] — The presence of mobility is one of the main features of an ad hoc network, which distinguishes it from traditional cellular networks and from the Internet. Currently there are two types of mobility models adopted in ad hoc networks [170], namely motion traces and synthetic models. Motion traces [168, 170, 172–174] are more accurate and realistic, but require large log files for monitoring the associated node mobility and behavior. Synthetic models [168–170, 175–180] are more prevalent and they realistically describe mobility without traces. A few examples of synthetic models are the random walk mobility model [168, 170], the restricted random model [170], the smooth random mobility model [168, 169], the random waypoint model [175–177], the random direction model [170, 178], the boundless simulation model [170], the Gauss-Markov mobility model [170], the mobility vector model [174], the city section mobility model [170], the graph-base mobility model [173], the random (Manhattan) drunk mobility model [168], and a number of group mobility models [170, 179, 180].

Table 2.9: Synthetic models.

Random Walk Mobility Model
The random walk mobility model is sometimes referred to as "Brownian motion" alluding to the random motion of electrons. In this model, a node moves from its current location to a new location by randomly choosing both a direction and a speed for its roaming [168, 170].
Restricted Random Model
The restricted random model usually introduces a bias between the current state and the next state of a node, e.g. the next value of the speed or the direction is randomly selected from a limited range based on the current value of the speed or the direction, respectively [170].
Smooth Random Mobility Model

In the smooth random mobility model, nodes are categorized into several types, e.g. pedestrian and vehicular, each with a set of characteristic movement parameters, which are tunable and correlated. Hence this model avoids sudden and unrealistic speed as well as direction changes which are often criticized in the random walk mobility model and in the restricted random model [168, 169].

Random Waypoint Model

The random waypoint model introduces a pause interval following a motion interval for each node. In the motion interval, a node behaves as that in the random walk mobility model. The length of the pause time is uniformly distributed in a given range [175–177].

Random Direction Model

The random direction model is a small variant of the random waypoint model and is designed for obtaining a uniform number of neighbours for each node [170, 178].

Boundless Simulation Model

The boundless simulation model is a vector-based implementation of the restricted random mobility model instead of imposing individual restrictions on the speed and direction of motion [170].

Gauss-Markov mobility model

The Gauss-Markov mobility model introduces a tuning parameter for varying the degree of randomness as well as for the auto-correlation of the speed and direction in a random mobility model [170].

Mobility Vector Model

The mobility vector model uses a base vector, a deviation vector and an acceleration factor for defining the mobility of a node. The base vector denotes the major speed and direction, while the deviation vector denotes the mobility deviation from the base vector [174].

City Section Mobility Model

The city section mobility model combines the random waypoint model and Manhattan-like scenarios. Each node selects a destination, then follows the most linear route towards its destination [170].

Graph-Base Mobility Model

In the graph-based mobility model each node moves along the edges of a graph, defining the infrastructure of the simulation area. The target destination is a randomly selected vertex in the graph [173].

Random (Manhattan) Drunk Mobility Model

The random drunk mobility model is similar to the city section mobility model, but does not define a target point. Instead, once a node reaches a new street crossing, it selects one of the available directions according to a given probability [168].

Group Mobility Models

In the group mobility models, each node decides its movement depending on other nodes in its group. How nodes are grouped may be related to position, speed (e.g. pedestrian, car, bicycle) or scenario (e.g. highway lane) [170, 179, 180].

- *Traffic Workload* [181–183] — Characterizing the network's teletraffic has been studied for years in telecommunication networks and for the Internet. Numerous different techniques may be applied in ad hoc networks. Usually the full load scenario is considered for evaluating the scalability and stability of the system, which investigates the worst-case scenario. In underloaded scenarios the Constant Bit Rate (CBR) [181, 182] and Variable Bit Rate (VBR) [182, 183] traffic models are commonly used.

Most simulations of ad hoc networks are implemented on asynchronous discrete-event network simulators, such as *ns*-2 (Network Simulator version 2) [184] and OPNET (OPtimized Network Engineering Tool) [185]. Every event implies the possible transition of the system's state and these events are identified by a unique timestamp. The family of discrete event simulation techniques may be categorized [167] into sequential and parallel approaches.

- *Sequential Simulation* — OPNET, *ns*-2 and OMNeT++ (Objective Modular Network Testbed in C++) [186] fall into this category and are most prevalent in both the academic and industrial communities. They implement the discrete events sequentially, which requires large-scale simulations.
- *Parallel and Distributed Simulation* — In order to reduce the above-mentioned excessive simulation time of sequential models, several parallel discrete-event techniques have been proposed, where synchronization becomes paramount for the sake of preventing dependent events from being executed in an incorrect order. A parallel simulator consists of a set of logic processes, which interact by event messages, each carrying an event and its timestamp. Naturally the results obtained from parallel simulations should be the same as those acquiring from sequential simulations. These techniques either conservatively avoid scheduling conflicts between dependent events by using a blocking mechanism, or optimistically detect

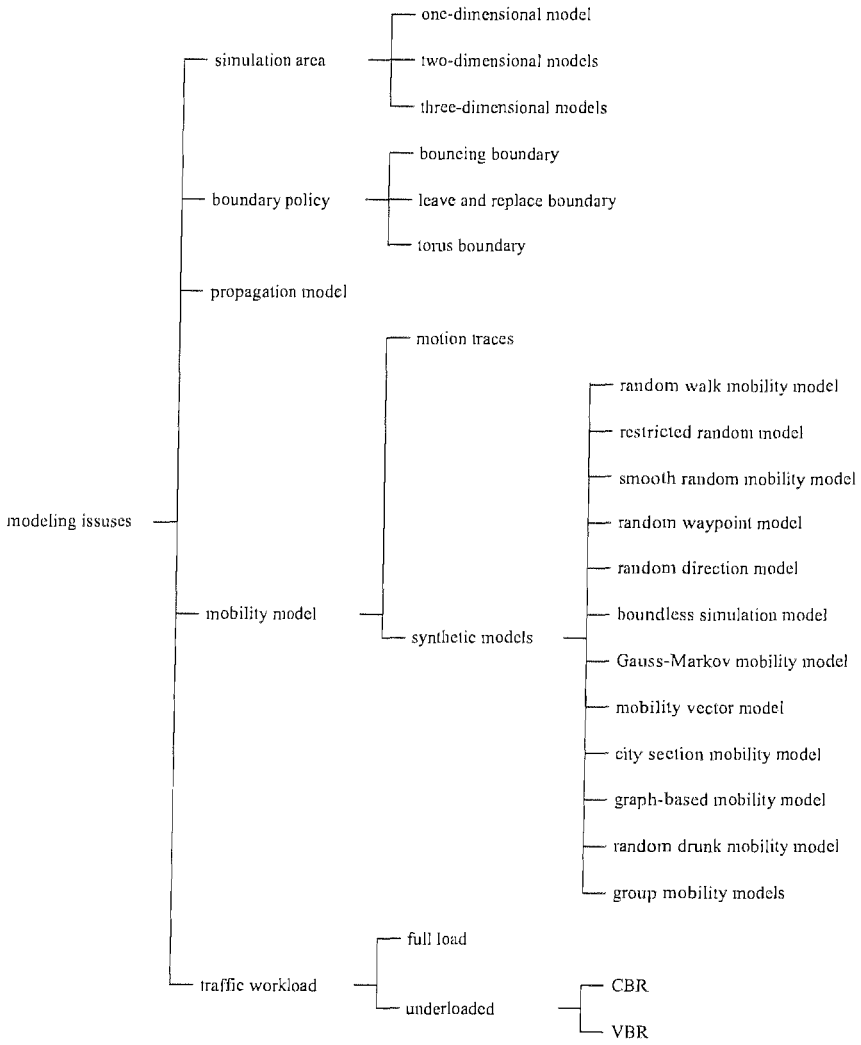

FIGURE 2.12: Modeling issues in ad hoc networks.

and recover synchronization errors by using a roolback mechanism. In the conservative simulations, each logic process executes an event only if it is certain that it will not receive an earlier event from other logic processes, otherwise it is blocked. In the optimistic simulations, each logic process greedily executes events in timestamp order until no event messages remain or until an earlier event message arrives. Upon receiving an earlier event message, the simulator restores the latest valid state and cancels all operations after this valid state, which is called rollback. A few examples of parallel simulators are the Parallel and Distributed *ns* (PDNS) [187], the Wireless Propagation and Protocol Testbed (Wippet) [188], the Global Mobile Information System Simulator (GloMoSim) [189], etc.

However, the simulation results of the above tools may not be always consistent with

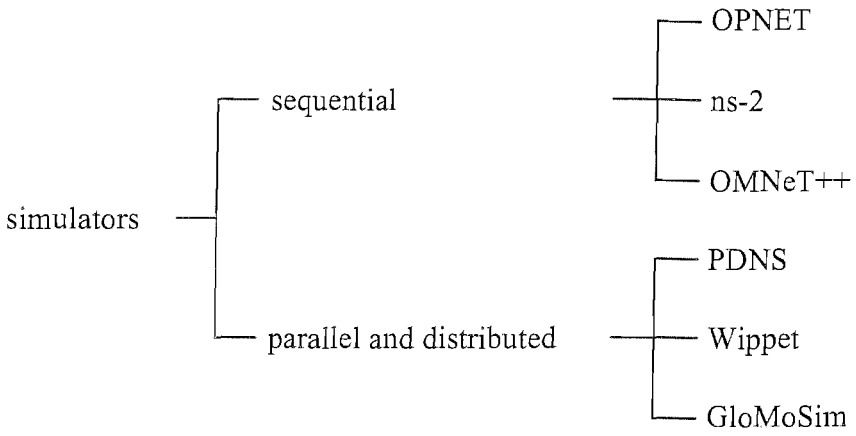

FIGURE 2.13: Simulators in ad hoc networks.

each other, typically owing to the employment of different modeling techniques and simplifying assumptions. Significant disparities between OPNET, *ns*-2 and GloMoSim have been revealed in both quantitative and qualitative terms in the literature [190].

2.4 Conclusion

In this chapter, we have provided a brief overview of the family of ad hoc networks, covering their basic concepts, evolution, standard activities and design challenges. Although they have a 30-year history, they are still in their infancy. Undoubtedly, their importance has been recognized by both the academic and industrial communities, as evidenced by the intensifying research and standardization activities in this area. They may also be expected to be amalgamated with the existing cellular network, which raises a further range of exciting research challenges.

Chapter 3

Rate Adaptation on the Throughput of Random Ad Hoc Networks

3.1 Introduction

An *ad hoc* network consists of a number of mobile nodes, which may communicate directly with each other over wireless links, but the *ad hoc* network has no base station infrastructure. One of the most fundamental characteristics of *ad hoc* networks is their *achievable capacity*, especially their *scalability*, i.e. how the achievable capacity scales as a function of the network size quantified in terms of the number of nodes in an *ad hoc* network.

More specifically, in their landmark paper [43] Gupta and Kumar studied the achievable capacity of *ad hoc* networks having n nodes, each capable of transmitting at W bits per second. They considered two types of network models, namely so-called *arbitrary networks*, which consist of arbitrarily located nodes generating an arbitrary traffic pattern, and *random networks* supporting randomly located nodes generating a random traffic pattern. Furthermore, Gupta and Kumar considered two types of propagation models [43]. The first one is the so-called *protocol model*, where the transmission of node i is successfully received by node j, provided that there is no other simultaneous transmission in the neighbouring area[1] of node j, as defined in Section 2.3.8. Secondly,

[1]This neighbouring area, also call the guard zone, is specified by the protocol to prevent a neighbouring node from transmitting on the same channel at the same time.

Gupta and Kumar also studied the effects of *physical model*, where the transmission of node i is successfully received by node j, if its Signal-to-Interference-plus-Noise Ratio (SINR) at the input of node j's receiver is not less than a given threshold, as defined in Section 3.2. Their results showed [43] that the achievable per-node throughput scaled according to the function $\Theta(\frac{W}{\sqrt{n}})$[2] for *arbitrary networks* and $\Theta(\frac{W}{\sqrt{n \log n}})$ for *random networks* obeying the *protocol model*. By contrast, it scaled according to the function $\Theta(\frac{W}{n^{\frac{1}{\alpha}}})$[3] for *arbitrary networks* and $\Theta(\frac{W}{\sqrt{n}})$ for *random networks* obeying the *physical model*. All these results implied that the per-node throughput of the network tended to zero, as the number of nodes tended to infinity. For a tangibly interpreted insight into these results, let us consider a source-destination node pair in a given area, where the communicating nodes are distributed. As the network size increases, the number of nodes between the source-destination pair of nodes increases and so does the number of hops required for conveying the traffic between these two nodes, provided that the nodes only communicated with their immediate neighbours, since the more distant nodes were beyond their power-limited transmission range. Hence the network's per-node throughput diminishes, since more of each node's throughput is assigned for forwarding the other nodes' traffic, hence reducing the effective per-node throughput. Furthermore, it was shown in [43] that using multi-channel transmission would not circumvent the problem of having a diminishing per-node throughput experienced in the case of the single-channel transmission. An example of multichannel transmission is constituted by a multiple-antenna aided transceiver , which has the potential of increasing the per-node throughput, but fails to prevent the gradual reduction of the per-node throughput.

However, the results of [43] are not terminally conclusive, since several idealistic simplifying assumptions were stipulated. For example, all the interference was treated as additional noise, although the central limit theorem only becomes valid in the presence of at least eight interfering nodes and in practice this may not be the case. Furthermore, the transmission rate was fixed, no pathloss, no fading and no mobility were considered.

At the time of writing, the exact capacity of wireless networks is unknown even for simple systems, such as the so-called interference channel of [191] portrayed in Figure 3.1 and the simplest possible two-hop relay channel of [191] seen in Figure 3.2. Numerous information-theoretic efforts have been invested in the capacity analysis of *ad hoc* networks [191–194]. Traditionally the *capacity region*, or *rate region*, which is the closure[4]

[2] A function is in $\Theta(f(n))$ if it is not much worse, but also not much better than $f(n)$, i.e. there exist two positive real constants, c_1 and c_2, and a positive integer, n_0, such that $c_1 n \leq \Theta(f(n)) \leq c_2 n$ for $\forall n \geq n_0$ [2].

[3] α is the power decay pathloss exponent.

[4] In linear algebra the closure of a set of vectors is the set of all linear combinations of the vectors [195].

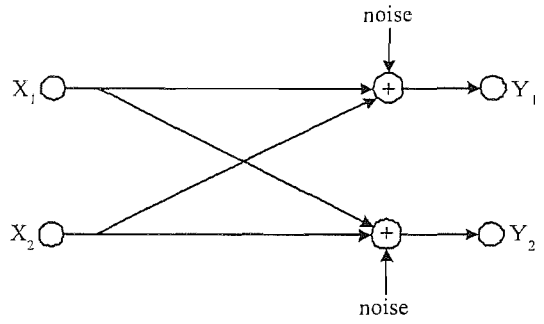

FIGURE 3.1: A simple four-node system having two sources and two destinations, which was termed as the interference channel [191].

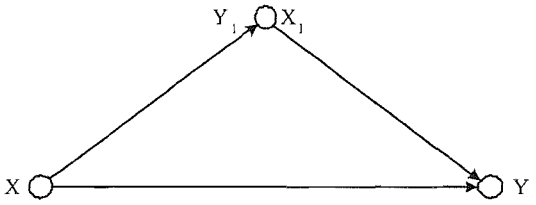

FIGURE 3.2: The simplest possible two-hop relay channel [191].

of all feasible vector rates, has been studied in information theory [43, 191–194]. An information-theoretic proof was given for the specific scenario of large *ad hoc* wireless networks having n randomly selected source-destination node pairs communicating at a fixed common rate, and it was shown [192] that the maximum common rate tended to zero, as the number of users was increased. Recently an important notion, namely that of the *transport capacity* of a network was introduced in [43] for characterising the traffic-carrying capacity of multihop wireless networks. Specially, the transport capacity was defined as the sum of the nodes' maximum achievable throughput weighted by the distances between the source-destination node pairs [43], and it has been investigated in numerous contributions [43, 191, 193, 194]. The rationale of this metric is that distant destinations may require several hops, potentially reserving a high relaying throughput and hence they contribute more substantially towards the transport capacity of the network. The family of wireless networks having an arbitrary size as well as topology and communicating over a general discrete memoryless channel was studied in [193], and its achievable *rate region* was determined. Furthermore, a specific network whose per-node *transport capacity* scaled as $\Theta(1)$[5] was constructed [193]. An information-theoretic model of wireless networks was studied in [191], which took into

[5]In physically tangible terms this implies that the per-node transport capacity remains the same order as the network size increases.

account the distances between nodes as well as the resultant attenuation of radio signals, which included both pathloss and absorption[6]. The results of [191] showed that in a relatively high-attenuation scenario, where absorption exists or the pathloss exponent is higher than 3, which is a realistic situation, the per-node *transport capacity* was bounded by $O(1)$[7], when the nodes were individually power limited. Furthermore, the per-node *transport capacity* order was $\Theta(1)$, when the traffic load was balanced across the network with the aid of multipath routing and the distance between each hop was bounded [191]. Some simple upper bounds of the *transport capacity* of *ad hoc* networks were provided also in [194], which were only dependent on the network topology and on the power constraints of the nodes. The related scaling law[8] results matched those of [43], both in the case of perfect Channel State Information (CSI)[9] and in the case of no CSI at all [194].

Besides information-theoretic approaches of [191–194], some other approaches have been developed for investigating the capacity of *ad hoc* networks [46, 197]. A mathematical framework was defined for studying the *rate region* of wireless *ad hoc* networks in [46]. The authors aimed for calculating the maximum common throughput, which was achieved by all source-destination node pairs in the network, rather than for studying the associated scaling law [46]. A deterministic network structure described by so-called squarelets[10] was proposed in [197] for studying the throughput *scalability*[11] of general networks in conjunction with various random node distributions and traffic patterns. The main results of [43] might be readily confirmed with the aid of the deterministic approach of [197].

Various capacity studies based on simulations, rather than on theoretical analysis have also been performed, for example in [51, 52]. Specifically, the interaction between the 802.11a MAC and *ad hoc* forwarding on the achievable network capacity was evaluated

[6]The transmission medium and obstacles can absorb radio waves as well as reflect them. The energy absorption by molecular resonance in the atmosphere dominates the propagation attenuation at high frequencies. It was characterised by a negative exponential function of the transmission distance in addition to the classic power law decay in [191, 196].

[7]A function is in $O(f(n))$, if it is less than some constant multiple of $f(n)$, i.e. a positive real constant, c, and a positive integer, n_0, exist such that $O(f(n)) \leq cf(n)$ for $\forall n \geq n_0$ [3].

[8]The scaling law in *ad hoc* networks characterizes how the network performance varies, as the number of nodes in the network tends to infinity. In this chapter the network performance is quantified in terms of the achievable per-node throughput.

[9]Perfect CSI means that the complete channel state information is known at both the receivers and transmitters.

[10]In [197] the communication area was assumed to be a square-shaped unit area, which was divided into a number of smaller squares, i.e. squarelets, for the sake of the analysis so that there was at least one node in each squarelet.

[11]Scalability in *ad hoc* networks quantifies whether the network is capable of providing an acceptable level of service, e.g. reasonable throughput or delay, when the number of nodes in the network tends to infinity [17].

in [51]. The results showed that the 802.11a system was capable of approaching the theoretically attainable per-node throughput scaling law of $O(\frac{1}{\sqrt{n}})$ in a large random network carrying random traffic [51]. The per-node throughput capacity of multi-channel multihop *ad hoc* networks based on the 802.11a MAC scheme was quantitatively evaluated in [52].

A variety of techniques may be used for improving the capacity of wireless networks, such as directional antennae [44, 45], power control [46], successive interference cancellation (SIC) [46] and variable-rate transmissions [46]. However, none of these techniques have been found to be capable of changing the scaling law of *ad hoc* networks. The results provided in [46] quantitatively showed that multihop routing, spatial reuse[12], SIC and variable-rate transmissions have the potential of significantly improving the achievable capacity. By contrast, the attainable performance improvement of power control was only significant, when rate adaptation was unavailable [46]. It was shown in [44, 45] that the *scalability* problem might be mitigated by increasing the number of antenna elements and the resultant antenna gain, which is a benefit of having a narrower beamwidth. However, despite its considerable complexity, beamforming does not dramatically change the scaling law due to the limitations of realistic systems [45].

The exploitation of intelligent scheduling in the network also has the potential of improving the attainable capacity by deferring those nodes's transmissions, which impose a high cost in terms of the required transmit power or the number of hops until the time instant, when it imposes a low cost [46–48]. The variation of communication channels caused by both the radio propagation phenomena [46, 198] and the node mobility [47, 48, 199] was exploited for the sake of increasing the achievable network capacity, provided that the potentially real-time source information of the nodes was capable of tolerating the associated delays, when the network was allowed to schedule the transmission of packets during favourable fading or mobility conditions [46]. Moreover, the fundamental scaling law was found to remain the same as that in [43] even when taking into account the effects of both pathloss and fading [198]. When absorption existed or the pathloss exponent was higher than 3, the per-node *transport capacity* was upper bounded by $O(1)$ even in the best-case scenario, where the CSI was perfectly known to both the receivers and transmitters. By contrast, in the worst-case scenario, where there is no CSI at all, the per-node transport capacity scaled as $\Theta(1)$. On the other hand, mobility was found to be capable of increasing the per-node throughput to $\Theta(1)$ with the aid of a two-hop

[12]Spatial reuse implies that more than one nodes are allowed to transmit in the same bandwidth and time slot.

strategy, even when the number of communicating nodes n was high, provided that the transmission delay was not taken into account [47]. However, the expected delay per packet imposed by the above strategy might be proportional to $\Theta(\log n)$ [48], which suggested that mobile *ad hoc* networks constituted by many nodes may not be scalable[13] in real-time applications. The exact capacity and the exact end-to-end delay of mobile *ad hoc* networks were quantified in [199]. The associated results showed that multiple-path transmission was capable of reducing the end-to-end delay, but was unable to improve the attainable capacity.

The capacity of an *ad hoc* network may also be improved by additional infrastructure support [49, 50, 200], such as that provided by base stations and access points, in the context of a hybrid wireless network. The results of [49, 50] showed that the per-node throughput of *ad hoc* networks was improved by the infrastructure support provided by both regularly allocated base stations [49] and randomly distributed access points [50]. More explicitly, the *scalability* of a hybrid *ad hoc* network was investigated in [200], where both the *ad hoc* nodes as well as their traffic patterns were randomly distributed, and additionally, the support infrastructure nodes were connected via high-capacity links. The system exhibited three different scaling regimes, depending on the relative increase of the number of infrastructure nodes, m, and the number of *ad hoc* nodes, n, in the hybrid network. The per-node throughput remained proportional to $\Theta\left(\frac{1}{\sqrt{n \log n}}\right)$, when m scaled according to a function, which increased more slowly than $\Theta\left(\sqrt{\frac{n}{\log n}}\right)$. These findings implied that the employment of infrastructure nodes might improve the capacity, but remains incapable of changing its scaling law. When m scales according to a function increasing between $\Theta\left(\sqrt{\frac{n}{\log n}}\right)$ and $\Theta\left(\frac{n}{\log n}\right)$, the per-node throughput scaled as a function of $\Theta(\frac{m}{n})$, which implied that the beneficial presence of base-station infrastructure was indeed capable of improving the scaling law. Finally, the per-node throughput scaled as a function of $\Theta\left(\frac{1}{\log n}\right)$, when the number of base-stations m scaled according to a function increasing faster than $\Theta\left(\frac{n}{\log n}\right)$, which implied that employing more infrastructure nodes would fail to further improve the throughput *scalability* of the system.

In most of the above-mentioned literature, a *fixed transmission rate* associated with a time-invariant modulation scheme was assumed [43–45, 47, 49, 50]. In practice, variable-rate transmissions [201, 202] using for example variable spreading factors, variable coding rates, variable modulation constellation sizes, etc., hold the promise of significantly

[13]A network is often referred to be scalable if it can provide acceptable service, e.g. reasonable throughput or delay, even when the network size tends to infinity.

improving the achievable throughput. Adaptive transceivers have now become part of the High Speed Downlink Packet Access (HSDPA) mode of the third generation systems [202] and hence they may be expected to find their way also into both pure *ad hoc* networks and hybrid networks. The implementation of such adaptive transceivers is discussed in [201], while the corresponding adaptive transceiver based cellular rather than *ad hoc* network aspects can be found in [202, 203]. As a further advance, a rigorous mathematical framework was proposed for numerically characterizing the effects of *rate adaptation* in [46], stating that the associated computational complexity of scheduling would increase exponentially, as the number of nodes increased.

Against this background, the new contribution of this chapter is that two formulas are provided for characterizing the benefits of rate adaptation on the achievable per-node throughput of random ad hoc networks both in the absence and in the presence of shadow fading. In Section 3.2, the system model of wireless *ad hoc* networks is introduced. In Section 3.3, the achievable throughput improvements of perfect *rate adaptation* are estimated without taking into account the effects of fading. To expound further, in Section 3.4 the effect of perfect *rate adaptation* under shadowing is analyzed. Examples of Adaptive Quadrature Amplitude Modulation (AQAM) simulations are provided in Section 3.5. Finally, Section 3.6 provides our conclusions.

3.2 System Model

Our model of the *ad hoc* network considered is similar to that used in [43], apart from a few modifications, which include the employment of perfect *rate adaptation* and the effects of a fading channel. In this chapter *perfect rate adaptation* means that both the receiving node and the transmitting node in communication have the perfect knowledge of the channel information, but not the channel information of other nodes. This implies that the transmitter automatically adjusts the transmission rate to match the SINR experienced at the receiver for the sake of approaching the Shannonian channel capacity [46]:

$$c = W \log_2(1 + \gamma), \tag{3.1}$$

where c is the channel capacity achievable with the aid of perfect Channel State Information (CSI), which is known to the receiver only [204][14], W is the channel's bandwidth

[14] In the case of a single transmitter-receiver pair, where perfect CSI is available to both the transmitter and receiver, the transmitter may invoke a variable-power, variable-rate scheme for improving both the achievable channel capacity as well as the resultant effective throughput in comparison to the scenario,

and γ is the SINR at the receiver[15].

Let us consider a random *ad hoc* network supporting n nodes uniformly and independently distributed in a unit area $\mathcal{S}$ [43], which is a planar disk. All nodes share the same bandwidth. No node is capable of simultaneously transmitting and receiving signals. Furthermore, the nodes are incapable of simultaneously transmitting/receiving signals to/from more than one node[16]. All packet-transmissions are slotted into perfectly synchronized time slots [17]. The power of each transmitting node is fixed to P_t Watts, i.e. no transmit power control is used, which is typical in cost-efficient *ad hoc* networks.

Let $\mathcal{N}_t$ be the subset of nodes simultaneously transmitting at some time instant. If node i, $i \notin \mathcal{N}_t$ is receiving signals from node j, $j \in \mathcal{N}_t$, then the Signal-to-Interference-plus-Noise Ratio (SINR) experienced at node i becomes:

$$\gamma_{ji} = \frac{P_t G_{ji}}{\sum_{k \in \mathcal{N}_t, k \neq j} P_t G_{ki} + \eta_i}, \tag{3.2}$$

where γ_{ji} is the SINR at node i experienced by the signal arriving from node j, while G_{ki} is the power gain between nodes k as well as i, and η_i is the background noise encountered at node i. The value of the power gain G_{ji} depends on the propagation model, which will be discussed in Sections 3.3 and 3.4, taking into account the absence of fading or the presence of log-normal shadow fading, respectively. The minimum SINR required for successful reception is β [43].

Every transmitting node assumes perfect knowledge of its link quality and hence we are estimating the achievable throughput upper bound with the advent of perfect adaptive-rate transmission, which is a prerequisite for approaching the Shannon limit [205]. The common reliable transmission range r_n of all nodes is chosen to guarantee the asymptotic

when perfect CSI is known to the receiver only [204]. However, in the case of multiple transmitter-receiver pairs communicating simultaneously, the employment of power control without the knowledge of the other nodes' power may lead to the system's instability. Optimal power control would require a complicated centralized control regime in the network, which is unaffordable for cost-efficient ad hoc networks. Hence we assume the employment of no power control, and therefore the channel capacity remains that achieved with the aid of perfect CSI known to the receiver only.

[15]For simplicity, we treat all interfering signals as noise in this chapter [46].

[16]This assumption implies that there is no multicast, which has the potential of improving the throughput [46].

[17]The design of medium access schemes for ad hoc networks has still numerous open problems. At the time of writing random access seems to be the favorite option [15, 43, 105, 107], where time slots are used for scheduling the transmissions of various nodes. This assumption is introduced for convenience of exposition and can be removed as suggested in [43]

connectivity of random networks [43, 206][18]. Initially the minimum distance between nodes is assumed to be r_{min}, which satisfies $r_{min} < r_n$, although later this assumption will be dropped, letting $r_{min} \to 0$.

3.3 The Effects of Path Loss

In the absence of fading, i.e. when the only propagation phenomenon considered is the pathloss, the signal power is assumed to decay upon increasing the distance r according to $r^{-\alpha}$, yielding:

$$G(r) = r^{-\alpha}, \tag{3.3}$$

where r and $G(r)$ are the distance and the power gain between two nodes, respectively, and α is the pathloss exponent. In general we have $2 \leq \alpha \leq 4$ in a typical pathloss model [207].

Consider node j is transmitting to node i at a distance less than r_n. The received SINR at node i is

$$\gamma_{ji} = \frac{P_t r_{ji}^{-\alpha}}{\sum_{k \in \mathcal{N}_t, k \neq j} P_t r_{ki}^{-\alpha} + \eta_i}. \tag{3.4}$$

Owing to the central limit theorem (CLT), the interference may be assumed to be approximately Gaussian when the number of interfering sources is higher than eight [208]. Thus only the fluctuation of the received signal power is considered. In the model of [43], the guard zone[19] is appropriately selected to guarantee that all nodes' transmissions to other nodes at a distance less than r_n achieve the minimum required SINR β, so that we have:

$$\gamma_{ji} = \beta \left(\frac{r_n}{r_{ji}} \right)^{\alpha}. \tag{3.5}$$

[18] In the protocol model of [43], a common range r_n is employed by all nodes for transmissions, i.e. the transmission is successfully received, when the distance between the transmitting node and the receiving node is less than r_n, provided that there is no other node simultaneously transmitting over the same channel in a neighbouring area. This common range r_n should be sufficiently high for the transmitter to reach its intended receiver, while imposing a low interference on other nodes sharing the same channel. In other words, this common range r_n should ensure that the network is connected with a probability of one as the number of nodes in the network tends to infinity [206]. We simply invoke this assumption for ensuring the network's connectivity.

[19] A guard zone is specified as a transmission exclusion zone imposed for the sake of preventing a neighbouring node from transmitting on a channel already activated within the zone at the same time.

If the transmission rate is fixed, the achievable throughput without rate adaptation, c_g, is also fixed and determined by the lower bound of the SINR, yielding[20]:

$$c_g = W \log_2(1+\beta). \tag{3.6}$$

In Section 3.2 we have assumed that node j is randomly and uniformly distributed in $\mathcal{S}$, which requires a relatively high number of communicating nodes, but may be achieved without any assumption considering the nodes' mobility model. Furthermore, given that r_{ji} is less than the reliable range r_n of transmission, the conditional Probability Density Function (PDF) of the distance r_{ji} and the conditional PDF of the SINR γ_{ji} can be shown to be[21]:

$$f_{r|r<r_n}(r_{ji}) = \frac{2r_{ji}}{r_n^2 - r_{min}^2}, \quad r_{min} < r_{ji} < r_n, \tag{3.7}$$

$$f_{\gamma|r<r_n}(\gamma_{ji}) = \frac{2\left(\frac{\gamma_{ji}}{\beta}\right)^{-\frac{2}{\alpha}-1}}{\alpha\beta\left[1-\left(\frac{r_{min}}{r_n}\right)^2\right]}, \quad \beta < \gamma_{ji} < \beta\left(\frac{r_n}{r_{min}}\right)^{\alpha}. \tag{3.8}$$

If perfect *rate adaptation* is available, the average achievable throughput with rate adaptation, c_a, can be shown to be[22]:

$$\begin{aligned} c_a &= \int_{r_{min}}^{r_n} f_{r|r<r_n}(r_{ji}) W \log_2(1+\gamma_{ji})\, \mathrm{d}r_{ji} \\ &= \int_{r_{min}}^{r_n} \frac{2r_{ji}}{r_n^2 - r_{min}^2} W \log_2\left[1+\beta\left(\frac{r_n}{r_{ji}}\right)^{\alpha}\right] \mathrm{d}r_{ji} \\ &= \frac{2W}{(r_n^2 - r_{min}^2)\ln 2} \int_{r_{min}}^{r_n} r_{ji} \ln\left[1+\beta\left(\frac{r_n}{r_{ji}}\right)^{\alpha}\right] \mathrm{d}r_{ji}. \end{aligned} \tag{3.9}$$

Hence it is possible to estimate the achievable normalized per-node throughput improvement of $c_i = \frac{c_a}{c_g}$ attained with the advent of perfect *rate adaptation* by numerical

[20]Since the minimum required SINR β is still achieved at the distance r_n, the maximum achievable throughput is the channel capacity $W\log_2(1+\beta)$. Although the channel capacity is higher than this value, when the distance is less than r_n, the achievable throughput cannot be improved due to the fixed-rate transmission.

[21]Since the position of node j is randomly and uniformly distributed in $\mathcal{S}$, it is also randomly and uniformly distributed in the circle having its center at node i and its radius of r_n conditioned on the distance r_{ji} is less than r_n. We ignore the edge effect in this chapter, which implies the assumption that this circle is far smaller than $\mathcal{S}$. Therefore, we arrive at Equation 3.7.

[22]With the aid of perfect rate adaptation, the transmitter may adjust the transmission rate for the sake of achieving the channel capacity according to the channel quality variation imposed by the pathloss.

integration:

$$c_i = \frac{2\int_{r_{min}}^{r_n} r_{ji} \ln\left[1+\beta\left(\frac{r_n}{r_{ji}}\right)^{\alpha}\right] \mathrm{d}r_{ji}}{(r_n^2 - r_{min}^2)\ln(1+\beta)}. \tag{3.10}$$

Upon substituting the normalized minimum distance of $u = \frac{r_{min}}{r_n}$ between *ad hoc* nodes as well as the normalized distance $s = \frac{r_{ji}}{r_n}$ into Equation 3.10, we arrive at the following theorem, quantifying the upper bound of the normalized per-node throughput improvement in the absence of fading but in the presence of perfect pathloss knowledge.

Theorem 3.1. *The achievable normalized throughput improvement c_i with the advent of perfect rate adaptation in the absence of fading is given by*

$$c_i = \frac{c_a}{c_g} = \frac{2\int_u^1 s\ln(1+\beta s^{-\alpha})\mathrm{d}s}{(1-u^2)\ln(1+\beta)} \leq \frac{2\int_0^1 s\ln(1+\beta s^{-\alpha})\mathrm{d}s}{\ln(1+\beta)} = c_i^0 < +\infty, \tag{3.11}$$

where the upper bound c_i^0 is the maximum achievable normalized throughput improvement c_i attained when we have $r_{min} = 0$. ■

The proof of Theorem 3.1 is outlined in Appendix A. Note in Theorem 3.1 that the upper bound c_i^0 is a constant that is independent of n, and it is determined purely by the propagation parameters, α and β. The achievable normalized per-node throughput improvement c_i with the aid of perfect rate adaptation in the absence of fading and its upper bound c_i^0 are plotted in Figures 3.3 - 3.6.

More specifically, Figures 3.3 and 3.4 show that the achievable normalized per-node throughput improvement c_i is a decreasing function of the normalized minimum distance $\frac{r_{min}}{r_n}$, as evidenced by the proof of Theorem 3.1. In other words, as the minimum distance between nodes decreases, the achievable normalized per-node throughput improvement increases, because the pathloss-related received signal power improves exponentially upon reducing the normalized minimum distance between nodes, as seen in Equation 3.11. By contrast, in cost-efficient *ad hoc* nodes using no power control *fixed rate transmission* fails to efficiently exploit the increased capacity, when the received signal quality is improved for example by reducing the minimum distance between nodes. The achievable normalized per-node throughput improvement c_i associated with different values of α converges to unity, when we have $r_{min} \to r_n$, since the received signal quality is constant at $r_{min} = r_n$, if we only consider the effects of pathloss, but assume that no shadow fading is experienced.

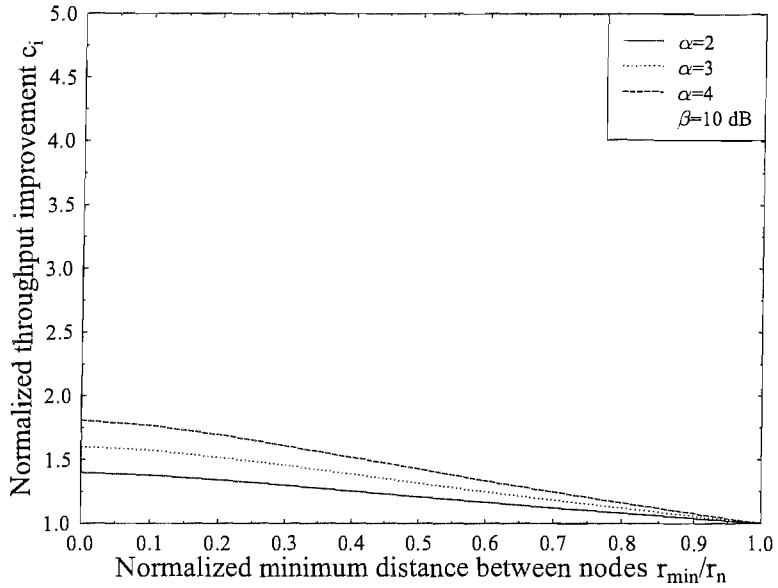

FIGURE 3.3: The normalized per-node throughput improvement c_i versus the normalized minimum distance $\frac{r_{min}}{r_n}$ between nodes plotted for different values of the pathloss exponent α at a target SINR value of $\beta = 10$ dB in the absence of fading, which is evaluated from Equation 3.11. The transmit power is fixed and perfect rate adaptation is assumed.

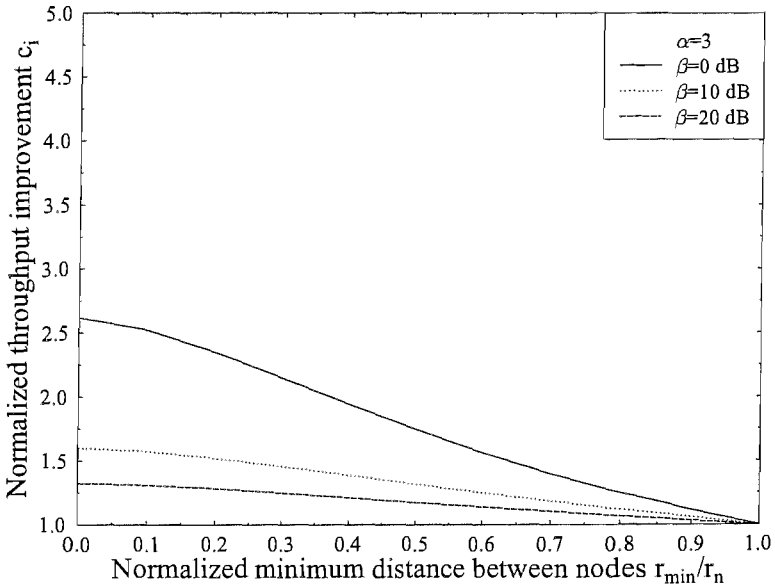

FIGURE 3.4: The normalized per-node throughput improvement c_i versus the normalized minimum distance $\frac{r_{min}}{r_n}$ between nodes plotted for different values of the target SINR β at a pathloss exponent of $\alpha = 3$ in the absence of fading, which is evaluated from Equation 3.11. The transmit power is fixed and perfect rate adaptation is assumed.

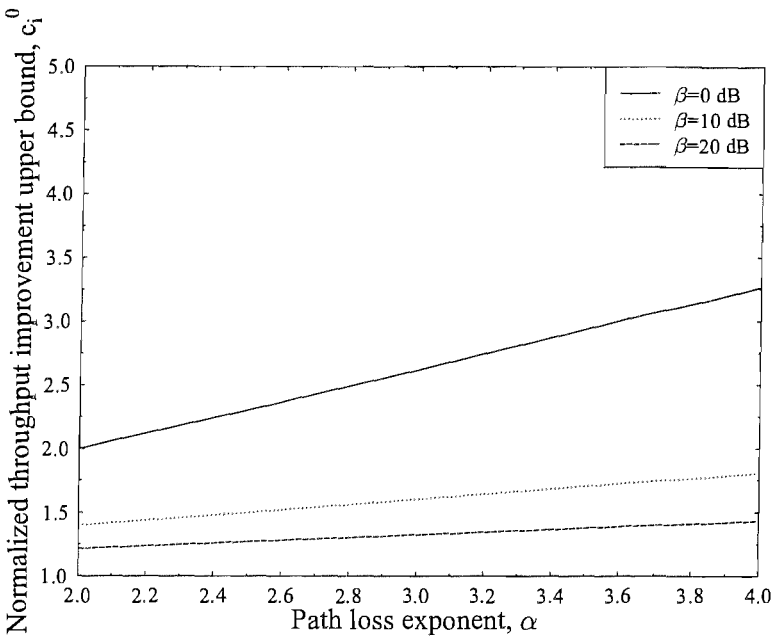

FIGURE 3.5: The normalized per-node throughput improvement upper bound c_i^0 versus the pathloss exponent α plotted for different values of the target SINR β in the absence of fading, which is evaluated from Equation 3.11. The transmit power is fixed and perfect rate adaptation is assumed.

Similar to Figure 3.3, Figure 3.5 also shows that the normalized per-node throughput improvement upper bound c_i^0 increases as a benefit of rate adaptation upon increasing the pathloss exponent from $\alpha = 2$ to $\alpha = 4$. This follows the intuition that *rate adaptation* is capable of improving the throughput more substantially in a higher-attenuation scenario, which is a consequence of the lower efficiency of the *fixed rate transmission* scheme in case of a larger fluctuation range of the received signal quality. As the pathloss exponent α increases, the gap between the received signal quality when $r_{ji} = r_n$ and that when $r_{ji} = r_{min}$ increases, hence the probability of high SINR value increases. While the rate of the *fixed rate transmission* scheme has to be fixed to its worst case value when $r_{ji} = r_n$, perfect *rate adaptation* is capable of compensating for the received signal quality fluctuation, and hence the normalized per-node throughput improvement c_i increases.

Similar to Figure 3.4, Figure 3.6 also shows that the normalized per-node throughput improvement upper bound c_i^0 decreases, as the required SINR β of the receiver increases, for example because a higher-throughput modulation scheme is used. This is because the channel capacity is a logarithmic function of the link SINR, as seen in Equation 3.1. Hence the slope of the channel capacity decreases, as the link SINR increases and so does the normalized per-node throughput improvement.

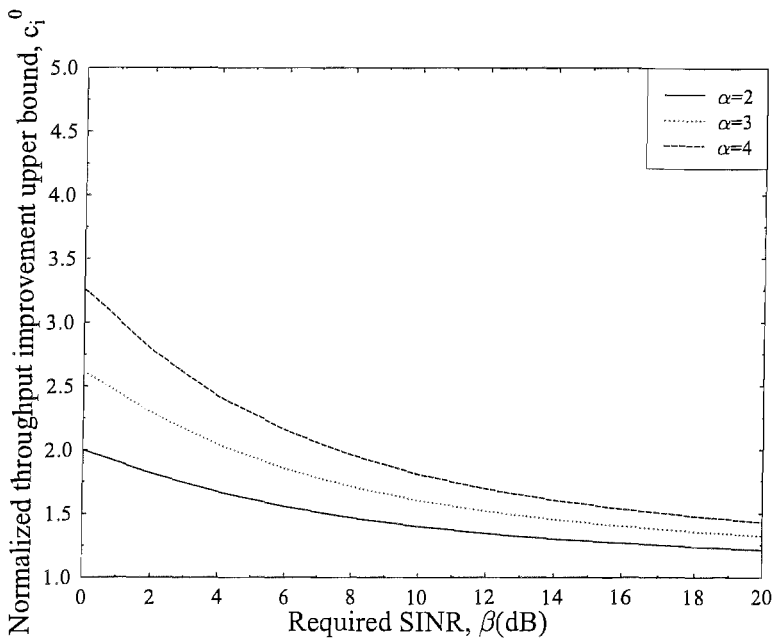

FIGURE 3.6: The normalized per-node throughput improvement upper bound c_i^0 versus the target SINR β plotted for different values of the pathloss exponent α in the absence of fading, which is evaluated from Equation 3.11. The transmit power is fixed and perfect rate adaptation is assumed.

3.4 The Effects of Shadow Fading

If additionally the effects of shadowing are taken into account, the shadow-faded power gain is log-normally distributed with a mean given by Equation 3.3. Then the conditional PDF of the shadow-faded power gain at a certain distance is given by [207]:

$$f_{G|r}(G) = \frac{1}{\sqrt{2\pi}\sigma G} e^{-\frac{(\ln G + \alpha \ln r)^2}{2\sigma^2}}, \tag{3.12}$$

where G and r are the power gain and the distance between two nodes, respectively and σ is the standard deviation of the lognormal shadowing in natural units. In practice the range of σ is $5 \sim 12$ dB and its typical value is 8 dB [207], which corresponds to $1.15 \sim 2.76$ and 1.84, respectively, in terms of natural units.

Owing to the central limit theorem, the interference is approximatively Gaussian distributed [208]. Hence only the fluctuation of the shadow-faded received signal power is considered. The guard zone of the *ad hoc* networks is appropriately selected to guarantee that all nodes' transmissions to other nodes at a distance less than r_n achieve the

minimum required SINR β on average, hence we have:

$$\gamma_{ji} = \beta r_n^{\alpha} G_{ji}, \tag{3.13}$$

where the shadow-faded power gain G_{ji} is log-normally distributed with a mean of $r_{ji}^{-\alpha}$.

Substituting Equation 3.13 into Equation 3.12 and applying the probability transformation formula [209], we have the conditional PDF of γ_{ji} at a given distance r_{ji}:

$$f_{\gamma|r_{ji}}(\gamma_{ji}) = \frac{1}{\sqrt{2\pi}\sigma\gamma_{ji}} e^{-\frac{(\ln\gamma_{ji}+\alpha\ln r_{ji}-\ln\beta-\alpha\ln r_n)^2}{2\sigma^2}}. \tag{3.14}$$

Upon substituting Equation 3.7 into Equation 3.14 and applying the theorem of total probability [209], we arrive at the PDF of γ_{ji} conditioned on $r_{ji} < r_n$:

$$\begin{aligned} f_{\gamma|r_{ji}<r_n}(\gamma_{ji}) &= \int_{r_{min}}^{r_n} f_{r|r<r_n}(r_{ji}) f_{\gamma|r_{ji}}(\gamma_{ji}) \mathrm{d}r_{ji} \\ &= \frac{2}{\sqrt{2\pi}\sigma\gamma_{ji}(r_n^2 - r_{min}^2)} \int_{r_{min}}^{r_n} r_{ji} e^{-\frac{(\ln\gamma_{ji}+\alpha\ln r_{ji}-\ln\beta-\alpha\ln r_n)^2}{2\sigma^2}} \mathrm{d}r_{ji}. \end{aligned} \tag{3.15}$$

Therefore the normalized per-node throughput improvement c_i achieved with the aid of perfect *rate adaptation* may be expressed as follows:

$$c_i = \frac{c_a}{c_g} = \frac{\int_{\beta}^{\infty} f_{\gamma|r<r_n}(\gamma_{ji}) \ln(1+\gamma_{ji}) \mathrm{d}\gamma_{ji}}{\ln(1+\beta) \int_{\beta}^{\infty} f_{\gamma|r<r_n}(\gamma_{ji}) \mathrm{d}\gamma_{ji}}. \tag{3.16}$$

Upon substituting the logarithmic normalized minimum distance of $u = \ln r_{min} - \ln r_n$ between *ad hoc* nodes as well as the logarithmic normalized distance of $s = \ln r_{ji} - \ln r_n$ and the logarithmic normalized SINR of $t = \ln\gamma_{ji} - \ln\beta$ into Equation 3.16, we arrive at the following theorem in the presence of shadow fading.

Theorem 3.2. *The normalized throughput improvement c_i achieved with the advent of perfect rate adaptation in the presence of shadow fading is given by*

$$\begin{aligned} c_i &= \frac{\int_0^{+\infty} \ln(1+\beta e^t)\mathrm{d}t \int_u^0 e^{2s} e^{-\frac{(t+\alpha s)^2}{2\sigma^2}} \mathrm{d}s}{\ln(1+\beta)\int_0^{+\infty} \mathrm{d}t \int_u^0 e^{2s} e^{-\frac{(t+\alpha s)^2}{2\sigma^2}} \mathrm{d}s} \\ &\leq \frac{\int_0^{+\infty} \ln(1+\beta e^t)\mathrm{d}t \int_{-\infty}^0 e^{2s} e^{-\frac{(t+\alpha s)^2}{2\sigma^2}} \mathrm{d}s}{\ln(1+\beta)\int_0^{+\infty} \mathrm{d}t \int_{-\infty}^0 e^{2s} e^{-\frac{(t+\alpha s)^2}{2\sigma^2}} \mathrm{d}s} \\ &= c_i^0 < +\infty, \end{aligned} \tag{3.17}$$

where the upper bound c_i^0 is the maximum achievable normalized throughput improvement c_i attained, when we have $r_{min} = 0$ ■

The proof of Theorem 3.2 is outlined in Appendix B. Observe in Equation 3.17 that the upper bound c_i^0 is still a constant, regardless of the specific value of n and it is purely determined by the propagation parameters α, β and σ. The achievable normalized per-node throughput improvement c_i attained with the aid of perfect rate adaptation in the presence of shadow fading and its upper bound c_i^0 are plotted in Figures 3.7 - 3.15.

More explicitly, Figures 3.7 - 3.9 show that the achievable normalized per-node throughput improvement c_i experienced in the presence of shadow fading is also a decreasing function of the normalized minimum distance $\frac{r_{min}}{r_n}$, and this trend is similar to that in the absence of shadowing, as it was evidenced by Figures 3.3 and 3.4. However, the achievable normalized per-node throughput improvement c_i is higher than unity even at $\frac{r_{min}}{r_n} = 1$, which is different from that in the absence of shadowing. This gain was achieved by counteracting the link quality variation imposed by shadow fading with the aid of perfect rate adaptation. Observe in Equation 3.17 that at $\frac{r_{min}}{r_n} = 1$ we have:

$$\begin{aligned} c_i|_{\frac{r_{min}}{r_n}=1} &= \frac{\int_\beta^{+\infty} f_{\gamma|r_{ji}=r_n}(\gamma_{ji}) \ln(1+\gamma_{ji})\mathrm{d}\gamma_{ji}}{\ln(1+\beta)\int_\beta^{+\infty} f_{\gamma|r_{ji}=r_n}(\gamma_{ji})\mathrm{d}\gamma_{ji}} \\ &= \frac{\int_0^{+\infty} \ln(1+\beta e^t) e^{-\frac{t^2}{2\sigma^2}} \mathrm{d}t}{\ln(1+\beta)\int_0^{+\infty} e^{-\frac{t^2}{2\sigma^2}} \mathrm{d}t} \\ &> 1. \end{aligned} \tag{3.18}$$

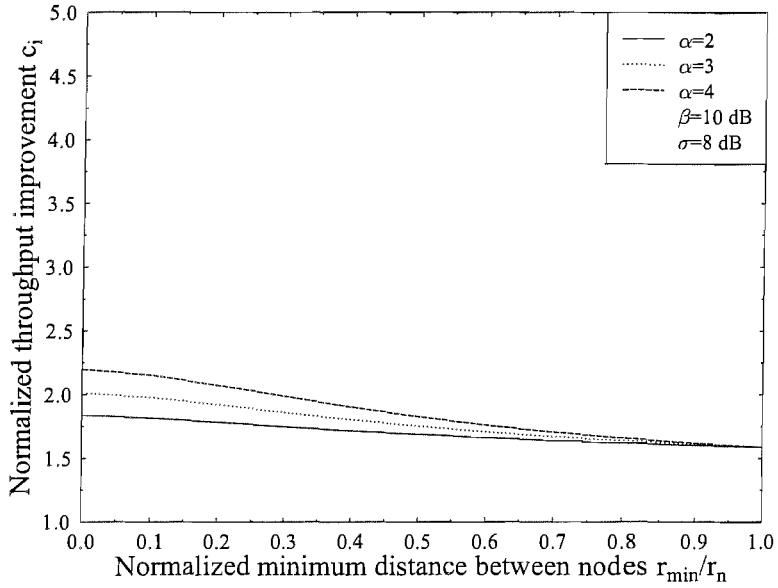

FIGURE 3.7: The normalized per-node throughput improvement c_i versus the normalized minimum distance r_{min}/r_n between nodes plotted for different values of the pathloss exponent α at a target SINR value of $\beta = 10$ dB and a lognormal shadowing standard deviation of $\sigma = 8$ dB in the presence of shadow fading, which is evaluated from Equation 3.17. The transmit power is fixed and perfect rate adaptation is assumed.

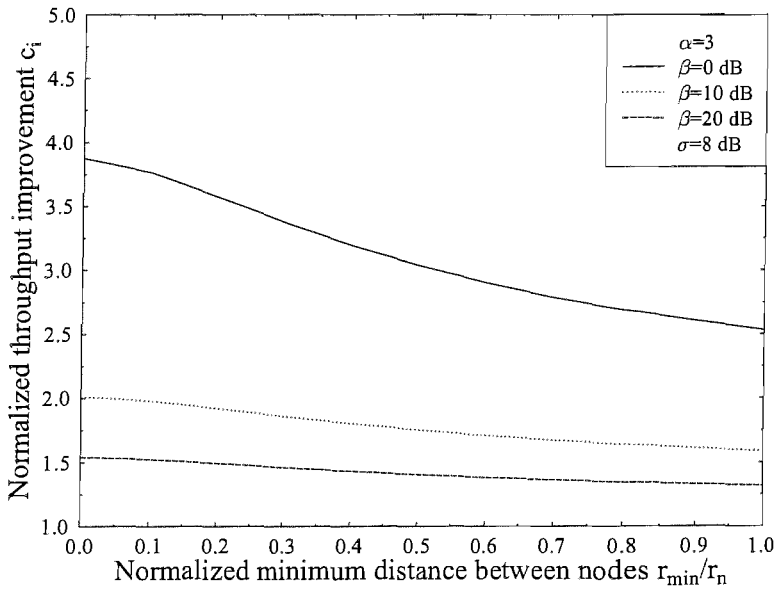

FIGURE 3.8: The normalized per-node throughput improvement c_i versus the normalized minimum distance r_{min}/r_n between nodes plotted for different values of the target SINR β at a pathloss exponent value of $\alpha = 3$ and a lognormal shadowing standard deviation of $\sigma = 8$ dB in the presence of shadow fading, which is evaluated from Equation 3.17. The transmit power is fixed and perfect rate adaptation is assumed.

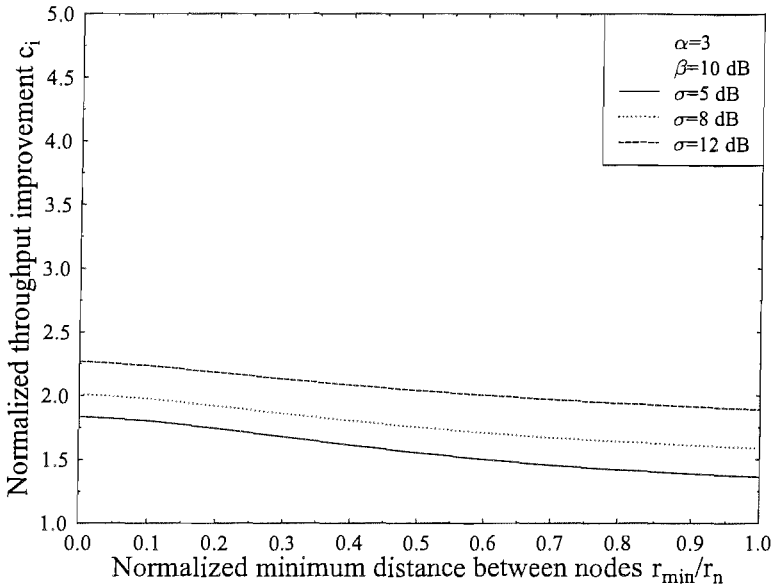

FIGURE 3.9: The normalized per-node throughput improvement c_i versus the normalized minimum distance r_{min}/r_n between nodes plotted for different values of the lognormal shadowing standard deviation σ at a pathloss exponent value of $\alpha = 3$ and a target SINR of $\beta = 10$ dB in the presence of shadow fading, which is evaluated from Equation 3.17. The transmit power is fixed and perfect rate adaptation is assumed.

We observe from Equation 3.18 that the normalized per-node throughput improvement c_i achieved at $\frac{r_{min}}{r_n} = 1$ is independent of the pathloss exponent α, and it is purely determined by the minimum SINR β of the specific receiver required for successful reception as well as by the lognormal shadowing standard deviation σ. This is because the conditional PDF of γ_{ji} at a given distance r_{ji} does not depend on α at $r_{min} = r_n$, as observed in Equation 3.14. Hence the curves associated with different values of α in Figure 3.7 converge, when we have $r_{min} \rightarrow r_n$, but this is not the case for different values of β, as seen in Figure 3.8 or for different values of σ, as portrayed in Figure 3.9.

Similar to Figure 3.7, Figures 3.10 and 3.11 show that the normalized per-node throughput improvement upper bound c_i^0 increases as a function of the pathloss exponent α also in the presence of shadow fading, as was the case in Figures 3.3 and 3.5 in the absence of shadowing. This is a consequence of the lower efficiency of the fixed-rate transmission schemes in case of a higher pathloss.

Similar to Figure 3.8, Figures 3.12 and 3.13 show that the normalized per-node throughput improvement upper bound c_i^0 is a decreasing function of the minimum SINR β of the receiver required for successful reception also in the presence of shadow fading, as was the case in Figures 3.4 and 3.6 in the absence of shadowing. This is also because

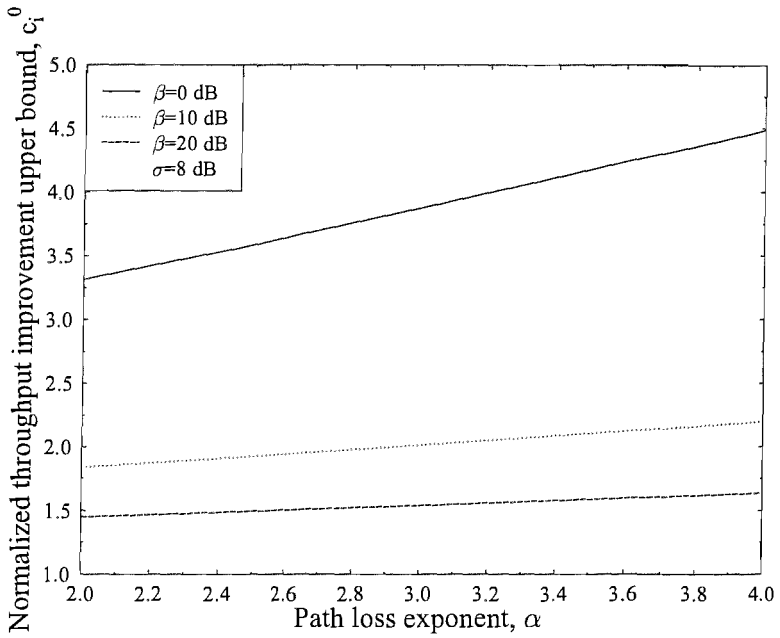

FIGURE 3.10: The normalized per-node throughput improvement upper bound c_i^0 versus the pathloss exponent α plotted for different values of the target SINR β at a lognormal shadowing standard deviation of $\sigma = 8$ dB in the presence of shadow fading, which is evaluated from Equation 3.17. The transmit power is fixed and perfect rate adaptation is assumed.

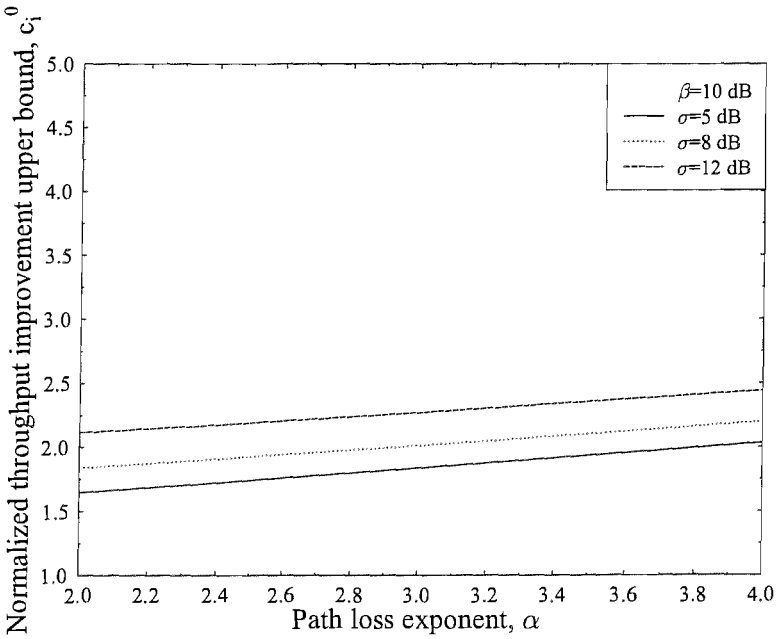

FIGURE 3.11: The normalized per-node throughput improvement upper bound c_i^0 versus the pathloss exponent α plotted for different values of the lognormal shadowing standard deviation σ at a target SINR of $\beta = 10$ dB in the presence of shadow fading, which is evaluated from Equation 3.17. The transmit power is fixed and perfect rate adaptation is assumed.

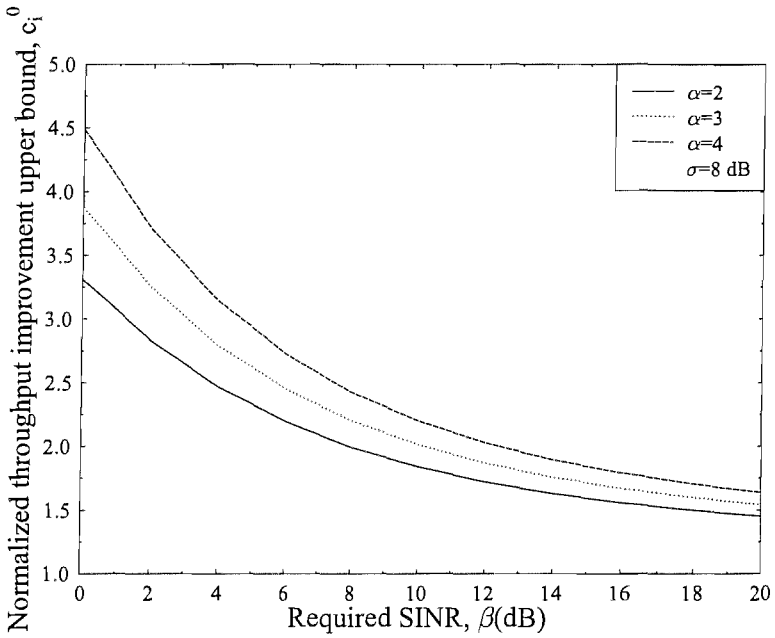

FIGURE 3.12: The normalized per-node throughput improvement upper bound c_i^0 versus the target SINR β plotted for different values of the pathloss exponent α at a lognormal shadowing standard deviation of $\sigma = 8$ dB in the presence of shadow fading, which is evaluated from Equation 3.17. The transmit power is fixed and perfect rate adaptation is assumed.

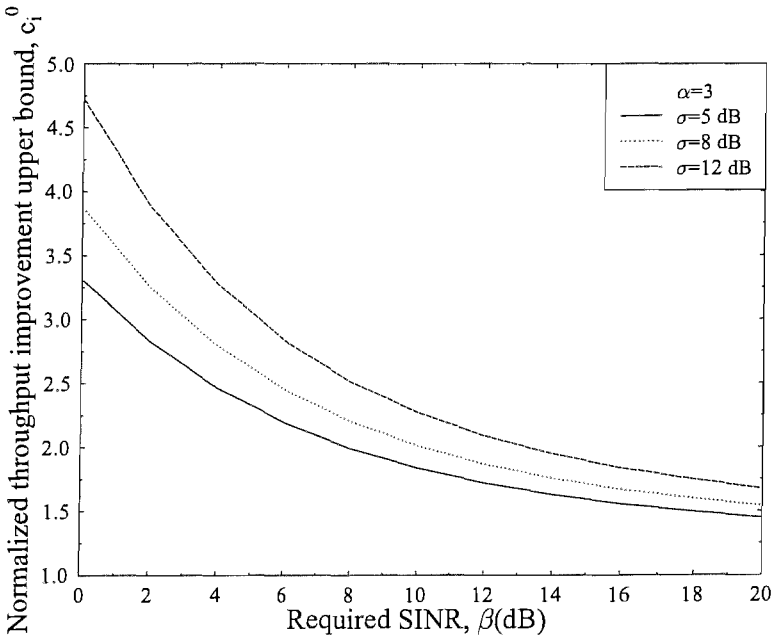

FIGURE 3.13: The normalized per-node throughput improvement upper bound c_i^0 versus the target SINR β plotted for different values of the lognormal shadowing standard deviation σ at a pathloss exponent of $\alpha = 3$ in the presence of shadow fading, which is evaluated from Equation 3.17. The transmit power is fixed and perfect rate adaptation is assumed.

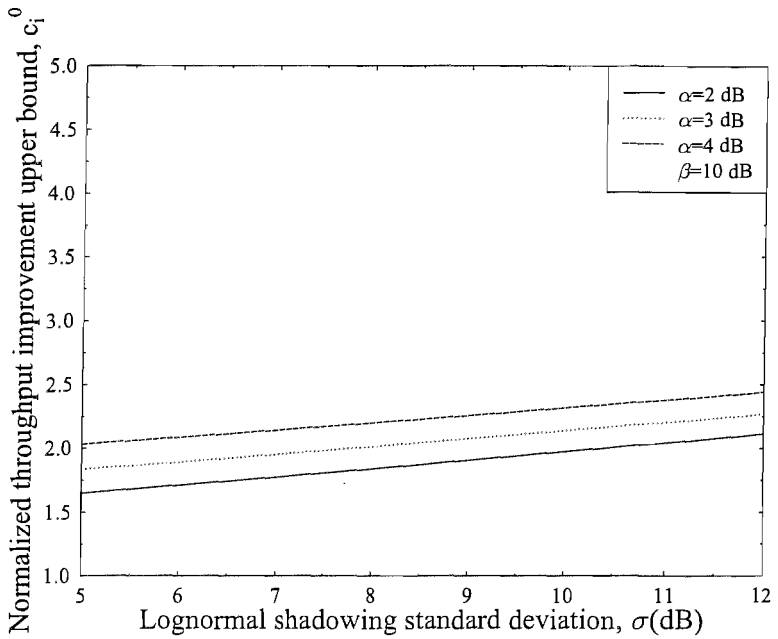

FIGURE 3.14: The normalized per-node throughput improvement upper bound c_i^0 versus the lognormal shadowing standard deviation σ plotted for different values of the pathloss exponent α at a target SINR of $\beta = 10$ dB in the presence of shadow fading, which is evaluated from Equation 3.17. The transmit power is fixed and perfect rate adaptation is assumed.

the channel capacity is a logarithmic function of the link SINR as seen in Equation 3.1, hence the slope of the channel capacity decreases as the link SINR increases, and so does the normalized per-node throughput improvement.

Similar to Figure 3.9, Figures 3.14 and 3.15 demonstrate that the normalized per-node throughput improvement c_i increases as a function of the lognormal shadowing standard deviation σ. This also obeys the intuition that rate adaptation improves the achievable throughput in case of a higher shadow fading standard deviation, as a consequence of the lower efficiency of the fixed rate transmission scheme in case of a larger fluctuation range of the link quality.

3.5 Example: AQAM

The family of AQAM schemes constitutes an efficient *rate adaptation* technique in mind for the sake of increasing the achievable throughput [201, 202, 210]. There are several criteria that may be invoked for choosing the switching levels between the adjacent AQAM modes [210, 211]. In the previous sections we used the idealized concept of

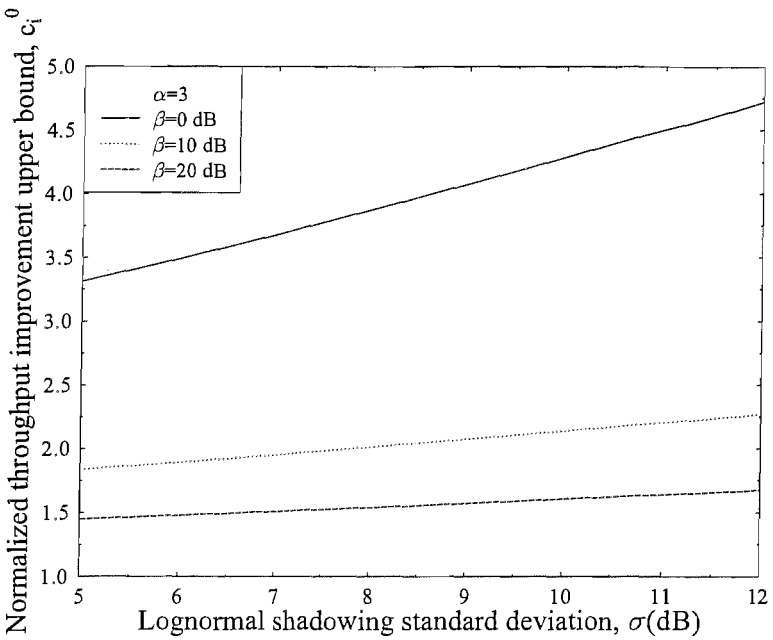

FIGURE 3.15: The normalized per-node throughput improvement upper bound c_i^0 versus the lognormal shadowing standard deviation σ plotted for different values of the target SINR β at a pathloss exponent of $\alpha = 3$ in the presence of shadow fading, which is evaluated from Equation 3.17. The transmit power is fixed and perfect rate adaptation is assumed.

instantaneous SINR as our channel quality measure for evaluating the beneficial effects of perfect *rate adaptation* on the achievable effective throughput upper bound.

In this section a K-mode adaptive square QAM scheme using Gray coding is investigated. The mode selection rule is formulated as follows [211]:

$$\text{Choose mode } k, \text{ when we have } s_k \leq \gamma_s < s_{k+1}, k \in \{0, ..., K\}, \tag{3.19}$$

where γ_s is the instantaneous SINR per symbol, s_k is the kth switching level and $s_0 = 0$, $s_{K+1} = \infty$. The AQAM constellation size is given by M_k phasors in mode k as follows:

$$M_0 = 0,$$
$$M_1 = 2,$$
$$M_k = 2^{2(k-1)}, k = 2, ..., K.$$

mode	k	M_k	b_k	s_k(dB)	
				BER = 10^{-3}	BER = 10^{-6}
No Tx	0	0	0	$-\infty$	$-\infty$
BPSK	1	2	1	6.7895	10.5298
QPSK	2	4	2	9.7998	13.5401
16-QAM	3	16	4	16.5430	20.4223
64-QAM	4	64	6	22.5490	26.5588
256-QAM	5	256	8	28.4147	32.5455
1024-QAM	6	1024	10	34.2607	38.5033

TABLE 3.1: The parameters of K-mode square AQAM systems using Gray coding and designed for maintaining BER = 10^{-3} and 10^{-6}, respectively. The switching thresholds were evaluated from Equations 3.20-3.21 and $\gamma_b = \gamma_s / \log_2 M$.

The number of Bits Per Symbol (BPS) b_k transmitted in mode k is given by:

$$b_0 = 0,$$
$$b_k = \log_2 M_k, k = 1, ..., K.$$

The general BER expression of M-ary square QAM using Gray coding for transmission over Additive White Gaussian Noise (AWGN) channels is given by [212]:

$$P_b = f_b(\gamma_b) = \frac{1}{\log_2 \sqrt{M}} \sum_{j=1}^{\log_2 \sqrt{M}} P_b(j), \tag{3.20}$$

$$P_b(j) = \frac{1}{\sqrt{M}} \sum_{i=0}^{(1-2^j)\sqrt{M}-1} \left\{ (-1)^{\left\lfloor \frac{i2^{j-1}}{\sqrt{M}} \right\rfloor} \left(2^{j-1} - \left\lfloor \frac{i2^{j-1}}{\sqrt{M}} + \frac{1}{2} \right\rfloor \right) \text{erfc}\left((2i+1) \sqrt{\frac{3\gamma_b \log_2 M}{2(M-1)}} \right) \right\}, \tag{3.21}$$

where $\gamma_b = \frac{\gamma_s}{\log_2 M}$ is the SINR per bit, and $\lfloor x \rfloor$ rounds x to the nearest smaller integer towards $-\infty$. Although it is impossible to obtain an analytical expression of its inverse function of $\gamma_b = f_b^{-1}(P_b)$, we can readily find its numerical solutions with the aid of one-dimensional root-finding [213], since $P_b = f_b(\gamma_b)$ is monotonically decreasing. Hence we arrive at the AQAM parameters listed in Table 3.1, which are independent of the associated SINR distribution. For example, if a 5-mode square AQAM scheme is adopted, the maximum constellation size will be $M_5 = 256$ and the highest switching level becomes $s_6 = \infty$, regardless of the target BER.

The average number of bits per symbol normalized to that of the fixed rate BPSK scheme is [211]:

$$B_i = \frac{\sum_{k=1}^{K} b_k \int_{s_k}^{s_{k+1}} f_{\gamma_s}(\gamma_s) \mathrm{d}\gamma_s}{B_{\mathrm{BPSK}}}, \tag{3.22}$$

where $f_{\gamma_s}(\gamma_s)$ is the PDF of the SINR per symbol and B_{BPSK} is the BPS throughput of the fixed rate BPSK scheme. In general a constant symbol rate is used in AQAM, regardless of the modulation mode selected, hence a constant bandwidth is required. Again, if we treat the co-channel interference as noise, which is justified by the central limit theorem, $f_{\gamma_s}(\gamma_s)$ is given by Equations 3.8 and 3.15 in the absence and in the presence of shadowing, respectively. The PDFs of the corresponding normalized SINR values associated with $r_{min} = 0$ are depicted in Figure 3.16. Since the SINR achieved at the fringes of the transmission range, i.e. at r_n, exactly satisfies the minimum SINR requirement β, provided that only the effect of path loss is considered. Hence the SINR normalized to β is always higher than or equal to 0 dB in the absence of fading, as suggested by Figure 3.16. The peak of the SINR PDF is reached at a normalized SINR abscissa value of less than 0 dB in the presence of shadowing, because the abscissa value of the peak $r^{-\alpha}e^{-\sigma^2}$ of the lognormal distribution in Equation 3.12 is less than the SINR's mean value of $r^{-\alpha}e^{-\sigma^2/2}$. The achievable normalized average BPS throughput B_i versus the number of different-throughput modulation modes K of square AQAM systems associated with $r_{min} = 0$ and $\beta = s_1$ is characterized in Figure 3.17, which was recorded both in the absence of fading and in the presence of shadowing.

Figure 3.17 shows that AQAM is capable of substantially improving the average BPS throughput both in the absence of fading and in the presence of shadowing compared to the fixed rate BPSK scheme. However, the additional throughput improvement achieved by a high-complexity scheme using more than four AQAM modes is marginal, because the probability of activating the high-BPS modes drops exponentially, when the SINR normalized to β increases, as suggested by the PDF seen in Figure 3.16. This result is in line with Theorem 3.1 and Theorem 3.2, suggesting that even perfect *rate adaptation* is incapable of improving the scaling law of the per-node throughput attained, regardless of the absence or presence of shadowing. The achievable normalized average BPS throughput recorded in the case of a higher switching threshold set designed for maintaining a more stringent requirement of BER $\leq 10^{-6}$ is only marginally lower than that in the case of a lower threshold set designed for maintaining the less stringent requirement of BER $\leq 10^{-3}$, since the distributions of the normalized SINR in the BER $= 10^{-6}$ and 10^{-3} scenarios are identical, as seen in Figure 3.16. This implies that a lower BPS

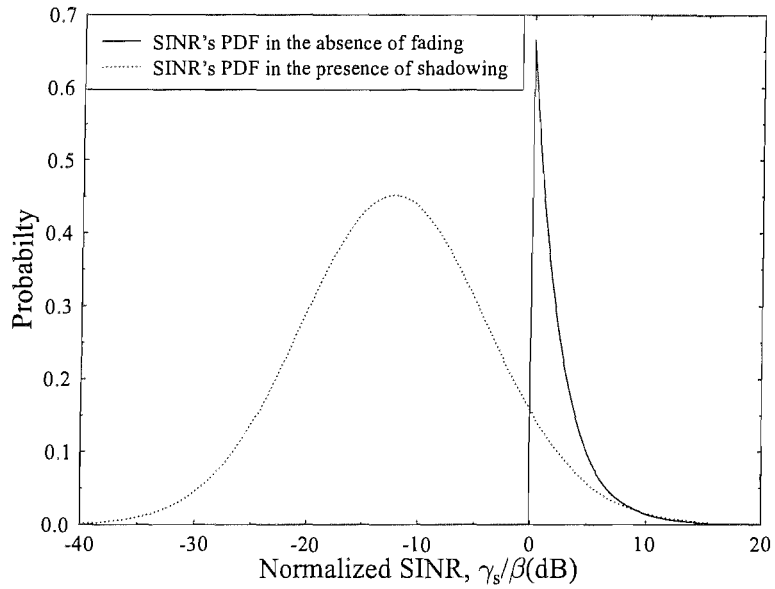

FIGURE 3.16: The PDFs of the SINRs normalized to the minimum SINR requirement β both in the absence of fading and in the presence of log-normal shadowing having $\alpha = 3$ and $\sigma = 8$ dB, which were computed from Equations 3.8 and 3.15 for $r_{min} = 0$, respectively.

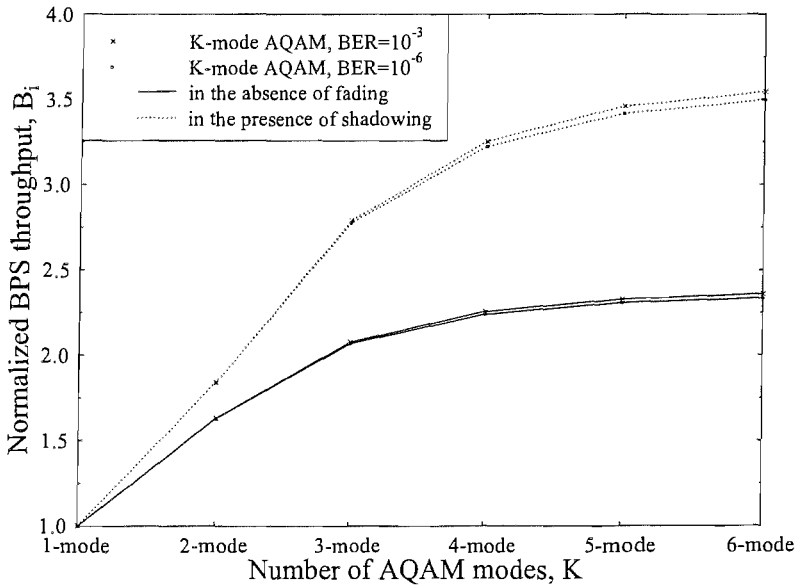

FIGURE 3.17: The achievable normalized per-node average BPS throughput B_i versus the number of modes K in K-mode square AQAM systems using Gray coding for a path loss exponent value of $\alpha = 3$, a lognormal shadowing standard deviation of $\sigma = 8$ dB and a target BER of 10^{-3} and 10^{-6}, respectively, recorded both in the absence of fading and in the presence of shadow fading in a random *ad hoc* network. The PDF $f_{\gamma_s}(\gamma_s)$ of the SINR per symbol is given by Equation 3.8 and Equation 3.15, respectively.

throughput improvement may be achieved in case of requiring a lower BER of 10^{-6}, which conforms to the trends observed in Figure 3.4. However, it does not imply that the AQAM scheme achieves a lower BPS throughput in the case of aiming for a lower instantaneous BER, since we normalize the BPS throughput to that of the fixed rate BPSK scheme, which is different for the scenarios of BER $= 10^{-3}$ and BER $= 10^{-6}$ owing to the different values of r_n.

3.6 Conclusion

In this chapter we have focused our attention on the effects of perfect *rate adaptation* on the achievable throughput of random *ad hoc* networks, which was discussed in the context of both pathloss and shadow fading. In conclusion, perfect *rate adaptation* has the potential of considerably improving the achievable throughput of the random *ad hoc* network compared to *fixed rate transmissions*, since *rate adaptation* is capable of mitigating the effects of link quality fluctuations, as shown in Figures 3.3 - 3.15. This conclusion was further confirmed by Figure 3.17 in the context of our AQAM examples. The normalized per-node throughput improvement upper bound c_i^0 achieved with the aid of perfect *rate adaptation* is determined purely by the pathloss exponent α, by the required minimum SINR β of the receiver and by the lognormal shadowing standard deviation σ. We observed in Figures 3.5 and 3.9 - 3.11 that the achievable normalized throughput c_i^0 increases, as α or σ increases, because perfect *rate adaptation* is capable of efficiently mitigating the pathloss- and shadowing-induced link quality variations. More explicitly, this was demonstrated in Figure 3.3 in the absence of fading, while in Figures 3.7 and 3.9 in the presence of shadowing, respectively. By contrast, c_i^0 decreases as the SINR β required by either a less sophisticated or by a higher-throughput receiver increases, which is a consequence of the fixed-mode scheme's higher throughput, as shown in Figures 3.4 and 3.6 in the absence of fading and in Figures 3.8, 3.12 and 3.13 in the presence of shadowing, respectively.

Chapter 4

Ad Hoc Networks Using Spreading Sequences Exhibiting an Interference-Free Window

4.1 Introduction

Code Division Multiple Access (CDMA) systems have substantial benefits and hence have found their way into the third-generation wireless systems. A set of ideal spreading sequences is expected to have zero off-peak auto-correlations and cross-correlations, which would eliminate both Inter Symbol Interference (ISI) and Multiple Access Interference (MAI) imposed, regardless whether they operate in synchronous or asynchronous scenarios. Unfortunately, such ideal spreading sequences do not exist. But nonetheless, it is possible to design sequences, which exhibit an Interference Free Window (IFW) over a limited duration [214]. A further design-trade-off is that maintaining low auto-correlations and cross-correlations outside the IFW contradict to each other [214] and these correlation side-lobes in fact are typically higher than those of classic spreading sequences. Despite these trade-offs, spreading codes having an IFW are attractive, since the ISI and MAI associated with the family of classic spreading sequences, such as orthogonal Walsh-Hadamard (WH) codes, Pseudo Noise (PN) sequences, Gold codes and Kasami codes [215], significantly impair the attainable capacity of traditional CDMA systems.

More explicitly, the achievable system capacity might be dramatically improved even with the aid of a limited-duration IFW, where the off-peak aperiodic auto-correlations

c_{xx} and cross-correlations c_{xy} become zero [216]:

$$c_{xx}(\tau) = \begin{cases} 1, \tau = 0, \\ 0, \tau \neq 0, \text{ and is within IFW}, \end{cases} \tag{4.1}$$

$$c_{xy}(\tau) = 0, \qquad \tau \text{ is within IFW}. \tag{4.2}$$

These attractive correlation properties assist us in eliminating the effects of both ISI and MAI. The family of Large Area Synchronous (LAS) [217] codes exhibits the above-mentioned favourable properties, which renders them a promising design alternative to traditional spreading codes. Initial comparative studies between LAS-CDMA and traditional CDMA were presented for example in [217].

LAS codes are generated by combining Large Area (LA) [218] codes and Loosely Synchronous (LS) [219] codes. Li [218] proposed various construction schemes for LA codes and analyzed the performance of LA-CDMA, which exhibited higher spectral efficiency than traditional CDMA. Stanczak *et al.* [219] focussed their attention on contriving systematic methods for the construction of LS codes. Choi and Hanzo [220] investigated the design of efficient and flexible LAS codes having an increased duty ratio, which resulted in a higher number of codes and hence a higher number of supported users than previous designs. An entire LAS-CDMA network was studied in [221].

More in-depth comparative studies between LAS codes and random sequences employed in the context of single- and multi-carrier DS-CDMA cellular networks were performed in [222]. These results indicated that LAS DS-CDMA significantly outperformed traditional DS-CDMA, provided that all nodes operated in a quasi-synchronous manner, where all multipath components arrived within the IFW.

Again, as a benefit of having an IFW, LAS codes have the ability to support asynchronous operation in ad hoc networks. In this chapter we will focus our attention on a comparative study of LAS codes and traditional spreading sequences in DS-CDMA ad hoc networks. For the detailed construction methods of LA, LS and LAS codes please refer to [218, 219].

The outline of this chapter is as follows. An infinite mesh of rectilinear node topology is introduced in Section 4.2 for the sake of evaluating the achievable BER performance. In Section 4.2 the system model of LAS DS-CDMA is also described. The BER performance of classic spreading sequences employed in such a system is investigated in Section 4.3. Our comparative study between LAS codes and traditional spreading sequences is presented in Section 4.4. Finally, Section 4.5 provides our conclusions.

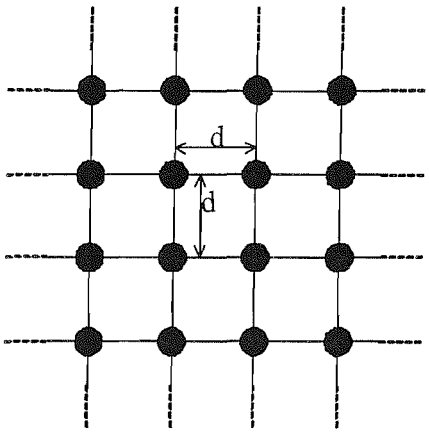

FIGURE 4.1: The infinite mesh of rectilinear node topology with considered. The distance between any two adjacent nodes is d.

4.2 System Model and Assumptions

For the sake of maintaining mathematical tractability and for gaining valuable insights into more realistic practical mobile wireless networks, we consider an infinite mesh of rectilinear topology having infinite nodes, as seen in Figure 4.1. Its regular topology exactly enables us to examine the system performance [191, 223, 224]. Its infinite structure results in a scenario having the highest possible interference and conveniently eliminates any effect the size of the node-grid would impose on the validity of the results. We use (ud, vd) for denoting the location of nodes on the two-dimensional plane, where u and v are integers and d is the minimum distance between any two adjacent nodes.

Every node in the network has four neighbours, connected by the edges, as seen in Figure 4.1. We assume that the maximum affordable transmit power only supports communications between neighbours. If a packet has to be sent from a source node to a destination node that is not an immediate neighbour, it has to be relayed by the intermediate nodes. Each node is assigned a spreading sequence for transmitting such that the shortest distance between any two nodes using the same spreading sequence is maximized. Each node is assumed to have the equal probability to transmit or receive signals to or from one of its neighbours. Under uniform traffic generation conditions, the network is homogeneous and hence it is possible for us to study a single receiving reference node, rather than considering all nodes.

We will focus our attention on the system's single-hop performance under the above assumptions, rather than considering a particular routing strategy. We assume that each node transmits or receives with the probability of 0.5, respectively, i.e. that there

is always sufficient data in the node's buffer. Without loss of generality, the receiving reference node is assumed to be located at the coordinate $(0,0)$ in the two-dimensional plane and receives from the transmitting node located at $(0,d)$. Hence all the other nodes are regarded as interferers, which interfere with a probability of 0.5.

Consider K simultaneously transmitting nodes in the context of wireless ad hoc networks, where each transmitting node transmits at the same constant power level P_t, since cost-efficient ad hoc networks routinely dispense with power control. The multipath channel has the channel impulse response (CIR) of [207]:

$$h_k(t) = \sum_{l=0}^{L_p-1} h_{kl}\delta(t - lT_c)e^{-j\vartheta_{kl}}, \tag{4.3}$$

where $h_k(t)$ is the complex-valued low-pass equivalent CIR of the multipath channel experienced by the transmitting node k. Furthermore, L_p is the total number of resolvable paths, which is assumed to be identical for all nodes, h_{kl} is the fading envelope of the lth path of the transmitting node k, $\delta(t)$ is the Dirac delta function, T_c is the chip duration and ϑ_{kl} is the phase-shift of the lth path of the transmitting node k. In general, the phase angles $\{\vartheta_{kl}\}$ are deemed to be independently and uniformly distributed in $[0, 2\pi)$, while the fading amplitudes $\{h_{kl}\}$ are independent Nakagami-m distributed random variables having a Probability Distribution Function (PDF) of $p(h_{kl})$ expressed as [207]:

$$p(h_{kl}) = \frac{2m_{kl}^{m_{kl}} h_{kl}^{2m_{kl}-1}}{\Gamma(m_{kl})\Omega_{kl}^{m_{kl}}} e^{-\frac{m_{kl}}{\Omega_{kl}}h_{kl}^2}. \tag{4.4}$$

In Equation 4.4 m_{kl} is the Nakagami-m fading parameter, which characterizes the severity of the fading on the lth path of the transmitting node k, Ω_{kl} is the second moment of h_{kl}, which corresponds to the average path loss on the lth path of the transmitting node k [207], and $\Gamma(\cdot)$ is the gamma function [1]. We assume a negative exponentially decaying Multipath Intensity Profile (MIP) given by [225, 226]:

$$\Omega_{kl} = \Omega_{k0}e^{-\eta l}, \quad k = 1, ...K \text{ and } l = 1, ..., L_p - 1, \tag{4.5}$$

$$\Omega_{k0} = \mathrm{E}\{h_{kl}^2\} = r_k^{-\alpha}, \tag{4.6}$$

where $\eta > 0$ is the rate of average power decay, which is assumed to be identical for all nodes, r_k is the distance between the reference receiving node and the transmitting node k, and $\alpha > 2$ is the path loss exponent [207], which is also assumed to be identical

for all nodes. Given the above-mentioned network topology, Equation 4.6 becomes

$$\Omega_{k0} = r_k^{-\alpha} = \left(u^2 + v^2\right)^{-\frac{\alpha}{2}} d^{-\alpha}. \tag{4.7}$$

The signal $x_k(t)$ transmitted by node k is given by [226–229]:

$$x_k(t) = \sqrt{2P_t} a_k(t) b_k(t) \Psi(t) e^{j\phi_k}, \tag{4.8}$$

where ϕ_k is the carrier phase of the transmitting node k, which is assumed to be uniformly distributed in $[0, 2\pi)$. The spreading code $a_k(t)$ is defined as:

$$a_k(t) = \sum_{j=-\infty}^{\infty} a_{kj} \varphi_{T_c}(t - jT_c), \tag{4.9}$$

where $a_{kj} \in \{-1, 1\}$ is a binary spreading sequence having a period L and the rectangular pulse $\varphi_T(t)$ having a period T is defined as:

$$\varphi_T(t) = \begin{cases} 1, t \in [0, T], \\ 0, \text{otherwise}. \end{cases} \tag{4.10}$$

The data signal $b_k(t)$ is defined as:

$$b_k(t) = \sum_{j=-\infty}^{\infty} b_{kj} \varphi_{T_s}(t - jT_s), \tag{4.11}$$

where $b_{kj} \in \{-1, 1\}$ is the binary data sequence and T_s is the symbol duration, which satisfies $T_s = LT_c$. The chip waveform $\Psi(t)$ is defined as:

$$\Psi(t) = \sum_{j=-\infty}^{\infty} \psi_{T_c}(t - jT_c), \tag{4.12}$$

where $\psi_{T_c}(t)$ is an arbitrary time-limited function, which satisfies $\psi_{T_c}(t) = 0$ for $t \notin [0, T_c]$ and is normalized to have an energy equal to T_c, i.e. we have $\int_0^{T_c} \psi_{T_c}^2(t)\mathrm{d}t = T_c$. For a rectangular chip waveform we have $\psi_{T_c}(t) = \varphi_{T_c}(t)$.

The signal $y(t)$ received by the reference node is given by:

$$y(t) = \sum_{k=1}^{K} \sum_{l=0}^{L_p - 1} \sqrt{2P_t} a_k(t - lT_c - \tau_k) b_k(t - lT_c - \tau_k) \Psi(t - lT_c - \tau_k) h_{kl} e^{j\theta_{kl}} + n(t), \tag{4.13}$$

where τ_k is the propagation delay of the transmitting node k, $\theta_{kl} = \phi_k - \vartheta_{kl}$ is the phase-shift of the lth path of the transmitting node k at the receiving reference node and $n(t)$ is the complex-valued low-pass equivalent AWGN having a double-sided spectral density of $N_0/2$. Generally, θ_{kl} is independently and uniformly distributed in $[0, 2\pi)$[1] and τ_k is assumed to be uniformly distributed in the range of $[\tau_{k0}, \tau_{k0} + \tau_{max}]$, where $\tau_{k0} = \frac{r_k}{c}$ is the shortest delay or Line-Of-Sight (LOS) delay between the transmitting node k and the reference node, where c is the velocity of light. Furthermore, τ_{max} is the maximum propagation delay relative to the LOS delay, which is assumed to be identical for all nodes.

4.3 BER Analysis

Let us assume that the reference node is receiving signals from the transmitting node q using maximal ratio combining (MRC) and the RAKE receiver combines a total of L_r branches. Then the output Z_{qi} of its correlation receiver at the ith branch is given by:

$$\begin{aligned} Z_{qi} &= \mathrm{Re}\left\{ \int_{iT_c+\tau_q}^{T_s+iT_c+\tau_q} y(t)\alpha_i e^{-j\theta_{qi}} a_q(t - iT_c - \tau_q)\Psi(t - iT_c - \tau_q)\mathrm{d}t \right\} \\ &= D_{qi} + I_{(S)qi} + I_{(M)qi} + n_{qi}, \end{aligned} \tag{4.14}$$

where α_i is the branch or finger weight of the RAKE receiver [226] , D_{qi} is the required signal, while $I_{(S)qi}$ is the multipath interference imposed by the other paths of node q, $I_{(M)qi}$ is the multiple access interference incurred by other nodes and n_{qi} is the noise. Following the procedures outlined in [226–228, 230], we can derive D_{qi}, $I_{(S)qi}$, $I_{(M)qi}$ and n_{qi} conditioned on the finger weights $\{\alpha_i\}$ of the RAKE receiver and the qth user's spreading sequence $a_q(t)$ [226].

The required signal D_{qi} can be expressed as:

$$D_{qi} = \sqrt{2P_t}T_s b_{q0} h_{qi} \alpha_i. \tag{4.15}$$

[1]Normally the sum or difference of two uniformly distributed random variables has a triangular distribution. However, the sum or difference of two random phases - both uniformly distributed in $[0, 2\pi)$ - is still uniformly distributed in $[0, 2\pi)$ due to the 2π periodicity of the phase.

The multipath interference $I_{(S)qi}$ and its variance $\sigma^2_{(S)qi}$ are given by[2]:

$$I_{(S)qi} = \sqrt{2P_t}T_c\alpha_i \sum_{\substack{l=0 \\ l\neq i}}^{L_p-1} h_{ql}\cos(\theta_{ql}-\theta_{qi})\left[b_{q,-1}c_{qq}(\xi-L)+b_{q0}c_{qq}(\xi)\right], \tag{4.16}$$

$$\sigma^2_{(S)qi} = P_tT_c^2\alpha_i^2 \sum_{\substack{l=0 \\ l\neq i}}^{L_p-1} \Omega_{q0}e^{-\eta l}\left[c^2_{qq}(\xi-L)+c^2_{qq}(\xi)\right], \tag{4.17}$$

where we have $\xi = l-i$, and $c_{kq}(\xi)$ is the discrete aperiodic cross-correlation function of the spreading sequences $\{a_{kj}|j=0,..,L-1\}$ and $\{a_{qj}|j=0,...,L-1\}$, which is defined as [228]:

$$c_{kq}(\xi) = \begin{cases} \sum_{j=0}^{L-1-\xi} a_{kj}a_{q,j+\xi}, 0\leq\xi\leq L-1, \\ \sum_{j=0}^{L-1+\xi} a_{k,j-\xi}a_{qj}, -(L-1)\leq\xi<0, \\ 0, \qquad\qquad |\xi|\geq L. \end{cases} \tag{4.18}$$

Equation 4.18 becomes the discrete aperiodic auto-correlation function $c_{qq}(\xi)$, if we have $k=q$.

The multiple access interference $I_{(M)qi}$ and its variance $\sigma^2_{(M)qi}$ are given by:

$$I_{(M)qi} = \sqrt{2P}T_c\alpha_i \sum_{\substack{k=1 \\ k\neq q}}^{K}\sum_{l=0}^{L_p-1} h_{kl}\cos(\theta_{kl}-\theta_{qi})\left[b_{k,-1}\rho_{kq}(\tau_c)+b_{k0}\varrho_{kq}(\tau_c)\right], \tag{4.19}$$

$$\sigma^2_{(M)qi} = PT_c^2\alpha_i^2 \sum_{\substack{k=1 \\ k\neq q}}^{K}\sum_{l=0}^{L_p-1} \Omega_{k0}e^{-\eta l}\int_{\tau_{q0}}^{\tau_{q0}+\tau_{max}}\int_{\tau_{k0}}^{\tau_{k0}+\tau_{max}} \frac{1}{\tau^2_{max}}[\rho^2_{kq}(\tau_c)+\varrho^2_{kq}(\tau_c)]\mathrm{d}\tau_q\mathrm{d}\tau_k. \tag{4.20}$$

The partial cross-correlation functions $\rho_{kq}(\tau_c)$ and $\varrho_{kq}(\tau_c)$ of the spreading codes are defined by the normalized partial auto-correlation functions $R_\psi(\tau_c)$ and $\hat{R}_\psi(\tau_c)$ of the

[2]This derivation of $\sigma^2_{(S)qi}$ was proposed by Eng and Milstein [226] and has been widely used in MPI analysis [231–236]. The difference between our results in this chapter and those in [226] is that we calculate the SINR value for each branch of the RAKE receiver and apply the results of [230], rather than summing the signals of all RAKE receiver branches and approximating the sum as the square of a Nakagami-m random variable [226]. However, we used the following simplifying assumption in this derivation, which has also been often used by numerous authors in the literature [226, 231–236]. The conditional BEP $P_b(\gamma)$ in Equation 4.32 is averaged over $\{\gamma_i\}$, which is dependent on $\{h_{qi}\}$, for arriving at the expression of P_b in Equation 4.34. However, the SINR value γ_i in Equation 4.31 is calculated by averaging over $\{h_{ql}\}$, where $l\neq i$. This implies that this derivation averages over $\{h_{qi}\}$ more than once. Although this is a non-exact simplifying assumption, the sheer fact of applying the Gaussian approximation itself inherently introduces some inaccuracy and there is no exact formula in the literature for calculating the MPI at the time of writing.

chip waveform $\psi_{T_c}(t)$ as:

$$\rho_{kq}(\tau_c) = c_{kq}(\zeta - L)\hat{R}_\psi(\tau_c) + c_{kq}(\zeta + 1 - L)R_\psi(\tau_c), \tag{4.21}$$

$$\varrho_{kq}(\tau_c) = c_{kq}(\zeta)\hat{R}_\psi(\tau_c) + c_{kq}(\zeta + 1)R_\psi(\tau_c), \tag{4.22}$$

$$R_\psi(\tau_c) = \frac{1}{T_c}\int_0^{\tau_c} \psi_{T_c}(t)\psi_{T_c}(t + T_c - \tau_c)\mathrm{d}t, \tag{4.23}$$

$$\hat{R}_\psi(\tau_c) = \frac{1}{T_c}\int_{\tau_c}^{T_c} \psi_{T_c}(t)\psi_{T_c}(t - \tau_c)\mathrm{d}t, \tag{4.24}$$

where we have $\zeta = \lfloor (l - i + \frac{\tau_k - \tau_q}{T_c}) \bmod L \rfloor$, $\tau_c = (l - i + \frac{\tau_k - \tau_q}{T_c}) \bmod L - \zeta$. Hence $0 \leq \zeta \leq \zeta + \tau_c \leq \zeta + 1 \leq L$. For a rectangular chip waveform, we have $R_\psi(\tau_c) = \tau_c$ and $\hat{R}_\psi(\tau_c) = 1 - \tau_c$. There is a double integral in Equation 4.20, which complicates its evaluation. However, since its integrand is determined entirely by the difference between τ_q and τ_k, and all the cross-correlation items $c_{kq}(\zeta - L)$, $c_{kq}(\zeta + 1 - L)$, $c_{kq}(\zeta)$, and $c_{kq}(\zeta + 1)$ remain constant, while we have $\frac{\tau_k - \tau_q}{T_c} \in [\zeta, \zeta + 1)$, and the double integral in Equation 4.20 can be simplified (see Appendix C for details) to the sum of a finite series, when a rectangular chip waveform is used:

$$\begin{aligned}\sigma^2_{(M)qi} = P_t T_c^2 \alpha_i^2 \sum_{\substack{k=1 \\ k\neq q}}^{K} \sum_{l=0}^{L_p - 1} \Omega_{k0} e^{-\eta l} \frac{T_c^2}{\tau_{max}^2} \\ \times \left[\sum_{j=\lambda_-}^{\lambda_0} S_j^{(1)}(t)\Big|_{\max\{\tau_- - j, 0\}}^{\min\{\tau_0 - j, 1\}} - \sum_{j=\lambda_0}^{\lambda_+} S_j^{(2)}(t)\Big|_{\max\{\tau_0 - j, 0\}}^{\min\{\tau_+ - j, 1\}} \right],\end{aligned} \tag{4.25}$$

where we have $\zeta = (l - i + j) \bmod L$ and the partial integral $S_j^{(i)}(t)\Big|_{t_1}^{t_2} = S_j^{(i)}(t_2) - S_j^{(i)}(t_1)$, and $S_j^{(i)}(t)$ is given by:

$$\begin{aligned}S_j^{(i)}(t) = \frac{1}{4}\omega_1(\zeta)t^4 + \frac{1}{3}\left[\omega_1(\zeta)(j - \tau_i) + 2\omega_2(\zeta)\right]t^3 + \frac{1}{2}\left[2\omega_2(\zeta)(j - \tau_i) + \omega_3(\zeta)\right]t^2 \\ + \omega_3(\zeta)(j - \tau_i)t,\end{aligned} \tag{4.26}$$

$$\tau_i = \begin{cases} \tau_-, \text{if } i = 1, \\ \tau_+, \text{if } i = 2. \end{cases} \tag{4.27}$$

The coefficients $\omega_1(\zeta)$, $\omega_2(\zeta)$ and $\omega_3(\zeta)$ in Equation 4.26 are given by:

$$\begin{aligned}\omega_1(\zeta) &= \left[c_{kq}(\zeta + 1 - L) - c_{kq}(\zeta - L)\right]^2 + \left[c_{kq}(\zeta + 1) - c_{kq}(\zeta)\right]^2, \\ \omega_2(\zeta) &= c_{kq}(\zeta - L)\left[c_{kq}(\zeta + 1 - L) - c_{kq}(\zeta - L)\right] + c_{kq}(\zeta)\left[c_{kq}(\zeta + 1) - c_{kq}(\zeta)\right], \\ \omega_3(\zeta) &= c_{kq}^2(\zeta - L) + c_{kq}^2(\zeta).\end{aligned} \tag{4.28}$$

The parameters τ_-, τ_0, τ_+ defining the integral area and their integer parts λ_-, λ_0, λ_+ are given by:

$$\begin{aligned}\tau_- &= \frac{\tau_{k0} - \tau_{q0} - \tau_{max}}{T_c}, \lambda_- = \lfloor \tau_- \rfloor, \\ \tau_0 &= \frac{\tau_{k0} - \tau_{q0}}{T_c}, \qquad \lambda_0 = \lfloor \tau_0 \rfloor, \\ \tau_+ &= \frac{\tau_{k0} - \tau_{q0} + \tau_{max}}{T_c}, \lambda_+ = \lfloor \tau_+ \rfloor.\end{aligned}$$

The Gaussian noise n_{qi} and its variance $\sigma^2_{(N)qi}$ are given by:

$$n_{qi} = \mathrm{Re}\left\{ \alpha_i \int_0^{T_s} n(t) a_q(t) \Psi(t) e^{j\theta_{qi}} \mathrm{d}t \right\}, \tag{4.29}$$

$$\sigma^2_{(N)qi} = \alpha_i^2 N_0 T_s. \tag{4.30}$$

Consequently, the SINR encountered on the ith path of the transmitting node q at the receiving reference node is denoted by $2\gamma_i$, where γ_i is given by:

$$\gamma_i = \frac{D^2_{qi}}{2\left[\sigma^2_{(S)qi} + \sigma^2_{(M)qi} + \sigma^2_{(N)qi}\right]}. \tag{4.31}$$

The term Bit Error Probability (BEP) will be used interchangeably with the BER $P_{b|\mathbf{h}}(\boldsymbol{\gamma})$, which is conditioned on the fading envelope vector $\mathbf{h}$. When using BPSK for transmitting from node n to the receiving reference node, the BEP is given by applying the Gaussian approximation as [230]:

$$P_b(\boldsymbol{\gamma}) = \mathrm{Q}\left(\sqrt{\sum_{i=0}^{L_r-1} 2\gamma_i} \right), \tag{4.32}$$

where $\boldsymbol{\gamma}$ represents the vector constituted by $\{\gamma_i\}$, L_r is the total number of RAKE receiver branches and $Q(x)$ is the Gaussian Q-function. For the sake of conveniently evaluating the average BER, we will use an alternative definite integral of the form of $Q(x)$ [230]:

$$Q(x) = \frac{1}{\pi} \int_0^{\frac{\pi}{2}} \exp\left(-\frac{x^2}{2\sin^2\theta} \right) \mathrm{d}\theta, \quad x \geq 0. \tag{4.33}$$

Finally, the average BER at the reference node receiving from the transmitting node q is given by [230]:

$$P_b = \frac{1}{\pi} \int_0^{\frac{\pi}{2}} \prod_{i=0}^{L_r-1} \left(\frac{m_i \sin^2\theta}{\bar{\gamma}_i + m_i \sin^2\theta} \right)^{m_i} \mathrm{d}\theta, \tag{4.34}$$

where $2\bar{\gamma}_i$ is the average SINR of the transmitting node q at the receiving reference node, and the SINR-related term $\bar{\gamma}_i$ in Equation 4.34 is given by:

$$\bar{\gamma}_i = \left[\frac{\Upsilon_S(i)}{L^2} + \frac{\Upsilon_M(i)}{L^2} + \frac{1}{\gamma_{\text{SNR}}}\right]^{-1} e^{-\eta i}, \tag{4.35}$$

where $\Upsilon_S(i)$ and $\Upsilon_M(i)$ are the multipath interference (MPI) and the MAI related terms, respectively, and γ_{SNR} is the received per-bit signal-to-interference ratio (SNR), which does not take into account the received interference power. They are formulated as:

$$\Upsilon_S(i) = \sum_{\substack{l=0 \\ l\neq i}}^{L_p-1} e^{-\eta l}[c_{qq}^2(\xi - L) + c_{qq}^2(\xi)], \tag{4.36}$$

$$\Upsilon_M(i) = \sum_{\substack{k=1 \\ k\neq q}}^{K} \sum_{l=0}^{L_p-1} \frac{\Omega_{k0}}{\Omega_{q0}} e^{-\eta l} \frac{T_c^2}{\tau_{max}^2} \left[\sum_{j=\lambda_-}^{\lambda_0} S_j^{(1)}(t)\Big|_{\max\{\tau_- - j,0\}}^{\min\{\tau_0 - j,1\}} - \sum_{j=\lambda_0}^{\lambda_+} S_j^{(2)}(t)\Big|_{\max\{\tau_0 - j,0\}}^{\min\{\tau_+ - j,1\}}\right], \tag{4.37}$$

$$\gamma_{\text{SNR}} = \frac{P_t L T_c \Omega_{q0}}{N_0}. \tag{4.38}$$

4.4 Performance of LAS DS-CDMA

4.4.1 Benchmark Systems

In this section we will compare the achievable performance of a number of systems, namely that of quasi-synchronous LAS DS-CDMA and quasi-synchronous DS-CDMA using WH codes and Orthogonal Gold (OG) codes, as well as asynchronous LAS DS-CDMA and asynchronous DS-CDMA using random signature sequences. BPSK modulation is used in all of the above systems.

We investigate the attainable performance of the LAS-CDMA 2000 system's physical layer [237], which was originally conceived for base-station-aided communications, rather than for ad hoc networks. In the LAS-CDMA 2000 system modified versions of the LA(L_A, M_A, K_A) and LS(N, P, W_0) codes are combined for the sake of generating the LAS codes [220, 237], where the length of the LA code becomes $L_A = 2552$ chips. The minimum spacing between non-zero spreading code pulses of the LA code becomes $M_A = 136$ chip durations, which is equal to the length of the constituent LS code based on Equation 10 in [220]. The number of non-zero pulses is $K_A = 17$ based on Figure 1 in [218], the length of the complementary code used in the generation of the LS code is $N = 4$ [220], the dimension of the WH matrix used for generating the LS

code is $P = 32$ [220] and the number of zeros at the beginning and in the center of the complementary code pair is $W_0 = 4$ [220]. Hence such a LAS code exhibits an IFW length of $[-\iota, \iota]$, where we have $\iota = \min\{W_0, N-1\} = 3$. The corresponding spreading gain becomes $G = \frac{L_A}{K_A} = 151$.

For the sake of a fair comparison we would need both WH and OG codes having a length of $L = 151$ chips. However, no such codes exist, and the most similar ones are those having a length of $L = 128$ and $L = 256$ chips.

If the LAS DS-CDMA system considered is asynchronous, i.e. if $\tau_k - \tau_q$ is uniformly distributed in $[0, LT_c)$, Equations 4.20 and 4.37 can be simplified, when a rectangular chip waveform is used as follows (see Appendix C for details):

$$\sigma^2_{(M)qi} = PT_c^2 h_{qi}^2 \sum_{\substack{k=1 \\ k\neq q}}^{K} \sum_{l=0}^{L_p-1} \Omega_{k0} e^{-\eta l} \frac{1}{L} \sum_{j=0}^{L-1} \left[\frac{1}{3}\omega_1(\zeta) + \omega_2(\zeta) + \omega_3(\zeta) \right], \tag{4.39}$$

$$\Upsilon_M(i) = \sum_{\substack{k=1 \\ k\neq q}}^{K} \sum_{l=0}^{L_p-1} \frac{\Omega_{k0}}{\Omega_{q0}} e^{-\eta l} \frac{1}{L} \sum_{j=0}^{L-1} \left[\frac{1}{3}\omega_1(\zeta) + \omega_2(\zeta) + \omega_3(\zeta) \right]. \tag{4.40}$$

All the other system parameters remain the same as those in quasi-synchronous LAS DS-CDMA.

When considering asynchronous DS-CDMA using random sequences, the random signature sequences have a zero off-peak auto-correlation and cross-correlation, hence based on Equation 4.17, 4.20 and 4.35 we have:

$$\sigma^2_{(S)qi} = PLT_c^2 h_{qi}^2 \left[g(L_p, \eta) - e^{-\eta i} \right] \Omega_{q0}, \tag{4.41}$$

$$\sigma^2_{(M)qi} = \frac{2}{3} PLT_c^2 h_{qi}^2 g(L_p, \eta) \sum_{\substack{k=1 \\ k\neq q}}^{K} \Omega_{k0}, \tag{4.42}$$

$$\gamma_c(i) = \left[\frac{g(L_p, \eta) - e^{-\eta i}}{L} + \frac{2g(L_p, \eta)}{3L} \sum_{(u,v)\neq(0,0),(0,1)} (u^2 + v^2)^{-\frac{\alpha}{2}} + \frac{1}{\gamma_{\mathrm{SNR}}} \right]^{-1}, \tag{4.43}$$

where

$$g(L_p, \eta) = \sum_{l=0}^{L_p-1} e^{-\eta l} = \frac{1 - e^{-\eta L_p}}{1 - e^{-\eta}}. \tag{4.44}$$

SNR (dB)	$\gamma_{\text{SNR}} = \infty$
Chip duration (μs)	$T_c = 1.0$
Minimum distance (light speed $\times$ T_c)	$d = 0.1$
Maximum propagation delay (T_c)	$\tau_{max} = 2$
Total number of resolvable paths	$L_p = 4$
Total number of RAKE branches	$L_r = 3$
IFW width	$\iota = 3$
Path loss exponent	$\alpha = 4.0$
Rate of average power decay	$\eta = 0.2$
Nakagami-m fading parameter	$m = 1.0$

TABLE 4.1: The parameters used for the comparative simulations between quasi-synchronous LAS DS-CDMA, quasi-synchronous DS-CDMA using Walsh-Hadamard and Orthogonal Gold codes, asynchronous LAS DS-CDMA, asynchronous DS-CDMA using random signature sequences.

For the sake of fair comparability, when considering asynchronous DS-CDMA using random sequences, we assume that the spreading gain of the random signature sequences is the same as that of the LAS-CDMA 2000 codes, namely $G = 151$, which is also equal to the length L of the random signature sequences.

For the sake of fair comparability, when considering asynchronous DS-CDMA using random sequences, we assume that the spreading gain of the random signature sequences is the same as that of the LAS-CDMA 2000 codes, namely $G = 151$, which is also equal to the length L of the random signature sequences.

4.4.2 Numerical Results

The system parameters used in our investigations are listed in Table 4.1, unless otherwise stated. The effects of the received per-bit SNR γ_{SNR}, the maximum propagation delay τ_{max}, the total number of resolvable paths L_p, the total number of RAKE receiver branches L_r and the Nakagami-m parameter m are characterized in Figures 4.2 - 4.9, respectively.

The effects of the received per-bit SNR γ_{SNR}

Figure 4.2 shows that the BERs of all the systems considered decrease, as the SNR increases. This can be readily seen from Equation 4.35, where $P_b(\gamma)$ is a monotonically decreasing function of γ_{SNR}. However, it may also be concluded from Equation 4.35 that increasing the transmitted power is only capable of mitigating the effects of the

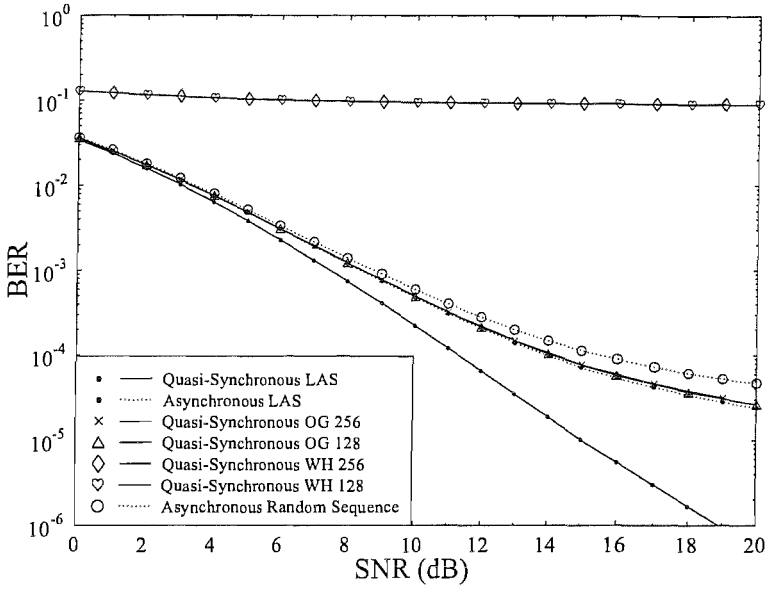

FIGURE 4.2: BER versus the received per-bit SNR γ_{SNR}. All nodes are assumed to transmit with a probability of 0.5 at the same power level P_t. An infinite number of nodes are placed on a simple infinite rectilinear grid, with the minimum distance between adjacent nodes $d = 30$ meters. The maximum propagation delay is $\tau_{max} = 2T_c$. The total number of resolvable paths is $L_p = 4$, and the RAKE receiver combines $L_r = 3$ paths. The IFW width is $\iota = 3$. The rate of average negative exponential power decay is $\eta = 0.2$. The Nakagami-m fading parameter is $m = 1.0$. The pathloss exponent is $\alpha = 4.0$. These results were evaluated from Equation 4.34.

background noise, but not of the MPI or MAI. This is the reason that increasing the transmitted power substantially improves the achievable BER performance of the quasi-synchronous LAS DS-CDMA system. The quasi-synchronous DS-CDMA systems using both 256-chip and 128-chip WH codes exhibit a poor performance owing to their high auto-correlation function side-lobes. The quasi-synchronous DS-CDMA systems using 256-chip and 128-chip Orthogonal Gold (OG) codes exhibit a moderate performance owing to their good correlation properties. Since the performance of quasi-synchronous DS-CDMA systems is mainly determined by the correlation values near $\xi = 0$ between the spreading sequences used by the desired node and interferers, and there are several cross-correlation values at $\xi = 0$ in OG codes, which are in proportion to their spreading gain. This is the reason that the quasi-synchronous DS-CDMA systems using 256-chip and 128-chip OG codes exhibit almost the same performance. The asynchronous LAS DS-CDMA system performs slightly better than the asynchronous DS-CDMA system using random sequences, as a consequence of its lower MPI resulting from its IFW, given the parameters of $L_p = 4$ and $\iota = 3$. The quasi-synchronous LAS DS-CDMA system performs best, since its IFW cancels most of the MPI, given the parameters of $L_p = 4$

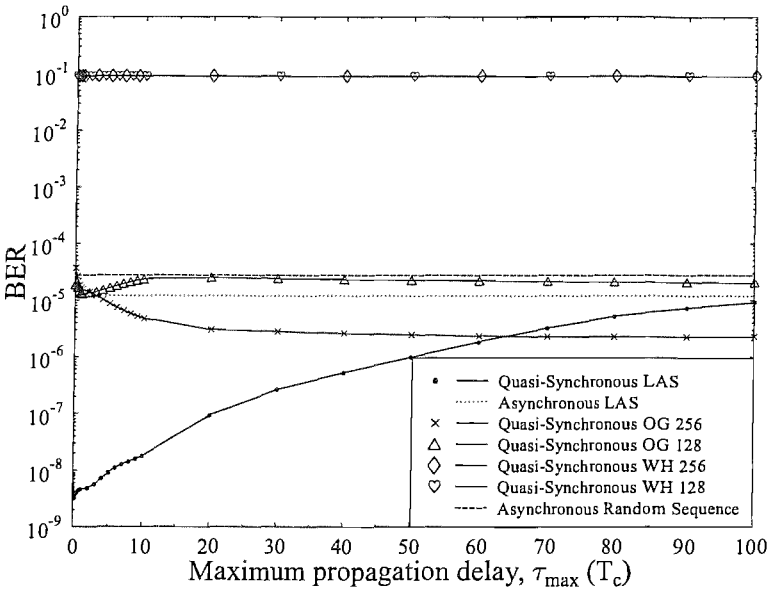

FIGURE 4.3: BER versus the maximum propagation delay τ_{max} expressed in terms of the chip duration T_c. All nodes are assumed to transmit with a probability of 0.5 at the same power level P_t. An infinite number of nodes are placed on a simple infinite rectilinear grid, with the minimum distance between adjacent nodes $d = 30$ meters. The maximum propagation delay is $\tau_{max} = 2T_c$. The total number of resolvable paths is $L_p = 4$, and the RAKE receiver combines $L_r = 3$ paths. The IFW width is $\iota = 3$. The rate of average negative exponential power decay is $\eta = 0.2$. The Nakagami-m fading parameter is $m = 1.0$. The pathloss exponent is $\alpha = 4.0$. These results were evaluated from Equation 4.34.

and $\iota = 3$. Hence the quasi-synchronous LAS DS-CDMA system becomes essentially noise-limited, rather than interference-limited, which is also the reason that it benefits most from increasing the transmitted power.

The effects of the maximum propagation delay τ_{max}

In order to demonstrate the capability of LAS codes for mitigating MPI and MAI, we let $\gamma_{SNR} \rightarrow \infty$ in Figure 4.3. Figure 4.3 shows that the attainable BER performance of the quasi-synchronous LAS DS-CDMA system decreases roughly, as the maximum propagation delay increases, since the effects of less accurate synchronization inflict a higher MAI. Even the asynchronous LAS DS-CDMA system performs slightly better than the asynchronous DS-CDMA arrangement using random sequences, since most of the MPI is eliminated in the asynchronous LAS DS-CDMA scheme, given the parameters of $L_p = 4$ and $\iota = 3$. The maximum propagation delay has a marginal effect on the quasi-synchronous DS-CDMA scheme using WH codes and the system having a higher

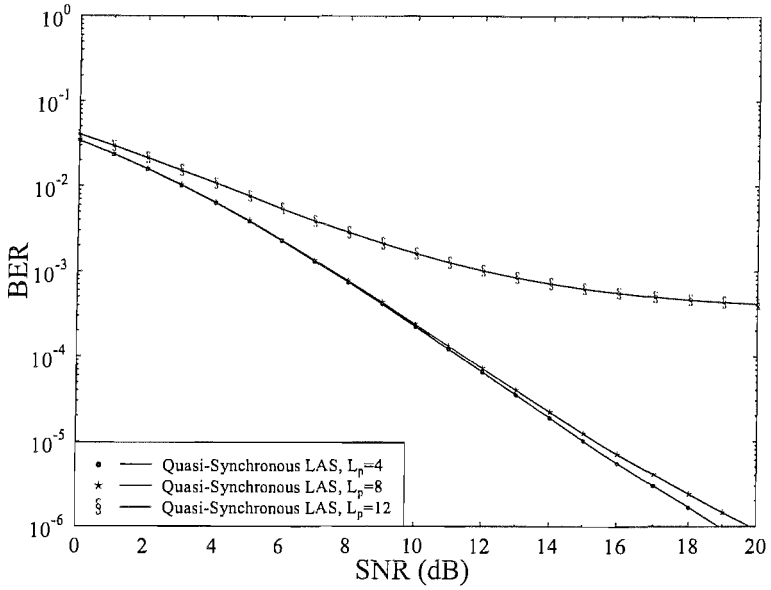

FIGURE 4.4: BER versus the received per-bit SNR γ_{SNR}. All nodes are assumed to transmit with a probability of 0.5 at the same power level P_t. An infinite number of nodes are placed on a simple infinite rectilinear grid, with the minimum distance between adjacent nodes $d = 30$ meters. The maximum propagation delay is $\tau_{max} = 2T_c$. The total number of resolvable paths is $L_p = 4, 8$ and 12, respectively, and the RAKE receiver combines $L_r = 3$ paths. The IFW width is $\iota = 3$. The rate of average negative exponential power decay is $\eta = 0.2$. The Nakagami-m fading parameter is $m = 1.0$. The pathloss exponent is $\alpha = 4.0$. These results were evaluated from Equation 4.34.

spreading gain has almost no advantages, since the MPI dominates the achievable performance, as it can be concluded from the associated auto-correlation and cross-correlation functions. The quasi-synchronous system using 256-chip OG codes performs best at a large maximum propagation delay, mainly as a consequence of its higher spreading gain and LAS codes' high side-lobes outside the IFW.

The effects of the total number of resolvable paths L_p

Figures 4.4 and 4.5 show that the BER versus SNR performance of the quasi-synchronous LAS DS-CDMA ad hoc nodes decreases, as the total number of resolvable paths increases and $L_r = 3$ of these components are combined by the RAKE receiver, since more paths will be located outside the IFW. Hence, when L_p is high, LAS DS-CDMA inevitably encounters serious MPI and MAI. There is a large BER discrepancy between $L_p = 8$ and $L_p = 12$, because there are very high auto-correlation side-lobes at $\xi = \pm 8$ outside the IFW.

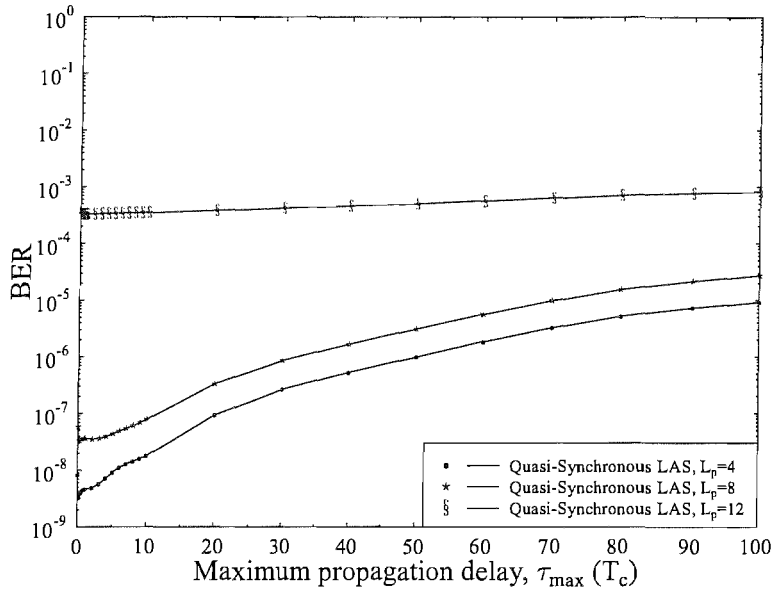

FIGURE 4.5: BER versus the maximum propagation delay τ_{max} expressed in terms of the chip duration T_c. All nodes are assumed to transmit with a probability of 0.5 at the same power level P_t. An infinite number of nodes are placed on a simple infinite rectilinear grid, with the minimum distance between adjacent nodes $d = 30$ meters. The maximum propagation delay is $\tau_{max} = 2T_c$. The total number of resolvable paths is $L_p = 4, 8$ and 12, respectively, and the RAKE receiver combines $L_r = 3$ paths. The IFW width is $\iota = 3$. The rate of average negative exponential power decay is $\eta = 0.2$. The Nakagami-m fading parameter is $m = 1.0$. The pathloss exponent is $\alpha = 4.0$. These results were evaluated from Equation 4.34.

The effects of the total number of RAKE receiver branches L_r

Figures 4.6 and 4.7 show that increasing the total number of RAKE receiver branches is capable of dramatically improving the performance of the quasi-synchronous LAS DS-CDMA system, when the total number of resolvable paths is assumed to be $L_p = 4$. This performance improvement is attributed to the RAKE receiver, which benefits from the associated time-diversity.

The effects of the Nakagami-m parameter

Figures 4.8 and 4.9 demonstrate that the quasi-synchronous LAS DS-CDMA system suffering from less severe fading in the presence of a higher Nakagami-m parameter performs better. This can be concluded from Equation 4.34 by letting $m_i = m$. Since

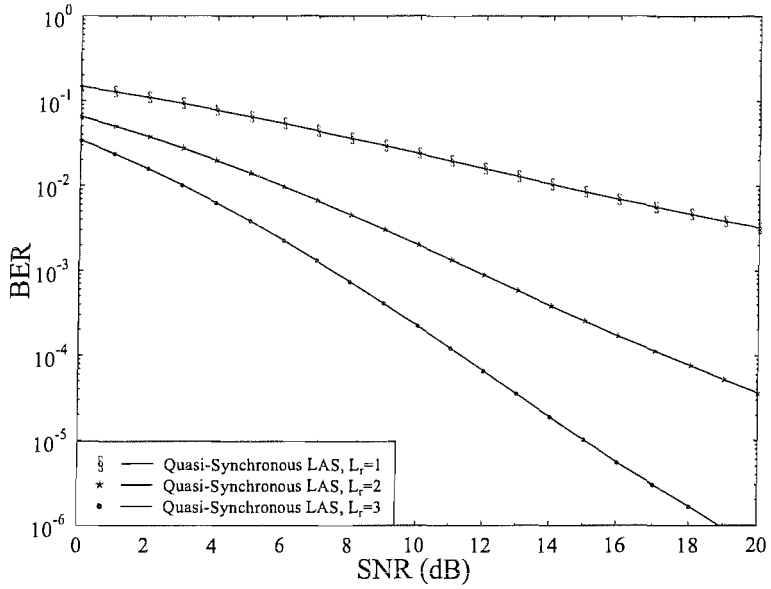

FIGURE 4.6: BER versus the received per-bit SNR γ_{SNR}. All nodes are assumed to transmit with a probability of 0.5 at the same power level P_t. An infinite number of nodes are placed on a simple infinite rectilinear grid, with the minimum distance between adjacent nodes $d = 30$ meters. The maximum propagation delay is $\tau_{max} = 2T_c$. The total number of resolvable paths is $L_p = 4$, and the RAKE receiver combines $L_r = 1, 2$ and 3 paths, respectively. The IFW width is $\iota = 3$. The rate of average negative exponential power decay is $\eta = 0.2$. The Nakagami-m fading parameter is $m = 1.0$. The pathloss exponent is $\alpha = 4.0$. These results were evaluated from Equation 4.34.

$\frac{x}{1+x} - \ln(1+x) \leq 0$ when $x \geq 0$ and $\frac{m\sin^2\theta}{\bar{\gamma}_i + m\sin^2\theta} \geq 0$, we have

$$\begin{aligned}
&\frac{\partial P_b(\gamma)}{\partial m} \\
&= \frac{1}{\pi}\int_0^{\frac{\pi}{2}} \sum_{j=0}^{L_r-1} \left[\frac{\bar{\gamma}_j}{\bar{\gamma}_j + m\sin^2\theta} - \ln\left(1 + \frac{\bar{\gamma}_j}{m\sin^2\theta}\right)\right] \prod_{i=0}^{L_r-1} \left(\frac{m\sin^2\theta}{\bar{\gamma}_i + m\sin^2\theta}\right)^m \mathrm{d}\theta \\
&\leq 0. \qquad (4.45)
\end{aligned}$$

More explicitly, we model a Rayleigh fading channel as $m = 1$, while $m \to \infty$ corresponds to an AWGN channel.

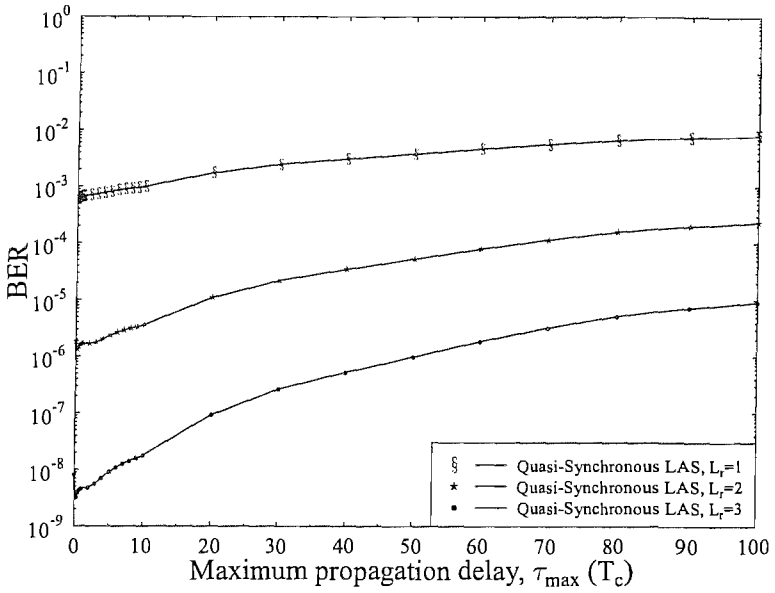

FIGURE 4.7: BER versus the maximum propagation delay τ_{max} expressed in terms of the chip duration T_c. All nodes are assumed to transmit with a probability of 0.5 at the same power level P_t. An infinite number of nodes are placed on a simple infinite rectilinear grid, with the minimum distance between adjacent nodes $d = 30$ meters. The maximum propagation delay is $\tau_{max} = 2T_c$. The total number of resolvable paths is $L_p = 4$, and the RAKE receiver combines $L_r = 1, 2$ and 3 paths, respectively. The IFW width is $\iota = 3$. The rate of average negative exponential power decay is $\eta = 0.2$. The Nakagami-m fading parameter is $m = 1.0$. The pathloss exponent is $\alpha = 4.0$. These results were evaluated from Equation 4.34.

4.5 Conclusion

In conclusion, LAS DS-CDMA was investigated in the context of an ad hoc network obeying an infinite rectilinear mesh topology. The system exhibits a significantly better performance than the family of traditional spreading sequences used in a quasi-synchronous DS-CDMA scenario having a low number of resolvable multipath components and a sufficiently high number of RAKE receiver branches. All these parameters are related to the chip rate. As the chip rate increases, the node density expressed in terms of the normalized distance travelled by the radio waves within a chip duration increases, while the total number of resolvable paths decreases, which therefore requires a low number of RAKE receiver branches. Hence, LAS DS-CDMA benefits from having a low chip rate. We may adjust the chip rate to correspond to the channel's coherence bandwidth, which avoids encountering frequency non-selective fading that would result in having no multipath diversity. If a high bit rate is required, multicarrier LAS DS-CDMA might be invoked for the sake of providing low-chip-rate parallel transmissions mapped to several

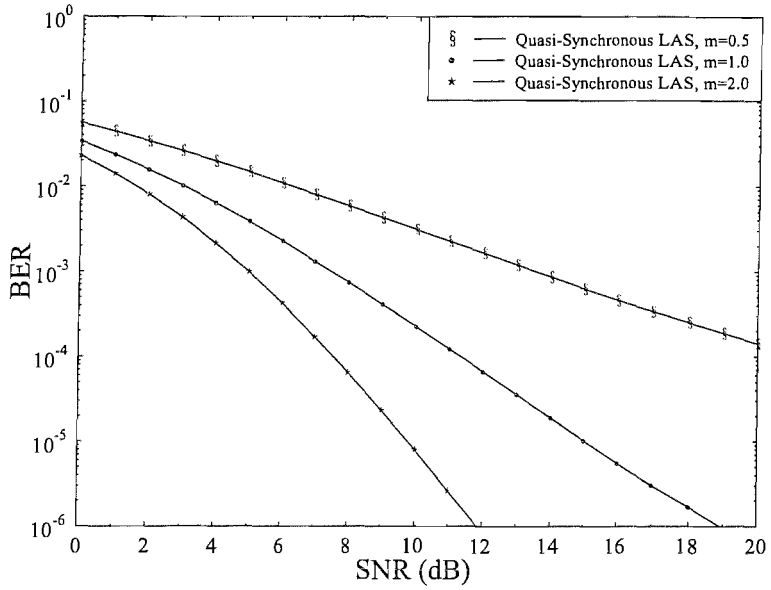

FIGURE 4.8: BER versus the received per-bit SNR γ_{SNR}. All nodes are assumed to transmit with a probability of 0.5 at the same power level P_t. An infinite nodes are placed on a simple infinite rectilinear grid, with the minimum distance between adjacent nodes $d = 30$ meters. The maximum propagation delay is $\tau_{max} = 2T_c$. The total number of resolvable paths is $L_p = 4$, and the RAKE receiver combines $L_r = 3$ paths. The IFW width is $\iota = 3$. The rate of average negative exponential power decay is $\eta = 0.2$. The Nakagami-m fading parameter is $m = 0.5, 1.0$ and 2.0, respectively. The pathloss exponent is $\alpha = 4.0$. These results were evaluated from Equation 4.34.

parallel subcarriers, which has however the following disadvantage. The number of resolvable multipath components is reduced proportionately to the number of subcarriers used, which reduces the maximum achievable diversity gain, although it has the benefit of proportionately extending the IFW width and hence the maximum cell-size, where interference-free communications are achievable.

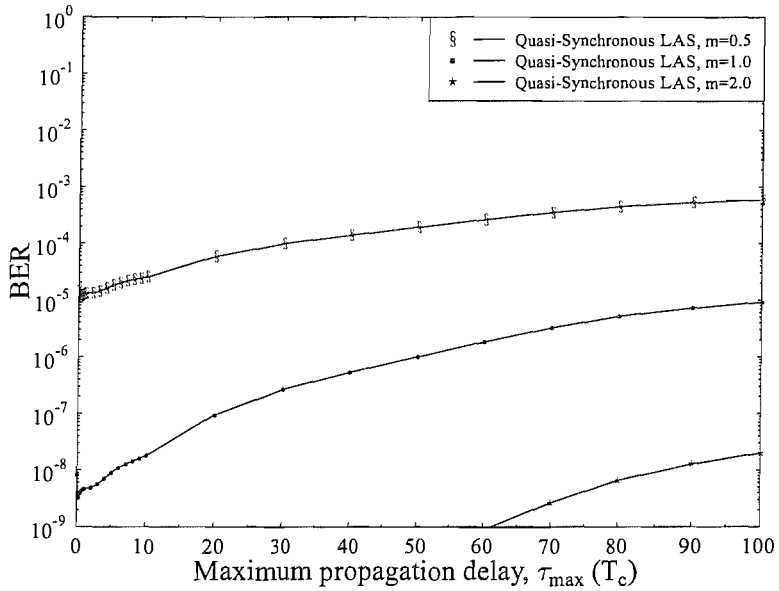

FIGURE 4.9: BER versus the maximum propagation delay τ_{max} expressed in terms of the chip duration T_c. All nodes are assumed to transmit with a probability of 0.5 at the same power level P_t. An infinite number of nodes are placed on a simple infinite rectilinear grid, with the minimum distance between adjacent nodes $d = 0.1$speed of light $\times T_c$. The maximum propagation delay is $\tau_{max} = 2T_c$. The total number of resolvable paths is $L_p = 4$, and the RAKE receiver combines $L_r = 3$ paths. The IFW width is $\iota = 3$. The rate of average negative exponential power decay is $\eta = 0.2$. The Nakagami-m fading parameter is $m = 0.5, 1.0$ and 2.0, respectively. The pathloss exponent is $\alpha = 4.0$. These results were evaluated from Equation 4.34.

Chapter 5

A Unified Exact BER Performance Analysis of Asynchronous DS-CDMA Systems Using BPSK Modulation over Flat Fading Channels

5.1 Introduction

CDMA has been one of the most successful radio access techniques since the 1990s and Direct Sequence (DS) CDMA has been integrated into the third generation mobile systems. The Bit Error Ratio (BER) is one of the most important performance metric in communication systems and hence it has been extensively studied in various DS-CDMA systems.

For the sake of computational simplicity, the most widely used approach of calculating the average BER of DS-CDMA systems is assuming that the Multiple Access Interference (MAI) is Gaussian distributed or conditional Gaussian distributed based on the Central Limit Theorem (CLT). Various Gaussian approximation techniques have been proposed, such as the Standard Gaussian Approximation (SGA) [208, 226–228, 238–247], the Improved Gaussian Approximation (IGA) [208, 239, 241, 242, 244, 245, 247–249], the Simplified IGA (SIGA) [208, 239, 241, 243, 245, 247], as well as the Improved Holtzman

Gaussian Approximation (IHGA) [243]. However, the accuracy of the various Gaussian approximation techniques depends on the specific configuration of the system. It is well known that the Gaussian approximation techniques become less accurate, when a low number of users is supported or when there is a dominant interferer [244].

Therefore the exact BER analysis dispensing with the previous assumptions on the MAI distribution is desirable. The exact BER performance of a system can be evaluated by typically integrating, i.e. averaging the generic BER formula over all random parameters of all users, but this requires the evaluation of multiple integrals [246], which is irrealistic when the number of users is high. Hence several exact BER evaluation techniques have also been developed without assuming a Gaussian MAI distribution, such as the series expansion [244, 245, 250–252], or the Fourier [208, 238, 243, 247, 250] and the Laplace [253] transform based methods. The latter two lead to the Characteristic Function (CF) and Moment Generating Function (MGF) based approaches and have been prevalent in the exact BER analysis of communication systems. These techniques typically achieve more accurate BER evaluation at the cost of a high computation complexity.

In the existing literature, most results are reported for the BERs of DS-CDMA systems communicating over Additive White Gaussian Noise (AWGN) channels [227–229, 239–242, 244, 245, 247, 248, 250–252, 254–257], and a few studies also considered Rayleigh channels [208, 244] as well as Nakagami-m channels [226, 238, 243, 249, 253]. Geraniotis and Pursley [250] were the first authors, who investigated the exact BER calculation of asynchronous DS-CDMA systems over AWGN channels using the CF approach. Then Cheng and Beaulieu extended the results to both Rayleigh [208] and Nakagami-m [238] channels. However, the results of [238] only apply to Nakagami-m fading associated with an integer fading parameter m.

The novel contribution of this chapter is that we provide a unified exact BER performance analysis of asynchronous DS-CDMA systems using BPSK modulation for transmissions over Rayleigh, Ricean, Hoyt and Nakagami-m flat fading channels. This chapter is organized as follows. In Section 5.2 the Rayleigh, Ricean, Hoyt and Nakagami-m fading channels are summarized. In Section 5.3 a general asynchronous DS-CDMA system using BPSK modulation and communicating over flat fading channels is presented. Then, in Section 5.4 its exact BER performance using random spreading sequences is investigated and in Section 5.5 our MAI analysis is performed based on the CF approach in the context of various fading channels. Our numerical results are presented in Section 5.6 and finally our conclusions are provided in Section 5.7.

5.2 Fading Channels

We consider a range of different fading channels in our analysis, namely the Rayleigh, Ricean, Hoyt and Nakagami-m channels. Note that a table of the corresponding fading PDFs and CFs has been given in [258]. We provide two new closed-form expressions for the CFs of the Ricean and Hoyt fading, respectively, rather than in the form of the sum of infinite series, as given by Table II of [258]. Furthermore, we present some important properties of different fading channels, when both the fading amplitude and the fading phase are considered.

The fading is characterized by the complex-valued random variable $\widetilde{h} = he^{j\varphi}$, where h and φ are the fading amplitude and phase, respectively. For the sake of simplifying our analysis, we also use an alternative expression of the fading variable, i.e. $\widetilde{h} = h_r + jh_i$, where h_r and h_i are the real and imaginary part, respectively.

5.2.1 Rayleigh Channels

The Rayleigh distribution has been widely used for modeling radio channels, where there is no Line-Of-Sight (LOS) propagation paths between the transmitter and the receiver [230]. If a complex-valued variable $\widetilde{h}$ is Rayleigh distributed, the PDF and CF of its modulus h are given by [258]:

$$f_h(x) = \frac{x}{\sigma^2}\exp\left(-\frac{x^2}{2\sigma^2}\right), x \geq 0, \tag{5.1}$$

$$\Phi_h(\omega) = {}_1\mathbb{F}_1\left(1;\frac{1}{2};-\frac{1}{2}\sigma^2\omega^2\right) + j\sigma\omega\sqrt{\frac{\pi}{2}}\exp\left(-\frac{1}{2}\sigma^2\omega^2\right), \tag{5.2}$$

where we have $\sigma > 0$ and $\Omega = 2\sigma^2$ is the average fading power, and ${}_1\mathbb{F}_1(\alpha;\beta;x)$ is the confluent hypergeometric function [259].

The phase φ of a Rayleigh variable is uniformly distributed over $[0, 2\pi)$ and independent of the fading amplitude h [260]. The PDF of the Rayleigh fading phase is given by:

$$f_\varphi(x) = \frac{1}{2\pi}, x \in [0, 2\pi). \tag{5.3}$$

One of the important properties of the complex-valued Rayleigh variable is that its real and imaginary parts, i.e. h_r and h_i, are mutually independent, zero-mean and real-valued Gaussian variables, both having a variance of σ^2 [261, 262]. This property is exploited, when generating Rayleigh distributed variables in this dissertation.

5.2.2 Ricean or Nakagami-n Channels

The Ricean distribution is also known as the Nakagami-n distribution [263, 264] and has been frequently used for modeling radio channels where there exists a LOS propagation path between the transmitter and the receiver, such as microcellular urban and suburban land mobile, as well as picocellular indoor and factory scenarios [230]. The Ricean fading process physically consists of a direct LOS component having a power of μ^2 and many weaker components having a total power of $2\sigma^2$. Hence the PDF and CF of the Ricean fading amplitude h are given by [258, 264]:

$$f_h(x) = \frac{x}{\sigma^2} \exp\left(-\frac{x^2+\mu^2}{2\sigma^2}\right) \mathbb{I}_0\left(\frac{x\mu}{\sigma^2}\right), x \geq 0, \tag{5.4}$$

$$\begin{aligned}\Phi_h(\omega) = &\exp\left(-\frac{\mu^2}{2\sigma^2}\right) \Psi_2\left(1; 1, \frac{1}{2}; \frac{\mu^2}{2\sigma^2}, -\frac{1}{2}\sigma^2\omega^2\right) \\ &+ j\sqrt{2}\sigma\omega \exp\left(-\frac{\mu^2}{2\sigma^2}\right) \Psi_2\left(\frac{3}{2}; 1, \frac{3}{2}; \frac{\mu^2}{2\sigma^2}, -\frac{1}{2}\sigma^2\omega^2\right),\end{aligned} \tag{5.5}$$

where we have $\mu \geq 0$ and $\sigma > 0$, $\Omega = \mu^2 + 2\sigma^2$ is the average fading power, $\mathbb{I}_0(x)$ is the zeroth-order modified Bessel function of the first kind [259] and $\Psi_2(\alpha; \gamma, \gamma'; x, y)$ is one of Horn's confluent hypergeometric functions of two variables [265, 266]. Equation 5.5 provides a closed-form expression for the CF of the Ricean fading amplitude, which is equivalent to the formula given by Table II of [258], but here it is represented in its more compact form, rather than as a sum of infinite series. Another alternative expression of the PDF of the Ricean fading amplitude is also often used [230, 258]. The Ricean K-factor is defined as:

$$\kappa = \frac{\mu^2}{2\sigma^2}. \tag{5.6}$$

The Ricean fading describes a range of channels, spanning from Rayleigh fading, associated with $\kappa = 0$, to no fading, when we have $\kappa = \infty$ [230].

The Ricean phase φ is neither uniformly distributed nor independent of the fading amplitude h [264]. Since it is not directly relevant to our analysis, we do not present the marginal PDF of the Ricean fading phase φ or the joint PDF of the Ricean fading amplitude h and the Ricean fading phase φ. However, these two PDFs may be readily

derived by capitalizing on the specific property of the Ricean distribution, that its real and imaginary parts, i.e. h_r and h_i, are mutually independent Gaussian variables [264]. The mean and variance of h_r and h_i are $\{\mu_r, \sigma^2\}$ and $\{\mu_i, \sigma^2\}$, respectively, where we have $\mu_r^2 + \mu_i^2 = \mu^2$. This property is exploited, when generating Ricean variables in this dissertation.

5.2.3 Hoyt or Nakagami-q Channels

The Hoyt distribution is also known as the Nakagami-q distribution [263, 267] and was originally used for modeling radio channels subject to strong ionospheric scintillation, such as satellite links [230, 268]. Recently, it has been used more frequently as one of the important models for the statistical description of fading mobile radio channels [230, 258]. The PDF and CF of the Hoyt fading amplitude h are given by [258]:

$$f_h(x) = \frac{(1+q^2)x}{q\Omega} \exp\left[-\frac{(1+q^2)x^2}{4q^2\Omega}\right] \mathbb{I}_0\left[\frac{(1-q^4)x^2}{4q^2\Omega}\right], x \geq 0, \tag{5.7}$$

$$\begin{aligned}\Phi_h(\omega) = &\frac{2q}{1+q^2}\mathbb{H}_7\left[1; 1, \frac{1}{2}; \frac{(1-q^2)^2}{4(1+q^2)^2}, -\frac{q^2\Omega}{(1+q^2)^2}\omega^2\right] \\ &+ j\frac{2q^2\sqrt{\pi\Omega}}{(1+q^2)^2}\omega\mathbb{H}_7\left[\frac{3}{2}; 1, \frac{3}{2}; \frac{(1-q^2)^2}{4(1+q^2)^2}, -\frac{q^2\Omega}{(1+q^2)^2}\omega^2\right],\end{aligned} \tag{5.8}$$

where $\Omega > 0$ is the average power and $\mathbb{H}_7(\alpha, \gamma, \delta, x, y)$ is one of Horn's confluent hypergeometric functions of two variables [265]. Equation 5.8 provides a closed-form expression for the CF of the Hoyt fading amplitude, which is equivalent to the formula given by Table II of [258], but here it is represented in its more compact form, rather than as a sum of infinite series. Another alternative expression of the PDF of the Hoyt fading amplitude is also often used [263]. The Hoyt fading includes channels spanning from the one-sided Gaussian fading, associated with $q = 0$, to the Rayleigh fading, having $q = 1$ [230].

Similar to the Ricean fading, the Hoyt fading phase φ is neither uniform distributed nor independent of the fading amplitude h [267]. Again, since it is not directly relevant to our analysis, we do not present here the marginal PDF of the Hoyt fading phase φ or the joint PDF of the Hoyt fading amplitude h and the Hoyt fading phase φ. However, these two PDFs may be readily derived by exploiting the specific property of the Hoyt distribution, that its real and imaginary parts, i.e. h_r and h_i, are mutually independent zero-mean Gaussian variables having a variance of σ_r^2 and σ_i^2, respectively [267], which

satisfy:

$$\Omega = \sigma_r^2 + \sigma_i^2, \tag{5.9}$$

$$q = \frac{\sigma_i}{\sigma_r}. \tag{5.10}$$

This property is exploited, when generating Hoyt distributed variables in this dissertation.

5.2.4 Nakagami-m Channels

The Nakagami-m distribution is a versatile statistical distribution which is capable of modelling a variety of fading environments, such as land mobile, as well as indoor mobile multipath propagation channels and ionospheric radio links [230]. The PDF and CF of the Nakagami-m fading amplitude h are given by [258]:

$$f_h(x) = \frac{2}{\Gamma(m)} \left(\frac{m}{\Omega}\right)^m x^{2m-1} \exp\left(-\frac{m}{\Omega}x^2\right), x \geq 0, \tag{5.11}$$

$$\begin{aligned}\Phi_h(\omega) = {}& {}_1\mathbb{F}_1\left(m; \frac{1}{2}; -\frac{\Omega}{4m}\omega^2\right) \\ & + j\omega \frac{\Gamma(m+\frac{1}{2})}{\Gamma(m)} \sqrt{\frac{\Omega}{m}} {}_1\mathbb{F}_1\left(m+\frac{1}{2}; \frac{3}{2}; -\frac{\Omega}{4m}\omega^2\right),\end{aligned} \tag{5.12}$$

where $\Omega > 0$ is the average power, $m \geq \frac{1}{2}$ is the Nakagami-m fading parameter and $\Gamma(x)$ is the Gamma function [259]. The Nakagami-m fading family includes channels as diverse, as the one-sided Gaussian fading associated with $m = \frac{1}{2}$, the Rayleigh fading, having $m = 1$, and no fading, corresponding to $m = \infty$ [230]. Since it is difficult to generate arbitrary Nakagami-m fading profiles, only some well-known special cases are considered in our simulations in this dissertation, such as integer values of $2m$. When $2m$ is an integer, a Nakagami-m variable may be generated from the square root of the sum of $2m$ independent Gaussian variables [207].

The distribution of the Nakagami-m fading phase φ is still unknown at the time of writing, but typically it is assumed to be uniform over $[0, 2\pi)$ [263].

5.3 System Model and Assumptions

We consider a general asynchronous BPSK modulated DS-CDMA system communicating over fading channels mentioned in Section 5.2. There are K simultaneously transmitting users in the system. Binary random spreading sequences having L chips and a rectangular chip waveform are employed.

The rectangular pulse having a duration of T is defined as:

$$p_T(t) = \begin{cases} 1, t \in [0, T), \\ 0, \text{otherwise.} \end{cases} \tag{5.13}$$

Hence the kth user's spreading signal $a_k(t)$ and data signal $b_k(t)$ can be expressed as:

$$a_k(t) = \sum_{m=-\infty}^{\infty} a_{k,m} p_{T_c}(t - mT_c), \tag{5.14}$$

$$b_k(t) = \sum_{m=-\infty}^{\infty} b_{k,m} p_{T_s}(t - mT_s), \tag{5.15}$$

where T_c and T_s are the chip and bit duration, respectively, satisfying $T_s = LT_c$. Both the spreading sequence $\{a_{k,m}\}_{m=0}^{L-1}$ and the data sequence $\{b_{k,m}\}_{m=-\infty}^{\infty}$ are mutually independent and symmetrically Bernoulli distributed [260], implying that we have $P\{a_{k,m} = \pm 1\} = P\{b_{k,m} = \pm 1\} = \frac{1}{2}$.

The received signal at the input of the coherent receiver is given by:

$$r(t) = \Re\left\{\sum_{k=0}^{K} \widetilde{h}_k a_k(t - \tau_k) b_k(t - \tau_k) e^{j[\omega_c(t-\tau_k)+\theta_k]}\right\} + \eta(t), \tag{5.16}$$

where $\Re\{\widetilde{x}\}$ denotes the real part of the complex number $\widetilde{x}$. Furthermore, the received complex equivalent signals $\{\widetilde{h}_k\}_{k=0}^{K-1}$ are mutually independent and conforms to one of the fading distributions mentioned in Section 5.2 with their average fading power $\{\Omega_k\}_{k=0}^{K-1}$. The carrier's angular frequency ω_c is common to all users, while the carrier phase shift $\{\theta_k\}_{k=0}^{K-1}$ and the time delay $\{\tau_k\}_{k=0}^{K-1}$ are independently and uniformly distributed in $[0, 2\pi)$ and $[0, T_s)$, respectively. Finally, $\eta(t)$ is the zero-mean stationary Additive White Gaussian Noise (AWGN) having a double-sided power spectral density of $\frac{N_0}{2}$. Hence the SNR of the received signal is $\frac{\Omega_0 LT_c}{N_0}$.

Without loss of generality, we assume that the 0th user's signal is the desired one. If both the chip synchronization and the phase estimation are perfect, the decision statistic

at the output of the coherent receiver is given by:

$$Z = h_0 L b_{0,0} + \sum_{k=1}^{K-1} \Re\left\{X_k \tilde{h}_k e^{j\Delta_k}\right\} + \eta, \tag{5.17}$$

where the noise component η is a zero-mean Gaussian random variable having a variance of $\sigma_\eta^2 = \frac{N_0 L}{T_c}$, while the phase shift difference $\Delta_k = -\omega_c(\tau_k - \tau_0) + (\theta_k - \theta_0)$ between the kth and 0th user is uniformly distributed in $[0, 2\pi)$[1]. The random variable X_k may be further expressed as [208, 228]:

$$X_k = \sum_{m=0}^{L-2} Y_{k,m}\left[(1-\nu_k) + a_{0,m}a_{0,m+1}\nu_k\right] + Y_{k,L-1}\nu_k + Y_{k,L}(1-\nu_k), \tag{5.18}$$

where the $(L+1)$ random variables $\{Y_{k,m}\}_{m=0}^{L}$ are mutually independent and symmetric Bernoulli distributed, conditioned on the 0th user's spreading sequence $\{a_{0,m}\}_{m=0}^{L-1}$. Furthermore, the relative chip shifts $\{\nu_k\}_{k=1}^{K-1}$ between the kth and 0th user normalized by the chip duration are mutually independent and uniformly distributed in $[0, 1)$ [208, 228].

5.4 BER Analysis

Let B and A denote the number of chip boundaries both with and without chip-value transitions within the 0th user's spreading sequence, respectively, and define two sets $\mathcal{A}$ and $\mathcal{B}$ as follows [208, 228]:

$$\begin{aligned} \mathcal{A} &= \{-A, -(A-2), ..., A-2, A\}, \\ \mathcal{B} &= \{-B, -(B-2), ..., B-2, B\}. \end{aligned} \tag{5.19}$$

Then we have $A + B = L - 1$.

Upon defining the Co-Channel Interference (CCI), $I_k = \Re\left\{X_k \tilde{h}_k e^{j\Delta_k}\right\}$, incurred by the kth user, the CCIs imposed by different interferers are mutually independent conditioned on B [208, 228]. It transpires that both the PDF, $f_{I_k|B}(x)$, and CF, $\Phi_{I_k|B}(\omega)$, of the CCI incurred by the kth user are even for all fading channels in Section 5.2.

[1]Again, similar to our discussions in Section 4.2, the sum or difference of two random phases, both uniformly distributed in $[0, 2\pi)$, is still uniformly distributed in $[0, 2\pi)$ due to the 2π periodicity of the phase. Furthermore, it can be shown that the distribution of Δ_k is independent of τ_k, because the distribution of Δ_k conditioned on τ_k is also uniform in $[0, 2\pi)$. Hence Δ_k and X_k are independent, which enables us to average them separately later in Section 5.5.

Applying Parseval's theorem [258], the 0th user's Bit Error Probability (BEP) $P_{e|B}$ conditioned on B may be shown to be:

$$P_{e|B} = \frac{1}{2} - \frac{1}{\pi}\int_0^\infty \frac{1}{\omega}\Phi_\eta(\omega)\Im\{\Phi_{h_0}(\omega L)\}\prod_{k=1}^{K-1}\Phi_{I_k|B}(\omega)\mathrm{d}\omega, \tag{5.20}$$

where $\Im\{\Phi_{h_0}(\omega)\}$ is the imaginary part of the CF of the 0th user's fading amplitude h_0. Alternatively, Equation 5.20 may also be derived by exchanging the order of integrals. Note that Equation 5.20 applies not only to the fadings mentioned in Section 5.2, but also to any arbitrarily distributed fading, whenever the PDF, or equivalently the CF, of the MAI is even even if different users suffer from different types of fading. When the Rayleigh or Nakagami-m fading is considered, Equation 5.20 reduces to Equation 39 of [208] and to Equation 21 of [238], respectively.

Finally, the overall average BEP is obtained by averaging $P_{e|B}$ over all spreading sequences, yielding:

$$P_e = 2^{-(L-1)}\sum_{B=0}^{L-1}\binom{L-1}{B}P_{e|B}. \tag{5.21}$$

For the sake of simplicity, we will only consider the CF range spanning over $\omega \geq 0$ in our later discussions in the context of Equation 5.20. Nevertheless, the CF range spanning over $\omega < 0$ can be readily derived from the range spanning over $\omega \geq 0$ by exploiting the following property of the CF [260]:

$$\Phi(-\omega) = \Phi^*(\omega), \tag{5.22}$$

where $\Phi^*(\omega)$ denotes the complex conjugate of $\Phi(\omega)$.

5.5 MAI Analysis

The only task that remained unsolved so far is the determination of the conditional CF, $\Phi_{I_k|B}(\omega)$, of the CCI incurred by the kth user. The CF of I_k conditioned on X_k, $\Phi_{I_k|X_k}(\omega)$, may be derived by the specific properties outlined in Section 5.2. Upon averaging $\Phi_{I_k|X_k}(\omega)$ over $\{Y_{k,m}\}_{m=0}^{L}$ and ν_k, we arrive at the CF of I_k conditioned on B in the following form:

$$\Phi_{I_k|B}(\omega) = 2^{-(L+1)}\sum_{d_1\in\mathcal{A}}\sum_{d_2\in\mathcal{B}}\binom{A}{\frac{d_1+A}{2}}\binom{B}{\frac{d_2+B}{2}}\sum_{Y_{k,L-1},Y_{k,L}\in\{\pm1\}}\Phi_{I_k|\lambda_0,\lambda_1}(\omega), \tag{5.23}$$

where $\Phi_{I_k|\lambda_0,\lambda_1}(\omega)$ is the CF of I_k conditioned on the coefficients λ_0 and λ_1. The coefficients λ_0 and λ_1 are defined as:

$$\lambda_0 = d_1 + d_2 + Y_{k,L} \tag{5.24}$$

$$\lambda_1 = -2d_2 + Y_{k,L-1} - Y_{k,L}. \tag{5.25}$$

The conditional CFs, $\Phi_{I_k|X_k}(\omega)$ and $\Phi_{I_k|\lambda_0,\lambda_1}(\omega)$, will be provided for various fading scenarios in the following subsections.

5.5.1 Rayleigh Channels

Upon exploiting the specific properties of the Rayleigh distribution which were outlined in Section 5.2.1, it is readily shown that I_k is conditioned on X_k and Δ_k is a zero-mean Gaussian random variable having a variance of $X_k^2\sigma_k^2$. Hence we have the CF of I_k conditioned on X_k in the following form:

$$\Phi_{I_k|X_k}(\omega) = \Phi_{I_k|X_k,\Delta_k}(\omega) = \exp\left(-\frac{1}{2}X_k^2\sigma_k^2\omega^2\right). \tag{5.26}$$

Finally, the conditional CF $\Phi_{I_k|B}(\omega)$ is expressed as Equation 5.23 and the conditional CF $\Phi_{I_k|\lambda_0,\lambda_1}(\omega)$ in Equation 5.23 may be shown to be:

$$\Phi_{I_k|\lambda_0,\lambda_1}(\omega) = \begin{cases} \dfrac{1}{\lambda_1\sigma_k\omega}\sqrt{\dfrac{\pi}{2}}\mathrm{erf}\left(\dfrac{x\sigma_k\omega}{\sqrt{2}}\right)\Big|_{\lambda_0}^{\lambda_0+\lambda_1}, & \lambda_1 \neq 0 \\ \exp\left(-\dfrac{1}{2}\lambda_0^2\sigma_k^2\omega^2\right), & \lambda_1 = 0, \end{cases} \tag{5.27}$$

where $\mathrm{erf}(x)$ is the error function [259] and $f(x)|_{x_1}^{x_2} = f(x_2) - f(x_1)$.

This result has been derived in [208] for the Rayleigh fading. However, we represent it here in a unified approach so that Equations 5.23 - 5.25 may be used for other fading channels in our later discussions.

5.5.2 Ricean or Nakagami-n Channels

Upon exploiting the property of the Ricean distribution in Section 5.2.2, it is readily to show that I_k conditioned on X_k and Δ_k is a Gaussian random variable. Hence we have

the CF of I_k conditioned on X_k in the following form:

$$\Phi_{I_k|X_k,\Delta_k}(\omega) = \exp\left[jX_k\mu_k\omega\cos(\Delta_k+\vartheta_k) - \frac{1}{2}X_k^2\sigma_k^2\omega^2\right], \tag{5.28}$$

where ϑ_k satisfies $\cos\vartheta_k = \frac{\mu_{kr}}{\mu_k}$ and $\sin\vartheta_k = \frac{\mu_{ki}}{\mu_k}$. Averaging $\Phi_{I_k|X_k,\Delta_k}(\omega)$ over $\Delta_k \in [0, 2\pi)$ with the aid of Equation 3.339 in [259], we have the CF of I_k conditioned on X_k in the following form:

$$\Phi_{I_k|X_k}(\omega) = \exp\left(-\frac{1}{2}X_k^2\sigma_k^2\omega^2\right)\mathbb{J}_0\left(X_k\mu_k\omega\right), \tag{5.29}$$

where $\mathbb{J}_0(x)$ is the zeroth-order Bessel function of the first kind [259]. Finally, the conditional CF $\Phi_{I_k|B}(\omega)$ is also expressed as Equation 5.23 and the conditional CF $\Phi_{I_k|\lambda_0,\lambda_1}(\omega)$ in Equation 5.23 may be shown to be:

$$\Phi_{I_k|\lambda_0,\lambda_1}(\omega) = \begin{cases} \frac{x}{\lambda_1}\mathbb{F}_{1:0;1}^{1:0;0}\left(\begin{matrix}\frac{1}{2}:-;-;\\ \frac{3}{2}:-;1;\end{matrix} -\frac{1}{2}x^2\sigma_k^2\omega^2, -\frac{1}{4}x^2\mu_k^2\omega^2\right)\Bigg|_{\lambda_0}^{\lambda_0+\lambda_1}, & \lambda_1 \neq 0, \\ \exp\left(-\frac{1}{2}\lambda_0^2\sigma_k^2\omega^2\right)\mathbb{J}_0\left(\lambda_0\mu_k\omega\right), & \lambda_1 = 0, \end{cases} \tag{5.30}$$

where $\mathbb{F}_{C:D;D'}^{A:B;B'}\left[\begin{matrix}(a):(b);(b');\\ (c):(d);(d');\end{matrix} x,y\right]$ is the Kampé de Fériet function [266, 269].

5.5.3 Hoyt or Nakagami-q Channels

Upon exploiting the property of the Hoyt distribution in Section 5.2.3, it can be readily shown that I_k conditioned on X_k and Δ_k is a zero-mean Gaussian random variable having a variance of $\left(\sigma_{kr}^2\cos^2\Delta_k + \sigma_{ki}^2\sin^2\Delta_k\right)X_k^2$. Hence we have the CF of I_k conditioned on X_k and Δ_k in the following form:

$$\Phi_{I_k|X_k,\Delta_k}(\omega) = \exp\left[-\frac{1}{2}\left(\sigma_{kr}^2\cos^2\Delta_k + \sigma_{ki}^2\sin^2\Delta_k\right)X_k^2\omega^2\right]. \tag{5.31}$$

Applying the integral identity of Equation 3.339 in [259], we arrive at the CF of I_k conditioned on X_k by averaging $\Phi_{I_k|X_k,\Delta_k}(\omega)$ over $\Delta_k \in [0, 2\pi)$ in the form of:

$$\Phi_{I_k|X_k}(\omega) = \exp\left[-\frac{1}{4}\left(\sigma_{kr}^2+\sigma_{ki}^2\right)X_k^2\omega^2\right]\mathbb{I}_0\left[\frac{1}{4}\left(\sigma_{kr}^2-\sigma_{ki}^2\right)X_k^2\omega^2\right]. \tag{5.32}$$

Finally, the conditional CF $\Phi_{I_k|B}(\omega)$ is also expressed as Equation 5.23 and the conditional CF $\Phi_{I_k|\lambda_0,\lambda_1}(\omega)$ in Equation 5.23 may be shown to be:

$$\Phi_{I_k|\lambda_0,\lambda_1}(\omega) = \tag{5.33}$$
$$\begin{cases} \frac{x}{\lambda_1}\,\mathbb{F}_{1:0;1}^{1:0;0}\left(\begin{matrix}\left[\left(\frac{1}{2}\right):1,2\right]:-\,;\quad -\quad ; \\ \left[\left(\frac{3}{2}\right):1,2\right]:-\,;\left[(1):1\right];\end{matrix} -\frac{x^2}{4}(\sigma_{kx}^2+\sigma_{ky}^2)\omega^2, \frac{x^4}{64}(\sigma_{kx}^2-\sigma_{ky}^2)^2\omega^4\right)\Bigg|_{\lambda_0}^{\lambda_0+\lambda_1}, & \lambda_1 \neq 0, \\ \exp\left[-\frac{1}{4}\left(\sigma_{kx}^2+\sigma_{ky}^2\right)\lambda_0^2\omega^2\right]\mathbb{I}_0\left[\frac{1}{4}\left(\sigma_{kx}^2-\sigma_{ky}^2\right)\lambda_0^2\omega^2\right], & \lambda_1 = 0, \end{cases}$$

where $\mathbb{F}_{C:D^{(1)};\ldots;D^{(n)}}^{A:B^{(1)};\ldots;B^{(n)}}\left(\begin{matrix}\left[(a):\theta^{(1)},\ldots,\theta^{(n)}\right]:\left[(b^{(1)}):\phi^{(1)}\right];\ldots;\left[(b^{(n)}):\phi^{(n)}\right]; \\ \left[(c):\psi^{(1)},\ldots,\psi^{(n)}\right]:\left[(d^{(1)}):\delta^{(1)}\right];\ldots;\left[(d^{(n)}):\delta^{(n)}\right];\end{matrix} x_1,\ldots,x_n\right)$ is the generalized Lauricella function of n variables defined as Equations 21 - 23 of [266].

5.5.4 Nakagami-m Channels

Upon exploiting the results of [253], we have the CF of I_k conditioned on X_k in the following form:

$$\Phi_{I_k|X_k}(\omega) = {}_1\mathbb{F}_1\left(m;1;-\frac{\Omega}{4m}X_k^2\omega^2\right). \tag{5.34}$$

Finally, the conditional CF $\Phi_{I_k|B}(\omega)$ is still expressed as Equation 5.23 and the conditional CF $\Phi_{I_k|\lambda_0,\lambda_1}(\omega)$ in Equation 5.23 may be shown to be:

$$\Phi_{I_k|\lambda_0,\lambda_1}(\omega) = \begin{cases} \frac{x}{\lambda_1}\,{}_2\mathbb{F}_2\left(m,\frac{1}{2};1,\frac{3}{2};-\frac{\Omega}{4m}x^2\omega^2\right)\Big|_{\lambda_0}^{\lambda_0+\lambda_1}, & \lambda_1 \neq 0 \\ {}_1\mathbb{F}_1\left(m;1;-\frac{\Omega}{4m}\lambda_0^2\omega^2\right), & \lambda_1 = 0, \end{cases} \tag{5.35}$$

where ${}_p\mathbb{F}_q(\alpha_1,\alpha_2,\ldots,\alpha_p;\beta_1,\beta_2,\ldots,\beta_q;x)$ is the generalized hypergeometric function [259]. The MAI analysis of DS-CDMA systems communicating over Nakagami-m channels has been studied in [238], but the results of [238] only apply to the scenarios, where the Nakagami-m fading parameter m is an integer. By contrast, Equation 5.35 applies to arbitrary values of m.

5.6 Numerical Results

In this section we will verify the accuracy of our exact BER analysis provided in Section 5.4 and demonstrate the limited accuracy of the SGA method by Monte Carlo

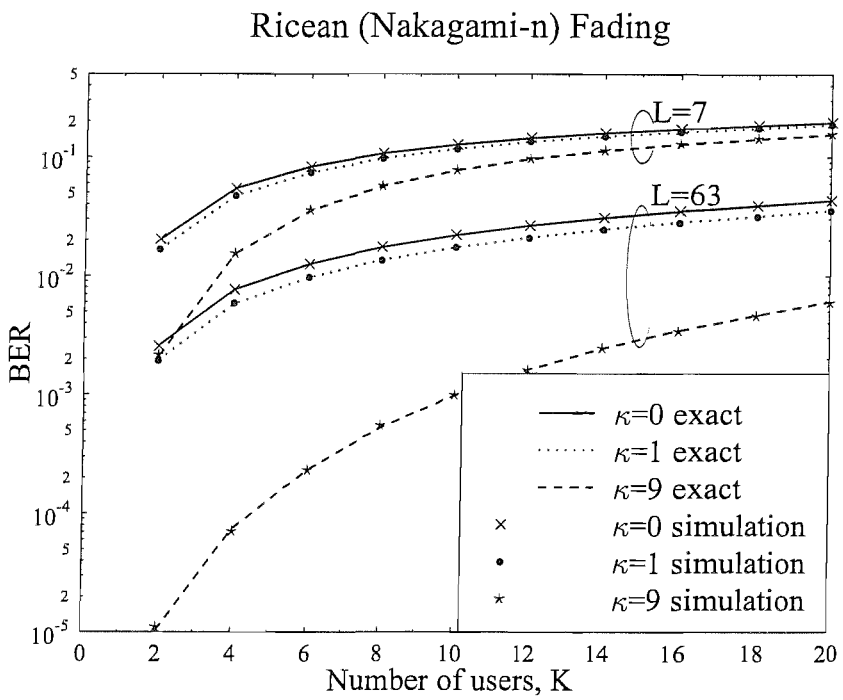

FIGURE 5.1: BER versus the number of users K in an asynchronous DS-CDMA system exposed to Ricean fading using random spreading sequences and BPSK modulation. The length of the random spreading sequences is $L = 7$ and 63. The Ricean K-factor is $\kappa = 0$ (Rayleigh), 1 and 9, which is common to all users. The average power of all users at the receiver is equal and the background noise is ignored, i.e. we have $\gamma_{\text{SNR}} = \infty$.

simulations.

5.6.1 Effects of the Number of Users

Figures 5.1 and 5.2 illustrate the average BER performance versus the number of users in the context of Ricean fading channels, when the effects of background noise are ignored. Figure 5.1 compares the results obtained from our exact BER analysis to our simulation results and shows that they match very well both for various spreading sequence lengths and for various Ricean K-factors. On the other hand, Figure 5.2 compares the results obtained using the SGA to our simulation results and shows an interesting phenomenon. It is widely recognized that the SGA slightly over-estimates the average BER, when the Ricean K-factor is $\kappa = 0$, i.e. for Rayleigh fading. This has also been reported in [208]. By contrast, when κ increases to 9, the SGA under-estimates the average BER. Although not shown explicitly here, if we have $\kappa \to \infty$, which corresponds to having no fading

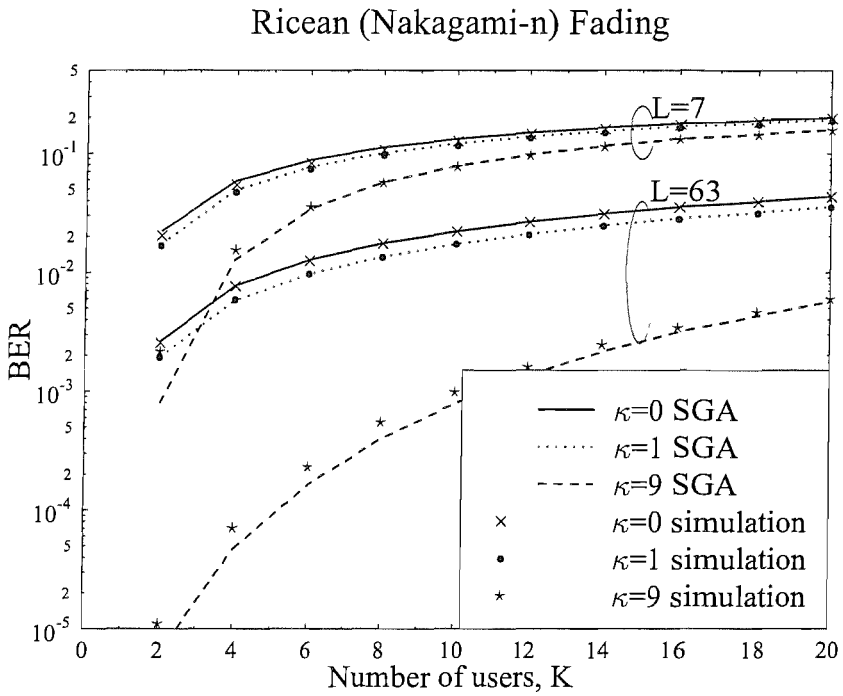

FIGURE 5.2: BER versus the number of users K in an asynchronous DS-CDMA system exposed to Ricean fading using random spreading sequences and BPSK modulation. The length of the random spreading sequences is $L = 7$ and 63. The Ricean K-factor is $\kappa = 0$ (Rayleigh), 1 and 9, which is common to all users. The average power of all users at the receiver is equal and the background noise is ignored, i.e. we have $\gamma_{\text{SNR}} = \infty$.

and no noise, only CCI, the SGA will more severely under-estimate the average BER, which has been reported in the context of AWGN channels [244].

Figures 5.3 and 5.4 illustrate the average BER performance versus the number of users, when the effects of background noise are ignored. Figure 5.3 compares the results obtained from our exact BER analysis to our simulation results and shows that they match very well both for different spreading sequence lengths and for various Hoyt fading parameters. On the other hand, Figure 5.4 compares the results obtained using the SGA to our simulation results and demonstrates that the SGA over-estimates the average BER, especially in the scenarios where either there is a limited number of interferers, or when the Hoyt fading parameter q is small or when short spreading sequences are used.

Figures 5.5 and 5.6 illustrate the achievable average BER performance versus the number of users in the context of Nakagami-m fading channels, when the effects of background noise are ignored. Figure 5.5 compares the results obtained from our exact BER analysis

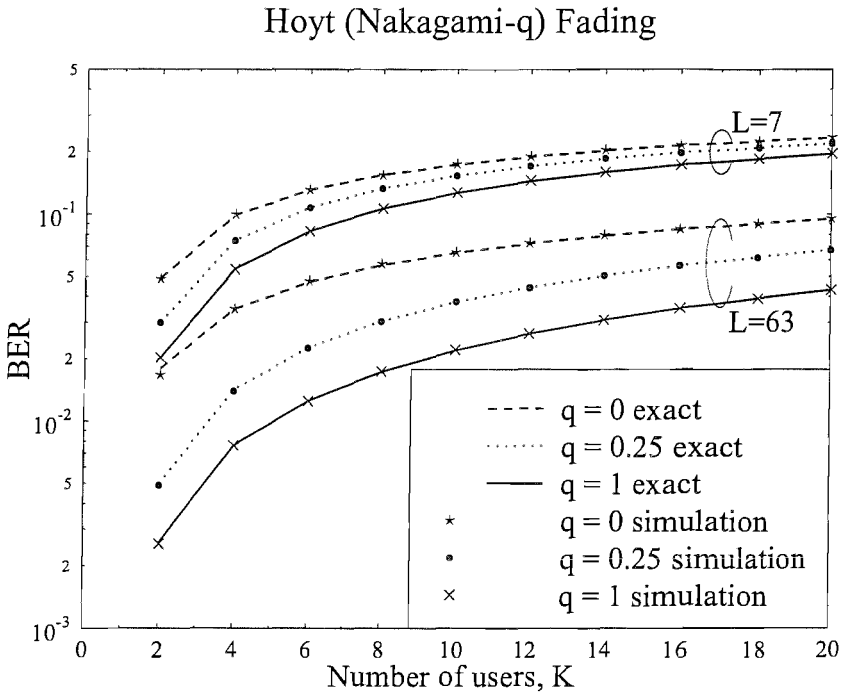

FIGURE 5.3: BER versus the number of users K in an asynchronous DS-CDMA system using random spreading sequences and BPSK modulation communicating over Hoyt channels. The length of the random spreading sequences is $L = 7$ and 63. The Hoyt fading parameter is $q = 0$ (one-sided Gauss), 0.25 and 1 (Rayleigh), which is common to all users. The average power of all users at the receiver is equal and the background noise is ignored, i.e. we have $\gamma_{\text{SNR}} = \infty$.

to our simulation results and shows that they match well both for various spreading sequence lengths and for various Nakagami-m fading parameters. On the other hand, Figure 5.6 compares the results obtained using the SGA to our simulation results and shows a similar phenomenon to that seen in Figure 5.2. The SGA over-estimates the average BER when the Nakagami-m fading parameter is low, while it under-estimates the average BER when the Nakagami-m fading parameter is high.

5.6.2 Effects of the Per-Bit SNR

Figures 5.7 and 5.8 illustrate the average BER performance versus the per-bit SNR, when the number of users is $K = 4$. Figure 5.7 compares the results obtained from our accurate BER analysis to the simulation results and shows that they match for both different spreading sequence lengths and for various Ricean fading parameters. On the

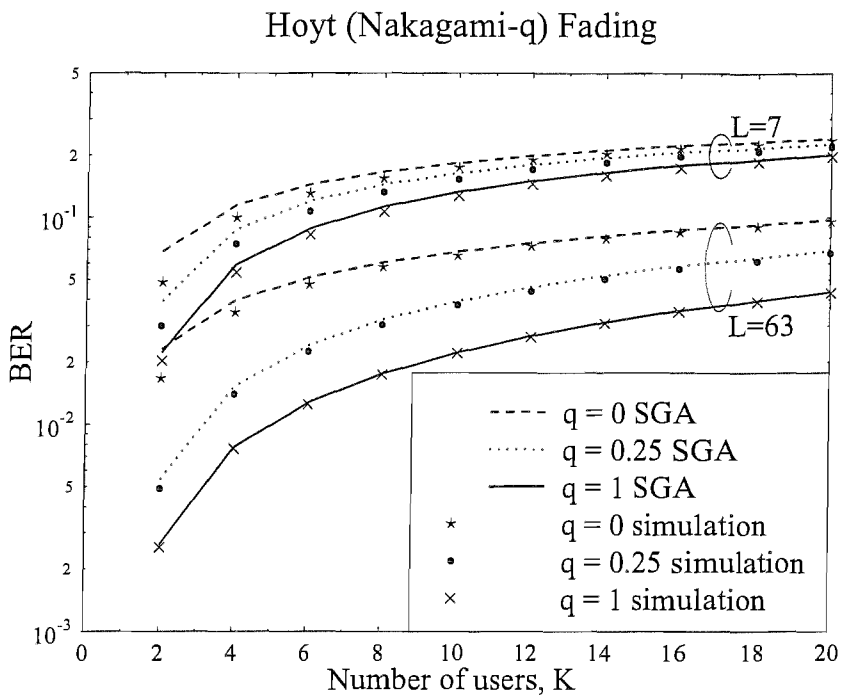

FIGURE 5.4: BER versus the number of users K in an asynchronous DS-CDMA system using random spreading sequences and BPSK modulation communicating over Hoyt channels. The length of the random spreading sequences is $L = 7$ and 63. The Hoyt fading parameter is $q = 0$ (one-sided Gauss), 0.25 and 1 (Rayleigh). The average power of all users at the receiver is equal and the background noise is ignored, i.e. we have $\gamma_{\text{SNR}} = \infty$.

other hand, Figure 5.8 compares the results obtained by the SGA to our simulation results and shows similar performance trends to those seen in Figure 5.2, when the Ricean K-factor κ increases. Furthermore, the SGA still fails to accurately evaluate the average BER performance, particularly when the SNR is high.

Figures 5.9 and 5.10 illustrate the average BER performance versus the per-bit SNR, when the number of users is $K = 4$. Figure 5.9 compares the results obtained from our exact BER analysis to our simulation results and shows that they match well both for different spreading sequence lengths and for various Hoyt fading parameters. On the other hand, Figure 5.10 compares the results obtained by the SGA to our simulation results and demonstrates the limited accuracy of the SGA, particularly when the SNR is high, the Hoyt fading parameter q is low and when short spreading sequences are used.

Figures 5.11 and 5.12 characterize the achievable average BER performance versus the per-bit SNR in the context of Nakagami-m fading channels, when the number of users is

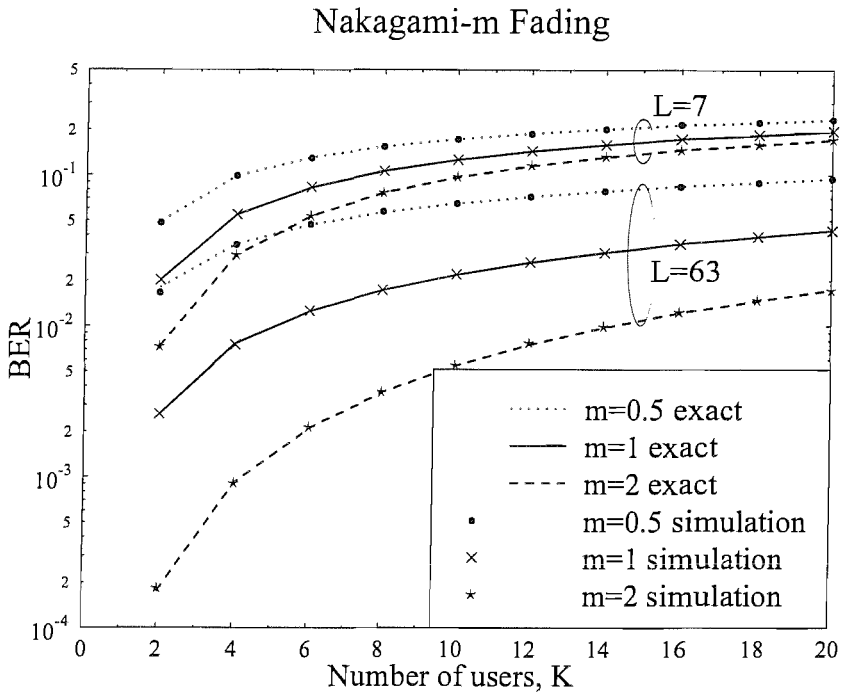

FIGURE 5.5: BER versus the number of users K in an asynchronous DS-CDMA system using random spreading sequences and BPSK modulation communicating over Nakgami-m channels. The length of the random spreading sequences is $L = 7$ and 63. The Nakgami-m fading parameter is $m = 0.5$ (one-sided Gauss), 1 (Rayleigh) and 2, which is common to all users. The average power of all users at the receiver is equal and the background noise is ignored, i.e. we have $\gamma_{\text{SNR}} = \infty$.

$K = 4$. Figure 5.11 compares the results obtained from our exact BER analysis to our simulation results and shows that they match well for both different spreading sequence lengths and for various Nakagami-m fading parameters. On the other hand, Figure 5.12 compares the results obtained by the SGA to our simulation results and exhibits similar performance trends to those seen in Figure 5.6, when the Nakagami-m fading parameter increases. The SGA over-estimates the average BER, when the Nakagami-m fading parameter is low, while it under-estimates the average BER, when the Nakagami-m fading parameter is high.

5.7 Conclusion

A unified approach has been proposed for the exact average BER analysis of an asynchronous DS-CDMA system using random spreading sequences and BPSK modulation

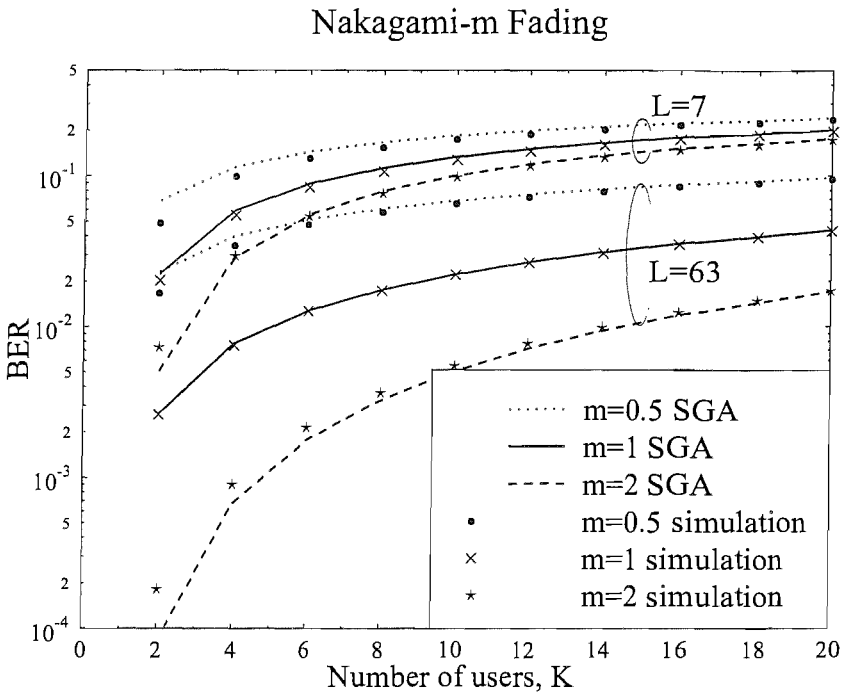

FIGURE 5.6: BER versus the number of users K in an asynchronous DS-CDMA system using random spreading sequences and BPSK modulation communicating over Nakagami-m channels. The length of the random spreading sequences is $L = 7$ and 63. The Nakagami-m fading parameter is $m = 0.5$ (one-sided Gauss), 1 (Rayleigh) and 2. The average power of all users at the receiver is equal and the background noise is ignored, i.e. we have $\gamma_{\text{SNR}} = \infty$.

for communicating over various fading channels. Several closed-form expressions were derived for the conditional CFs of the interfering signals in various fading channels. A unified exact BER expression was provided, which requires only a single numerical integration. Our simulation results verified the accuracy of our exact BER analysis for various combinations of the spreading sequence length and the fading severity. By contrast, the SGA demonstrated limited accuracy compared to our simulation results. It over-estimates the average BER when the fading severe, while it under-estimates the average BER performance when the fading is benign, especially when either there is a low number of interferers, or the SNR is high and short spreading sequences are used.

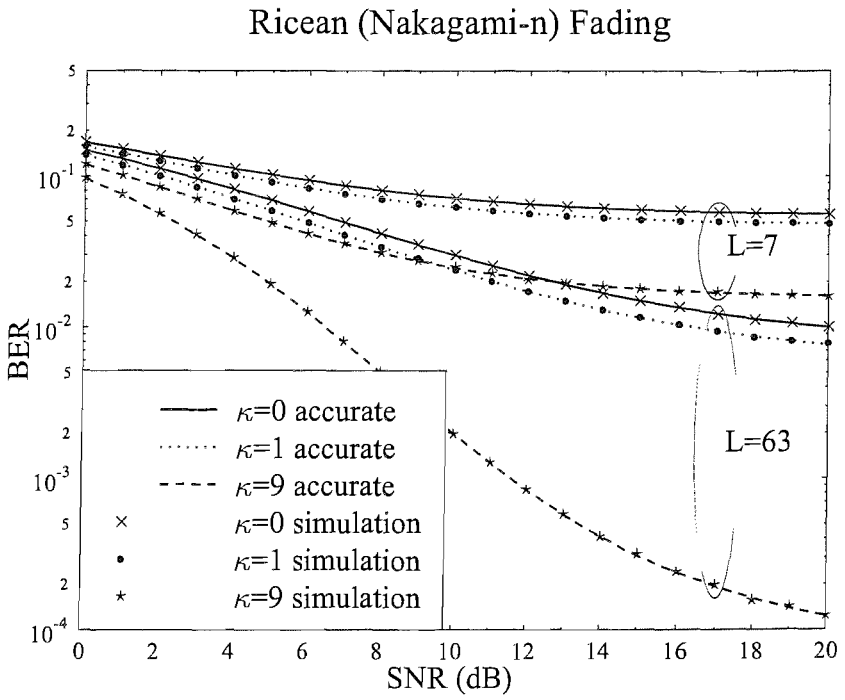

FIGURE 5.7: BER versus per-bit SNR in an asynchronous DS-CDMA system exposed to Ricean fading using random spreading sequences and BPSK modulation. The length of the random spreading sequences is $L = 7$ and 63. The Ricean K-factor is $\kappa = 0$, 1 and 9, which is common to all users. The average power of all users at the receiver is equal. The number of users is $K = 4$.

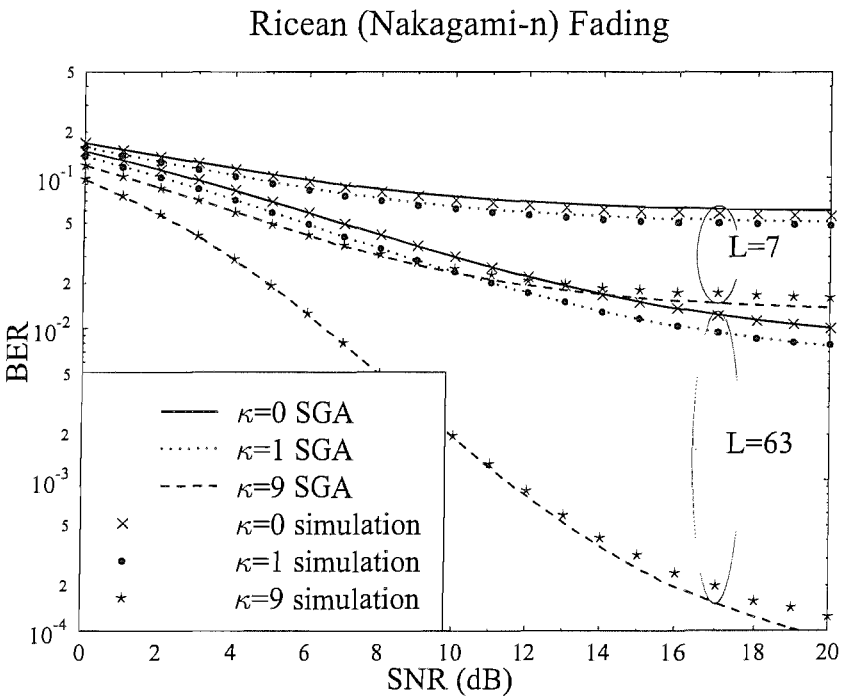

FIGURE 5.8: BER versus per-bit SNR in an asynchronous DS-CDMA system exposed to Ricean fading using random spreading sequences and BPSK modulation. The length of the random spreading sequences is $L = 7$ and 63. The Ricean K-factor is $\kappa = 0$, 1 and 9, which is common to all users. The average power of all users at the receiver is equal. The number of users is $K = 4$.

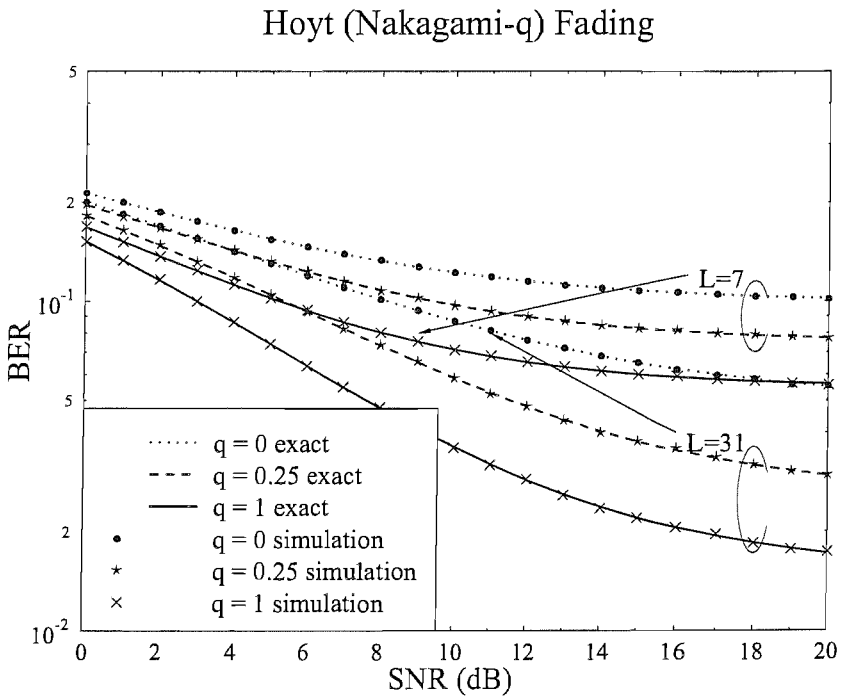

FIGURE 5.9: BER versus per-bit SNR in an asynchronous DS-CDMA system using random spreading sequences and BPSK modulation communicating over Hoyt channels. The length of the random spreading sequences is $L = 7$ and 31. The Hoyt fading parameter is $q = 0$, 0.25 and 1. The average power of all users at the receiver is equal. The number of users is $K = 4$.

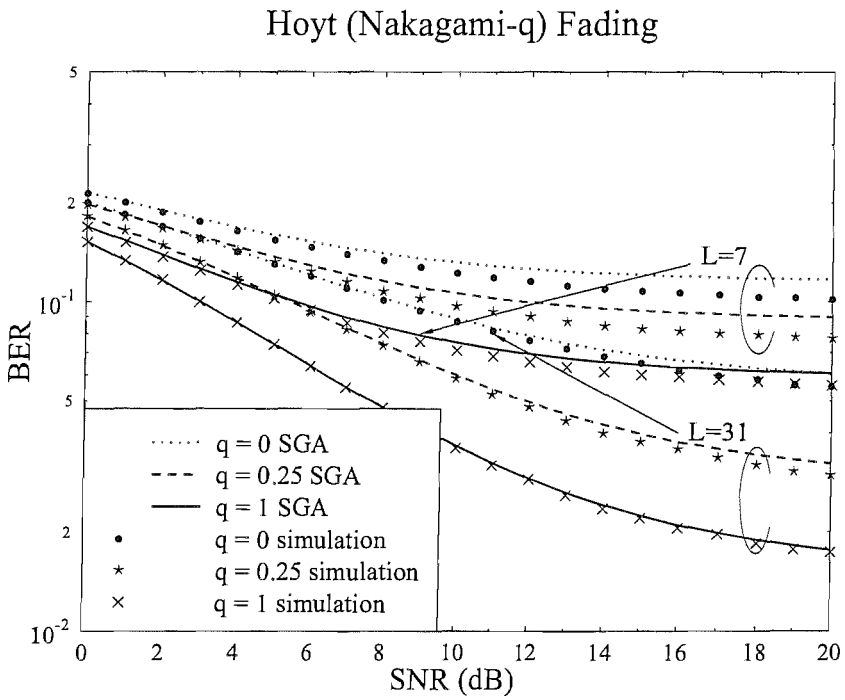

FIGURE 5.10: BER versus per-bit SNR in an asynchronous DS-CDMA system using random spreading sequences and BPSK modulation communicating over Hoyt channels. The length of the random spreading sequences is $L = 7$ and 31. The Hoyt fading parameter is $q = 0$, 0.25 and 1. The average power of all users at the receiver is equal. The number of users is $K = 4$.

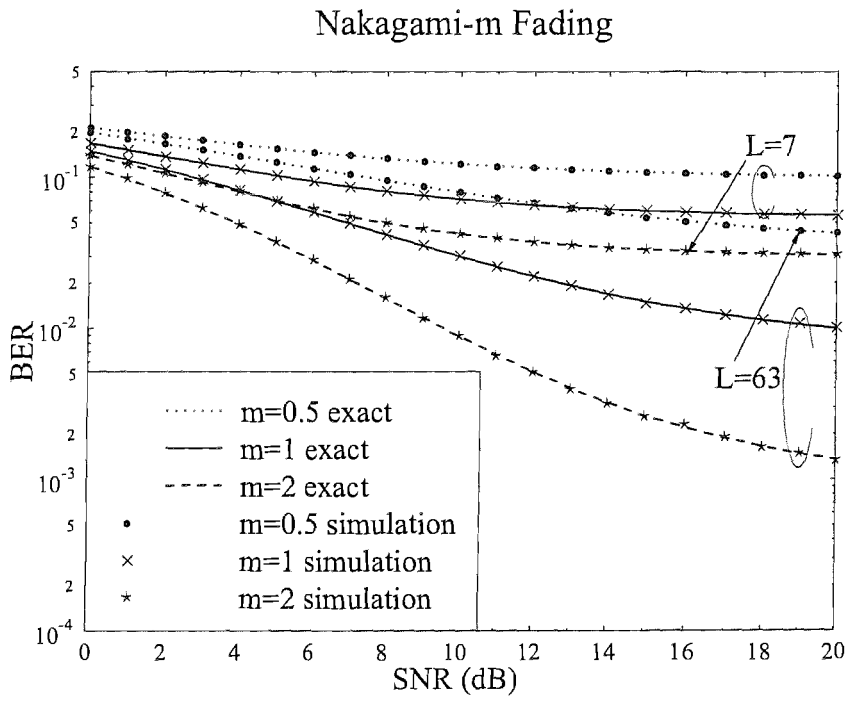

FIGURE 5.11: BER versus per-bit SNR in an asynchronous DS-CDMA system exposed to Nakagami-m fading using random spreading sequences and BPSK modulation. The length of the random spreading sequences is $L = 7$ and 63. The Nakagami-m fading parameter is $m = 0.5$, 1 and 2, which is common to all users. The average power of all users at the receiver is equal. The number of users is $K = 4$.

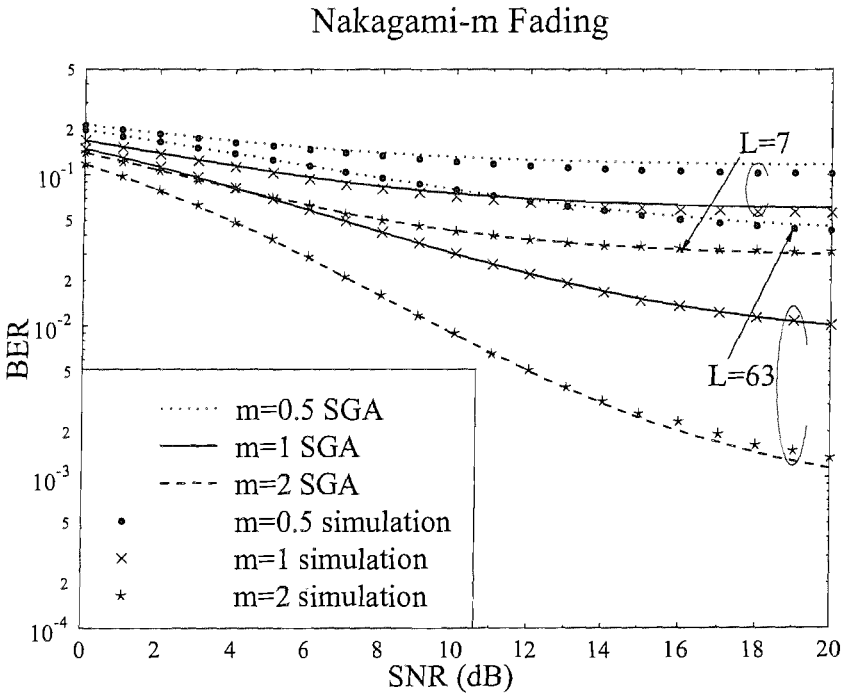

FIGURE 5.12: BER versus per-bit SNR in an asynchronous DS-CDMA system exposed to Nakagami-m fading using random spreading sequences and BPSK modulation. The length of the random spreading sequences is $L = 7$ and 63. The Nakagami-m fading parameter is $\kappa = 0$, 1 and 9, which is common to all users. The average power of all users at the receiver is equal. The number of users is $K = 4$.

Chapter 6

Exact BER of Rectangular-Constellation QAM Subjected to Asynchronous Co-Channel Interference and Nakagami-m Fading

6.1 Introduction

The family of Quadrature Amplitude Modulation (QAM) [201, 202, 210, 215] schemes has found its way into virtually all recent wireless standards, including the third-generation (3G) High-Speed Downlink Packet Access (HSDPA), the 802.11 Wireless Local Area Network (WLAN) family, as well as the Digital Audio Broadcast (DAB) and Video Broadcast (DVB) systems. The maximum-minimum distance rectangular QAM (R-QAM) constellation is popular, since it achieves the best BER in uncoded Gaussian scenarios.

The Symbol Error Rate (SER) performance of R-QAM has been studied using various exact computation techniques in [207, 270–273]. By contrast, the novel contribution of this chapter is that we evaluate the BER performance of R-QAM, when additionally the Co-Channel Interference (CCI) is taken into account. Conventionally, the R-QAM BER has been estimated by using various approximations or bounds [207, 274]. However,

using exact BER calculation is still desirable for verifying the accuracy of various approximation and bounding techniques. The exact BER expressions derived for 16-QAM and 64-QAM constellations were provided in [201]. A general recursive algorithm devised for the exact BER computation of Square QAM (S-QAM) was presented in [275], while an exact and general closed-form BER expression of R-QAM[1] was derived for arbitrary constellation sizes in [212]. Most of these results were obtained for Additive White Gaussian Noise (AWGN) channels. The AWGN result of [212] was later extended to Nakagami-m [276, 277] and Ricean [278] fading channels. A signal-space partitioning method was proposed for calculating the exact SER/BER of arbitrary two-dimensional signaling in the context of various fading channels in [279].

The exact QAM BER calculation becomes even more challenging, when the CCI is taken into account. Conventionally, the CCI is assumed to be Gaussian distributed for the sake of computational simplicity [280]. However, the Gaussian Approximation (GA) is accurate only, when we have a large number of interferers owning to the Central Limit Theorem (CLT) [260]. Moreover, to the best of the authors' knowledge, the exact and general BER expression of R-QAM systems corrupted by CCI has not been derived. In the existing literature, most exact BER analyses procedures were performed for BPSK [281–290] and QPSK [289–292] systems.

Hence, again, the contribution of this chapter is that we derive an exact and general BER expression for general R-QAM systems corrupted by both asynchronous CCI and Nakagami-m fading, while dispensing with the Gaussian distributed CCI assumption. This provides an accurate alternative to simulations when the Gaussian approximation fails to give accurate analysis. This paper is organized as follows. In Section 6.2 a general R-QAM system subject to asynchronous CCI and Nakagami-m fading is described. Its exact BER performance is investigated based on the Characteristic Function (CF) approach in Section 6.3. Our numerical results are presented in Section 6.4, where we verify the accuracy of our exact BER expression and demonstrate the limited accuracy of the GA method. Finally, we conclude this paper in Section 6.5.

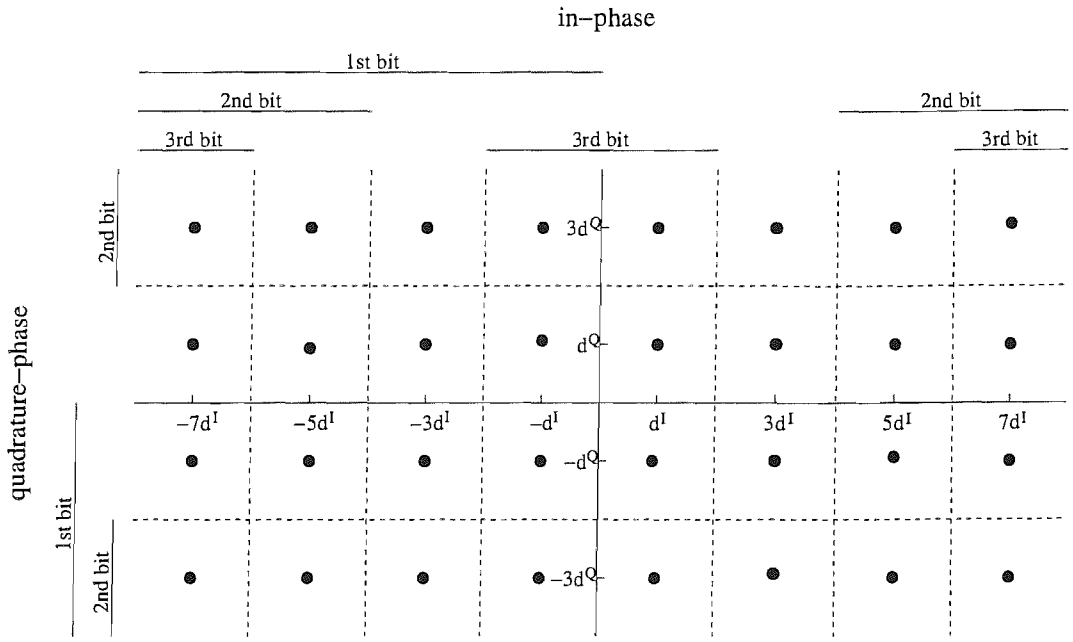

FIGURE 6.1: Illustration of an (8×4)-point R-QAM signal constellation [276, 277].

6.2 System Model and Assumptions

The R-QAM signal consists of two independent amplitude-modulated signals and can be expressed as [276]:

$$s(t) = d^I b^I(t)\cos(\omega_c t + \theta) + d^Q b^Q(t)\sin(\omega_c t + \theta), \tag{6.1}$$

where ω_c and θ are the common carrier frequency and the carrier phase shift. As illustrated in [212], $2d^I$ and $2d^Q$ are the minimum distance between signal constellation points along the in-phase and quadrature-phase axes, respectively. Note that d^I and d^Q are not necessarily equal in the general rectangular QAM constellation. The in-phase and quadrature-phase data signals, $b^I(t)$ and $b^Q(t)$, are given by:

$$b^I(t) = \sum_{n=-\infty}^{\infty} b_n^I p_{T_s}(t - nT_s), \tag{6.2}$$

$$b^Q(t) = \sum_{n=-\infty}^{\infty} b_n^Q p_{T_s}(t - nT_s), \tag{6.3}$$

[1]The generic class of R-QAM contains both the specific subclass of square-shaped S-QAM constellations, as well as non-square constellations.

where $\left\{b_n^I\right\}_{n=-\infty}^{\infty}$ and $\left\{b_n^Q\right\}_{n=-\infty}^{\infty}$ are the in-phase and quadrature-phase data symbols, respectively. The symbol duration is denoted as T_s and $p_T(t)$ is the rectangular pulse having a duration of T, i.e. we have

$$p_T(t) = \begin{cases} 1, t \in [0, T), \\ 0, \text{otherwise.} \end{cases} \tag{6.4}$$

In the M-ary R-QAM scheme, where we have $M = M^I \times M^Q$, $\log_2 M^I$ and $\log_2 M^Q$ bits are Gray encoded and mapped onto the in-phase and quadrature-phase components [201, 212], respectively. Hence, the in-phase and quadrature data symbols, b_n^I and b_n^Q, are selected from the set of $\mathcal{A}^I$ and $\mathcal{A}^Q$, respectively:

$$\mathcal{A}^I = \{\pm 1, \pm 3, ..., \pm(M^I - 1)\} \tag{6.5}$$

$$\mathcal{A}^Q = \{\pm 1, \pm 3, ..., \pm(M^Q - 1)\} \tag{6.6}$$

Hence, the average per-bit energy E_b may be expressed as [276]:

$$E_b = \Omega \frac{(d^I)^2 \left[(M^I)^2 - 1\right] + (d^Q)^2 \left[(M^Q)^2 - 1\right]}{3 \log_2 M}, \tag{6.7}$$

where Ω is the signal's average fading power.

We consider a general R-QAM system subjected to K asynchronous co-channel interferers as illustrated in Figure 6.2. The received signal $r(t)$ subjected to fading may be written as:

$$\begin{aligned} r(t) = \sum_{k=0}^{K} h_k \{ & d_k^I b_k^I (t - \tau_k) \cos[\omega_c (t - \tau_k) + \theta_k + \varphi_k] \\ & + d_k^Q b_k^Q (t - \tau_k) \sin[\omega_c (t - \tau_k) + \theta_k + \varphi_k] \} + \eta(t), \end{aligned} \tag{6.8}$$

where the fading amplitude h_k obeys the Nakagami-m distribution having parameters $\{m_k, \Omega_k\}$ [263], the fading phase φ_k is typically assumed to be uniformly distributed over $[0, 2\pi)$ [263], the time delay τ_k of the kth user is uniformly distributed over $[0, T_s)$, and the Additive White Gaussian Noise (AWGN) $\eta(t)$ has a double-sided power spectral density of $N_0/2$. Neglecting the subscript k, the PDF $f_h(x)$ of the fading amplitude h is given by [263]:

$$f_h(x) = \frac{2}{\Gamma(m)} \left(\frac{m}{\Omega}\right)^m x^{2m-1} \exp\left(-\frac{m}{\Omega} x^2\right), x \geq 0, \tag{6.9}$$

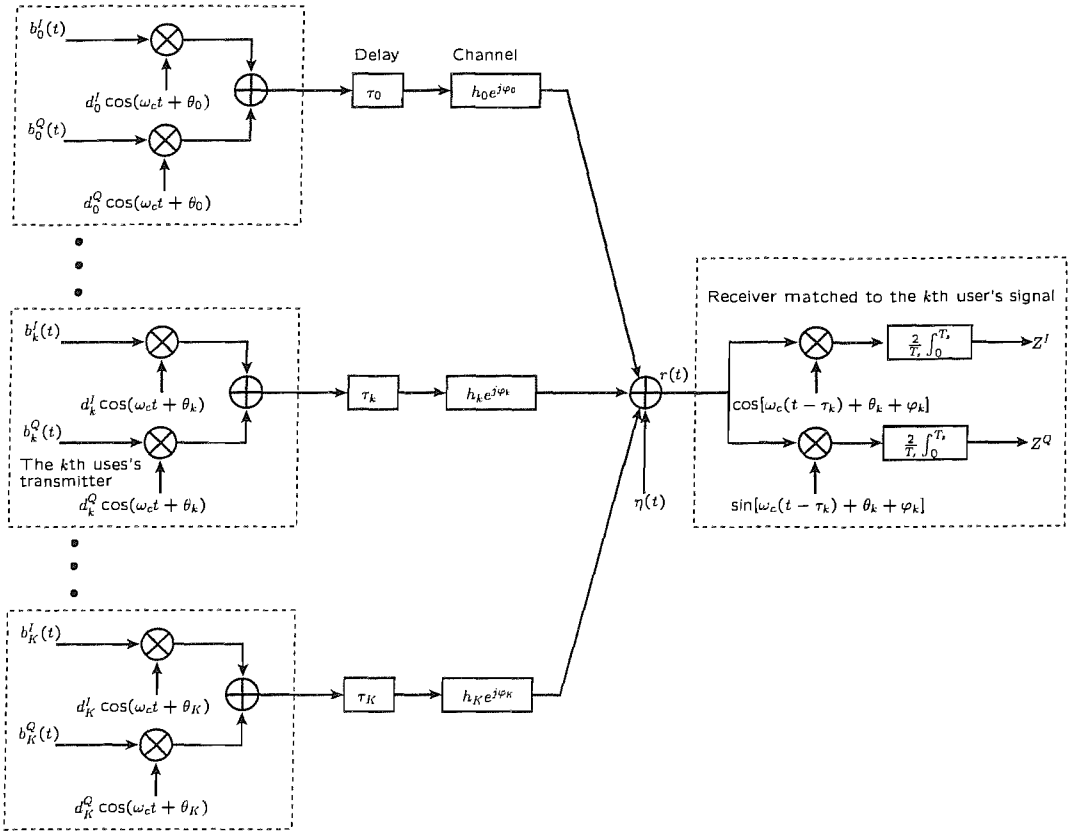

FIGURE 6.2: A general R-QAM system subjected to K asynchronous co-channel interferers.

where Ω is the average fading power and m is the Nakagami-m fading parameter.

Without loss of generality, we assume that the 0th user is the desired one. In the case of coherent demodulation as well as perfect channel estimation, the in-phase and quadrature-phase decision statistics, Z^I and Z^Q, are given by:

$$Z^I = d_0^I h_0 b_{0,0}^I + \sum_{k=1}^{K} I_k^I + \eta^I, \tag{6.10}$$

$$Z^Q = d_0^Q h_0 b_{0,0}^Q + \sum_{k=1}^{K} I_k^Q + \eta^Q, \tag{6.11}$$

where the noise components η^I and η^Q can be shown to be zero-mean Gaussian distributed random variables, both having a variance of N_0/T_s. The in-phase and quadrature-phase CCIs, I_k^I and I_k^Q, incurred by the kth user are given by:

$$I_k^I = h_k \left(X_k^I \cos \Delta_k + X_k^Q \sin \Delta_k \right), \tag{6.12}$$

$$I_k^Q = h_k \left(X_k^Q \cos \Delta_k - X_k^I \sin \Delta_k \right), \tag{6.13}$$

where the phase shift difference $\Delta_k = -\omega_c(\tau_k - \tau_0) + (\theta_k - \theta_0) + (\varphi_k - \varphi_0)$ between the kth interferer and the desired user is uniformly distributed over $[0, 2\pi)$[2]. The random variables X_k^I and X_k^Q are defined as:

$$X_k^I = d_k^I[b_{k,-1}^I \nu_k + b_{k,0}^I(1-\nu_k)], \tag{6.14}$$

$$X_k^Q = d_k^Q[b_{k,-1}^Q \nu_k + b_{k,0}^Q(1-\nu_k)], \tag{6.15}$$

where $\nu_k = \tau_k/T_s$ is the time delay of the kth interferer normalized by the symbol duration.

6.3 BER Analysis

6.3.1 Exact Analysis

Let us now continue by analyzing the error probability of the in-phase component based on the CF approach. The error probability of the quadrature component may be derived in the same way.

Upon exploiting the results of [253], we have the CF of I_k^I conditioned on X_k^I and X_k^Q in the following form:

$$\Phi_{I_k^I|X_k^I,X_k^Q}(\omega) = {}_1\mathbb{F}_1\left(m_k; 1; -\frac{\Omega_k}{4m_k}\left[(X_k^I)^2 + (X_k^Q)^2\right]\omega^2\right), \tag{6.16}$$

where ${}_1\mathbb{F}_1(\alpha;\beta;x)$ is the confluent hypergeometric function [259]. Upon averaging $\Phi_{I_k^I|X_k^I,X_k^Q}(\omega)$ over the kth interferer's data symbols $b_{k,-1}^I$, $b_{k,-1}^Q$, $b_{k,0}^I$, $b_{k,0}^Q$ and the time delay τ_k, we obtain the CF of I_k^I, $\Phi_{I_k^I}(\omega)$, as follows:

$$\Phi_{I_k^I}(\omega) = \frac{1}{M_k^2}\sum_{b_{k,-1}^I, b_{k,0}^I \in \mathcal{A}_k^I}\sum_{b_{k,-1}^Q, b_{k,0}^Q \in \mathcal{A}_k^Q} \Phi_{I_k^I|\lambda_0,\lambda_1,\lambda_2}(\omega), \tag{6.17}$$

where the coefficients λ_0, λ_1 and λ_2 are defined as:

$$\lambda_0 = (d_k^I)^2(b_{k,0}^I)^2 + (d_k^Q)^2(b_{k,0}^Q)^2, \tag{6.18}$$

$$\lambda_1 = (d_k^I)^2 b_{k,0}^I(b_{k,-1}^I - b_{k,0}^I) + (d_k^Q)^2 b_{k,0}^Q(b_{k,-1}^Q - b_{k,0}^Q), \tag{6.19}$$

$$\lambda_2 = (d_k^I)^2(b_{k,-1}^I - b_{k,0}^I)^2 + (d_k^Q)^2(b_{k,-1}^Q - b_{k,0}^Q)^2. \tag{6.20}$$

[2]Similar to our discussions in Section 5.3, Δ_k is uniformly distributed in $[0, 2\pi)$ and is independent of τ_k. Hence Δ_k is independent of X_k^I and X_k^Q, which enables us to average them separately later in Section 6.3.

The conditional CF, $\Phi_{I_k^I|\lambda_0,\lambda_1,\lambda_2}(\omega)$, may be shown to be given by:

$$\Phi_{I_k^I|\lambda_0,\lambda_1,\lambda_2}(\omega) = \tag{6.21}$$
$$\begin{cases} {}_1\mathbb{F}_1\left(m_k;1;-\dfrac{\Omega_k}{4m_k}\lambda_0\omega^2\right), & \lambda_2 = 0, \\ \dfrac{x}{\lambda_2}\,\mathbb{F}_{1:0;1}^{1:0;1}\left(\begin{matrix}[(m_k):1,1]:-;[(\frac{1}{2}):1]; \\ [(1):1,1]\ :-;[(\frac{3}{2}):1];\end{matrix} -\left(\lambda_0-\dfrac{\lambda_1^2}{\lambda_2}\right)\dfrac{\Omega_k\omega^2}{4m_k}, -\dfrac{\Omega_k\omega^2x^2}{4\lambda_2 m_k}\right)\Bigg|_{\lambda_1}^{\lambda_1+\lambda_2}, & \lambda_2 \neq 0, \end{cases}$$

where $\mathbb{F}_{C:D^{(1)};\ldots;D^{(n)}}^{A:B^{(1)};\ldots;B^{(n)}}\left(\begin{matrix}[(a):\theta^{(1)},\ldots,\theta^{(n)}]:[(b^{(1)}):\phi^{(1)}];\ldots;[(b^{(n)}):\phi^{(n)}]; \\ [(c):\psi^{(1)},\ldots,\psi^{(n)}]:[(d^{(1)}):\delta^{(1)}];\ldots;[(d^{(n)}):\delta^{(n)}];\end{matrix} x_1,\ldots,x_n\right)$ is the generalized Lauricella function of n variables defined as Equations 21 - 23 of [266] and $f(x)|_{x_1}^{x_2} = f(x_2) - f(x_1)$.

When we have $M_k = 2$, i.e. the kth interferer adopts BPSK modulation and experiences Nakagami-m fading, Equation 6.21 reduces to Equations 8 and 9 of [290]. By contrast, when $M_k = 4$, $d_k^I = d_k^Q$ and $m = 1$, i.e. the kth interferer adopts QPSK modulation and experiences Rayleigh fading, Equation 6.21 reduces to Equations 17, 19 and 21 of [290].

The in-phase CCI I_k^I imposed by the different interferers is mutually independent. Upon defining the total in-phase interference plus noise term as $\xi^I = \sum_{k=1}^{K} I_k^I + \eta^I$, it transpires that both its PDF $f_{\xi^I}(x)$ and its CF $\Phi_{\xi^I}(\omega) = \Phi_{\eta^I}(\omega)\prod_{k=1}^{K}\Phi_{I_k^I}(\omega)$ are even. Hence the Cumulative Distribution Function (CDF) $\mathrm{F}_{\xi^I}(x)$ of the total in-phase interference plus noise can be shown to be:

$$\mathrm{F}_{\xi^I}(x) = \frac{1}{2} + \frac{1}{\pi}\int_0^\infty \frac{\sin(\omega x)}{\omega}\Phi_{\xi^I}(\omega)\mathrm{d}\omega. \tag{6.22}$$

Extending the AWGN result of [212] to the scenarios encountered in presence of interference plus noise, the conditional error probability of the uth bit of the in-phase

component, $P^I_{b|h_0}(u)$, can be expressed as follows, when $f_{\xi^I}(x)$ is even[3]:

$$P^I_{b|h_0}(u) = \frac{1}{M^I_k} \times \sum_{l=0}^{(1-2^{-u})M^I_k-1} \left\{ (-1)^{\left\lfloor \frac{l2^{u-1}}{M^I_k} \right\rfloor} \left(2^{u-1} - \left\lfloor \frac{l2^{u-1}}{M^I_k} + \frac{1}{2} \right\rfloor \right) \left[2\left(1 - \mathrm{F}_{\xi^I}\left((2l+1)d^I_0 h_0\right)\right)\right] \right\}, \tag{6.23}$$

where $\lfloor x \rfloor$ denotes the largest integer no greater than x. Upon averaging $P^I_{b|h_0}(u)$ over h_0 and applying Parseval's theorem [258], we obtain the error probability $P^I_b(u)$ of the uth bit of the in-phase component in the form of:

$$P^I_b(u) = \frac{1}{2} - \frac{2}{\pi M^I_k} \int_0^\infty \frac{\Phi_{\xi^I}(\omega)}{\omega} \times \sum_{l=0}^{(1-2^{-u})M^I_k-1} \left\{ (-1)^{\left\lfloor \frac{l2^{u-1}}{M^I_k} \right\rfloor} \left(2^{u-1} - \left\lfloor \frac{l2^{u-1}}{M^I_k} + \frac{1}{2} \right\rfloor \right) \Im\left\{ \Phi_{h_0}\left[(2l+1)d^I_0\omega\right]\right\} \right\} \mathrm{d}\omega, \tag{6.24}$$

where $\Im\{\Phi_{h_0}(\omega)\}$ is the imaginary part of the CF of the desired user's fading amplitude, h_0. The CF $\Phi_h(\omega)$ of the Nakagami-m fading amplitude h is given by [258]:

$$\Phi_h(\omega) = {}_1\mathbb{F}_1\left(m; \frac{1}{2}; -\frac{\Omega}{4m}\omega^2\right) + j\omega \frac{\Gamma(m+\frac{1}{2})}{\Gamma(m)} \sqrt{\frac{\Omega}{m}}\, {}_1\mathbb{F}_1\left(m+\frac{1}{2}; \frac{3}{2}; -\frac{\Omega}{m}\omega^2\right). \tag{6.25}$$

Following the same approach, we may derive the error probability $P^Q_b(u)$ of the uth bit of the quadrature-phase component in the form of:

$$P^Q_b(u) = \frac{1}{2} - \frac{2}{\pi M^Q_k} \int_0^\infty \frac{\Phi_{\xi^Q}(\omega)}{\omega} \times \sum_{l=0}^{(1-2^{-u})M^Q_k-1} \left\{ (-1)^{\left\lfloor \frac{l2^{u-1}}{M^Q_k} \right\rfloor} \left(2^{u-1} - \left\lfloor \frac{l2^{u-1}}{M^Q_k} + \frac{1}{2} \right\rfloor \right) \Im\left\{ \Phi_{h_0}\left[(2l+1)d^Q_0\omega\right]\right\} \right\} \mathrm{d}\omega. \tag{6.26}$$

Finally, the average BER of M-ary general R-QAM can be obtained by averaging the error probabilities given by Equations 6.24 and 6.26 [212]:

$$P_b = \frac{1}{\log_2 M_0} \left(\sum_{u=1}^{\log_2 M^I_0} P^I_b(u) + \sum_{u=1}^{\log_2 M^Q_0} P^Q_b(u) \right). \tag{6.27}$$

[3]The calculation of the QAM BER conditioned on h_0 is closely related to the probability $P_{\xi^I}\{x > dh_0\}$, given a distance d from the decision boundary. When $f_{\xi^I}(x)$ is even, we have $P_{\xi^I}\{x > dh_0\} = 1 - \mathrm{F}_{\xi^I}(dh_0)$. When ξ^I is Gaussian, this probability reduces to $\frac{1}{2}\mathrm{erfc}(\frac{dh_0}{\sqrt{N_0}})$, which is the result in [212].

When there is no interference, i.e. we have $K = 0$, Equations 6.24 and 6.26 reduce to the single-user results of [276, 277]. As expected, when only BPSK or QPSK are considered, i.e. we have $d_k^I = d_k^Q$ and $M_k = 2, 4$ for all users, Equations 6.24 and 6.26 reduce to the results of [290].

6.3.2 Special Cases

6.3.2.1 Error Probability of Square QAM

When only S-QAM is considered, i.e. we have $d_k^I = d_k^Q$ and $M_k^I = M_k^Q = \sqrt{M_k}$ for all users, therefore we arrive at $P_b^I(u) = P_b^Q(u)$. Hence Equation 6.27 reduces to:

$$P_b = \frac{2}{\log_2 M_0} \sum_{u=1}^{\log_2 M_0^I} P_b^I(u), \tag{6.28}$$

which requires only a single numerical integration.

6.3.2.2 Error Probability of QPSK in the Presence of Rayleigh Interferers

When only QPSK is considered and all interferers are subjected to Rayleigh fading, i.e. we have $M_k^I = M_k^Q = 2$ for all users and $m_k = 1$ for $k = 1, ..., K$, Equation 6.21 reduces to:

$$\Phi_{I_k^I|\lambda_0,\lambda_1,\lambda_2}(\omega) = \begin{cases} \exp\left(-\frac{\Omega_k}{4}\lambda_0\omega^2\right), & \lambda_2 = 0, \\ \sqrt{\frac{\pi}{\lambda_2\Omega_k\omega^2}} \exp\left[-\left(\lambda_0 - \frac{\lambda_1^2}{\lambda_2}\right)\frac{\Omega_k\omega^2}{4}\right] \operatorname{erf}\left(x\sqrt{\frac{\Omega_k\omega^2}{4\lambda_2}}\right)\Bigg|_{\lambda_1}^{\lambda_1+\lambda_2}, & \lambda_2 \neq 0, \end{cases} \tag{6.29}$$

where $\operatorname{erf}(x)$ is the error function [259].

Taking into account that $M_k^I = M_k^Q = 2$, Equations 6.24 and 6.26 reduce to:

$$P_b^I(1) = \frac{1}{2} - \frac{\Gamma\left(m_0 + \frac{1}{2}\right)}{\pi\Gamma(m_0)}\sqrt{\frac{\Omega_0}{m_0}}\int_0^\infty \Phi_{\xi^I}(\omega)\,{}_1\mathbb{F}_1\left(m_0 + \frac{1}{2}; \frac{3}{2}; -\frac{\Omega_0}{m_0}\left(d_0^I\right)^2\omega^2\right), \tag{6.30}$$

$$P_b^Q(1) = \frac{1}{2} - \frac{\Gamma\left(m_0 + \frac{1}{2}\right)}{\pi\Gamma(m_0)}\sqrt{\frac{\Omega_0}{m_0}}\int_0^\infty \Phi_{\xi^Q}(\omega)\,{}_1\mathbb{F}_1\left(m_0 + \frac{1}{2}; \frac{3}{2}; -\frac{\Omega_0}{m_0}\left(d_0^Q\right)^2\omega^2\right). \tag{6.31}$$

Accordingly, Equation 6.27 reduces to:

$$P_b = \frac{1}{2}\left[P_b^I(1) + P_b^Q(1)\right]. \tag{6.32}$$

Furthermore, if the minimum distance between signal points on both the in-phase and quadrature-phase axes is the same, i.e. we have $d_k^I = d_k^Q$, then we arrive at $P_b^I(1) = P_b^Q(1)$. Hence, Equations 6.30 - 6.32 may be further simplified to:

$$P_b = \frac{1}{2} - \frac{\Gamma\left(m_0 + \frac{1}{2}\right)}{\pi\Gamma(m_0)}\sqrt{\frac{\Omega_0}{m_0}}\int_0^\infty \Phi_{\xi^I}(\omega)\,{}_1\mathbb{F}_1\left(m_0 + \frac{1}{2}; \frac{3}{2}; -\frac{\Omega_0}{m_0}\left(d_0^I\right)^2\omega^2\right), \tag{6.33}$$

which has been been given in [290].

6.3.2.3 Error Probability of PAM in the Presence of Interference

When the real-valued one-dimensional Pulse Amplitude Modulation (PAM) is considered, i.e. we have $M_k = M_k^I$ and $d_k^Q = 0$, there is no crosstalk imposed by the quadrature-phase component on the in-phase component. Hence, Equation 6.17 reduces to:

$$\Phi_{I_k^I}(\omega) = \frac{1}{M_k^2}\sum_{b_{k,-1}^I, b_{k,0}^I \in \mathcal{A}_k^I} \Phi_{I_k^I|b_{k,-1}^I, b_{k,0}^I}(\omega), \tag{6.34}$$

where the conditional CF, $\Phi_{I_k^I|b_{k,-1}^I, b_{k,0}^I}(\omega)$, may be shown to be given by:

$$\Phi_{I_k^I|b_{k,-1}^I, b_{k,0}^I}(\omega) = \begin{cases} {}_1\mathbb{F}_1\left[m_k; 1; -\frac{\Omega_k}{4m_k}\left(d_k^I b_{k,0}^I\right)^2\omega^2\right], & b_{k,-1}^I = b_{k,0}^I, \\ \frac{x}{b_{k,-1}^I - b_{k,0}^I}\,{}_2\mathbb{F}_2\left[m_k, \frac{1}{2}; 1, \frac{3}{2}; -\frac{\Omega_k}{4m_k}\left(d_k^I\right)^2\omega^2 x^2\right]\Big|_{b_{k,0}^I}^{b_{k,-1}^I}, & b_{k,-1}^I \neq b_{k,0}^I. \end{cases} \tag{6.35}$$

where ${}_p\mathbb{F}_q(\alpha_1, \alpha_2, ..., \alpha_p; \beta_1, \beta_2, ..., \beta_q; x)$ is the generalized hypergeometric function [259]. Furthermore, Equation 6.27 reduces to:

$$P_b = \frac{1}{\log_2 M_0}\sum_{u=1}^{\log_2 M_0} P_b^I(u), \tag{6.36}$$

where $P_b^I(u)$ is calculated from Equation 6.24 as in the complex-valued scenario of Section 6.3.1.

6.3.2.4 Error Probability of BPSK

When BPSK is considered, i.e. we have $M_k = M_k^I = 2$ and $d_k^Q = 0$, the results of Section 6.3.1 may be further simplified. Equation 6.17 reduces to:

$$\Phi_{I_k^I}(\omega) = \frac{1}{2}{}_1\mathbb{F}_1\left[m_k; 1; -\frac{\Omega_k}{4m_k}\left(d_k^I\right)^2\omega^2\right] + \frac{1}{2}{}_2\mathbb{F}_2\left[m_k, \frac{1}{2}; 1, \frac{3}{2}; -\frac{\Omega_k}{4m_k}\left(d_k^I\right)^2\omega^2\right]. \quad (6.37)$$

Furthermore, Equations 6.24 and 6.27 reduce to:

$$P_b = P_b^I(1) = \frac{1}{2} - \frac{\Gamma\left(m_0 + \frac{1}{2}\right)}{\pi\Gamma(m_0)}\sqrt{\frac{\Omega_0}{m_0}}\int_0^\infty \Phi_{\xi^I}(\omega){}_1\mathbb{F}_1\left[m_0 + \frac{1}{2}; \frac{3}{2}; -\frac{\Omega_0}{m_0}\left(d_0^I\right)^2\omega^2\right]. \quad (6.38)$$

These results have been given in [290].

6.3.2.5 Error Probability R-QAM in the Absence of Interference

When there is no interference, i.e. we have $K = 0$, the results in Section 6.3.1 reduce to the single-user results. More specifically, Equations 6.24 and 6.26 reduce to:

$$P_b^I(u) = \frac{\Gamma\left(m_0 + \frac{1}{2}\right)}{\sqrt{\pi}M_k^I\Gamma(m_0+1)}\sum_{l=0}^{(1-2^{-u})M_k^I-1}(-1)^{\left\lfloor\frac{l2^{u-1}}{M_k^I}\right\rfloor}\left(2^{u-1} - \left\lfloor\frac{l2^{u-1}}{M_k^I} + \frac{1}{2}\right\rfloor\right)$$
$$\times\left[\frac{m_0N_0}{\Omega_0(2l+1)^2\left(d_0^I\right)^2}\right]^{m_0}{}_2\mathbb{F}_1\left[m_0, m_0+\frac{1}{2}; m_0+1; -\frac{m_0N_0}{\Omega_0(2l+1)^2\left(d_0^I\right)^2}\right], \quad (6.39)$$

$$P_b^Q(u) = \frac{\Gamma\left(m_0 + \frac{1}{2}\right)}{\sqrt{\pi}M_k^Q\Gamma(m_0+1)}\sum_{l=0}^{(1-2^{-u})M_k^Q-1}(-1)^{\left\lfloor\frac{l2^{u-1}}{M_k^Q}\right\rfloor}\left(2^{u-1} - \left\lfloor\frac{l2^{u-1}}{M_k^Q} + \frac{1}{2}\right\rfloor\right)$$
$$\times\left[\frac{m_0N_0}{\Omega_0(2l+1)^2\left(d_0^Q\right)^2}\right]^{m_0}{}_2\mathbb{F}_1\left[m_0, m_0+\frac{1}{2}; m_0+1; -\frac{m_0N_0}{\Omega_0(2l+1)^2\left(d_0^Q\right)^2}\right] \quad (6.40)$$

where ${}_2\mathbb{F}_1(\alpha, \beta; \gamma; x)$ is the hypergeometric function [259]. These results are equivalent to Equation 12 in [276].

6.3.3 Gaussian Approximation

Owing to its simplicity, the Gaussian Approximation (GA) is widely used for modeling interference, when the number of interferers is sufficiently high. Owing to the Central Limit Theorem (CLT), the in-phase CCI I_k^I may be assumed to be approximately

Gaussian distributed and its variance may be shown to be:

$$\sigma_{I_k^I}^2 = \frac{\Omega_k}{9}\left\{\left(d_k^I\right)^2\left[\left(M_k^I\right)^2-1\right]+\left(d_k^Q\right)^2\left[\left(M_k^Q\right)^2-1\right]\right\}. \tag{6.41}$$

Treating the in-phase CCI as noise, i.e. replacing N_0 with $N_0+2\sum_{k=1}^{K}\sigma_{I_k^I}^2$ in Equation 6.39, we arrive at the corresponding formula for $P_b^I(u)$. Following the same approach, we may derive the Gaussian-approximation based expression for $P_b^Q(u)$.

$$P_b^I(u) \approx \frac{\Gamma\left(m_0+\frac{1}{2}\right)}{\sqrt{\pi}M_k^I\Gamma(m_0+1)}\sum_{l=0}^{(1-2^{-u})M_k^I-1}(-1)^{\left\lfloor\frac{l2^{u-1}}{M_k^I}\right\rfloor}\left(2^{u-1}-\left\lfloor\frac{l2^{u-1}}{M_k^I}+\frac{1}{2}\right\rfloor\right)$$
$$\times\left[\frac{m_0\left(N_0+2\sum_{k=1}^{K}\sigma_{I_k^I}^2\right)}{\Omega_0(2l+1)^2\left(d_0^I\right)^2}\right]^{m_0}{}_2\mathbb{F}_1\left[m_0,m_0+\frac{1}{2};m_0+1;-\frac{m_0\left(N_0+2\sum_{k=1}^{K}\sigma_{I_k^I}^2\right)}{\Omega_0(2l+1)^2\left(d_0^I\right)^2}\right] \tag{6.42}$$

$$P_b^Q(u) \approx \frac{\Gamma\left(m_0+\frac{1}{2}\right)}{\sqrt{\pi}M_k^Q\Gamma(m_0+1)}\sum_{l=0}^{(1-2^{-u})M_k^Q-1}(-1)^{\left\lfloor\frac{l2^{u-1}}{M_k^Q}\right\rfloor}\left(2^{u-1}-\left\lfloor\frac{l2^{u-1}}{M_k^Q}+\frac{1}{2}\right\rfloor\right)$$
$$\times\left[\frac{m_0\left(N_0+2\sum_{k=1}^{K}\sigma_{I_k^Q}^2\right)}{\Omega_0(2l+1)^2\left(d_0^Q\right)^2}\right]^{m_0}{}_2\mathbb{F}_1\left[m_0,m_0+\frac{1}{2};m_0+1;-\frac{m_0\left(N_0+2\sum_{k=1}^{K}\sigma_{I_k^Q}^2\right)}{\Omega_0(2l+1)^2\left(d_0^Q\right)^2}\right] \tag{6.43}$$

6.4 Numerical Results

In this section, we will verify the accuracy of our exact BER expression provided in Section 6.3 and demonstrate the limited accuracy of the GA method by Monte Carlo simulations.

We assume that the minimum distance between signal points of the in-phase and quadrature-phase components is the same, i.e. we have $d_k^I = d_k^Q$, which is typical in QAM, although our analysis outlined in Section 6.3 also applies to more general cases, where d_k^I and d_k^Q are not necessarily equal. Furthermore, the average interference power imposed by each interferer is common and they experience the same fading statistics as the desired signal, i.e. we have the same m_k value for all users, $k = 0, 1, ..., K$. Nevertheless, our analysis outlined in Section 6.3 applies to various general cases, where the average power of each

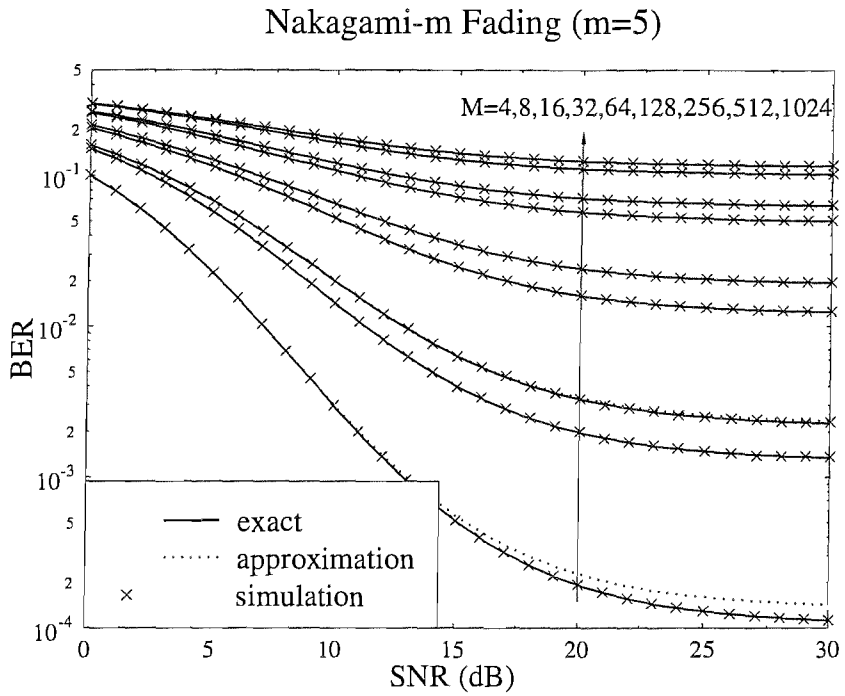

FIGURE 6.3: BER versus the per-bit SNR in a R-QAM system subjected to asynchronous CCI and Nakagami-m fading. All users have the same constellation size, i.e. $M_k = M$. The constellation size assumes values of $M = 4$, 8, 16, 32, 64, 128, 256, 512 and 1024, respectively. The minimum distances between signal points of the in-phase and quadrature-phase components are the same, i.e. $d_k^I = d_k^Q$. The number of interferers is $K = 6$. The per-bit SIR is 10dB. The average power of each interferer is identical and they experience the same fading distribution as the desired signal, i.e. we have $m_k = 5$.

interferer is different or where each user experiences different fading distributions. We define the per-bit Signal-to-Interference Ratio (SIR) as:

$$\mathrm{SIR} = \frac{1}{\log_2 M_0} \frac{\Omega_0 \left\{ (d_0^I)^2 \left[\left(M_0^I\right)^2 - 1 \right] + (d_0^Q)^2 \left[\left(M_0^Q\right)^2 - 1 \right] \right\}}{\sum_{k=1}^{K} \Omega_k \left\{ (d_k^I)^2 \left[\left(M_k^I\right)^2 - 1 \right] + (d_k^Q)^2 \left[\left(M_k^Q\right)^2 - 1 \right] \right\}}. \tag{6.44}$$

6.4.1 Effects of the SNR

Figures 6.3 and 6.4 illustrate the average BER performance versus the per-bit SNR expressed in dB in the context of Nakagami-m fading channels associated with the parameters of $m = 5$ and $m = 10$, respectively. We assume that the number of interferers

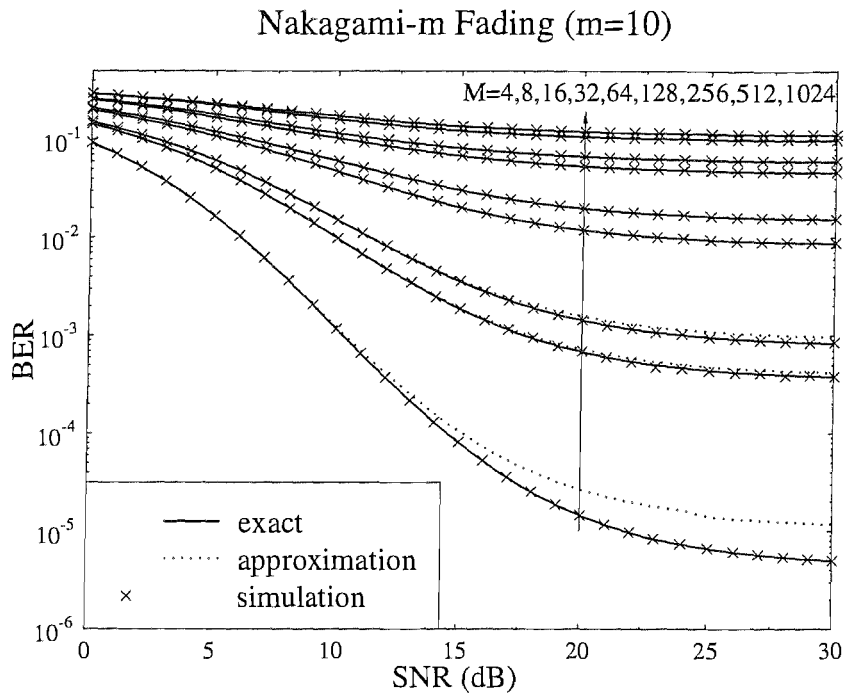

FIGURE 6.4: BER versus the per-bit SNR in a R-QAM system subjected to asynchronous CCI and Nakagami-m fading. All users have the same constellation size, i.e. $M_k = M$. The constellation size assumes values of M = 4, 8, 16, 32, 64, 128, 256, 512 and 1024, respectively. The minimum distances between signal points of the in-phase and quadrature-phase components are the same, i.e. $d_k^I = d_k^Q$. The number of interferers is $K = 6$. The per-bit SIR is 10dB. The average power of each interferer is identical and they experience the same fading distribution as the desired signal, i.e. we have $m_k = 10$.

is $K = 6$ in both figures. This is typical in the hexagonal cellular model of TDMA cellular networks, where each cell is surrounded by $K = 6$ adjacent so-called first-tier interfering cells and usually only the interference imposed by these $K = 6$ adjacent cells is considered. As seen in both figures, the results calculated by our exact BER analysis and the simulation results match both for various constellation sizes and for various Nakagami-m fading parameters. On the other hand, the GA over-estimates the average BER. When the per-bit SNR is high, the effects of SIR become dominant. Since the SIR distribution is non-Gaussian, the GA becomes less accurate. When the fading becomes less severe, i.e. the Nakagami-m parameter increases, the interferers' Line-Of-Sight (LOS) components become dominant, hence the CCI is less accurately approximated by a Gaussian variable. When the number of bits/symbol is low, the Central Limit Theorem (CLT) no longer applies and hence the GA becomes less accurate.

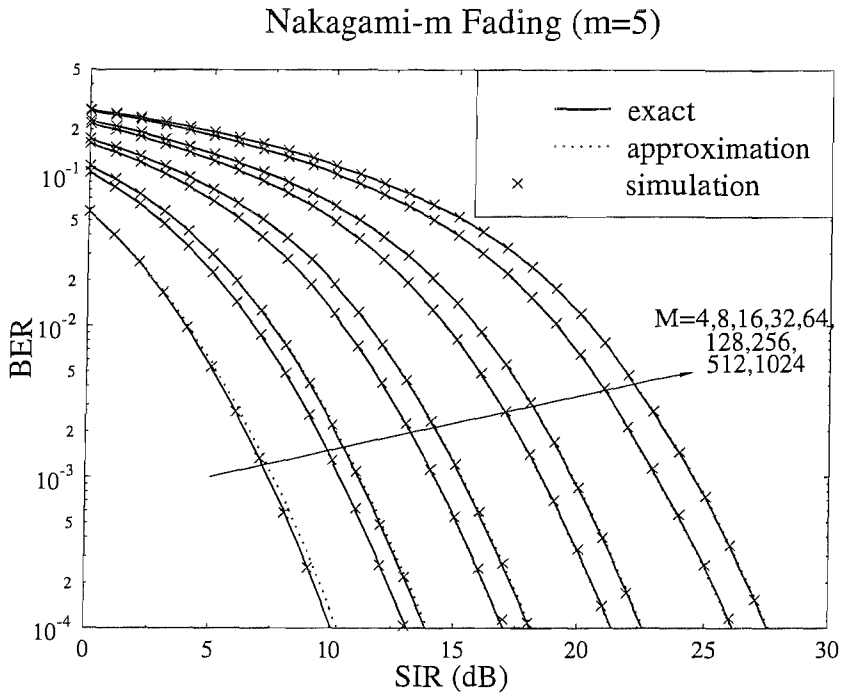

FIGURE 6.5: BER versus the per-bit SIR in a R-QAM system subjected to asynchronous CCI and Nakagami-m fading. All users have the same constellation size, i.e. $M_k = M$. The constellation size assumes values of $M = 4$, 8, 16, 32, 64, 128, 256, 512 and 1024, respectively. The minimum distances between signal points of the in-phase and quadrature-phase components are the same, i.e. $d_k^I = d_k^Q$. The number of interferers is $K = 6$. The average power of each interferer is common and they experience the same fading distribution as the desired signal, i.e. we have $m_k = 5$. The background noise is ignored.

6.4.2 Effects of the SIR

Figures 6.5 and 6.6 illustrate the average BER performance versus the per-bit SIR expressed in dB in the context of Nakagami-m fading channels associated with the parameters of $m = 5$ and $m = 10$, respectively. Since the evaluation of the effects of CCI on the QAM BER is the main objective of our analysis, we assume that the effects of noise are negligible. As seen in Figures 6.5 and 6.6, the results calculated by our exact BER analysis and the simulation results match both for various constellation sizes and for various Nakagami-m fading parameters. On the other hand, the GA slightly over-estimates the average BER. As expected, when the per-bit SIR is high, the fading becomes less severe and the number of bits/symbol is low, hence the GA becomes less accurate.

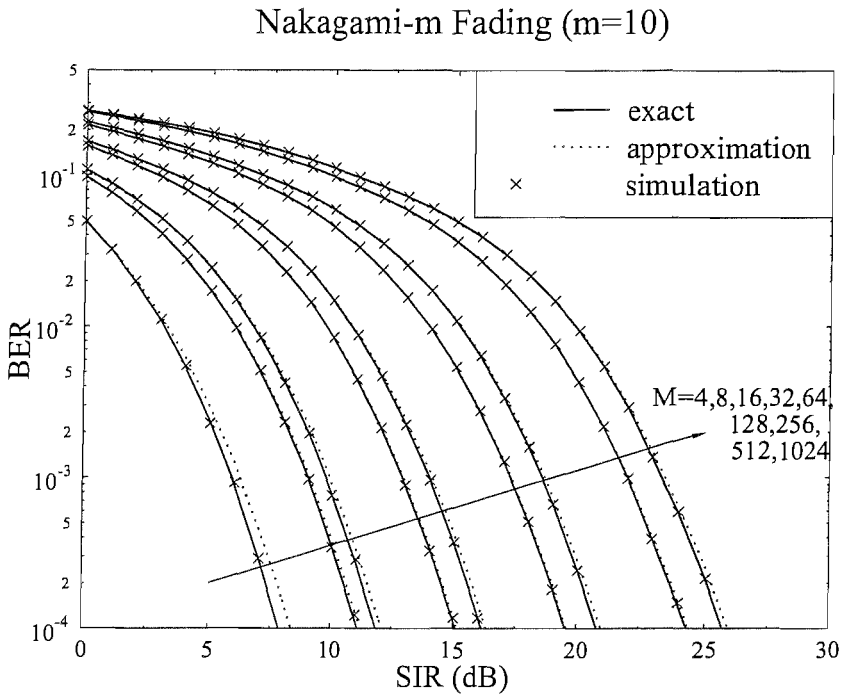

FIGURE 6.6: BER versus the per-bit SIR in a R-QAM system subjected to asynchronous CCI and Nakagami-m fading. All users have the same constellation size, i.e. $M_k = M$. The constellation size assumes values of M = 4, 8, 16, 32, 64, 128, 256, 512 and 1024, respectively. The minimum distances between signal points of the in-phase and quadrature-phase components are the same, i.e. $d_k^I = d_k^Q$. The number of interferers is $K = 6$. The average power of each interferer is common and they experience the same fading distribution as the desired signal, i.e. we have $m_k = 10$. The background noise is ignored.

6.4.3 Effects of the Number of Interferers

Although there are six adjacent first-tier interfering cells, different interferers may have different levels of influence. It is typical that there are one or two dominant interferers. Figures 6.7 and 6.8 illustrate the average BER performance versus the number of interferers. For the sake of simplicity, we assume that the average power of all dominant interferers is the same and the influence of all non-dominant interferers is negligible. As we expected, the results obtained by our exact BER analysis and the simulation results match for various constellation sizes and various Nakagami-m fading parameters. On the other hand, the GA over-estimates the average BER, especially when the constellation size is small, the fading becomes less severe and the number of interferers is small.

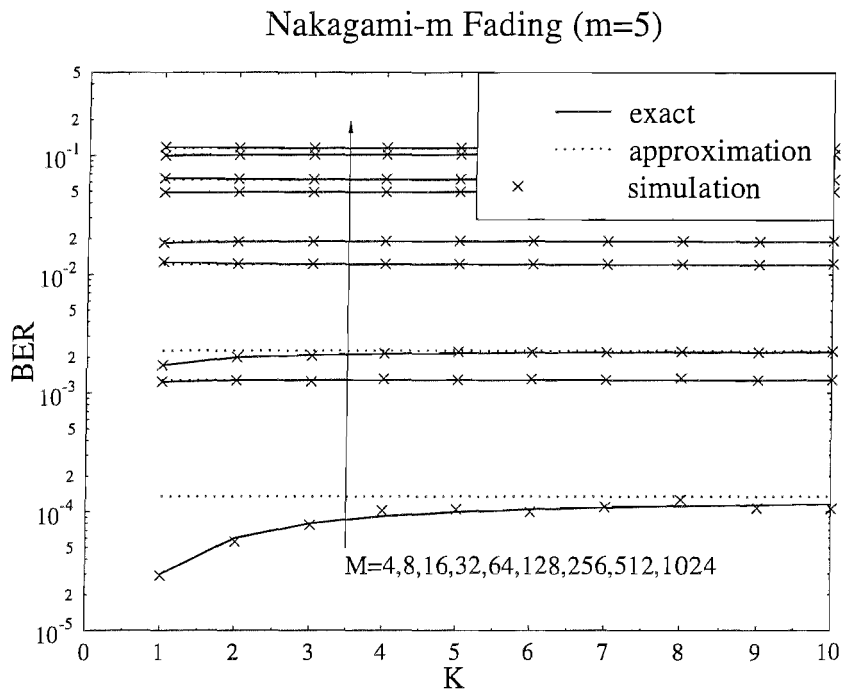

FIGURE 6.7: BER versus the number of interferers in a R-QAM system subjected to asynchronous CCI and Nakagami-m fading. All users have the same constellation size, i.e. $M_k = M$. The constellation size assumes values of $M = 4$, 8, 16, 32, 64, 128, 256, 512 and 1024, respectively. The minimum distances between signal points of the in-phase and quadrature-phase components are the same, i.e. $d_k^I = d_k^Q$. The per-bit SIR is 10dB. The average power of each interferer is common and they experience the same fading distribution as the desired signal, i.e. we have $m_k = 5$. The background noise is ignored.

6.4.4 Comparison between the BPSK and QPSK systems

It is widely recognized that the BPSK and QPSK systems have the same BER performance at the same per-bit SNR value in the absence of the CCI. Although the Gaussian approximations outlined in Section 6.3.3 also have the same BER formulae results for BPSK and QPSK scenarios, this does not mean that these two systems actually perform identically. Figures 6.9 - 6.11 compare the average BER performance of BPSK and QPSK schemes in the presence of CCI. Note that the Gaussian approximations based BER results of for these two schemes are the same in Figures 6.9 - 6.11. However, as seen from these figures, the results obtained from our exact analysis and from our simulations diverge, especially when the SNR value is high, the SIR value is high, the number of interferers is low and the fading becomes less severe. This might be caused

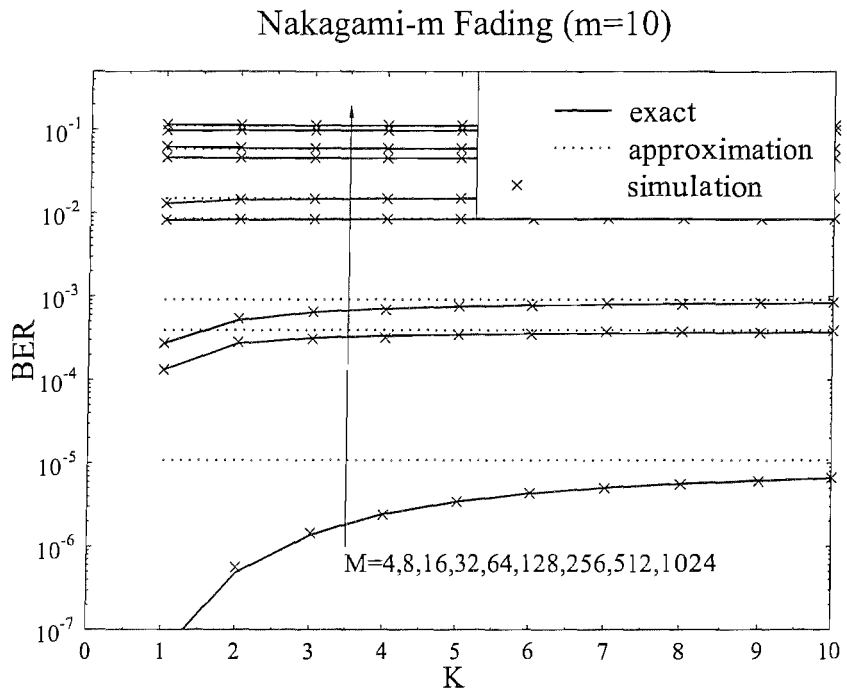

FIGURE 6.8: BER versus the number of interferers in a R-QAM system subjected to asynchronous CCI and Nakagami-m fading. All users have the same constellation size, i.e. $M_k = M$. The constellation size assumes values of $M = 4$, 8, 16, 32, 64, 128, 256, 512 and 1024, respectively. The minimum distances between signal points of the in-phase and quadrature-phase components are the same, i.e. $d_k^I = d_k^Q$. The per-bit SIR is 10dB. The average power of each interferer is common and they experience the same fading distribution as the desired signal, i.e. we have $m_k = 10$. The background noise is ignored.

by the inter-dependence of the random variables, X_k^I and X_k^Q, which may be concluded from Equations 6.14 - 6.15.

6.5 Conclusion

An exact and general BER expression has been derived for general R-QAM systems subjected to asynchronous CCI and Nakagami-m fading, which requires only two single numerical integrations. A new closed-form formula was provided for the CF of the CCI with the aid of the generalized Lauricella function of n variables [266]. Our simulation results verified the accuracy of our exact BER analysis for different constellation sizes and for various channel statistics. By contrast, the Gaussian model of CCI fails to accurately predict the QAM BER performance.

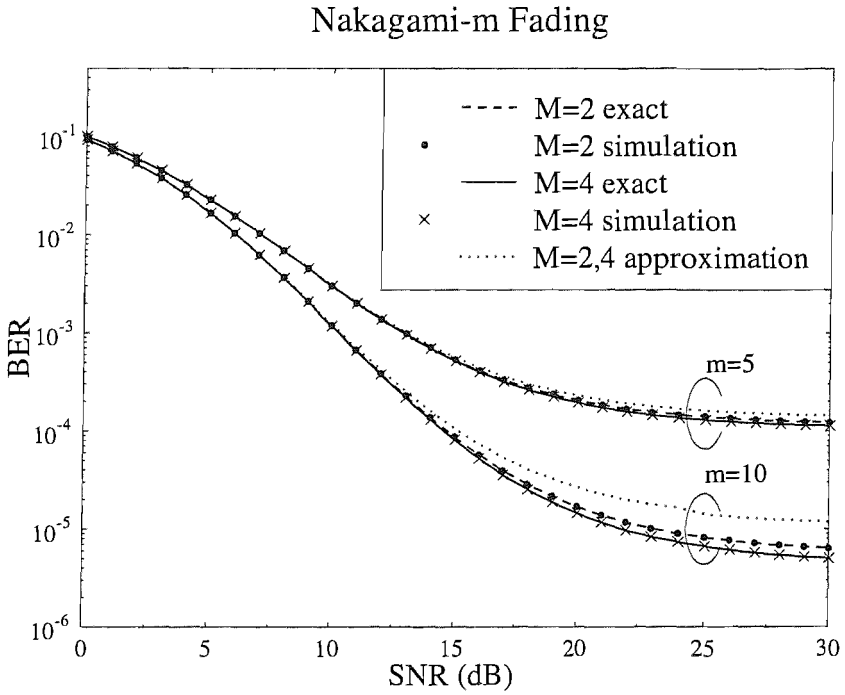

FIGURE 6.9: BER versus the per-bit SNR in a R-QAM system subjected to asynchronous CCI and Nakagami-m fading. All users have the same constellation size, i.e. $M_k = M$. The constellation size assumes values of $M = 2$ and 4, respectively. The minimum distances between signal points of the in-phase and quadrature-phase components are the same, i.e. $d_k^I = d_k^Q$. The number of interferers is $K = 6$. The per-bit SIR is 10dB. The average power of each interferer is identical and they experience the same fading distribution as the desired signal, i.e. we have $m_k = m$. The Nakagami-m parameter assumes values of $m = 5$ and 10, respectively.

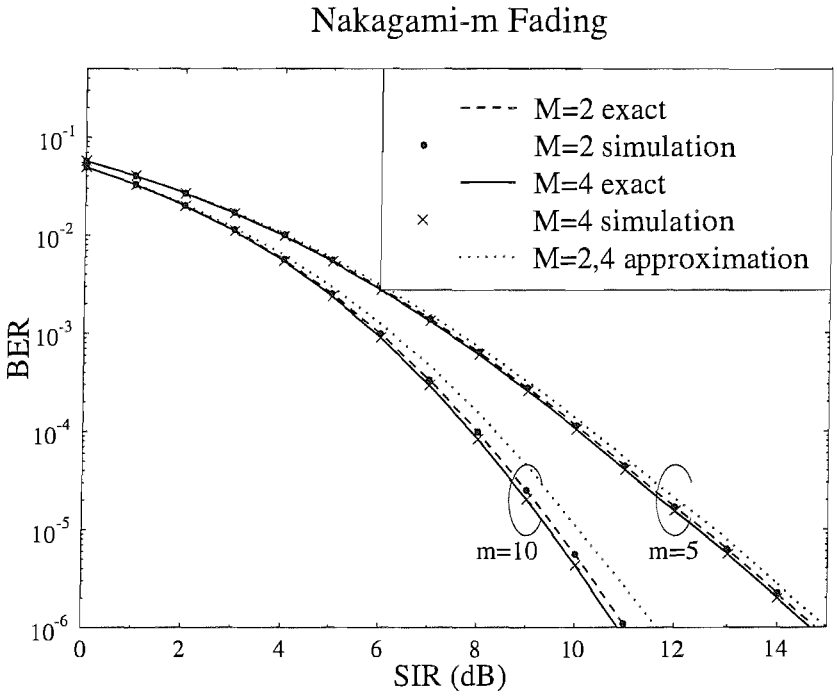

FIGURE 6.10: BER versus the per-bit SIR in a R-QAM system subjected to asynchronous CCI and Nakagami-m fading. All users have the same constellation size, i.e. $M_k = M$. The constellation size assumes values of $M = 2$ and 4, respectively. The minimum distances between signal points of the in-phase and quadrature-phase components are the same, i.e. $d_k^I = d_k^Q$. The number of interferers is $K = 6$. The average power of each interferer is common and they experience the same fading distribution as the desired signal, i.e. we have $m_k = m$. The Nakagami-m parameter assumes values of $m = 5$ and 10, respectively. The background noise is ignored.

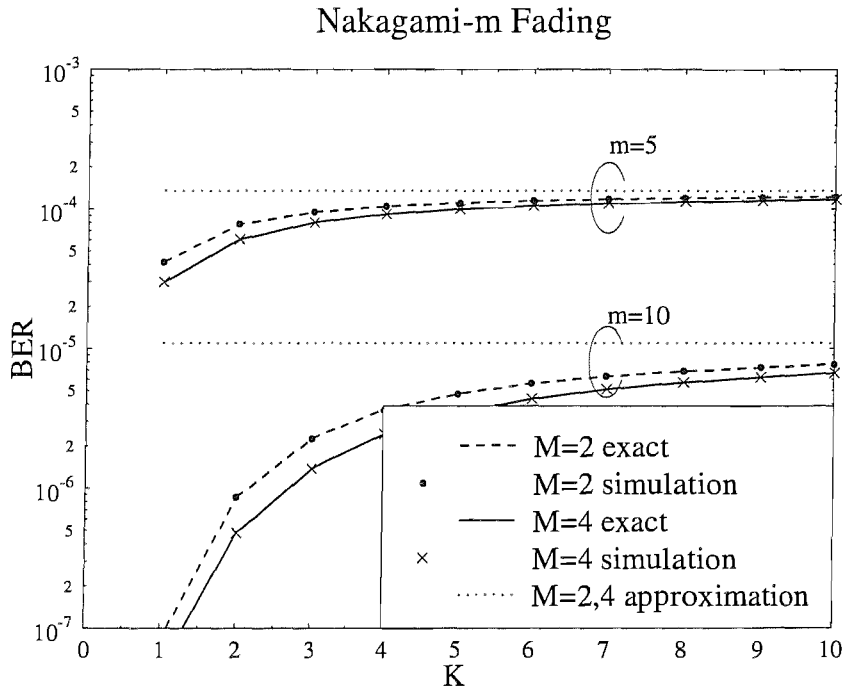

FIGURE 6.11: BER versus the number of interferers in a R-QAM system subjected to asynchronous CCI and Nakagami-m fading. All users have the same constellation size, i.e. $M_k = M$. The constellation size assumes values of $M = 2$ and 4, respectively. The minimum distances between signal points of the in-phase and quadrature-phase components are the same, i.e. $d_k^I = d_k^Q$. The per-bit SIR is 10dB. The average power of each interferer is common and they experience the same fading distribution as the desired signal, i.e. we have $m_k = m$. The Nakagami-m parameter assumes values of $m = 5$ and 10, respectively. The background noise is ignored.

Chapter 7

Exact BER Analysis of OFDM Systems Communicating over Frequency-Selective Fading Channels in the Presence of Both Carrier Frequency Offset and Channel Estimation Errors

7.1 Introduction

In recent years Orthogonal Frequency Division Multiplexing (OFDM) [215] has attracted intensive research efforts and, as a result, has found its way into numerous wireless standards. However, OFDM is sensitive to the effects of Carrier Frequency Offset (CFO), which destroys the orthogonality of the OFDM subcarriers and inflicts Inter-Carrier Interference (ICI). The performance degradation imposed by the CFO has been extensively studied in the open literature [293–305].

As a benefit of the associated mathematical simplicity, the Signal-to-Interference-plus-Noise Ratio (SINR) or Signal-to-Noise Ratio (SNR) have been the predominantly quantified performance metrics over the past decade [293–298]. Nevertheless, the most important performance evaluation metrics are the Bit Error Ratio (BER) [299–301] and

the Symbol Error Ratio (SER) [298, 302], which characterize the associated performance degradation more accurately.

One of the difficulties in the analysis of the performance degradation caused by CFO in OFDM systems is the statistical characterization of the ICI. Typically the ICI is assumed to be approximately Gaussian distributed [298–301, 303], which is based on the Central Limit Theorem (CLT) [260]. However, the accuracy of the Gaussian Approximation (GA) is limited [299], especially when the SNR encountered is high. This is because at high SNRs the effects of ICI become more dominant, particularly at low Doppler frequencies, when the ICI is typically constituted by a low number of immediately adjacent subcarriers. In this scenario the CLT is not satisfied. The exact analysis of the ICI distribution was provided based on either multiple integrals [301] or on the Characteristic Function (CF) [302–304].

At the time of writing the exact analytical BER/SER degradation caused by CFO in OFDM systems has been quantified in the context of Additive White Gaussian Noise (AWGN) channels [302–304], Rayleigh fading channels [301, 303, 305] and Ricean fading channels [301]. Moreover, to the best of the authors' knowledge, there are no studies in the open literature on the exact analytical BER performance of OFDM systems in the context of communicating over Nakagami-m fading channels in the presence of CFO. *Against this background, the novel contribution of this chapter is that we provide a closed-form expression, rather than a sum of the infinite series in [302, 303], for the average BER calculation of OFDM systems in the presence of both CFO and Phase Estimation Error (PER) in the context of frequency-selective Nakagami-m fading channels.*

This chapter is organized as follows. In Section 7.2 an OFDM system using BPSK/QPSK modulation communicating over frequency-selective Nakagami-m channels in the presence of CFO is presented. Then, in Section 7.3 its exact BER performance is investigated based on the CF approach. Our numerical results are presented in Section 7.4 and finally, our conclusions are provided in Section 7.5.

7.2 System Model and Assumptions

We consider an OFDM system having N subcarriers using BPSK or QPSK modulation for communicating over frequency-selective Nakagami-m slow-fading channels.

Let us assume that the data symbols $\{\widetilde{A}_k\}_{k=0}^{N-1}$ transmitted over the N subcarriers are mutually independent and selected from the constellation set according to a uniform

probability distribution. The transmitted equivalent baseband OFDM signal $\widetilde{s}(t)$ can be expressed in the time-domain as [305]:

$$\widetilde{s}(t) = \frac{1}{\sqrt{N}} \sum_{k=0}^{N-1} \widetilde{A}_k e^{j\frac{2\pi kt}{T_u}}, -T_g \leq t < T_u, \tag{7.1}$$

where T_g and T_u are the duration of the cyclic prefix and the useful data signal segment, respectively, $\widetilde{A}_k$ is the information symbol modulating the kth subcarrier in the Frequency-Domain (FD) and N is the number of OFDM subcarriers.

We consider a time-invariant frequency-selective fading channel. Typically the length T_g of the cyclic prefix is designed so that it becomes longer than the maximum propagation delay. Hence the Inter-Symbol Interference (ISI) between consecutive OFDM symbols is considered to be negligible in our analysis. Then the received signal $\widetilde{r}(t)$ encountered in the presence of CFO can be expressed as:

$$\widetilde{r}(t) = \frac{1}{\sqrt{N}} e^{j2\pi f_\Delta t} \sum_{k=0}^{N-1} \widetilde{A}_k \widetilde{h}_k + \widetilde{\eta}(t), -T_g \leq t < T_u, \tag{7.2}$$

where f_Δ denotes the carrier frequency offset between the transmitter and the receiver, and $\widetilde{\eta}(t)$ denotes the zero-mean complex-valued AWGN. More explicitly, $\widetilde{h}_k = h_k e^{j\theta_k}$ represents the complex-valued Frequency-Domain (FD) channel transfer factor (FDCHTF) of the kth subcarrier, where all FDCHTFs are considered to be mutually independent for simplicity. This is an often stipulated assumption in theoretical studies, although in practice the adjacent subcarriers are correlated, unless the Channel Impulse Response (CIR) tends to an infinite duration. In practice this assumption becomes valid, when the channel is quite dispersive and hence the CIR becomes significantly longer than the bit duration at the input of the OFDM modem. The FDCHTF h_k is characterized with the aid of the parameters $\{m_k, \Omega_k\}$, where m_k and Ω_k are the Nakagami-m fading parameter and the average power of the kth subcarrier, respectively[1] [306]. The associated Probability Density Function (PDF) and Characteristic Function (CF) of the FDCHTF h_k were given in [258], while the fading phase θ_k is typically assumed to be uniformly distributed over the interval of $[0, 2\pi)$ [263].

The received signal is sampled within an OFDM symbol at the time instants:

$$t_n = \frac{nT_u}{N}, n = 0, 1, ..., N-1. \tag{7.3}$$

[1]When the time-domain fading is Nakagami-m distributed, it is not strictly true that the frequency-domain fading is also Nakagami-m distributed. Nevertheless, this is a reasonable approximation, as it was argued in [306] and hence it will be exploited in this treatise.

Then the N Time-Domain (TD) samples $\{\widetilde{b}_n\}_{n=0}^{N-1}$ within an OFDM symbol are given by:

$$\widetilde{b}_n = \widetilde{r}(t_n) = \frac{1}{\sqrt{N}} e^{j\frac{2\pi n\epsilon}{N}} \sum_{k=0}^{N-1} \widetilde{A}_k e^{j\frac{2\pi kn}{N}} \widetilde{h}_k + \widetilde{\eta}_n, \tag{7.4}$$

where $\epsilon = f_\Delta T_u$ is the normalized CFO and $\widetilde{\eta}_n = \widetilde{\eta}(t_n)$ is the noise sample at the nth sampling instant within an OFDM symbol.

Upon performing Fast Fourier Transform (FFT) based demodulation [215], the Frequency-Domain (FD) symbols $\{\widetilde{B}_{k'}\}_{k'=0}^{N-1}$ can be expressed as:

$$\begin{aligned}\widetilde{B}_{k'} &= \frac{1}{\sqrt{N}} \sum_{n=0}^{N-1} \widetilde{b}_n e^{-j\frac{2\pi k'n}{N}} \\ &= \sum_{k=0}^{N-1} \widetilde{A}_k \widetilde{d}_{k-k'} \widetilde{h}_k + \frac{1}{\sqrt{N}} \sum_{n=0}^{N-1} \widetilde{\eta}_n e^{-j\frac{2\pi k'n}{N}},\end{aligned} \tag{7.5}$$

where the frequency-offset-dependent complex-valued FDCHTF-contribution $\widetilde{d}_k$ [300–302] induced by the CFO of the kth subcarrier is given by:

$$\widetilde{d}_k = d_k e^{j\psi_k} = \frac{\sin[\pi(k+\epsilon)]}{N\sin[\frac{\pi}{N}(k+\epsilon)]} e^{j\pi(1-\frac{1}{N})(k+\epsilon)}. \tag{7.6}$$

If the receiver is capable of compensating for the aggregate phase-shift $(\psi_0 + \theta_{k'})$ of the k'th subcarrier experiencing a phase estimation error of $\varsigma_{k'}$, $|\varsigma_{k'}| \leq \frac{\pi}{4}$, the decision statistics $\widetilde{Z}_{k'}$ may be written as:

$$\widetilde{Z}_{k'} = \widetilde{D}_{k'} + \sum_{k=0, k\neq k'}^{N-1} \widetilde{I}_{k'k} + \widetilde{\Lambda}_{k'}, \tag{7.7}$$

where the signal component $\widetilde{D}_{k'}$, the ICI component $\widetilde{I}_{k'k}$ imposed on the kth subcarrier and the noise component $\widetilde{\Lambda}_{k'}$ are given by:

$$\widetilde{D}_{k'} = \widetilde{A}_{k'} d_0 h_{k'} e^{j\varsigma_{k'}} \tag{7.8}$$

$$\widetilde{I}_{k'k} = \widetilde{A}_k \widetilde{d}_{k-k'} \widetilde{h}_k e^{-j(\psi_0+\theta_{k'})+j\varsigma_{k'}} \tag{7.9}$$

$$\widetilde{\Lambda}_{k'} = \frac{1}{\sqrt{N}} e^{-j(\psi_0+\theta_{k'})+j\varsigma_{k'}} \sum_{n=0}^{N-1} \widetilde{\eta}_n e^{-j\frac{2\pi k'n}{N}}. \tag{7.10}$$

If we assume furthermore that the noise samples $\widetilde{\eta}_n$, $n = 0, 1, ..., N-1$ are independently and identically distributed zero-mean complex Gaussian variables having a variance of

$2\sigma_\eta^2$, $\widetilde{\Lambda}_{k'}$ may be shown to be a zero-mean complex-valued Gaussian random variable having a variance of $2\sigma_\eta^2$.

7.3 BER Analysis

The analysis procedure of the average Bit Error Probability (BEP) performance based on the CF approach is illustrated at a glance in Figure 7.1. As an extension of the previous related work [208, 238, 243, 247, 250, 302–304], we summarize the analysis procedure concerned as follows:

Step 1 Since the CF of $\Re\{\widetilde{h}_k\}$ is well-known when $\widetilde{h}_k$ is a complex-valued Nakagami-m distributed variable [253], we may readily derive the conditional CF $\Phi_{\Re\{\widetilde{I}_{k'k}\}|\widetilde{A}_k}(\omega)$ of the real ICI component imposed by the kth subcarrier.

Step 2 Averaging $\Phi_{\Re\{\widetilde{I}_{k'k}\}|\widetilde{A}_k}(\omega)$ over all the possible values of $\widetilde{A}_k$, we have the CF $\Phi_{\Re\{\widetilde{I}_{k'k}\}}(\omega)$ of the real ICI component imposed by the kth subcarrier.

Step 3 It may be readily shown that the ICIs $\widetilde{I}_{k'k}$, $k = 0, 1, ..., N-1$ and $k \neq k'$, imposed by the different subcarriers are mutually independent. Upon defining the total interference plus noise $\widetilde{\xi}_{k'}$ experienced by the k'th subcarrier as:

$$\widetilde{\xi}_{k'} = \sum_{k=0, k\neq k'}^{N-1} \widetilde{I}_{k'k} + \widetilde{\Lambda}_{k'}, \tag{7.11}$$

it transpires that both the PDF $f_{\Re\{\widetilde{\xi}_{k'}\}}(x)$ and the CF $\Phi_{\Re\{\widetilde{\xi}_{k'}\}}(\omega)$ of $\Re\{\widetilde{\xi}_{k'}\}$ are even functions. The CF $\Phi_{\Re\{\widetilde{\xi}_{k'}\}}(\omega)$ may be expressed as:

$$\Phi_{\Re\{\widetilde{\xi}_{k'}\}}(\omega) = \Phi_{\Re\{\widetilde{\Lambda}_{k'}\}}(\omega) \prod_{k=0, k\neq k'}^{N-1} \Phi_{\Re\{\widetilde{I}_{k'k}\}}(\omega). \tag{7.12}$$

Step 4 Upon performing the inverse Fourier transform on $\Phi_{\Re\{\widetilde{\xi}_{k'}\}}(\omega)$, we arrive at the PDF $f_{\Re\{\widetilde{\xi}_{k'}\}}(x)$ of $\Re\{\widetilde{\xi}_{k'}\}$. Then upon integrating $f_{\Re\{\widetilde{\xi}_{k'}\}}(x)$, we generate the Cumulative Distribution Function (CDF) $F_{\Re\{\widetilde{\xi}_{k'}\}}(x)$ of $\Re\{\widetilde{\xi}_{k'}\}$. The average BEP $P_{e|\widetilde{A}_{k'},h_{k'}}(k')$ conditioned on the transmitted symbol $\widetilde{A}_{k'}$ and the fading amplitude $h_{k'}$ is given by:

$$P_{e|\widetilde{A}_{k'},h_{k'}}(k') = P\left\{\Re\{\widetilde{\xi}_{k'}\} < \left|\Re\{\widetilde{D}_{k'}\}\right|\right\} = 1 - F_{\Re\{\widetilde{\xi}_{k'}\}}\left(\left|\Re\{\widetilde{D}_{k'}\}\right|\right). \tag{7.13}$$

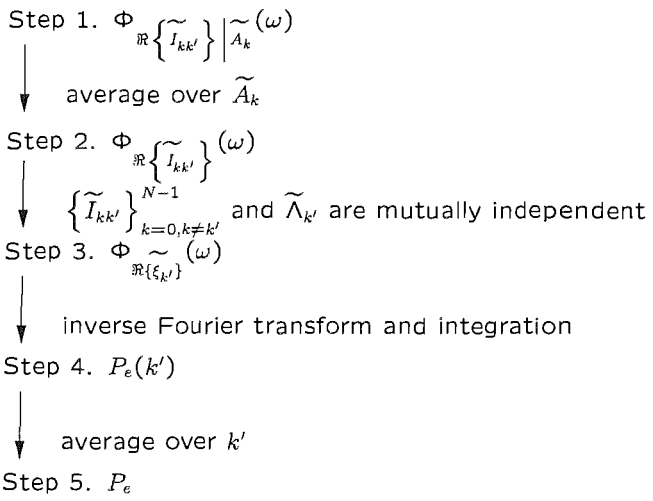

FIGURE 7.1: The analysis procedure of the average BEP performance evaluation based on the CF approach.

Upon integrating $P_{e|\widetilde{A}_{k'},h_{k'}}(k')$ over $\widetilde{A}_{k'}$ and $h_{k'}$, we arrive at the average BEP $P_e(k')$ of the k'th subcarrier. Actually, the procedures outlined in Step 4 are equivalent to applying Parseval's theorem [258], which is more elegant.

Step 5 Upon averaging $P_e(k')$ over all subcarriers, we arrive at the overall average BEP P_e as:

$$P_e = \frac{1}{N}\sum_{k'=1}^{N} P_e(k'). \tag{7.14}$$

7.3.1 BPSK modulation

If BPSK modulation is used and the data symbol $\widetilde{A}_k$ transmitted over the kth subcarrier obeys the symmetric Bernoulli distribution, i.e. we have $P\left\{\widetilde{A}_k = \pm 1\right\} = \frac{1}{2}$, then the conditional CF $\Phi_{\Re\{\widetilde{I}_{k'k}\}|\widetilde{A}_k}(\omega)$ of the real ICI component imposed by the kth subcarrier may be expressed as [253]:

$$\Phi_{\Re\{\widetilde{I}_{k'k}\}|\widetilde{A}_k}(\omega) = {}_1\mathbb{F}_1\left(m_k; 1; -\frac{\Omega_k}{4m_k} d_{k-k'}^2 \omega^2\right). \tag{7.15}$$

Since $\Phi_{\Re\{\widetilde{I}_{k'k}\}|\widetilde{A}_k}(\omega)$ is independent of the transmitted symbol $\widetilde{A}_k$, the CF $\Phi_{\Re\{\widetilde{I}_{k'k}\}}(\omega)$ of the real ICI component imposed by the kth subcarrier may be formulated as:

$$\Phi_{\Re\{\widetilde{I}_{k'k}\}}(\omega) = \Phi_{\Re\{\widetilde{I}_{k'k}\}|\widetilde{A}_{k'}}(\omega). \tag{7.16}$$

Upon applying Parseval's theorem [258], we can express the average BEP of the real component of the k'th subcarrier as:

$$P_e^B(k') = \frac{1}{2} - \frac{1}{\pi}\int_0^\infty \frac{1}{\omega}\Phi_{\Re\{\tilde{\xi}_{k'}\}}(\omega)\Im\left\{\Phi_{h_{k'}}(d_0\omega\cos\varsigma_{k'})\right\}\mathrm{d}\omega, \tag{7.17}$$

where $\Phi_{h_{k'}}(\omega)$ is the imaginary part of the CF of the fading amplitude $h_{k'}$ of the k'th subcarrier, which is given by Table II of [258]. Upon exploiting the integral identity of Equation 5.2.4.35 in [269], we arrive at the closed-form version of Equation 7.17 in the form of:

$$P_e^B(k') = \frac{1}{2} - \frac{\Gamma(m_{k'}+\frac{1}{2})}{\Gamma(m_{k'})}\sqrt{\frac{\gamma_{k'}}{\pi m_{k'}}}\mathbb{F}_A^{(N)}\left(\frac{1}{2}, \alpha_0, ..., \alpha_{N-1}; \beta_0, ..., \beta_{N-1}; -\frac{\gamma_0}{m_0}, ..., -\frac{\gamma_{N-1}}{m_{N-1}}\right), \tag{7.18}$$

where $\mathbb{F}_A^{(n)}(\lambda, \alpha_1, ..., \alpha_n; \beta_1, ..., \beta_n; x_1, ..., x_n)$ is the Lauricella function of n variables [269]. The coefficients of α_k, β_k and γ_k, $k = 0, 1, ..., N-1$, are given by:

$$\alpha_k = \begin{cases} m_{k'} + \frac{1}{2}, k = k', \\ m_{k'}, \quad k \neq k', \end{cases} \tag{7.19}$$

$$\beta_k = \begin{cases} \frac{3}{2}, k = k', \\ \frac{1}{2}, k \neq k', \end{cases} \tag{7.20}$$

$$\gamma_k = \begin{cases} \frac{\Omega_{k'}}{2\sigma_\eta^2} d_0^2 \cos^2\varsigma_{k'}, k = k', \\ \frac{\Omega_k}{2\sigma_\eta^2} d_{k-k'}^2, \quad k \neq k'. \end{cases} \tag{7.21}$$

As seen from Equations 7.19 and 7.20, there are only five distinct parameter values for λ, $\{\alpha_k\}$ and β_k in Equation 7.18. As seen from Equations 7.6 and 7.21, all N variables $\{\frac{\gamma_k}{m_k}\}$ may be calculated from N, ϵ, k', $\varsigma_{k'}$, Ω and m when all subcarriers have the same channel fading statistics $\{\Omega, m\}$. Hence Equation 7.18 is mathematically tractable using the equivalent integral representation provided in Appendix E.6, even when N is large, although formally there are $(3N+1)$ arguments in the Lauricella function $\mathbb{F}_A^{(n)}(\lambda, \alpha_1, ..., \alpha_n; \beta_1, ..., \beta_n; x_1, ..., x_n)$.

If there is no CFO, i.e. we have $\epsilon = 0$, there will be no ICI and the system is equivalent to a single-carrier and single-user Nakagami-m fading model [307]. Accordingly, Equation 7.18 reduces to

$$P_e^B(k') = \frac{1}{2} - \frac{\Gamma(m_{k'}+\frac{1}{2})}{\Gamma(m_{k'})}\sqrt{\frac{\gamma_{k'}}{\pi m_{k'}}}{}_2\mathbb{F}_1\left(m_{k'}+\frac{1}{2}, \frac{1}{2}; \frac{3}{2}; -\frac{\gamma_{k'}}{m_{k'}}\right), \tag{7.22}$$

where ${}_2\mathbb{F}_1(\alpha, \beta; \gamma; x)$ is the hypergeometric function [259]. Equation 7.22 is equivalent to

Equation 8.106 in [307] for BPSK, except that there is a multiplicative factor of $\cos^2 \varsigma_{k'}$ in Equation 7.21, which is induced by the phase estimation error.

7.3.2 QPSK modulation

If QPSK modulation is used and the data symbol $\widetilde{A}_k$ transmitted over the kth subcarrier is uniformly distributed, i.e. we have $P\left\{\widetilde{A}_k = \pm 1 \pm j\right\} = \frac{1}{4}$, the average BEPs $P_e^r(k')$ and $P_e^i(k')$ of the real and imaginary components of each subcarrier are identical due to the associated symmetry, i.e. we have $P_e(k') = P_e^r(k') = P_e^i(k')$. Hence we will only analyze the average BEP $P_e^r(k')$ of the real component of the k'th subcarrier in this subsection.

Since $|\widetilde{A}_k| = \sqrt{2}$, similar to the derivation in Section 7.3.1 we have the CF $\Phi_{\Re\{\widetilde{I}_{k'k}\}}(\omega)$ of the real ICI component imposed by the kth subcarrier as [253]:

$$\Phi_{\Re\{\widetilde{I}_{k'k}\}}(\omega) = \Phi_{\Re\{\widetilde{I}_{k'k}\}|\widetilde{A}_k}(\omega) = {}_1\mathbb{F}_1\left(m_k; 1; -\frac{\Omega_k}{2m_k} d_{k-k'}^2 \omega^2\right). \tag{7.23}$$

Following the same procedure as in Section 7.3.1, the BEP $P^r_{e|\widetilde{A}_{k'}}(k')$ conditioned on the transmitted symbol $\widetilde{A}_{k'}$ of the k'th subcarrier can be shown to be:

$$P^r_{e|\widetilde{A}_{k'}=1+j}(k') = P^r_{e|\widetilde{A}_{k'}=-1-j}(k') \tag{7.24}$$
$$= \frac{1}{2} - \frac{\Gamma(m_{k'} + \frac{1}{2})}{\Gamma(m_{k'})} \sqrt{\frac{\gamma_{k'}^+}{\pi m_{k'}}} \mathbb{F}_A^{(N)}\left(\frac{1}{2}, \alpha_0, ..., \alpha_{N-1}; \beta_0, ..., \beta_{N-1}; -\frac{\gamma_0^+}{m_0}, ..., -\frac{\gamma_{N-1}^+}{m_{N-1}}\right),$$
$$P^r_{e|\widetilde{A}_{k'}=1-j}(k') = P^r_{e|\widetilde{A}_{k'}=-1+j}(k') \tag{7.25}$$
$$= \frac{1}{2} - \frac{\Gamma(m_{k'} + \frac{1}{2})}{\Gamma(m_{k'})} \sqrt{\frac{\gamma_{k'}^-}{\pi m_{k'}}} \mathbb{F}_A^{(N)}\left(\frac{1}{2}, \alpha_0, ..., \alpha_{N-1}; \beta_0, ..., \beta_{N-1}; -\frac{\gamma_0^-}{m_0}, ..., -\frac{\gamma_{N-1}^-}{m_{N-1}}\right),$$

where the coefficients of α_k and β_k, $k = 0, 1, ..., N-1$, are given by Equations 7.19 and 7.20, respectively, and the coefficients of $\gamma_k^{\pm}$, $k = 0, ..., N-1$, are given by:

$$\gamma_k^{\pm} = \begin{cases} \frac{\Omega_{k'}}{\sigma_\eta^2} d_0^2 \cos^2(\varsigma_{k'} \pm \frac{\pi}{4}), & k = k', \\ \frac{\Omega_k}{\sigma_\eta^2} d_{k-k'}^2, & k \neq k'. \end{cases} \tag{7.26}$$

Finally, the average BEP $P_e(k')$ of the k'th subcarrier is obtained by averaging $P^r_{e|\widetilde{A}_{k'}}(k')$ over $\widetilde{A}_{k'}$, yielding:

$$P_e^Q(k') = \frac{1}{2} - \frac{\Gamma(m_{k'}+\frac{1}{2})}{2\Gamma(m_{k'})}\left[\sqrt{\frac{\gamma_{k'}^+}{\pi m_{k'}}}\mathbb{F}_A^{(N)}\left(\frac{1}{2},\alpha_0,...,\alpha_{N-1};\beta_0,...,\beta_{N-1};-\frac{\gamma_0^+}{m_0},...,-\frac{\gamma_{N-1}^+}{m_{N-1}}\right)\right.$$
$$\left. + \sqrt{\frac{\gamma_{k'}^-}{\pi m_{k'}}}\mathbb{F}_A^{(N)}\left(\frac{1}{2},\alpha_0,...,\alpha_{N-1};\beta_0,...,\beta_{N-1};-\frac{\gamma_0^-}{m_0},...,-\frac{\gamma_{N-1}^-}{m_{N-1}}\right)\right]. \quad (7.27)$$

If neither CFO nor PER is encountered, i.e. we have $\epsilon = 0$ and $\varsigma_{k'} = 0$, the system is equivalent to a single-carrier and single-user system communicating over a Nakagami-m fading channel [307], hence Equation 7.27 reduces to Equation 8.106 of [307] for QPSK modulation.

7.3.3 Special Case: Rayleigh Fading

When all subcarriers are subjected to Rayleigh fading, i.e. we have $m_k = 1$ for $k = 0, 1, ..., N-1$, Equations 7.15 and 7.23 reduce to:

$$\Phi_{\Re\{\widetilde{I}_{k'k}\}}(\omega) = \Phi_{\Re\{\widetilde{I}_{k'k}\}|\widetilde{A}_k}(\omega) = \exp\left(-\frac{1}{4}d_{k-k'}^2\Omega_k\omega^2\right), \text{for BPSK,} \quad (7.28)$$

$$\Phi_{\Re\{\widetilde{I}_{k'k}\}}(\omega) = \Phi_{\Re\{\widetilde{I}_{k'k}\}|\widetilde{A}_k}(\omega) = \exp\left(-\frac{1}{2}d_{k-k'}^2\Omega_k\omega^2\right), \text{for QPSK.} \quad (7.29)$$

Furthermore, Equations 7.18 and 7.27 reduce to:

$$P_e^B(k') = \frac{1}{2}\left(1 - \frac{1}{\sqrt{1+\frac{1}{\gamma_{k'}}+\sum_{k=0,k\neq k'}^{N-1}\frac{\gamma_k}{\gamma_{k'}}}}\right), \quad (7.30)$$

$$P_e^Q(k') = \frac{1}{2} - \frac{1}{4}\left(\frac{1}{\sqrt{1+\frac{1}{\gamma_{k'}^+}+\sum_{k=0,k\neq k'}^{N-1}\frac{\gamma_k^+}{\gamma_{k'}^+}}} + \frac{1}{\sqrt{1+\frac{1}{\gamma_{k'}^-}+\sum_{k=0,k\neq k'}^{N-1}\frac{\gamma_k^-}{\gamma_{k'}^-}}}\right), \quad (7.31)$$

where γ_k and $\gamma_k^\pm$ are given by Equations 7.21 and 7.26, respectively.

7.3.4 Gaussian Approximation

Typically the ICI is assumed to be approximately Gaussian distributed [298–301, 303] and hence the ICI may be treated as additional AWGN. Hence the CF $\Phi_{\Re\{\tilde{I}_{k'k}\}}(\omega)$ of the real ICI component imposed by the kth subcarrier may be approximated using Equation 7.28 for BPSK modulation and by Equation 7.29 for QPSK transmissions, respectively. Therefore, this scenario is also equivalent to the single-carrier and single-user Nakagami-m fading model, except that the noise is replaced by the combined interference-plus-noise component. The average BERs expressed in Equations 7.18 and 7.27 may be shown to be approximated as:

$$P_e^B(k') \approx \frac{1}{2} - \frac{\Gamma(m_{k'}+\frac{1}{2})}{\Gamma(m_{k'})} \times \sqrt{\frac{\gamma_{k'}}{\pi m_{k'}\left(1+\sum_{k=0,k\neq k'}^{N-1}\gamma_k\right)}}\,{}_2\mathbb{F}_1\left[m_{k'}+\frac{1}{2},\frac{1}{2};\frac{3}{2};-\frac{\gamma_{k'}}{m_{k'}\left(1+\sum_{k=0,k\neq k'}^{N-1}\gamma_k\right)}\right], \tag{7.32}$$

$$P_e^Q(k') \approx \frac{1}{2} - \frac{\Gamma(m_{k'}+\frac{1}{2})}{2\Gamma(m_{k'})\sqrt{\pi m_{k'}}} \times \left\{\sqrt{\frac{\gamma_{k'}^+}{1+\sum_{k=0,k\neq k'}^{N-1}\gamma_k^+}}\,{}_2\mathbb{F}_1\left[m_{k'}+\frac{1}{2},\frac{1}{2};\frac{3}{2};-\frac{\gamma_{k'}^+}{m_{k'}\left(1+\sum_{k=0,k\neq k'}^{N-1}\gamma_k^+\right)}\right]\right. + \left.\sqrt{\frac{\gamma_{k'}^-}{1+\sum_{k=0,k\neq k'}^{N-1}\gamma_k^-}}\,{}_2\mathbb{F}_1\left[m_{k'}+\frac{1}{2},\frac{1}{2};\frac{3}{2};-\frac{\gamma_{k'}^-}{m_{k'}\left(1+\sum_{k=0,k\neq k'}^{N-1}\gamma_k^-\right)}\right]\right\}, \tag{7.33}$$

where γ_k and $\gamma_k^{\pm}$ are given by Equations 7.21 and 7.26, respectively, while ${}_2\mathbb{F}_1(a,b;c;x)$ is the hypergeometric function [259]. In fact, the GA corresponds to the case, when all interfering subcarriers are subjected to Rayleigh fading, although there is no reason for the desired subcarrier to suffer from fading statistics different from those of other subcarriers. If all subcarriers are subjected to Rayleigh fading, Equations 7.32 and 7.33 reduce to Equations 7.30 and 7.31. In this case the results obtained by the Gaussian approximation coincide with those obtained by our exact analysis and this has been reported in [300, 301].

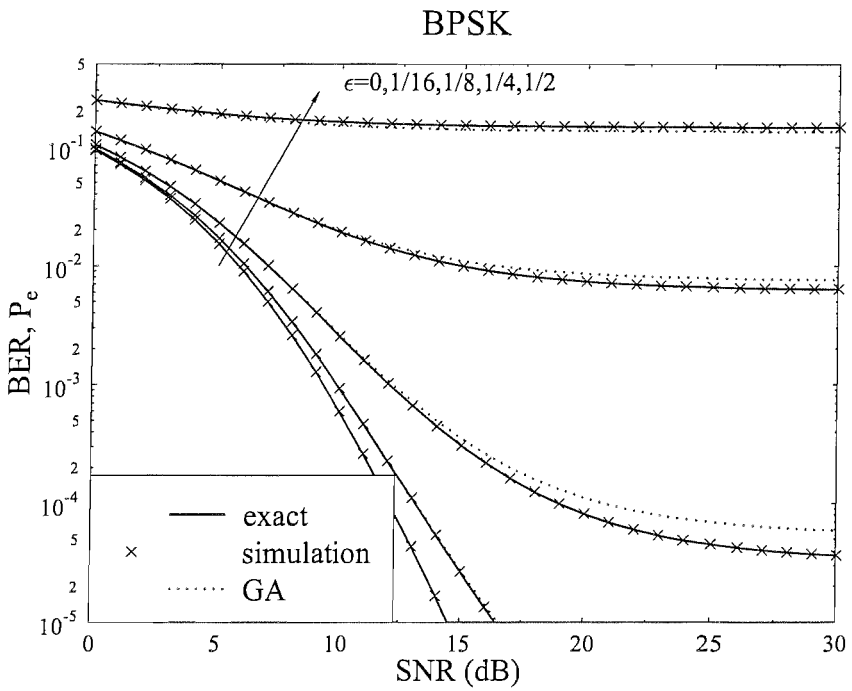

FIGURE 7.2: BER versus the per-bit SNR in a BPSK-modulated OFDM system subjected to frequency-selective Nakagami-m fading. All OFDM subcarriers experience the same fading distribution, i.e. we have $m_k = m = 5$. The number of OFDM subcarriers is $N = 64$. The normalized CFO is $\epsilon = 0$, $\frac{1}{16}$, $\frac{1}{8}$, $\frac{1}{4}$ and $\frac{1}{2}$, respectively. Perfect channel estimation is assumed, i.e. we have $\varsigma = 0$.

7.4 Numerical Results

7.4.1 The Effects of the Carrier Frequency Offset

In this subsection we will verify the accuracy of our exact BER analysis provided in Sections 7.3.1 for BPSK modulation and in Section 7.3.2 for QPSK modulation by Monte Carlo simulations. We will also demonstrate the relatively high accuracy of the Gaussian ICI approximation provided in Section 7.3.4. We will only consider the effects of the CFO, i.e. we assume having no PER, yielding $\varsigma_{k'} = 0$.

Figures 7.2 and 7.3 illustrate the average BER performance versus the per-bit SNR in conjunction with various normalized CFO values in a BSPK- and QPSK-modulated OFDM system, respectively, in the presence of CFO and frequency-selective Nakagami-m fading. When there is no CFO or PER, there is no cross-talk between the in-phase

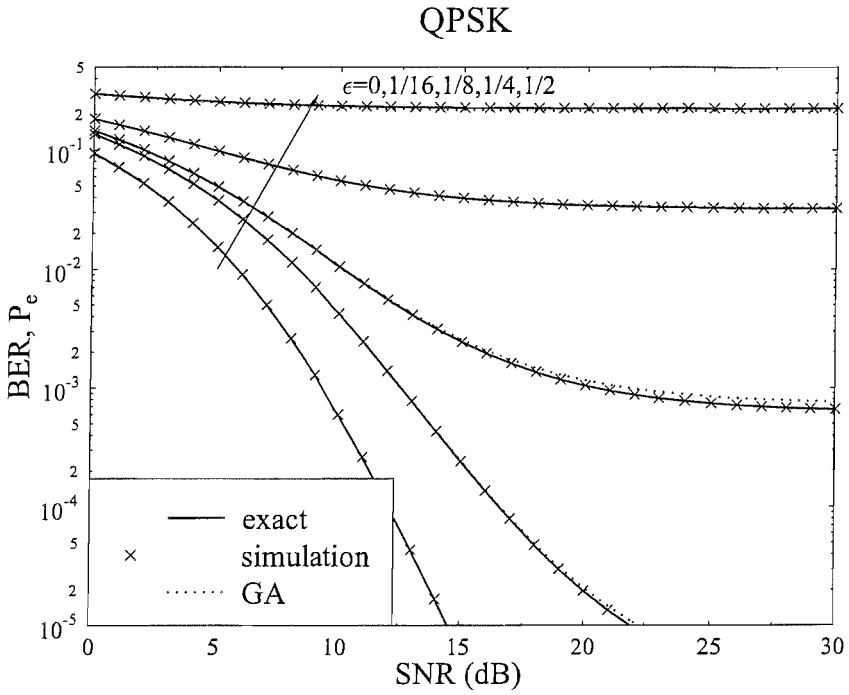

FIGURE 7.3: BER versus the per-bit SNR in a QPSK-modulated OFDM system subjected to frequency-selective Nakagami-m fading. All OFDM subcarriers experience the same fading distribution, i.e. we have $m_k = m = 5$. The number of OFDM subcarriers is $N = 64$. The normalized CFO is $\epsilon = 0$, $\frac{1}{16}$, $\frac{1}{8}$, $\frac{1}{4}$ and $\frac{1}{2}$, respectively. Perfect channel estimation is assumed, i.e. we have $\varsigma = 0$.

and quadrature-phase components. Therefore the QPSK-modulated OFDM system associated with $\epsilon = 0$ and characterized in Figure 7.3 has the same BER performance as the BPSK-modulated OFDM system having $\epsilon = 0$ in Figure 7.2. Furthermore, we included no GA results in Figures 7.2 and 7.3 when we have $\epsilon = 0$, since there is no ICI. However, if there exists CFO in both systems, the QPSK-modulated OFDM system suffers from more severe performance degradations than the BPSK-modulated OFDM system. We may see from Equations 7.15 and 7.23 that the interference energy in the QPSK-modulated OFDM system is twice as high as that in the BPSK-modulated OFDM system due to the associated I/Q cross-talk. We can see from both figures that generally speaking the BER decreases as the SNR value increases, but eventually remains limited by the ICI, leading to an error floor. There are two exceptions, namely when we have $\epsilon = 0$ and $\frac{1}{2}$. When there is no CFO, i.e. we have $\epsilon = 0$, the BPSK- and QPSK-modulated OFDM systems are noise-limited. By contrast, when the CFO is relatively high, i.e. we have $\epsilon = \frac{1}{2}$, both systems behave interference-limited. Furthermore, both

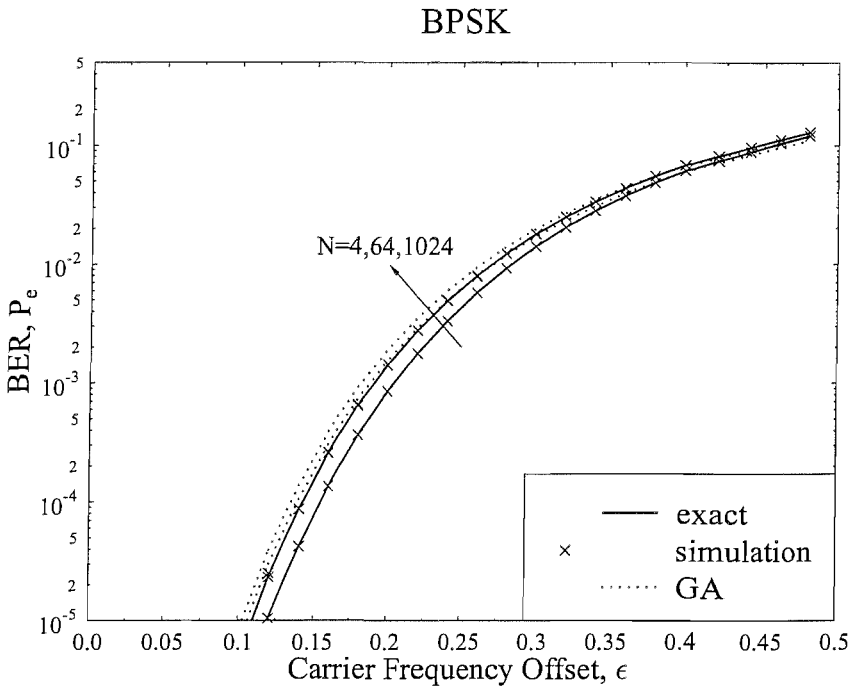

FIGURE 7.4: BER versus the normalized CFO in a BPSK-modulated OFDM system subjected to frequency-selective Nakagami-m fading. All OFDM subcarriers experience the same fading distribution, i.e. we have $m_k = m = 5$. The number of OFDM subcarriers is $N = 4$, 64 and 1024, respectively, but the associated BER curves of $N = 64$ and 1024 are indistinguishable for both the exact results and for the GA. Perfect channel estimation is assumed, i.e. we have $\varsigma = 0$. The background noise is ignored, i.e. we have $\sigma_\eta = 0$.

figures show that the results obtained from our exact BEP analysis and those accruing from simulations match well for various normalized CFO values. The GA is also fairly accurate, but it slightly over-estimates the BER in both Figures 7.2 and 7.3, especially when the SNR is high and when the normalized CFO is low. Moreover, the GA estimates the BER performance more accurately in the QPSK-modulated OFDM system than in the BPSK-modulated OFDM system, since the QPSK-modulated OFDM system suffers from more severe ICI due to the ICI-induced I/Q cross-talk.

Figures 7.4 and 7.5 illustrate the average BER performance versus the normalized CFO in conjunction with various numbers of OFDM subcarriers in a BSPK- and QPSK-modulated OFDM system, respectively, in the context of frequency-selective Nakagami-m fading. Note that there should be no bit errors in the context of a single-carrier

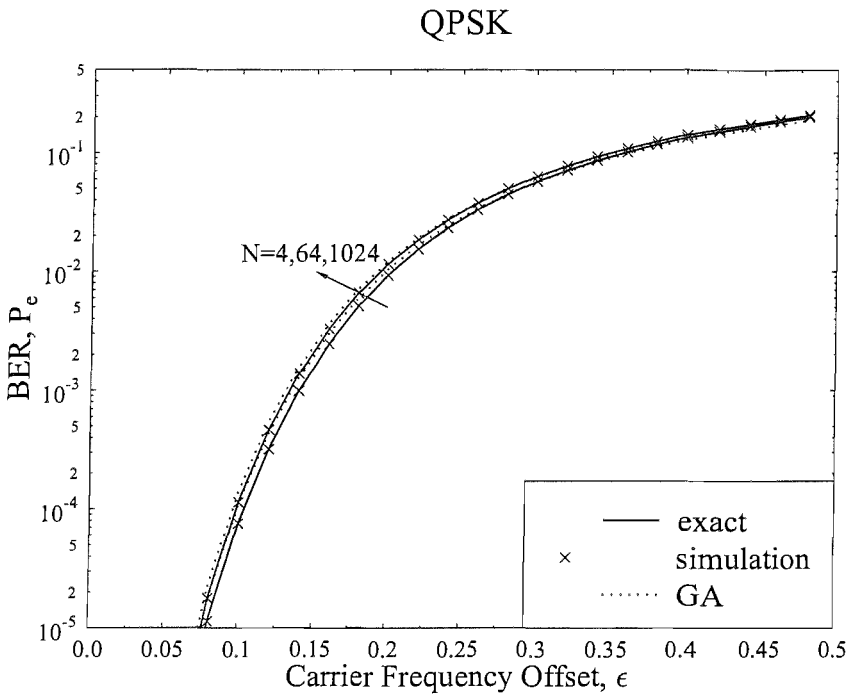

FIGURE 7.5: BER versus the normalized CFO in a QPSK-modulated OFDM system subjected to frequency-selective Nakagami-m fading. All OFDM subcarriers experience the same fading distribution, i.e. we have $m_k = m = 5$. The number of OFDM subcarriers is $N = 4$, 64 and 1024, respectively, but the associated BER curves of $N = 64$ and 1024 are indistinguishable for both the exact results and for the GA. Perfect channel estimation is assumed, i.e. we have $\varsigma = 0$. The background noise is ignored, i.e. we have $\sigma_\eta = 0$.

BPSK- or QPSK-modulated OFDM system, when the effects of noise are ignored. However, when multi-carrier modulation is adopted, the ICI induced by the CFO limits the achievable BER performance. Nevertheless, as the number of OFDM subcarriers is increased, the BER performance degradation is not aggravated further, provided that the number of OFDM subcarriers is sufficiently high. Upon their further increase, the associated BER curve of 64-subcarrier OFDM and of 1024-subcarrier OFDM becomes indistinguishable in both the BPSK- and the QPSK-modulated OFDM systems. The BER performance of the QPSK-modulated OFDM system seen in Figure 7.5 is worse than that of the BPSK-modulated OFDM system characterized in Figure 7.4 owing to the ICI-induced I/Q cross-talk of the QPSK-modulated OFDM system. We can see from both figures that the CFO significantly degrades the achievable BER performance of the OFDM systems. When there is no CFO, there are no bit errors, since stated before that we have ignored the effects of background noise. When the normalized CFO is low, the

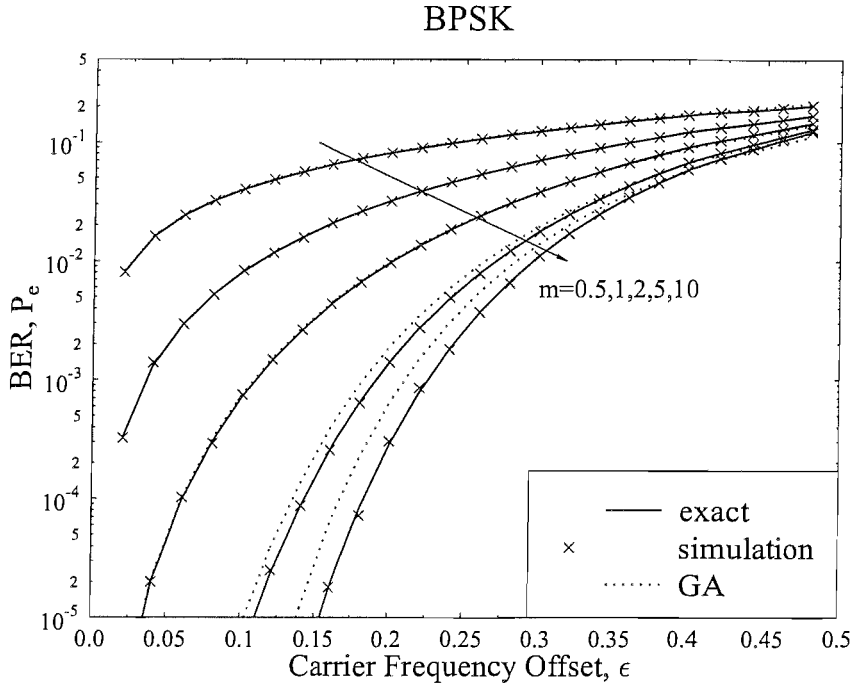

FIGURE 7.6: BER versus the normalized carrier frequency offset in a BPSK-modulated OFDM system subjected to frequency-selective Nakagami-m fading. All OFDM subcarriers experience the same fading distribution, i.e. we have $m_k = m$. The Nakagami-m parameter is $m = 0.5$, 1, 2, 5 and 10, respectively. Note that the BER curves obtained by our exact analysis and by the Gaussian approximation are not distinguishable when $m = 0.5$, 1 and 2. The number of OFDM subcarriers is $N = 64$. Perfect channel estimation is assumed, i.e. we have $\varsigma = 0$. The background noise is ignored, i.e. we have $\sigma_\eta = 0$.

BER increases exponentially with the normalized CFO. Again, both figures show that the results obtained from our exact analysis and those accruing from our simulations match well for various numbers of OFDM subcarriers. Similarly, the GA estimates the BER performance in both figures fairly accurately, although the BER is slightly overestimated, especially when the normalized CFO is low and when the number of OFDM subcarriers is low. Moreover, the GA estimates the BER performance more accurately in the QPSK-modulated OFDM system than it in the BPSK-modulated OFDM system, since the QPSK-modulated OFDM system is exposed to a higher number of interferers due to due to the ICI-induced cross-talk, which renders the interference more Gaussian.

Figures 7.6 and 7.7 illustrate the achievable average BER performance versus the normalized CFO in conjunction with various Nakagami-m fading parameters in a BSPK- and QPSK-modulated OFDM system, respectively, in the context of frequency-selective

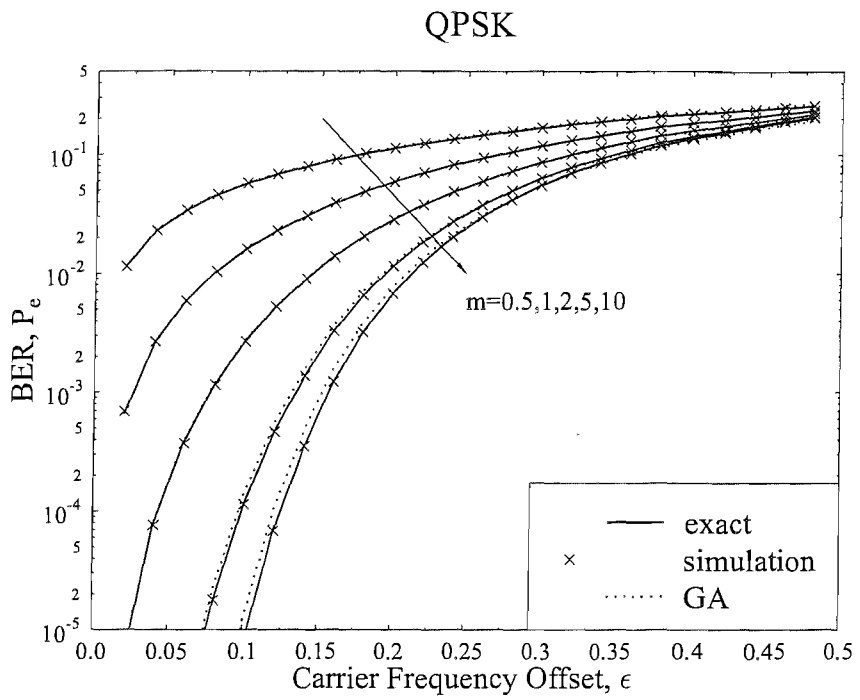

FIGURE 7.7: BER versus the normalized carrier frequency offset in a QPSK-modulated OFDM system subjected to frequency-selective Nakagami-m fading. All OFDM subcarriers experience the same fading distribution, i.e. we have $m_k = m$. The Nakagami-m parameter is $m = 0.5$, 1, 2, 5 and 10, respectively. Note that the BER curves obtained by our exact analysis and by the Gaussian approximation are not distinguishable when $m = 0.5$, 1 and 2. The number of OFDM subcarriers is $N = 64$. Perfect channel estimation is assumed, i.e. we have $\varsigma = 0$. The background noise is ignored, i.e. we have $\sigma_\eta = 0$.

Nakagami-m fading. Although we do not plot the curves for small values of the normalized CFO, i.e. for $\epsilon < 0.02$, the BERs recorded for all Nakagami-m fading parameters should be zero, when there is no CFO, i.e. for $\epsilon = 0$, since we have ignored the effects of noise. Therefore, we can see from Figures 7.6 and 7.7 that the CFO has a more detrimental impact on the systems suffering from more severe fading, i.e. when the Nakagami-m parameter is lower. When the normalized CFO is low, the BER increases exponentially with the normalized CFO. The BER performance of the QPSK-modulated OFDM system seen in Figure 7.7 is worse than that of the BPSK-modulated OFDM system characterized in Figure 7.6 due to the ICI-induced I/Q cross-talk of the QPSK-modulated OFDM system. Again, both figures show that the results obtained from our exact analysis and those accruing from our simulations match well for the various numbers of OFDM subcarriers considered. As stated in Section 7.3.4, the results obtained

by the GA in both figures match with those generated by our exact analysis, when the fading is Rayleigh, i.e. when we have $m = 1$. However, the GA slightly over-estimates the BER, when the fading is less severe, i.e. when the Nakagami-m fading parameter is high, especially when the normalized CFO is low. Moreover, the GA estimates the BER performance more accurately in the QPSK-modulated OFDM system than in the BPSK-modulated OFDM system, since the QPSK-modulated OFDM system is exposed to a higher number of interferers due to the ICI-induced I/Q cross-talk.

7.4.2 The Effects of the Phase Estimation Error

In this subsection we will verify the accuracy of our exact BER analysis provided in Section 7.3.1 for BPSK modulation and in Section 7.3.2 for QPSK modulation by Monte Carlo simulations. We will only consider the effects of the PER, i.e. we assume having $\epsilon = 0$. Since there is no CFO, there will be no ICI and hence no GA results are provided. Therefore the systems having different number of OFDM subcarriers perform similarly.

Figures 7.8 and 7.9 illustrate the average BER performance versus the per-bit SNR in conjunction with various PER values in a BPSK- and QPSK-modulated OFDM system, respectively, in the context of frequency-selective Nakagami-m fading. The associated BER decreases in both figures, as the SNR value increases. There is one exception in Figure 7.9, when we have $\varsigma = \frac{\pi}{4}$ for the QPSK-modulated OFDM system. In this scenario the ICI-induced cross-talk between the in-phase and quadrature-phase components outweighs the noise. When there is no PER, i.e. we have $\varsigma = 0$, there is no cross-talk between the in-phase and quadrature-phase components. Therefore the QPSK-modulated OFDM system having $\varsigma = 0$ in Figure 7.9 has the same BER performance as the BPSK-modulated OFDM system having $\varsigma = 0$ in Figure 7.8. However, if PER is present in both systems, the QPSK-modulated OFDM system suffers from a more severe performance degradation than the BPSK-modulated OFDM system, as a consequence of the cross-talk experienced by the QPSK-modulated OFDM system. Furthermore, both figures show that our exact analysis results and simulation results match well for various PER values. Comparing Figures 7.8 and 7.9 with Figures 7.2 and 7.3, the OFDM systems still appear to be noise-limited, when only the effects of PER are considered, while they become interference-limited when only the impact of CFO is considered. From this observation we conclude that OFDM systems are more sensitive to CFO than to PER.

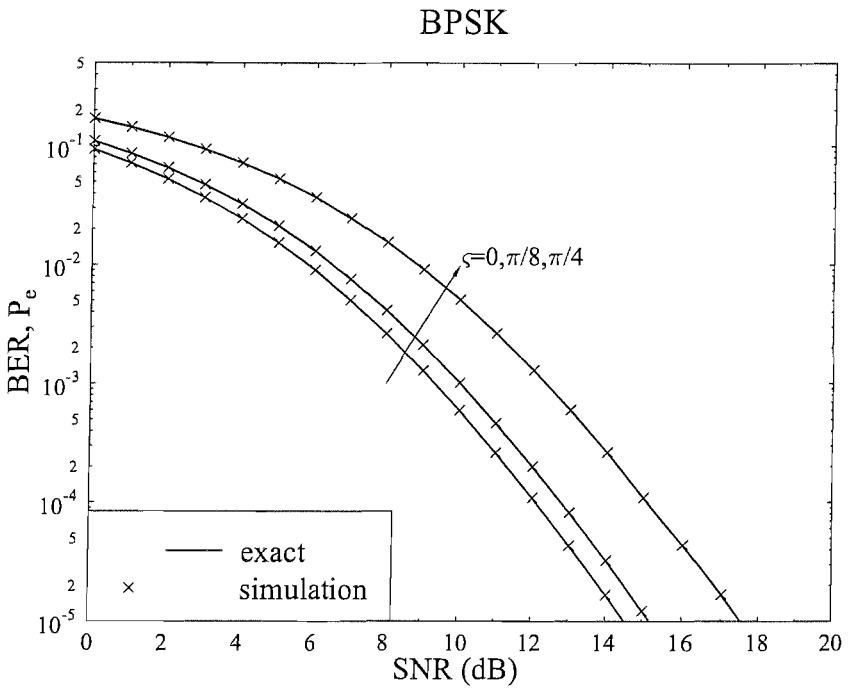

FIGURE 7.8: BER versus the per-bit SNR in a BPSK-modulated OFDM system subjected to Nakagami-m fading. All OFDM subcarriers experience the same fading distribution, i.e. we have $m_k = m = 5$. Perfect carrier synchronization is assumed, i.e. we have $\epsilon = 0$, hence the systems having different number of OFDM subcarriers have the same BER performance. The phase estimation error is $\varsigma = 0$, $\frac{\pi}{8}$, and $\frac{\pi}{4}$ respectively.

Figures 7.10 and 7.11 illustrate the average BER performance versus the PER for various Nakagami-m fading parameters in a BPSK- and QPSK-modulated OFDM system, respectively, in the context of frequency-selective Nakagami-m fading. Since there would be no bit errors, if both the CFO and the background noise are ignored in the BPSK-modulated OFDM system, we used an SNR value of 10dB in both figures. In line with our expectations, the BER increases, as the PER increases in both figures. The systems suffering from more severe fading become more sensitive to the effects of PER. Moreover, the PER has a more substantial impact on the QPSK-modulated OFDM system characterized in Figure 7.11 than on the BPSK-modulated OFDM system associated with Figure 7.10 due to the ICI-induced I/Q cross-talk in the QPSK-modulated OFDM system.

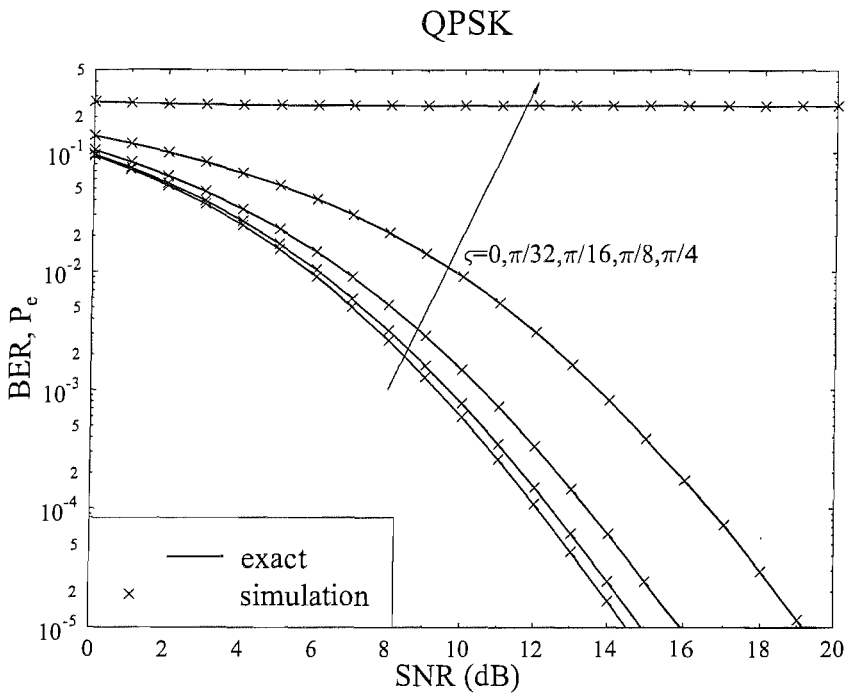

FIGURE 7.9: BER versus the per-bit SNR in a QPSK-modulated OFDM system subjected to Nakagami-m fading. All OFDM subcarriers experience the same fading distribution, i.e. we have $m_k = m = 5$. Perfect carrier synchronization is assumed, i.e. we have $\epsilon = 0$, hence the systems having different number of OFDM subcarriers have the same BER performance. The phase estimation error is $\varsigma = 0$, $\frac{\pi}{32}$, $\frac{\pi}{16}$, $\frac{\pi}{8}$, and $\frac{\pi}{4}$ respectively.

7.5 Conclusion

We have analyzed the BER degradation induced by both the CFO and the PER in both BPSK- as well as QPSK-modulated systems in the context of frequency-selective Nakagami-m fading channels. In contrast to the sum of the infinite series provided in [302, 303], several closed-form expressions were provided for calculating the average BER of such OFDM systems, which were derived based on the CF approach. Our simulation results verified the accuracy of our exact BER analysis for various combinations of the normalized CFO value, the PER value, the number of OFDM subcarriers and the Nakagami-m fading parameter. The Gaussian approximation of the ICI also estimates the average BER fairly accurately, although when the per-bit SNR is high, the normalized CFO is small, the number of OFDM subcarriers is low and when the fading is less severe, the GA slightly over-estimates the BER. Moreover, the GA estimates the

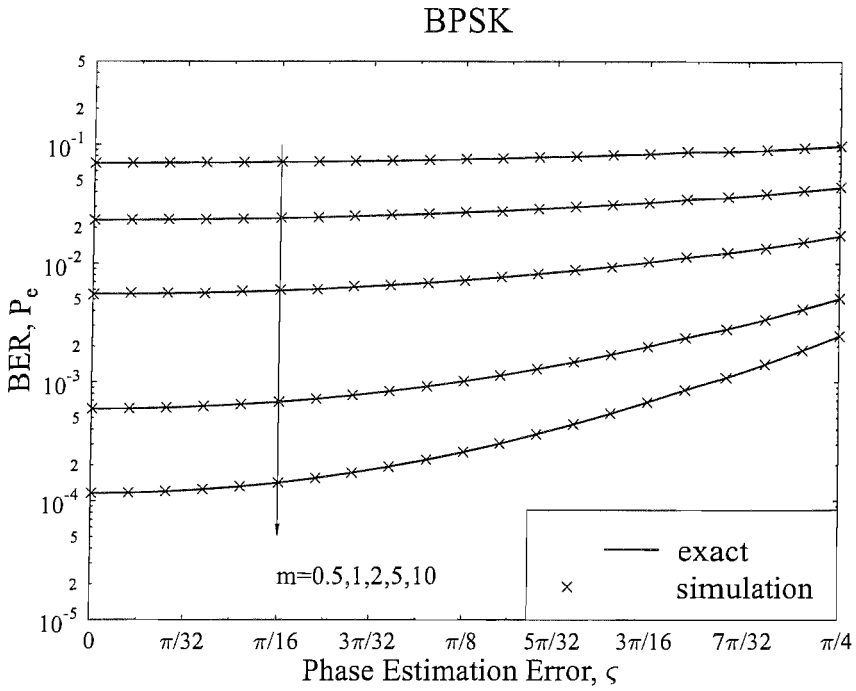

FIGURE 7.10: BER versus the phase estimation error in a BPSK-modulated OFDM system subjected to Nakagami-m fading. All OFDM subcarriers experience the same fading distribution, i.e. we have $m_k = m$. The Nakagami-m parameter is $m = 0.5$, 1, 2, 5 and 10, respectively. Perfect carrier synchronization is assumed, i.e. we have $\epsilon = 0$, hence the systems having different number of OFDM subcarriers have the same BER performance. The per-bit SNR on each OFDM subcarrier is assumed to be 10dB.

BER performance more accurately in the QPSK-modulated OFDM system than in the BPSK-modulated OFDM system, since the QPSK-modulated OFDM system is exposed to a higher number of interferers owing to the ICI-induced I/Q cross-talk experienced by in the QPSK-modulated OFDM system. The results obtained by GA coincide with those obtained by our exact analysis, when the fading is Rayleigh, i.e. when we have $m = 1$. Our future research may consider the ICI effects of higher-order modulation schemes.

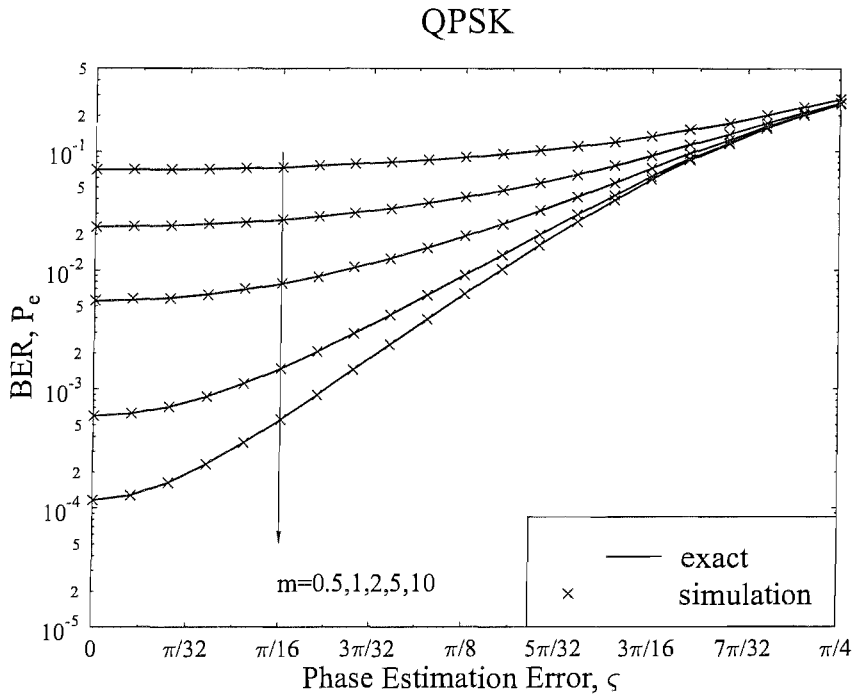

FIGURE 7.11: BER versus the phase estimation error in a QPSK-modulated OFDM system subjected to Nakagami-m fading. All OFDM subcarriers experience the same fading distribution, i.e. we have $m_k = m$. The Nakagami-m parameter is $m = 0.5$, 1, 2, 5 and 10, respectively. Perfect carrier synchronization is assumed, i.e. we have $\epsilon = 0$, hence the systems having different number of OFDM subcarriers have the same BER performance. The per-bit SNR on each OFDM subcarrier is assumed to be 10dB.

Chapter 8

Thesis Summary and Future Research

8.1 Summary

The penetration of wireless communication services has experienced an exponential growth during the past decade or so, causing numerous performance analysis problems. In this thesis we formulate and solve several of these open problems. The summary of each chapter is as follows:

8.1.1 Chapter 2

In this chapter we provided a brief overview of ad hoc networks. We began the chapter with an introduction of the basic concepts of ad hoc networks in Section 2.1. Section 2.2 outlined the evolution and the standardization activities of ad hoc networks. Section 2.3 presented a number of design challenges of ad hoc networks, such as capacity, routing, broadcast/multicast/geocast, medium access control, security, Quality of Service, energy efficiency, modeling/simulation, etc. Section 2.3.1 provided capacity studies of ad hoc networks, investigating the network's scalability and a range of techniques which may be used for improving the network's attainable capacity. Unfortunately most ad hoc networks relying on realistic operating conditions are not scalable, even when invoking the most powerful enabling techniques. The dynamic properties of ad hoc networks render the design of routing protocols a challenging task. Section 2.3.2 outlined a range of existing proactive, reactive and hybrid routing protocols designed for ad hoc networks,

focussing on the specifics of how routing information is obtained. From the perspective of how transmissions are carried out, routing protocols were categorized as unicast, broadcast, multicast and geocast techniques as detailed in Section 2.3.3. MAC protocols define how the nodes may access their shared channel. Section 2.3.4 identified the hidden node and exposed node problems in MAC protocol design and presented existing MAC protocols. Owing to their inherently open and shared broadcast radio channels, ad hoc networks are more vulnerable against security attacks. The various network-layer as well as link-layer security issues and the selfishness problem were summarized in Section 2.3.5. Each application may require a set of services to be supported by the ad hoc network. Section 2.3.6 addressed the QoS issue from four different perspectives, considering QoS models, QoS routing, QoS signalling and QoS MAC protocols. Energy efficieny is one of the main concerns in battery-powered ad hoc networks. Current energy-efficient communications techniques, such as transmission power control, load distribution and power-save modes, were briefly discussed in Section 2.3.7. Modeling and simulation enable us to study the system's behaviour economically and flexibly, hence they play important roles in the research of ad hoc networks and were addressed in Section 2.3.8. Finally, Section 2.4 concluded this chapter.

8.1.2 Chapter 3

Increasing the achievable capacity is one of the important design objectives of ad hoc networks, as addressed in Section 2.3.1. We commenced the chapter with an overview of related work on the capacity of ad hoc networks in Section 3.1, where various capacity studies based on information theory, simulation and other approaches were presented and where a variety of techniques capable of improving the network capacity were also investigated. Then we focussed our attention on the effects of perfect rate adaptation on the achievable throughput of random ad hoc networks, which was discussed in the context of pathloss and shadow fading in Section 3.3 and Section 3.4, respectively. We concluded that perfect rate adaptation had the potential of considerably improving the achievable throughput of the random ad hoc network compared to fixed rate transmissions, since rate adaptation was capable of mitigating the effects of link quality fluctuations. This conclusion was further confirmed by our simulations in the context of our AQAM examples in Section 3.5. Finally, we concluded the chapter in Section 3.6.

8.1.3 Chapter 4

The family of Large Area Synchronous (LAS) DS-CDMA spreading codes exhibits an Interference Free Window (IFW) over a limited duration, which renders them potentially applicable in DS-CDMA ad hoc networks. We began the chapter with an overview of related research on LAS codes in Section 4.1. Section 4.2 described an DS-CDMA ad hoc network obeying an infinite rectilinear mesh topology. Then the BER performance of such a network using LAS codes was investigated in Section 4.3. We detailed our results in Section 4.4. Section 4.4.1 detailed the benchmark system used, which was quasi-synchronous LAS DS-CDMA and quasi-synchronous DS-CDMA using both Walsh-Hadamard codes and Orthogonal Gold codes, as well as asynchronous LAS DS-CDMA and asynchronous DS-CDMA employing random signature sequences. Section 4.4.2 compared the performance of LAS DS-CDMA systems with our benchmark systems outlined in Section 4.4.1. Our results showed that the LAS ad hoc system exhibits a significantly better performance than the family of traditional spreading sequences used in a quasi-synchronous DS-CDMA scenario having a low number of resolvable multipath components and a sufficiently high number of RAKE receiver branches. Finally, we concluded the chapter in Section 4.5.

8.1.4 Chapter 5

Random signature sequences have been employed by the benchmark schemes used for the performance evaluation of DS-CDMA systems. We commenced the chapter with an overview of related research on the average BER calculation of asynchronous DS-CDMA systems in Section 5.1. Section 5.2 summarized the Rayleigh, Ricean, Hoyt and Nakagami-m fading channels and presented some important properties of different fading channels, when both the fading amplitude and the fading phase are considered. Then a general asynchronous DS-CDMA system using BPSK modulation for communicating over fading channels was presented in Section 5.3. We considered the exact BER calculation of these systems using random spreading sequences in Section 5.4 and provided a unified exact BER expression, which requires only a single numerical integration. In Section 5.5 the detailed MAI analysis of the system was presented based on the CF approach in the context of various fading channels and several closed-form expressions have been derived for the conditional CFs of the interfering signals in various fading channels. In Section 5.6 our numerical results verified the accuracy of our exact BER analysis for various combinations of the spreading sequence length and fading parameters and they

also demonstrated the reasonable accuracy of the Standard Gaussian Approximation (SGA) of the Multiple Access Interference (MAI). The SGA over-estimates the average BER when the fading severe, while it under-estimates it, when the fading is benign, especially when either there is a low number of interferers, or the SNR is high and short spreading sequences are used. Finally our conclusions were provided in Section 5.7.

8.1.5 Chapter 6

The family of QAM schemes constitutes a bandwidth-efficient transmission technique and hence has found its way into virtually all recent wireless standards. We commenced our discourse with an overview of related work on the average BER calculation of QAM systems communicating over AWGN or fading channels in Section 6.1. Then a general R-QAM scheme subject to asynchronous CCI and Nakagami-m fading was described in Section 6.2. Its exact BER performance was investigated based on the CF approach in Section 6.3. An exact and general BER expression was derived, which requires only two single numerical integrations and a new closed-form formula was provided for the CF of the CCI. Our numerical results were presented in Section 6.4, where we verified the accuracy of our exact BER expression for different constellation sizes and for various channel statistics. As expected, the GA technique demonstrated a good accuracy, although its accuracy became lower when the per-bit SIR was high, the fading was less severe, the constellation size was small and hence the number of bits/symbol was low. Finally, we concluded in Section 6.5.

8.1.6 Chapter 7

OFDM has been employed in numerous wireless standards and has emerged as one of the promising candidates to be employed in next-generation communication systems. However, the performance of OFDM systems is sensitive to the Carrier Frequency Offset (CFO), which destroys the orthogonality of the OFDM subcarriers and inflicts Inter-Carrier Interference (ICI). In Section 7.1 we provided an overview of the related work on the BER degradation induced by CFO in OFDM systems. Then an OFDM system using BPSK/QPSK modulation for communicating over frequency-selective Nakagami-m channels in the presence of both the CFO and the Phase Estimation Error (PER) was presented in Section 7.2. Its exact BER performance was investigated based on the CF approach in Section 7.3. Several new closed-form expressions were derived for calculating the average BER of a BPSK- or QPSK-modulated OFDM system. In Section 7.4

our numerical results verified the accuracy of our exact BER analysis for various combinations of the normalized CFO values, the PER value, the number of OFDM subcarriers and the Nakagami-m fading parameter. By contrast, the Gaussian approximation was shown to slightly over-estimate the average BER, especially when the normalized CFO was small, the number of OFDM subcarriers was low and when the fading was less severe. Finally, our conclusions were provided in Section 7.5.

8.2 Suggestions for Future Work

In this dissertation we have studied various performance evaluation problems of wireless systems. However, there are still numerous open problems in these areas. We will briefly outline a few ideas for our future work as follows.

In Chapter 5 we only investigated the exact BER performance of BPSK systems. The work may be readily extended to QPSK systems. However, the exact analysis of Multiple Access Interference (MAI) may be a bit more challenging. The analytical expressions of the MAI's CF for QPSK systems subjected to Rayleigh fading have been derived in [308, 309] and those for QPSK systems subjected to Nakagami-m fading may also be readily derived with the aid of the generalized Lauricella function of n variables [266]. However, those for QPSK systems subjected to Ricean or Hoyt fading are unavailable at the time of writing. The extension of the work to QAM systems is significantly more challenging, since there is no available analytical solution to the sum of several arbitrary integers.

In Chapter 5 we only investigated the exact BER performance of asynchronous Single-Carrier (SC) DS-CDMA systems. The work may be extended to MC DS-CDMA systems using random spreading sequences. However, the dependency between the interference imposed by the different frequencies renders the exact BER calculation more challenging. Fortunately, this dependency appears to be trivial in practice [310], if conditioned on the desired user's spreading sequence, hence the Multiple Access Interference (MAI) induced by the different subcarriers of various interferers may be approximately regarded as conditionally independent. Nevertheless, the results obtained by neglecting this dependency should be verified by simulations, since there is no proof justifying that they indeed may be neglected. Furthermore, the consideration of the Multi-Path Interference (MPI) in the exact BER calculation may impose further difficulties, since there is

no generic approach that may be invoked for modeling the MPI. Typically the MPI of random spreading sequences is approximated as Gaussian distributed [231].

Another possible future research item is constituted by the design of spreading sequences. Our results provided in Chapter 5 may be used as a benchmark. However, the exact BER expressions derived for deterministic spreading sequences may not be obtained, unless the cross-correlation functions of the deterministic spreading sequences considered may be expressed in an analytical form. Typically the performance of deterministic spreading sequences is evaluated by simulations [250, 253–257] at the cost of a high computational complexity. The main benefit of using simulations is that there is no difficulty in handling dependencies caused by the MAI or MPI.

In Chapter 6 we did not consider the benefits of receiver diversity. However, diversity combining techniques such as Selection Combining (SC), Maximal-Ratio Combining (MRC) and Equal-Gain Combining (EGC) [311] have been widely employed in wireless communication systems. Our results may be readily extended to SC and EGC aided scenarios. However, we might encounter more difficulties, when considering the MRC scenario, since the multiplication by the channel gain will introduce dependency between the desired signal and the interference.

Finally, in Chapter 7 we assumed that the fading channels of the individual OFDM subcarriers are mutually independent in the frequency-domain. We may consider the more general cases associated with correlation between the fading channels of the subcarriers. However, the derivation of the exact BER expressions may become more challenging, if not impossible, when the only solution may be to evaluate the performance by simulations, instead of mathematical analysis.

Appendix A

Proof of Theorem 3.1

Before proving Theorem 3.1, we will introduce a lemma, which shows that $s\ln(1+\beta s^{-\alpha})$ in the numerator of Equation 3.11 is bounded.

Lemma A.1. *Assume we have $\alpha > 1$, $\beta > 0$, and define*

$$h(x) = x\ln(1+\beta x^{-\alpha}), \quad x \in (0, +\infty).$$

Then it may be readily shown that $h(x)$ is bounded, and achieves its maximum at $x_M = (-\frac{\beta\omega}{\alpha+\omega})^{\frac{1}{\alpha}}$, yielding:

$$h(x_M) = (\alpha+\omega)(-\frac{\beta\omega}{\alpha+\omega})^{\frac{1}{\alpha}},$$

where $\omega \in (-1, 0)$ satisfies

$$\omega e^{\omega} = -\alpha e^{-\alpha}. \tag{A.1}$$

This is a so-called Lambert W function $\omega(x(\alpha)) = \mathrm{LambertW}(x) = \mathrm{LambertW}(-\alpha e^{-\alpha})$ [312]. Furthermore, we have $-\alpha < \omega < 0$ since $\alpha > 1$. ■

Proof. First we will derive two limits with the aid of L'Hospital's rule [213]:

$$\begin{aligned}
\lim_{x\to 0^+} h(x) &= \lim_{x\to 0^+} \frac{\ln(1+\beta x^{-\alpha})}{x^{-1}} \overset{L'Hospital}{=} \lim_{x\to 0^+} \frac{-\frac{\beta\alpha x^{-(\alpha+1)}}{1+\beta x^{-\alpha}}}{-x^{-2}} \\
&= \lim_{x\to 0^+} \frac{\beta\alpha x}{\beta + x^{\alpha}} \qquad = \qquad \frac{\lim\limits_{x\to 0^+} \beta\alpha x}{\beta + \lim\limits_{x\to 0^+} x^{-\alpha}} \\
&= 0,
\end{aligned} \tag{A.2}$$

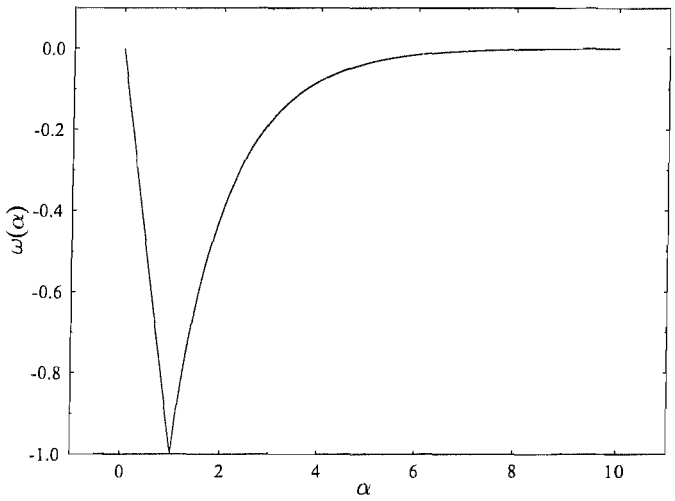

FIGURE A.1: The curve of $\omega(\alpha) = \text{LambertW}(-\alpha e^{-\alpha})$

$$\begin{aligned}\lim_{x\to+\infty} h(x) &= \lim_{x\to+\infty} \frac{\ln(1+\beta x^{-\alpha})}{x^{-1}} \overset{L'Hospital}{=} \lim_{x\to+\infty} \frac{-\frac{\beta\alpha x^{-(\alpha+1)}}{1+\beta x^{-\alpha}}}{-x^{-2}} \\ &= \lim_{x\to+\infty} \frac{\beta\alpha x}{\beta + x^{\alpha}} \overset{L'Hospital}{=} \lim_{x\to+\infty} \frac{\beta\alpha}{\alpha x^{\alpha-1}} \\ &= 0,\end{aligned} \tag{A.3}$$

where $h(x) > 0$ and $h(x)$ is continuous as well as differentiable in $(0, +\infty)$. Therefore there must exist a maximum x_M in $(0, +\infty)$ for $h(x)$, and this maximum satisfies

$$\left.\frac{\mathrm{d}h(x)}{\mathrm{d}x}\right|_{x=x_M} = \ln(1+\beta x_M^{-\alpha}) - \frac{\beta\alpha}{\beta + x_M^{\alpha}} = 0. \tag{A.4}$$

Solving the above equation, the following solution is obtained:

$$x_M = \left(-\frac{\beta\omega}{\alpha+\omega}\right)^{\frac{1}{\alpha}}, \tag{A.5}$$

at which $h(x)$ achieves the maximum of:

$$h(x_M) = (\alpha+\omega)(-\frac{\beta\omega}{\alpha+\omega})^{\frac{1}{\alpha}}, \tag{A.6}$$

where $\omega \in (-1, 0)$ satisfies

$$\omega e^{\omega} = -\alpha e^{-\alpha}. \tag{A.7}$$

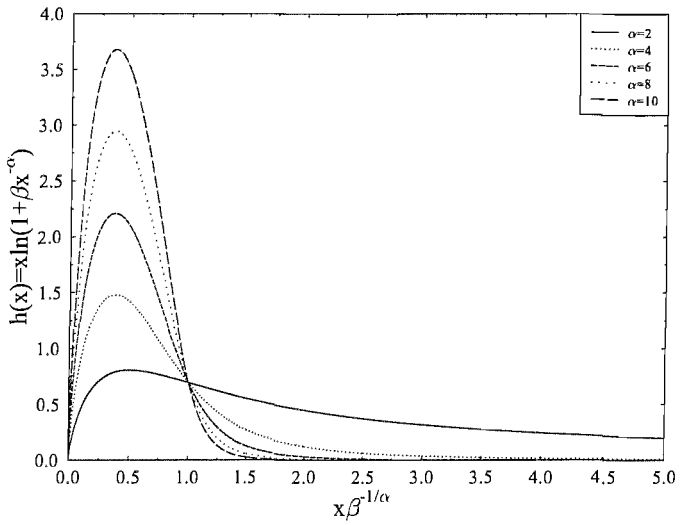

FIGURE A.2: The curve of $h(x) = x\ln(1+\beta x^{-\alpha})$

This is a Lambert W function $\omega(x(\alpha)) = \text{LambertW}(x) = \text{LambertW}(-\alpha e^{-\alpha})$ [312]. Furthermore, we have $-\alpha < \omega < 0$ since $\alpha > 1$. □

The curve corresponding to $\omega(\alpha)$ is plotted in Figure A.1, while that of $h(x)$ is plotted in Figure A.2.

Now we are ready to use Lemma A.1 for proving Theorem 3.1.

Proof. Since $u \in [0,1)$, $s \in [u,1]$ and α, $\beta > 0$, we have

$$\begin{aligned}\frac{\partial c_i}{\partial u} &= \frac{2u}{(1-u^2)^2\ln(1+\beta)}\left[2\int_u^1 s\ln(1+\beta s^{-\alpha})\mathrm{d}s - (1-u^2)\ln(1+\beta u^{-\alpha})\right] \\ &\leq \frac{2u}{(1-u^2)^2\ln(1+\beta)}\left[2\int_u^1 s\ln(1+\beta u^{-\alpha})\mathrm{d}s - (1-u^2)\ln(1+\beta u^{-\alpha})\right] \\ &= 0. \end{aligned} \tag{A.8}$$

This implies that the achievable normalized per-node throughput improvement c_i decreases as the normalized minimum distance $u = \frac{r_{min}}{r_n}$ increases, hence it may be concluded that we have $c_i \leq c_i^0$. The existence of the upper bound c_i^0 can be shown by using

Lemma A.1, yielding:

$$
\begin{aligned}
c_i^0 &= \frac{2\int_0^1 s\ln(1+\beta s^{-\alpha})\mathrm{d}s}{\ln(1+\beta)} \\
&< \frac{2s_M\ln(1+\beta s_M^{-\alpha})\int_0^1 \mathrm{d}s}{\ln(1+\beta)} = \frac{2(\omega+\alpha)}{\ln(1+\beta)}\left(-\frac{\beta\omega}{\omega+\alpha}\right)^{\frac{1}{\alpha}} \\
&< +\infty. \qquad \text{(A.9)}
\end{aligned}
$$

□

Appendix B

Proof of Theorem 3.2

Before proving Theorem 3.2, we will introduce a lemma, which shows that the achievable normalized per-node throughput improvement c_i is a monotonically decreasing function of the logarithmic normalized minimum distance of $u = \ln(\frac{r_{min}}{r_n})$ ad hoc nodes, if the following expression is a monotonically decreasing function of u:

$$\frac{\int_0^{+\infty} e^{-\frac{(t+\alpha u)^2}{2\sigma^2}} \ln(1+\beta e^t)\mathrm{d}t}{\ln(1+\beta)\int_0^{+\infty} e^{-\frac{(t+\alpha u)^2}{2\sigma^2}}\mathrm{d}t}, \tag{B.1}$$

which denotes the normalized capacity improvement at a given value of u.

Lemma B.1. *Let us assume that $g(x)$ and $h(x)$ are positive and integrable over the interval $[a, b]$, and define*

$$f_u(x) = \frac{\int_a^x g(t)\mathrm{d}t}{\int_a^x h(t)\mathrm{d}t},\ f_u(a) = \frac{g(a)}{h(a)},\ x \in [a, b],$$
$$f_d(x) = \frac{\int_x^b g(t)\mathrm{d}t}{\int_x^b h(t)\mathrm{d}t},\ f_d(b) = \frac{g(b)}{h(b)},\ x \in [a, b].$$

Then

(1) $f_u(x)$ is monotonically increasing and $f_d(x)$ is monotonically decreasing, if $\frac{g(x)}{h(x)}$ is monotonically increasing;

(2) $f_u(x)$ is monotonically decreasing and $f_d(x)$ is monotonically increasing, if $\frac{g(x)}{h(x)}$ is monotonically decreasing;

(3) The above results still hold when the domain of the variable x is extended to $(-\infty, b]$, $[a, +\infty)$ or $(-\infty, +\infty)$. ■

Proof. We will prove that $f_u(x)$ is monotonically increasing in the first case (1), and omit the proofs for the rest of (1), and for (2) and (3) since their principles are the same. If $\frac{g(x)}{h(x)}$ is monotonically increasing, we have

$$\begin{aligned}\frac{\mathrm{d}f_u(x)}{\mathrm{d}x} &= \frac{g(x)\int_a^x h(t)\mathrm{d}t - h(x)\int_a^x g(t)\mathrm{d}t}{\left[\int_a^x h(t)\mathrm{d}t\right]^2} \\ &= \frac{h(x)\left[\int_a^x \frac{g(x)}{h(x)}h(t)\mathrm{d}t - \int_a^x g(t)\mathrm{d}t\right]}{\left[\int_a^x h(t)\mathrm{d}t\right]^2} \\ &\geq \frac{h(x)\left[\int_a^x \frac{g(t)}{h(t)}h(t)\mathrm{d}t - \int_a^x g(t)\mathrm{d}t\right]}{\left[\int_a^x h(t)\mathrm{d}t\right]^2} \\ &= 0, \end{aligned} \tag{B.2}$$

where the equality only holds when $\frac{g(x)}{h(x)}$ is a constant. This proves the lemma. □

Here, we are ready to use Lemma B.1 for proving Theorem 3.2.

Proof. Let

$$g(u) = \int_0^{+\infty} e^{-\frac{(t+\alpha u)^2}{2\sigma^2}} \ln(1+\beta e^t)\mathrm{d}t, \tag{B.3}$$

$$h(u) = \ln(1+\beta)\int_0^{+\infty} e^{-\frac{(t+\alpha u)^2}{2\sigma^2}}\mathrm{d}t. \tag{B.4}$$

It is evident that $g(r)$ and $h(r)$ are positive and integrable over the interval $(-\infty, 0]$. Furthermore, we have

$$\begin{aligned}
\frac{\mathrm{d}\left(\frac{g(u)}{h(u)}\right)}{\mathrm{d}u} &= \frac{h(u)\frac{\mathrm{d}g(u)}{\mathrm{d}u} - g(u)\frac{\mathrm{d}h(u)}{\mathrm{d}u}}{[h(u)]^2} \\
&= -\frac{\alpha \ln(1+\beta)}{\sigma^2 [h(u)]^2}\left[\int_0^{+\infty}\mathrm{d}t\int_0^{+\infty}(t-s)e^{-\frac{(t+\alpha u)^2+(s+\alpha u)^2}{2\sigma^2}}\ln(1+\beta e^t)\mathrm{d}s\right] \\
&= -\frac{\alpha \ln(1+\beta)}{\sigma^2 [h(u)]^2}\left[\int_0^{+\infty}\mathrm{d}t\int_0^{t}(t-s)e^{-\frac{(t+\alpha u)^2+(s+\alpha u)^2}{2\sigma^2}}\ln(1+\beta e^t)\mathrm{d}s\right. \\
&\qquad \left. +\int_0^{+\infty}\mathrm{d}s\int_0^{s}(t-s)e^{-\frac{(t+\alpha u)^2+(s+\alpha u)^2}{2\sigma^2}}\ln(1+\beta e^t)\mathrm{d}t\right] \\
&= -\frac{\alpha \ln(1+\beta)}{\sigma^2 [h(u)]^2}\left[\int_0^{+\infty}\mathrm{d}t\int_0^{t}(t-s)e^{-\frac{(t+\alpha u)^2+(s+\alpha u)^2}{2\sigma^2}}\ln(1+\beta e^t)\mathrm{d}s\right. \\
&\qquad \left. +\int_0^{+\infty}\mathrm{d}t\int_0^{t}(s-t)e^{-\frac{(t+\alpha u)^2+(s+\alpha u)^2}{2\sigma^2}}\ln(1+\beta e^s)\mathrm{d}s\right] \\
&= -\frac{\alpha \ln(1+\beta)}{\sigma^2 [h(u)]^2}\left\{\int_0^{+\infty}\mathrm{d}t\int_0^{t}(t-s)e^{-\frac{(t+\alpha u)^2+(s+\alpha u)^2}{2\sigma^2}}\right. \\
&\qquad \left. \times\left[\ln(1+\beta e^t)-\ln(1+\beta e^s)\right]\mathrm{d}s\right\} \\
&< 0, \qquad \text{(B.5)}
\end{aligned}$$

where the inequality holds, since $(t-s)[\ln(1+\beta e^t) - \ln(1+\beta e^s] \geq 0$, but not equal to 0 everywhere. Using Lemma B.1, we have the first inequality $c_i \leq c_i^0$ in Equation 3.17.

The existence of c_i^0 can be proven as follows:

$$
\begin{aligned}
c_i^0 &= \frac{\int_0^{+\infty} \ln(1+\beta e^t)\mathrm{d}t \int_{-\infty}^{0} e^{2s} e^{-\frac{(t+\alpha s)^2}{2\sigma^2}} \mathrm{d}s}{\ln(1+\beta)\int_0^{+\infty} \mathrm{d}t \int_{-\infty}^{0} e^{2s} e^{-\frac{(t+\alpha s)^2}{2\sigma^2}} \mathrm{d}s} \\
&= \frac{\int_0^{+\infty} \ln(1+\beta e^t) e^{-\frac{2}{\alpha}t} \left[\mathrm{erf}(\frac{\alpha t - 2\sigma^2}{\sqrt{2}\alpha\sigma}) + 1\right] \mathrm{d}t}{\ln(1+\beta)\int_0^{+\infty} e^{-\frac{2}{\alpha}t} \left[\mathrm{erf}(\frac{\alpha t - 2\sigma^2}{\sqrt{2}\alpha\sigma}) + 1\right] \mathrm{d}t} \\
&< \frac{\int_0^{+\infty} 2\ln(1+\beta e^t) e^{-\frac{2}{\alpha}t} \mathrm{d}t}{\ln(1+\beta)\int_0^{+\infty} e^{-\frac{2}{\alpha}t} \left[\mathrm{erf}(\frac{-2\sigma^2}{\sqrt{2}\alpha\sigma}) + 1\right] \mathrm{d}t} \\
&< \frac{2\int_0^{+\infty} \ln(e^t + \beta e^t) e^{-\frac{2}{\alpha}t}}{\ln(1+\beta)\left[1 - \mathrm{erf}(\frac{\sqrt{2}\sigma}{\alpha})\right]\int_0^{+\infty} e^{-\frac{2}{\alpha}t} \mathrm{d}t} \\
&= \frac{2\ln(1+\beta) + \alpha}{\ln(1+\beta)\left[1 - \mathrm{erf}(\frac{\sqrt{2}\sigma}{\alpha})\right]} \\
&< +\infty,
\end{aligned}
\tag{B.6}
$$

where $\mathrm{erf}(x)$ is the error function, which is defined as

$$
\mathrm{erf}(x) = \frac{2}{\sqrt{\pi}} \int_0^x e^{-t^2} \mathrm{d}t, \tag{B.7}
$$

and satisfies $\mathrm{erf}(x) \in [-1, 1]$ and $\mathrm{erf}(-x) = -\mathrm{erf}(x)$ for $x \in (-\infty, +\infty)$. □

Appendix C

Simplified Expression in MAI

For the MAI expression of general spreading sequences in a quasi-synchronous system, since τ_c is only determined by $\tau = \frac{\tau_k - \tau_q}{T_c}$, the double integral in Equation 4.20 can be rewritten as:

$$\begin{aligned}
S &= \int_{\tau_{q0}}^{\tau_{q0}+\tau_{max}} \int_{\tau_{k0}}^{\tau_{k0}+\tau_{max}} \frac{1}{\tau_{max}^2} [\rho_{kq}^2(\tau_c) + \varrho_{kq}^2(\tau_c)] \mathrm{d}\tau_q \mathrm{d}\tau_k \\
&= \frac{1}{\tau_{max}^2} \left\{ \int_{\tau_{k0}-\tau_{q0}-\tau_{max}}^{\tau_{k0}-\tau_{q0}} [\rho_{kq}^2(\tau_c) + \varrho_{kq}^2(\tau_c)] \mathrm{d}(\tau T_c) \int_{\tau_{k0}-\tau}^{\tau_{q0}+\tau_{max}} \mathrm{d}\tau_q \right. \\
&\qquad \left. + \int_{\tau_{k0}-\tau_{q0}}^{\tau_{k0}-\tau_{q0}+\tau_{max}} [\rho_{kq}^2(\tau_c) + \varrho_{kq}^2(\tau_c)] \mathrm{d}(\tau T_c) \int_{\tau_{q0}}^{\tau_{k0}+\tau_{max}-\tau} \mathrm{d}\tau_q \right\} \\
&= \frac{1}{\tau_{max}^2} \left\{ \int_{\tau_{k0}-\tau_{q0}-\tau_{max}}^{\tau_{k0}-\tau_{q0}} [\rho_{kq}^2(\tau_c) + \varrho_{kq}^2(\tau_c)] (\tau T_c - \tau_{k0} + \tau_{q0} + \tau_{max}) \mathrm{d}(\tau T_c) \right. \\
&\qquad \left. - \int_{\tau_{k0}-\tau_{q0}}^{\tau_{k0}-\tau_{q0}+\tau_{max}} [\rho_{kq}^2(\tau_c) + \varrho_{kq}^2(\tau_c)] (\tau T_c - \tau_{k0} + \tau_{q0} - \tau_{max}) \mathrm{d}(\tau T_c) \right\} \\
&= \frac{T_c^2}{\tau_{max}^2} \left\{ \int_{\tau_-}^{\tau_0} [\rho_{kq}^2(\tau_c) + \varrho_{kq}^2(\tau_c)] (\tau - \tau_-) \mathrm{d}\tau - \int_{\tau_0}^{\tau_+} [\rho_{kq}^2(\tau_c) + \varrho_{kq}^2(\tau_c)] (\tau - \tau_+) \mathrm{d}\tau \right\}
\end{aligned} \tag{C.1}$$

where τ_-, τ_0 and τ_+ are defined as Equation 4.3.

From Equation 4.21 - 4.24, we have the following result when a rectangular chip waveform is used.

$$\begin{aligned}
&\rho_{kq}^2(\tau_c) + \varrho_{kq}^2(\tau_c) \\
&= [c_{kq}(\zeta - L)(1-\tau_c) + c_{kq}(\zeta + 1 - L)\tau_c]^2 + [c_{kq}(\zeta)(1-\tau_c) + c_{kq}(\zeta+1)\tau_c]^2 \\
&= \left\{ [c_{kq}(\zeta - L) - c_{kq}(\zeta + 1 - L)]^2 + [c_{kq}(\zeta) - c_{kq}(\zeta+1)]^2 \right\} \tau_c^2 \\
&\quad + 2\left\{ c_{kq}(\zeta - L)\left[c_{kq}(\zeta + 1 - L) - c_{kq}(\zeta - L)\right] + c_{kq}(\zeta)\left[c_{kq}(\zeta+1) - c_{kq}(\zeta)\right] \right\} \tau_c \\
&\quad + \left[c_{kq}^2(\zeta - L) + c_{kq}^2(\zeta)\right] \\
&= \omega_1(\zeta)\tau_c^2 + \omega_2(\zeta)\tau_c + \omega_3(\zeta)
\end{aligned} \tag{C.2}$$

where $\omega_1(\zeta)$, $\omega_2(\zeta)$ and $\omega_3(\zeta)$ are defined as Equation 4.28.

Substituting C.2 into C.1 and noticing that $\omega_1(\zeta)$, $\omega_2(\zeta)$ and $\omega_3(\zeta)$ keep constant while $\tau \in [j, j+1)$, we have

$$\begin{aligned}
S &= \frac{T_c^2}{\tau_{max}^2} \left\{ \int_{\tau_-}^{\tau_0} \left[\omega_1(\zeta)\tau_c^2 + \omega_2(\zeta)\tau_c + \omega_3(\zeta)\right](\tau - \tau_-)\mathrm{d}\tau \right. \\
&\qquad \left. - \int_{\tau_0}^{\tau_+} \left[\omega_1(\zeta)\tau_c^2 + \omega_2(\zeta)\tau_c + \omega_3(\zeta)\right](\tau - \tau_+)\mathrm{d}\tau \right\} \\
&= \frac{T_c^2}{\tau_{max}^2} \left\{ \sum_{j=\lambda_-}^{\lambda_0} \int_{\max\{\tau_- - j, 0\}}^{\min\{\tau_0 - j, 1\}} \left[\omega_1(\zeta)\tau_c^2 + 2\omega_2(\zeta)\tau_c + \omega_3(\zeta)\right](j + \tau_c - \tau_-)\mathrm{d}\tau_c \right. \\
&\qquad \left. - \sum_{j=\lambda_0}^{\lambda_+} \int_{\max\{\tau_0 - j, 0\}}^{\min\{\tau_+ - j, 1\}} \left[\omega_1(\zeta)\tau_c^2 + 2\omega_2(\zeta)\tau_c + \omega_3(\zeta)\right](j + \tau_c - \tau_+)\mathrm{d}\tau_c \right\} \\
&= \frac{T_c^2}{\tau_{max}^2} \left[\sum_{j=\lambda_-}^{\lambda_0} S_j^{(1)}(t)\Big|_{\max\{\tau_- - j, 0\}}^{\min\{\tau_0 - j, 1\}} - \sum_{j=\lambda_0}^{\lambda_+} S_j^{(2)}(t)\Big|_{\max\{\tau_0 - j, 0\}}^{\min\{\tau_+ - j, 1\}} \right]
\end{aligned} \tag{C.3}$$

where λ_-, λ_0 and λ_+ are defined as Equation 4.3, and $S_j^{(i)}$ is defined as Equation 4.26. Equation 4.25 is obtained by substituting Equation C.3 into Equation 4.20.

If the system is asynchronous, i.e., $\tau = \frac{\tau_k - \tau_q}{T_c}$ is uniformly distributed in $[0, L)$, the double integral in Equation 4.20 can be rewritten as:

$$\begin{aligned} S &= \frac{1}{LT_c} \int_0^{LT_c} [\rho_{kq}^2(\tau_c) + \varrho_{kq}^2(\tau_c)] \mathrm{d}(\tau T_c) \\ &= \frac{1}{L} \sum_{j=0}^{L-1} \int_j^{j+1} [\rho_{kq}^2(\tau_c) + \varrho_{kq}^2(\tau_c)] \mathrm{d}\tau \\ &= \frac{1}{L} \sum_{j=0}^{L-1} \int_0^1 \left[\omega_1(\zeta)\tau_c^2 + 2\omega_2(\zeta)\tau_c + \omega_3(\zeta)\right] \mathrm{d}\tau_c \\ &= \frac{1}{L} \sum_{j=0}^{L-1} \left[\frac{1}{3}\omega_1(\zeta) + \omega_2(\zeta) + \omega_3(\zeta)\right] \end{aligned} \tag{C.4}$$

Equation 4.39 and 4.40 are obtained by substituting Equation C.4 into Equation 4.20 and Equation 4.37, respectively.

Appendix D

The Characteristic Function

In probability theory, the Characteristic Function (CF) $\Phi_x(\omega)$ of a random variable x is defined as [260]:

$$\Phi_x(\omega) = E\{e^{j\omega x}\}, \tag{D.1}$$

where E denotes the expected value.

If there exists a Probability Density Function (PDF) $f(x)$, Equation D.1 may be expressed as [260]:

$$\Phi_x(\omega) = \int_{-\infty}^{\infty} f(x)e^{j\omega x}\mathrm{d}x. \tag{D.2}$$

As we have seen in Equation D.2 from a tangible physical perspective that the CF $\Phi_x(\omega)$ is the Fourier transform of the PDF $f(x)$ [260]. Hence $f(x)$ is the inverse Fourier transform of $\Phi_x(\omega)$ [260]:

$$f(x) = \frac{1}{2\pi}\int_{-\infty}^{\infty} \Phi_x(\omega)e^{-j\omega x}\mathrm{d}\omega. \tag{D.3}$$

Appendix E

The Hypergeometric Functions

In this appendix we provide a brief overview of several hypergeometric functions used in this dissertation. For notational convenience, we commence by introducing the Pochhammer symbol (x, n) [259, 265, 266, 269], which is defined as [269]:

$$(x, n) = x(x+1)...(x+n-1) = \frac{\Gamma(x+n)}{\Gamma(x)}, \tag{E.1}$$

where $\Gamma(x)$ is the gamma function [1] and n is a non-negative integer. In this dissertation we only consider real values of x, although it may be extended to complex values.

There are many types of hypergeometric functions. Since the Gauss hypergeometric function ${}_2\mathbb{F}_1(\alpha, \beta; \gamma; x)$ is the historically first hypergeometric function, it is often simply referred to as *the hypergeometric function* [269].

E.1 The Confluent Hypergeometric Function

The confluent hypergeometric function ${}_1\mathbb{F}_1(\alpha; \beta; x)$, also known as the Kummer function, is defined as [259, 265, 266, 269]:

$${}_1\mathbb{F}_1(\alpha; \beta; x) = \sum_{n=0}^{\infty} \frac{(\alpha, n)}{(\beta, n)} \frac{x^n}{n!}. \tag{E.2}$$

The confluent hypergeometric function ${}_1\mathbb{F}_1(\alpha; \beta; x)$ is undefined, when β is a non-positive integer, unless α is also a non-positive integer satisfying $\alpha \geq \beta$. It is convergent within the region of $x \in (-\infty, \infty)$ [269]. The confluent hypergeometric function ${}_1\mathbb{F}_1(\alpha; \beta; x)$

has been implemented in the commercial Mathematica software package [313] and its practical evaluation has been described in [314].

E.2 The Hypergeometric Function

The hypergeometric function ${}_2\mathbb{F}_1(\alpha,\beta;\gamma;x)$, which is also known as the Gauss hypergeometric function, is defined as [259, 265, 266, 269]:

$$ {}_2\mathbb{F}_1(\alpha,\beta;\gamma;x) = \sum_{n=0}^{\infty} \frac{(\alpha,n)(\beta,n)}{(\gamma,n)} \frac{x^n}{n!}. \tag{E.3}$$

The hypergeometric function ${}_2\mathbb{F}_1(\alpha,\beta;\gamma;x)$ is undefined when γ is a non-positive integer, unless one of the parameters, α or β, is also a non-positive integer satisfying $\alpha \geq \gamma$ or $\beta \geq \gamma$. Alternatively, ${}_2\mathbb{F}_1(\alpha,\beta;\gamma;x)$ is simply denoted as $\mathbb{F}(\alpha,\beta;\gamma;x)$ [259]. The confluent hypergeometric function ${}_1\mathbb{F}_1(\alpha;\beta;x)$ is a special case of the hypergeometric function ${}_2\mathbb{F}_1(\alpha,\beta;\gamma;x)$ [269]:

$$ {}_1\mathbb{F}_1(\alpha;\gamma;x) = \lim_{\beta\to\infty} {}_2\mathbb{F}_1(\alpha,\beta;\gamma;\frac{x}{\beta}). \tag{E.4}$$

The hypergeometric function ${}_2\mathbb{F}_1(\alpha,\beta;\gamma;x)$ converges, when $|x| < 1$ and diverges, when $|x| > 1$. Its convergence becomes less consistent on the unit circle [259, 269]. The hypergeometric function ${}_2\mathbb{F}_1(\alpha,\beta;\gamma;x)$ has been implemented in Mathematica [315] and its computation algorithm has been described in [314].

E.3 The Generalized Hypergeometric Function

The generalized hypergeometric function ${}_p\mathbb{F}_q(\alpha_1,\alpha_2,...,\alpha_p;\beta_1,\beta_2,...,\beta_q;x)$ is defined as [269]:

$$ {}_p\mathbb{F}_q(\alpha_1,\alpha_2,...,\alpha_p;\beta_1,\beta_2,...,\beta_q;x) = \sum_{n=0}^{\infty} \frac{(\alpha_1,n)(\alpha_2,n)\ldots(\alpha_p,n)}{(\beta_1,n)(\beta_2,n)\ldots(\beta_q,n)} \frac{x^n}{n!}, \tag{E.5}$$

where both p and q are non-negative integers. It converges for all finite x, when $p \leq q$. Its convergence becomes less predictable, when we have $p > q$ [269].

It may be readily shown that the confluent hypergeometric function ${}_1\mathbb{F}_1(\alpha;\beta;x)$ and the hypergeometric function ${}_2\mathbb{F}_1(\alpha,\beta;\gamma;x)$ are the special cases of the generalized hypergeometric function ${}_p\mathbb{F}_q(\alpha_1,\alpha_2,...,\alpha_p;\beta_1,\beta_2,...,\beta_q;x)$, when we have $p=1,q=1$ and $p=2,q=1$, respectively. The generalized hypergeometric function has been implemented in Mathematica [316]. As the simple case of ${}_2\mathbb{F}_2$ is concerned in Equation 5.35, it is more efficient to integrate Equation 5.34 directly.

E.4 Horn's Confluent Hypergeometric Functions of Two Variables

Horn investigated 34 distinct hypergeometric functions of two variables and in this set there are 14 confluent functions [265, 266]. In this dissertation we used two of Horn's confluent hypergeometric functions of two variables, which are defined as [265, 266]:

$$\Psi_2(\alpha;\gamma,\gamma';x,y)=\sum_{n=0}^{\infty}\sum_{m=0}^{\infty}\frac{(\alpha,m+n)}{(\gamma,m)(\gamma',n)}\frac{x^m y^n}{m!n!}, \tag{E.6}$$

$$\mathbb{H}_7(\alpha;\gamma,\delta;x,y)=\sum_{n=0}^{\infty}\sum_{m=0}^{\infty}\frac{(\alpha,2m+n)}{(\gamma,m)(\delta,n)}\frac{x^m y^n}{m!n!}, \tag{E.7}$$

and $\Psi_2(\alpha;\gamma,\gamma';x,y)$ is convergent for all finite values of x and y, while $\mathbb{H}_7(\alpha;\gamma,\delta;x,y)$ is convergent only when $|x|<\frac{1}{4}$. At the time of writing Horn's functions have not been implemented in any prevalent mathematical software. It is more efficient to compute Horn's functions from their equivalent integral representations, rather than from their definitions of Equations E.6 and E.7 [265]. It is sufficient for our investigations in this dissertation to integrate Equations 5.4 and 5.7 in order to obtain Equations 5.5 and 5.8, respectively.

E.5 The Kampé de Fériet Function

The Kampé de Fériet function $\mathbb{F}^{A:B;B'}_{C:D;D'}\left[\begin{matrix}(a):(b)\,;(b')\,;\\(c):(d)\,;(d')\,;\end{matrix}x,y\right]$ is a generalized hypergeometric function of two variables, which is defined as [266, 269]:

$$\mathbb{F}^{A:B;B'}_{C:D;D'}\left[\begin{matrix}(a):(b)\,;(b')\,;\\(c):(d)\,;(d')\,;\end{matrix}x,y\right]=\sum_{n=0}^{\infty}\sum_{m=0}^{\infty}\frac{\prod_{k=1}^{A}(a_k,m+n)\prod_{k=1}^{B}(b_k,m)\prod_{k=1}^{B'}(b'_k,n)}{\prod_{k=1}^{C}(c_k,m+n)\prod_{k=1}^{D}(d_k,m)\prod_{k=1}^{D'}(d'_k,n)}\frac{x^m y^n}{m!n!}, \tag{E.8}$$

where (a) abbreviates the array of A parameters $a_1,...,a_A$, while (b), (b'), (c), (d) and (d') have similar interpretations. The Kampé de Fériet function is convergent for all finite values of x and y, when we have $A+B<C+D+1$ and $A+B'<C+D'+1$, while its convergence becomes less predictable in other scenarios [266, 269]. At the time of writing the Kampé de Fériet function has not been implemented in any commercial mathematical software. As the simple case of $\mathbb{F}^{1:0;0}_{1:0;1}$ is concerned in Equation 5.30, it is more efficient to integrate Equation 5.29 directly.

E.6 The Lauricella Functions of n Variables

The Lauricella functions are generalized from the Gauss hypergeometric functions to multiple variables. There are four functions defined by Lauricella [266, 269]. In this dissertation we used one of these Lauricella functions, which is defined as [266, 269]:

$$\begin{aligned}&\mathbb{F}^{(n)}_A(\alpha;\beta_1,...,\beta_n;\gamma_1,...,\gamma_n;x_1,...,x_n)\\&=\sum_{m_1=0}^{\infty}\cdots\sum_{m_n=0}^{\infty}\frac{(\alpha,m_1+\cdots+m_n)(\beta_1,m_1)\ldots(\beta_n,m_n)}{(\gamma_1,m_1)\ldots(\gamma_n,m_n)}\frac{x_1^{m_1}\ldots x_n^{m_n}}{m_1!\ldots m_n!}.\end{aligned} \tag{E.9}$$

It is convergent within the region $\sum_{i=1}^{n}|x_i|<1$ [269]. At the time of writing the Lauricella function has not been implemented by any prevalent commercial mathematical software. However, its equivalent integral representation provides an efficient technique for its evaluation [266]:

$$\mathbb{F}^{(n)}_A(\alpha;\beta_1,...,\beta_n;\gamma_1,...,\gamma_n;x_1,...,x_n)=\frac{1}{\Gamma(\alpha)}\int_0^{\infty}e^{-t}t^{\alpha-1}\prod_{k=1}^{n}{}_1\mathbb{F}_1(\beta_k;\gamma_k;x_kt)\mathrm{d}t. \tag{E.10}$$

E.7 The Generalized Lauricella Function of n Variables

The generalized Lauricella function is defined as [266, 269]:

$$\mathbb{F}_{C:D^{(1)};\ldots;D^{(n)}}^{A:B^{(1)};\ldots;B^{(n)}}\left(\begin{matrix}\left[(a):\theta^{(1)},\ldots,\theta^{(n)}\right]:\left[(b^{(1)}):\phi^{(1)}\right];\ldots;\left[(b^{(n)}):\phi^{(n)}\right];\\ \left[(c):\psi^{(1)},\ldots,\psi^{(n)}\right]:\left[(d^{(1)}):\delta^{(1)}\right];\ldots;\left[(d^{(n)}):\delta^{(n)}\right];\end{matrix} x_1,\ldots,x_n\right) \tag{E.11}$$

$$=\sum_{m_1=0}^{\infty}\cdots\sum_{m_n=0}^{\infty}\frac{\prod_{k=1}^{A}(a_k,\sum_{i=1}^{n}m_i\theta_k^{(i)})\prod_{k=1}^{B^{(1)}}(b_k^{(1)},m_1\phi_k^{(1)})\cdots\prod_{k=1}^{B^{(n)}}(b_k^{(n)},m_n\phi_k^{(n)})}{\prod_{k=1}^{C}(c_k,\sum_{i=1}^{n}m_i\psi_k^{(i)})\prod_{k=1}^{D^{(1)}}(d_k^{(1)},m_1\delta_k^{(1)})\cdots\prod_{k=1}^{D^{(n)}}(d_k^{(n)},m_n\delta_k^{(n)})}\frac{x_1^{m_1}\ldots x_n^{m_n}}{m_1!\ldots m_n!},$$

where the coefficients $\theta_k^{(i)}$, $\phi_k^{(i)}$, $\psi_k^{(i)}$ and $\delta_k^{(i)}$ are positive constants or zero. The convergence of the generalized Lauricella function is unpredictable and has been discussed in [317]. As the simple case of $\mathbb{F}_{1:0;1}^{1:0;0}$ is concerned in Equation 5.33, it is the special case of the generalized Lauricella function with $n = 2$ and it is also the generalization of the Kampé de Fériet Function in Section E.5. Using Horn's convergence rule for the general hypergeometric functions of two variables [266, 269], $\mathbb{F}_{1:0;1}^{1:0;0}$ in Equation 5.33 converges for all finite values of x_1 and x_2. Furthermore, it is more efficient to integrate Equation 5.32 directly for its numerical evaluation, rather than to use its definition of Equation E.11.

Bibliography

[1] M. Abramowitz and I. A. Stegun, *Handbook of Mathematical Functions, with Formulas, Graphs, and Mathematical Tables.* Department of Commerce, USA, 1972.

[2] E. W. Weisstein, "Big-Theta Notation." MathWorld–A Wolfram Web Resource. http://mathworld.wolfram.com/Big-ThetaNotation.html.

[3] E. W. Weisstein, "Landau Symbols." MathWorld–A Wolfram Web Resource. http://mathworld.wolfram.com/LandauSymbols.html.

[4] J. J.-N. Liu and I. Chlamtac, "Mobile Ad-Hoc Networking with a View of 4G Wireless: Imperatives and Challenges," in *Mobile Ad Hoc Networking* (S. Basagni, M. Conti, S. Giordano, and I. Stojmenovic, eds.), ch. 1, pp. 1–46, Wiley-IEEE Press, 2004.

[5] X. Liu and L. Hanzo, "Effects of Rate Adaptation on the Throughput of Random Ad Hoc Networks," in *IEEE Vehicular Technology Conference*, vol. 3, (Dallas, TX, USA), pp. 1887–1891, 25-28 September 2005.

[6] X. Liu, H. Wei, and L. Hanzo, "Analytical BER Performance of DS-CDMA Ad Hoc Networks Using Large Area Synchronized Spreading Codes," in *Sixth International Conference on 3G and Beyond - 3G 2005*, (London, UK), pp. 249–253, 07-09 November 2005.

[7] X. Liu, H. Wei, and L. Hanzo, "Analytical BER Performance of LAS DS-CDMA Ad Hoc Networks," *submitted to IEE Proceedings Communications*, 2005.

[8] X. Liu and L. Hanzo, "A Unified Exact BER Performance Analysis of Asynchronous DS-CDMA Systems Using BPSK Modulation over Fading Channels," *accepted subjected to revision for publication in IEEE Transactions on Vehicular Technology*, 2006.

[9] X. Liu and L. Hanzo, "Accurate BER Analysis of Asynchronous DS-CDMA Systems in Ricean Channels," in *IEEE Vehicular Technology Conference*, (Montreal, Quebec, Canada), 25-28 May September 2006.

[10] X. Liu and L. Hanzo, "Exact BER Calculation of Asynchronous DS-CDMA Systems Communicating over Hoyt Channels," in *Ninth International Symposium on Spread Spectrum Techniques and Applications*, (Manaus, Brazil), 28-31 August 2006.

[11] X. Liu and L. Hanzo, "Exact BER of Rectangular-Constellation Quadrature Amplitude Modulation Subjected to Asynchronous Co-Channel Interference and Nakagami-m Fading," *to appear in Electronics Letters*, vol. 42, July 2006.

[12] X. Liu and L. Hanzo, "Exact BER of Rectangular-Constellation Quadrature Amplitude Modulation Subjected to Asynchronous Co-Channel Interference and Nakagami-m Fading," in *IEEE Vehicular Technology Conference (to be submitted)*, (Dublin, Ireland), 23-25 April 2007.

[13] X. Liu and L. Hanzo, "Exact BER Analysis of OFDM Systems Communicating over Frequency-Selective Fading Channels in the Presence of Both Carrier Frequency Offset and Channel Estimation Errors," in *IEEE Vehicular Technology Conference (to be submitted)*, (Dublin, Ireland), 23-25 April 2007.

[14] "Cambridge Learner's Dictionary." Cambridge University Press, 2004. http://dictionary.cambridge.org/.

[15] ANSI/IEEE Std 802.11, 1999 Edition, *Wireless LAN Medium Access Control (MAC) and Physical Layer (PHY) Specifications*, 1999.

[16] S. Corson and J. Macker, *Request for Comments - Mobile Ad Hoc Networking (MANET): Routing Protocol Performance Issues and Evaluation Considerations.* Internet Engineering Task Force (IETF), January 1999. http://www.ietf.org/rfc/rfc2501.txt.

[17] R. Ramanathan and J. Redi, "A Brief Overview of Ad Hoc Networks: Challenges and Directions," *IEEE Communications Magazine*, vol. 40, pp. 20–22, May 2002.

[18] J. Jubin and J. D. Tornow, "The DARPA Packet Radio Network Protocols," *roceedings of the IEEE*, vol. 75, pp. 21–32, January 1987.

[19] D. A. Beyer, "Accomplishments of the DARPA SURAN Program," in *IEEE Military Communications Conference*, vol. 2, (Monterey, CA, USA), pp. 855–862, 30 September-3 October 1990.

[20] W. Fifer and F. Bruno, "The Low-Cost Packet Radio," *Proceedings of the IEEE*, vol. 75, pp. 33–42, January 1987.

[21] B. Leiner, R. Ruther, and A. Sastry, "Goals and Challenges of the DARPA GloMo Program," *IEEE Personal Communications*, vol. 3, pp. 34–43, December 1996.

[22] J. Garcia-Luna-Aceves, C. Fullmer, E. Madruga, D. Beyer, and T. Frivold, "Wireless Internet Gateways (WINGs)," in *IEEE Military Communications Conference*, vol. 3, (Monterey, CA, USA), pp. 1271–1276, 2-5 November 1997.

[23] R. Ramanathan and M. Steenstrup, "Hierarchically-Organized, Multihop Mobile Wireless Networks for Quality-of-Service Support," *ACM/Baltzer Mobile Networks and Applications*, vol. 3, pp. 101–119, June 1998.

[24] R. Ruppe, S. Griswald, P. Walsh, and R. Martin, "Near Term Digital Radio (NTDR) System," in *IEEE Military Communications Conference*, vol. 3, (Monterey, CA, USA), pp. 1282–1287, 2-5 November 1997.

[25] D. Hall, "Tactical Internet System Architecture for Task Force XXI," in *Tactical Communications Conference*, (Fort Wayne, IN, USA), pp. 219–230, 30 April-2 May 1996.

[26] IEEE Std 802.11-1997, *Wireless LAN Medium Access Control (MAC) and Physical Layer (PHY) Specifications*, 1997.

[27] IEEE Std 802.11b-1999, *Wireless LAN Medium Access Control (MAC) And Physical Layer (PHY) Specifications: Higher-Speed Physical Layer Extension In The 2.4 GHz Band*, 1999.

[28] D. B. Johnson, D. A. Maltz, and Y.-C. Hu, *Internet Draft - The Dynamic Source Routing Protocol for Mobile Ad Hoc Networks (DSR)*. Internet Engineering Task Force (IETF), July 2004. http://www.ietf.org/internet-drafts/draft-ietf-manet-dsr-10.txt.

[29] IEEE Std 802.15.1-2002, *Wireless Medium Access Control (MAC) and Physical Layer (PHY) Specifications for Wireless Personal Area Networks (WPANs)*, 2002.

[30] IEEE Std 802.11g-2003, *Wireless LAN Medium Access Control (MAC) and Pphysical Layer (PHY) Specifications*, 2003.

[31] IEEE Std 802.15.3-2003, *Wireless Medium Access Control (MAC) and Physical Layer (PHY) Specifications for High Rate Wireless Personal Area Networks (WPANs)*, 2003.

[32] IEEE Std 802.15.4-2003, *Wireless Medium Access Control (MAC) and Physical Layer (PHY) Specifications for Low-Rate Wireless Personal Area Networks (LR-WPANs)*, 2003.

[33] C. Perkins, E. Belding-Royer, and S. Das, *RFC3561 - Ad hoc On-Demand Distance Vector (AODV) Routing.* Internet Engineering Task Force (IETF), July 2003. http://www.ietf.org/rfc/rfc3561.txt.

[34] T. Clausen and P. Jacquet, *RFC3626 - Optimized Link State Routing Protocol (OLSR).* Internet Engineering Task Force (IETF), October 2003. http://www.ietf.org/rfc/rfc3626.txt.

[35] IEEE Std 802.16-2004 (Revision of IEEE Std 802.16-2001), *Air Interface for Fixed Broadband Wireless Access Systems*, 2004.

[36] R. Ogier, F. Templin, and M. Lewis, *RFC3684 - Topology Dissemination Based on Reverse-Path Forwarding (TBRPF).* Internet Engineering Task Force (IETF), February 2004. http://www.ietf.org/rfc/rfc3684.txt.

[37] I. Chakeres, E. Belding-Royer, and C. Perkins, *Internet-Draft - Dynamic MANET On-demand (DYMO) Routing.* Internet Engineering Task Force (IETF), June 2005. http://www.ietf.org/internet-drafts/draft-ietf-manet-dymo-02.txt.

[38] J. A. Freebersyser and B. Leiner, "A DoD Perspective on Mobile Ad Hoc Networks," in *Ad Hoc Networking*, pp. 29–51, Addison-Wesley Longman Publishing Co., Boston, MA, USA, 2001.

[39] N. Abramson, "Development of the ALOHANET," *IEEE Transactions on Information Theory*, vol. 31, pp. 119–123, March 1985.

[40] L. Kleinrock and F. A. Tobagi, "Packet Switching in Radio Channels: Part I–Carrier Sense Multiple-Access Modes and Their Throughput-Delay Characteristics," *IEEE Transactions on Communications*, vol. 23, pp. 1400–1416, December 1975.

[41] R. Bruno, M. Conti, and E. Gregori, "Mesh Networks: Commodity Multihop Ad Hoc Networks," *IEEE Communications Magazine*, vol. 43, pp. 123–131, March 2005.

[42] IEEE 802.20 Working Group, "IEEE 802.20 Mobile Broadband Wireless Access (MBWA)." http://grouper.ieee.org/groups/802/20/.

[43] P. Gupta and P. Kumar, "The Capacity of Wireless Networks," *IEEE Transactions on Information Theory*, vol. 46, pp. 388–404, March 2000.

[44] A. Spyropoulos and C. Raghavendra, "Capacity Bounds for Ad-Hoc Networks Using Directional Antennas," in *IEEE International Conference on Communications*, vol. 1, (Anchorage, Alaska, USA), pp. 348–352, 11-15 May 2003.

[45] A. Spyropoulos and C. Raghavendra, "Asympotic Capacity Bounds for Ad-Hoc Networks Revisited: the Directional and Smart Antenna Cases," in *IEEE Global Telecommunications Conference*, vol. 3, (San Francisco, California, USA), pp. 1216–1220, 1-5 December 2003.

[46] S. Toumpis and A. J. Goldsmith, "Capacity Regions for Wireless Ad Hoc Networks," *IEEE Transactions on Wireless Communications*, vol. 2, pp. 736–748, July 2003.

[47] M. Grossglauser and D. Tse, "Mobility Increases the Capacity of Ad Hoc Wireless Networks," *IEEE/ACM Transactions on Networking*, vol. 10, pp. 477–486, August 2002.

[48] D. S. Heberto del Rio, "Logarithmic Expected Packet Delivery Delay in Mobile Ad Hoc Wireless Networks," *Wiley Journal on Wireless Communications and Mobile Computing*, vol. 4, pp. 281–287, May 2004.

[49] B. Liu, Z. Liu, and D. Towsley, "On the Capacity of Hybrid Wireless Networks," in *IEEE INFOCOM*, vol. 2, (San Francisco, Carlifornia, USA), pp. 1543 –1552, 30 March-3 April 2003.

[50] U. C. Kozat and L. Tassiulas, "Throughput Capacity of Random Ad Hoc Networks with Infrastructure Support," in *International Conference on Mobile Computing and Networking*, (San Diego, Carlifornia, USA), pp. 55–65, 14-19 September 2003.

[51] J. Li, C. Blake, D. S. J. D. Couto, H. I. Lee, and R. Morris, "Capacity of Ad Hoc Wireless Networks," in *ACM/IEEE International Conference on Mobile Computing and Networking*, (Rome, Italy), pp. 61–69, 16-21 July 2001.

[52] J. Li, Z. Haas, and M. Sheng, "Capacity Evaluation of Multi-Channel Multi-Hop Ad Hoc Networks," in *IEEE International Conference on Personal Wireless Communications*, (New Delhi, India), pp. 211–214, 15-17 December 2002.

[53] C. E. Perkins and P. Bhagwat, "Highly Dynamic Destination-Sequenced Distance-Vector Routing (DSDV) for Mobile Computers," in *ACM/SIGCOMM Conference on Communications Architectures, Protocols and Applications*, (London, United Kingdom), pp. 234–244, December 1994.

[54] S. Murthy and J. J. Garcia-Luna-Aceves, "An Efficient Routing Protocol for Wireless Networks," *ACM Mobile Networks and Applications*, vol. 1, pp. 183–197, October 1996. Special Issue on Routing in Mobile Communications Networks.

[55] T.-W. Chen and M. Gerla, "Global State Routing: A New Routing Scheme for Ad-Hoc Wireless Networks," in *IEEE International Conference on Communications*, vol. 1, (Atlanta, GA, USA), pp. 171–175, 7-11 June 1998.

[56] A. Iwata, C.-C. Chiang, G. Pei, M. Gerla, and T.-W. Chen, "Scalable routing strategies for ad hoc wireless networks," *IEEE Journal on Selected Areas in Communications*, vol. 17, pp. 1369–1379, August 1999.

[57] J. Garcia-Luna-Aceves and M. Spohn, "Source-Tree Routing in Wireless Networks," in *Seventh International Conference on Network Protocols*, (Toronto, Canada), pp. 273–282, 31 October-3 November 1999.

[58] S. Basagni, I. Chlamtac, V. R. Syrotiuk, and B. A. Woodward, "A Distance Routing Effect Algorithm for Mobility (DREAM)," in *The 4th Annual ACM/IEEE International Conference on Mobile Computing and Networking*, (Dallas, TX, USA), pp. 76–84, 1998.

[59] K. Kasera and R. Ramanathan, "A Location Management Protocol for Hierarchically Organized Multihop Mobile Wireless Networks," in *IEEE 6th International Conference on Universal Personal Communications*, vol. 1, (San Diego, CA, USA), pp. 158–162, 12-16 October 1997.

[60] C. Chiang, H. Wu, W. Liu, and M. Gerla, "Routing in Clustered Multihop, Mobile Wireless Networks," in *IEEE Singapore International Conference on Networks*, (Singapore), pp. 197–211, 16-17 April 1997.

[61] J. Raju and J. Garcia-Luna-Aceves, "A New Approach to On-Demand Loop-Free Multipath Routing," in *The 8th IEEE International Conference on Computer Communications and Networks*, (Boston, MA, USA), pp. 522–527, 11-13 October 1999.

[62] M. S. Corson and A. Ephremides, "A Distributed Routing Algorithm for Mobile Wireless Networks," *ACM Journal on Wireless Networks*, vol. 1, pp. 61–81, February 1995.

[63] V. Park and M. Corson, "A Highly Adaptive Distributed Routing Algorithm for Mobile Wireless Networks," in *IEEE INFOCOM*, vol. 3, (Kobe, Japan), pp. 1405–1413, 7-11 April 1997.

[64] C.-K. Toh, "A Novel Distributed Routing Protocol to Support Ad-Hoc Mobile Computing," in *IEEE Fifteenth Annual International Phoenix Conference on Computers and Communications*, (Scottsdale, AZ, USA), pp. 480–486, 27-29 March 1996.

[65] R. Dube, C. Rais, K.-Y. Wang, and S. Tripathi, "Signal Stability-Based Adaptive Routing (SSA) for Ad Hoc Mobile Networks," *IEEE Personal Communications*, vol. 4, pp. 36–45, February 1997.

[66] G. Aggelou and R. Tafazolli, "RDMAR: A Bandwidth-Efficient Routing Protocol for Mobile Ad Hoc Networks," in *The 2nd ACM International Workshop on Wireless Mobile Multimedia*, (Seattle, WA, USA), pp. 26–33, August 1999.

[67] Y.-B. Ko and N. H. Vaidya, "Location-Aided Routing (LAR) in Mobile Ad Hoc Networks," in *The 4th Annual ACM/IEEE International Conference on Mobile Computing and Networking*, (Dallas, TX, USA), pp. 66–75, October 1998.

[68] M. Gunes, U. Sorges, and I. Bouazizi, "ARA-The Ant-Colony Based Routing Algorithm for MANETs," in *IEEE International Conference on Parallel Processing Workshops*, pp. 79–85, 18-21 August 2002.

[69] W. Su and M. Gerla, "IPv6 Flow Handoff in Ad Hoc Wireless Networks Using Mobility Prediction," in *IEEE Global Telecommunications Conference*, vol. 1A, (Rio de Janeireo, Brazil), pp. 271–275, 5-9 December 1999.

[70] M. Jiang, J. Li, and Y. C. Tay, *Internet Draft - Cluster Based Routing Protocol(CBRP) Functional Specification).* Internet Engineering Task Force (IETF), August 1998. http://www.ietf.org/proceedings/98aug/I-D/draft-ietf-manet-cbrp-spec-00.txt.

[71] Z. Haas, "A New Routing Protocol for the Reconfigurable Wireless Networks," in *IEEE 6th International Conference on Universal Personal Communications Record*, vol. 2, (San Diego, CA, USA), pp. 562–566, 12-16 October 1997.

[72] M. Joa-Ng and I.-T. Lu, "A Peer-to-Peer Zone-Bbased Two-Level Link State Routing for Mobile Ad Hoc Networks," *IEEE Journal on Selected Areas in Communications*, vol. 17, pp. 1415–1425, August 1999.

[73] S.-C. M. Woo and S. Singh, "Scalable Routing Protocol for Ad Hoc Networks," *ACM Journal on Wireless Networks*, vol. 7, pp. 513–529, September 2001.

[74] S. Radhakrishnan, G. Racherla, C. Sekharan, N. Rao, and S. Batsell, "DST-A Routing Protocol for Ad Hoc Networks Using Distributed Spanning Trees," in *IEEE Wireless Communications and Networking Conference*, vol. 3, (New Orleans, LA, USA), pp. 1543–1547, 21-24 September 1999.

[75] N. Nikaein, H. Labiod, and C. Bonnet, "DDR: Distributed Dynamic Routing Algorithm for Mobile Ad Hoc Networks," in *The 1st ACM International Symposium on Mobile Ad Hoc Networking and Computing*, (Boston, MA, USA), pp. 19–27, September 2000.

[76] C. Metz, "At the Core of IP Networks: Link-State Routing Protocols," *IEEE Internet Computing*, vol. 3, pp. 72–77, September-October 1999.

[77] C. Hedrick, *RFC1058 - Routing Information Protocol.* Internet Engineering Task Force (IETF), June 1988. http://www.ietf.org/rfc/rfc1058.txt.

[78] E. M. Royer and C.-K. Toh, "A Review of Current Routing Protocols for Ad Hoc Mobile Wireless Networks," *IEEE Personal Communications*, vol. 6, pp. 46–55, April 1999.

[79] M. Abolhasan, T. Wysocki, and E. Dutkiewicz, "A Review of Routing Protocols for Mobile Ad Hoc Networks," *Elsevier Science Ad Hoc Networks*, vol. 2, pp. 1–22, January 2004.

[80] Z. Ren and W. Guo, "Unicast Routing in Mobile Ad Hoc Networks: Present and Future Directions," in *IEEE The Fourth International Conference on Parallel and Distributed Computing, Applications and Technologies*, pp. 340–344, 27-29 August 2003.

[81] B. Williams and T. Camp, "Comparison of Broadcasting Techniques for Mobile Ad Hoc Networks," in *International Symposium on Mobile Ad Hoc Networking and Computing*, (Lausanne, Switzerland), pp. 194–205, June 2002.

[82] C. de Morais Cordeiro, H. Gossain, and D. P. Agrawal, "Multicast over Wireless Mobile Ad Hoc Networks: Present and Future Directions," *IEEE Network*, vol. 17, pp. 52–59, January/February 2003.

[83] X. Jiang and T. Camp, "A Review of Geocasting Protocols for a Mobile Ad Hoc Network," in *Grace Hopper Celebration of Women in Computing 2002*, (Hyatt Regency Vancouver, British Columbia, Canada), 9-12 October 2002.

[84] C. Ho, K. Obraczka, G. Tsudik, and K. Viswanath, "Flooding for Reliable Multicast in Multi-Hop Ad Hoc Networks," in *The 3rd International Workshop on Discrete Algorithms and Methods for Mobile Computing and Communications*, (Seattle, WA, USA), pp. 64–71, 1999.

[85] S.-Y. Ni, Y.-C. Tseng, Y.-S. Chen, and J.-P. Sheu, "The Broadcast Storm Problem in A Mobile Ad Hoc Network," in *The 5th Annual ACM/IEEE International Conference on Mobile Computing and Networking*, (Seattle, WA, USA), pp. 151–162, 1999.

[86] H. Lim and C. Kim, "Multicast Tree Construction and Flooding in Wireless Ad Hoc Networks," in *the 3rd ACM International Workshop on Modeling, Analysis and Simulation of Wireless and Mobile Systems*, pp. 61–68, Boston, MA, USA 2000.

[87] W. Peng and X.-C. Lu, "On the Reduction of Broadcast Redundancy in Mobile Ad Hoc Networks," in *The 1st ACM International Symposium on Mobile Ad Hoc Networking and Computing*, (Boston, MA, USA), pp. 129–130, 2000.

[88] D. Waitzman and S. Deering, *RFC1075 - Distance Vector Multicast Routing Protocol.* Internet Engineering Task Force (IETF), November 1988. http://www.ietf.org/rfc/rfc1075.txt.

[89] C. Wu and Y. Tay, "AMRIS: A Multicast Protocol for Ad Hoc Wireless Networks," in *IEEE Military Communications Conference*, vol. 1, (Atlantic City, NJ, USA), pp. 25–29, 31 October-3 November 1999.

[90] E. M. Royer and C. E. Perkins, "Multicast Operation of the Ad-Hoc On-Demand Distance Vector Routing Protocol," in *The 5th Annual ACM/IEEE International Conference on Mobile Computing and Networking*, (Seattle, WA, USA), pp. 207–218, 1999.

[91] L. Ji and M. Corson, "A Lightweight Adaptive Multicast Algorithm," in *IEEE Global Telecommunications Conference*, vol. 2, (Sydney, NSW, Australia), pp. 1036–1042, 8-12 November 1998.

[92] K. Chen and K. Nahrstedt, "Effective Location-Guided Tree Construction Algorithms for Small Group Multicast in MANET," in *IEEE INFOCOM 2002*, vol. 3, pp. 1180–1189, 23-27 June 2002.

[93] S. J. Lee, W. Su, and M. Gerla, "On-Demand Multicast Routing Protocol in Multihop Wireless Mobile Networks," *ACM Mobile Networks and Applications*, vol. 7, pp. 441–453, December 2002.

[94] J. Garcia-Luna-Aceves and E. Madruga, "The Core-Assisted Mesh Protocol," *IEEE Journal on Selected Areas in Communications*, vol. 17, pp. 1380–1394, August 1999.

[95] C.-C. Chiang, M. Gerla, and L. Zhang, "Forwarding Group Multicast Protocol (FGMP) for Multihop, Mobile Wireless Networks," *ACM-Baltzer Journal of Cluster Computing: Special Issue on Mobile Computing*, vol. 1, no. 2, pp. 187–196, 1998.

[96] L. Ji and M. Corson, "Differential Destination Multicast-A MANET Multicast Routing Protocol for Small Groups," in *IEEE INFOCOM 2001*, vol. 2, (Anchorage, AK, USA), pp. 1192–1201, 22-26 April 2001.

[97] J. Xie, R. R. Talpade, A. Mcauley, and M. Liu, "AMRoute: Ad Hoc Multicast Routing Protocol," *ACM Mobile Networks and Applications*, vol. 7, pp. 429–439, December 2002.

[98] P. Sinha, R. Sivakumar, and V. Bharghavan, "MCEDAR: Multicast Core-Extraction Distributed Ad Hoc Routing," in *IEEE Wireless Communications and Networking Conference*, vol. 3, (New Orleans, LA, USA), pp. 1313–1317, 21-24 September 1999.

[99] Y.-B. Ko and N. Vaidya, "Geocasting in Mobile Ad Hoc Networks: Location-Based Multicast Algorithms," in *Second IEEE Workshop on Mobile Computing Systems and Applications*, (New Orleans, LA, USA), pp. 101–110, 25-26 February 1999.

[100] I. Stojmenovic, A. Ruhil, and D. Lobiyal, "Voronoi Diagram and Convex Hull Based Geocasting and Routing in Wireless Networks," in *Eighth IEEE International Symposium on Computers and Communication*, vol. 1, (Kemer-Antalya, Turkey), pp. 51–56, July 2003.

[101] W.-H. Liao, Y.-C. Tseng, and J.-P. Sheu, "GeoGRID: A Geocasting Protocol for Mobile Ad Hoc Networks Based on GRID," *Journal of Internet Technology*, vol. 1, no. 2, pp. 23–32, 2000.

[102] Y.-B. Ko and N. Vaidya, "GeoTORA: A Protocol for Geocasting in Mobile Ad Hoc Networks," in *IEEE International Conference on Network Protocols*, (Osaka, Japan), pp. 240–250, 14-17 November 2000.

[103] J. Boleng, T. Camp, and V. Tolety, "Mesh-Based Geocast Routing Protocols in An Ad Hoc Network," in *15th International Parallel and Distributed Processing Symposium*, pp. 1924–1933, 23-27 April 2001.

[104] T. Issariyakul, E. Hossain, and D. I. Kim, "Medium Access Control Protocols for Wireless Mobile Ad Hoc Networks: Issues and Approaches," *Wiley Journal on Wireless Communications and Mobile Computing*, vol. 3, pp. 935–958, December 2003.

[105] P. Karn, "MACA: A New Channel Access Method for Packet Radio," in *The 9th ARRL/CRRL Amateur Radio Computer Networking Conference*, (London, Ontario, Canada), pp. 134–140, 1990.

[106] C. L. Fullmer and J. J. Garcia-Luna-Aceves, "Solutions to Hidden Terminal Problems in Wireless Networks," in *The ACM Conference on Applications, Technologies, Architectures, and Protocols for Computer Communication*, (Cannes, France), pp. 39–49, 1997.

[107] V. Bharghavan, A. Demers, S. Shenker, and L. Zhang, "MACAW: A Media Access Protocol for Wireless LANs," *ACM SIGCOMM Computer Communication Review*, vol. 24, pp. 212–225, October 1994.

[108] M. Joa-Ng and I.-T. Lu, "Spread Spectrum Medium Access Protocol with Collision Avoidance in Mobile Ad-Hoc Wireless Network," in *IEEE INFOCOM'99*, vol. 2, (New York, NY, USA), pp. 776–783, 21-25 March 1999.

[109] A. Tzamaloukas and J. Garcia-Luna-Aceves, "A Receiver-Initiated Collision-Avoidance Protocol for Multi-Channel Networks," in *IEEE INFOCOM 2001*, vol. 1, (Anchorage, AK, USA), pp. 189–198, 22-26 April 2001.

[110] F. Tobagi and L. Kleinrock, "Packet Switching in Radio Channels: Part II–The Hidden Terminal Problem in Carrier Sense Multiple-Access and the Busy-Tone

Solution," *IEEE Transactions on Communications*, vol. 23, pp. 1417–1433, December 1975.

[111] J. Monks, V. Bharghavan, and W.-M. Hwu, "A Power Controlled Multiple Access Protocol for Wireless Packet Networks," in *IEEE INFOCOM 2001*, vol. 1, (Anchorage, AK, USA), pp. 219–228, 22-26 April 2001.

[112] Y.-B. Ko, V. Shankarkumar, and N. Vaidya, "Medium Access Control Protocols Using Directional Antennas in Ad Hoc Networks," in *IEEE INFOCOM 2000*, vol. 1, (Tel Aviv, Israel), pp. 13–21, 26-30 March 2000.

[113] T. Nandagopal, T.-E. Kim, X. Gao, and V. Bharghavan, "Achieving MAC Layer Fairness in Wireless Packet Networks," in *The 6th ACM Annual International Conference on Mobile Computing and Networking*, (Boston, MA, USA), pp. 87–98, August 2000.

[114] P. Ramanathan and P. Agrawal, "Adapting Packet Fair Queueing Algorithms to Wireless Networks," in *The 4th Annual ACM/IEEE International Conference on Mobile Computing and Networking*, (Dallas, TX, USA), pp. 1–9, 1998.

[115] N. H. Vaidya, P. Bahl, and S. Gupta, "Distributed Fair Scheduling in A Wireless LAN," in *The 6th ACM Annual International Conference on Mobile Computing and Networking*, (Boston, MA, USA), pp. 167–178, 2000.

[116] H. Takagi and L. Kleinrock, "Optimal Transmission Ranges for Randomly Distributed Packet Radio Terminals," *IEEE Transactions on Communications*, vol. 32, pp. 246–257, March 1984.

[117] T.-C. Hou and V. Li, "Transmission Range Control in Multihop Packet Radio Networks," *IEEE Transactions on Communications*, vol. 34, pp. 38–44, January 1986.

[118] S. Singh and C. Raghavendra, "PAMAS: Power Aware Multi-Access Protocol with Signalling for Ad Hoc Networks," *ACM ComputerCommunications Reviews*, vol. 28, pp. 5–26, July 1998.

[119] K.-T. Jin and D.-H. Cho, "Optimal Threshold Energy Level of Energy Efficient MAC for Energy-Limited Ad-Hoc Networks," in *IEEE Global Telecommunications Conference*, vol. 5, (San Antonio, TX, USA), pp. 2932–2936, 25-29 November 2001.

[120] B. Sadeghi, V. Kanodia, A. Sabharwal, and E. Knightly, "Opportunistic Media Access for Multirate Ad Hoc Networks," in *The 8th ACM Annual International*

Conference on Mobile Computing and Networking, (Atlanta, GA, USA), pp. 24–35, 2002.

[121] H. Xiao, K. C. Chua, W. Seah, and A. Lo, "On Service Prioritization in Mobile Ad-Hoc Networks," in *IEEE International Conference on Communications*, vol. 6, (Helsinki, Finland), pp. 1900–1904, 11-14 June 2001.

[122] X. Pallot and L. Miller, "Implementing Message Priority Policies over An 802.11 Based Mobile Ad Hoc Network," in *IEEE Military Communications Conference*, vol. 2, pp. 860–864, 28-31 October 2001.

[123] A. Veres, A. Campbell, M. Barry, and L.-H. Sun, "Supporting Service Differentiation in Wireless Packet Networks Using Distributed Control," *IEEE Journal on Selected Areas in Communications*, vol. 19, pp. 2081–2093, October 2001.

[124] H.-K. Wu and P.-H. Chuang, "Dynamic QoS Allocation for Multimedia Ad Hoc Wireless Networks," *ACM Journal on Mobile Networks and Applications*, vol. 6, pp. 377–384, August 2001.

[125] S.-T. Sheu and T.-F. Sheu, "A Bandwidth Allocation/Sharing/Extension Protocol for Multimedia over IEEE 802.11 Ad Hoc Wireless LANs," *IEEE Journal on Selected Areas in Communications*, vol. 19, pp. 2065–2080, October 2001.

[126] L. Zhou and Z. J. Haas, "Securing ad hoc networks," *IEEE Network*, vol. 13, pp. 24–30, November-December 1999.

[127] H. Yang, H. Luo, F. Ye, S. Lu, and L. Zhang, "Security in Mobile Ad Hoc Networks: Challenges and Solutions," *IEEE Wireless Communications*, vol. 11, pp. 38–47, February 2004.

[128] Y.-C. Hu, A. Perrig, and D. B. Johnson, "Ariadne: A Secure On-Demand Routing Protocol for Ad Hoc Networks," in *The 8th ACM Annual International Conference on Mobile Computing and Networking*, (Atlanta, GA, USA), pp. 12–23, 2002.

[129] M. G. Zapata and N. Asokan, "Securing Ad Hoc Routing Protocols," in *The ACM Workshop on Wireless Security*, (Atlanta, GA, USA), pp. 1–10, 2002.

[130] Y.-C. Hu, D. B. Johnson, and A. Perrig, "SEAD: Secure Efficient Distance Vector Routing for Mobile Wireless Ad Hoc Networks," in *The Fourth IEEE Workshop on Mobile Computing Systems and Applications*, (Calicoon, NY, USA), pp. 1775–1779, 20-21 June 2002.

[131] Y.-C. Hu, A. Perrig, and D. Johnson, "Packet Leashes: A Defense against Wormhole Attacks in Wireless Networks," in *IEEE INFOCOM 2003*, vol. 3, pp. 1976–1986, 30 March-3 April 2003.

[132] P. Papadimitratos and Z. Haas, "Secure Link State Routing for Mobile Ad Hoc Networks," in *The 20003 IEEE Symposium on Applications and the Internet Workshops*, pp. 379–383, 27-31 January 2003.

[133] K. Sanzgiri, B. Dahill, B. Levine, C. Shields, and E. Belding-Royer, "A Secure Routing Protocol for Ad Hoc Networks," in *The 10th IEEE International Conference on Network Protocols*, (Paris, France), pp. 78–87, 12-15 November 2002.

[134] B. Awerbuch, D. Holmer, C. Nita-Rotaru, and H. Rubens, "An On-Demand Secure Routing Protocol Resilient to Byzantine Failures," in *The ACM Workshop on Wireless Security*, (Atlanta, GA, USA), pp. 21–30, 2002.

[135] S. Marti, T. J. Giuli, K. Lai, and M. Baker, "Mitigating Routing Misbehavior in Mobile Ad Hoc Networks," in *The 6th Annual International Conference on Mobile Computing and Networking*, (Boston, MA, USA), pp. 255–265, 2000.

[136] H. Yang, X. Meng, and S. Lu, "Self-Organized Network-Layer Security in Mobile Ad Hoc Networks," in *The ACM Workshop on Wireless Security*, (Atlanta, GA, USA), pp. 11–20, 2002.

[137] P. Michiardi and R. Molva, "Ad Hoc Network Security," in *Mobile Ad Hoc Networking* (S. Basagni, M. Conti, S. Giordano, and I. Stojmenovic, eds.), ch. 12, pp. 329–354, Wiley-IEEE Press, 2004.

[138] L. Buttyan and J.-P. Hubaux, "Nuglets: A virtual currency to stimulate cooperation in self-organized ad hoc networks," Tech. Rep. Technical Report DSC/2001/001, Department of Communication Systems, Swiss Federal Institute of Technology, Lausanne, Switzerland, January 2001.

[139] S. Buchegger and J.-Y. Le Boudec, "Nodes Bearing Grudges: Towards Routing Security, Fairness, and Robustness in Mobile Ad Hoc Networks," in *The 10th Euromicro Workshop on Parallel, Distributed and Network-Based Processing*, (Canary Islands, Spain), pp. 403–410, 9-11 January 2002.

[140] S. Buchegger and J.-Y. Le Boudec, "Performance Analysis of the CONFIDANT Protocol," in *The 3rd ACM International Symposium on Mobile Ad Hoc Networking and Computing*, (Lausanne, Switzerland), pp. 226–236, 2002.

[141] P. Michiardi and R. Molva, "CORE: A COllaborative REputation Mechanism to Enforce Node Cooperation in Mobile Ad Hoc Networks," in *IFIP Communication and Multimedia Security Conference*, pp. 107–121, 26-27 September 2002.

[142] P. Michiardi and R. Molva, "A game theoretical approach to evaluate cooperation enforcement mechanisms in mobile ad hoc networks," in *The 1st IEEE International Symposium on Modeling and Optimization in Mobile, Ad Hoc and Wireless Networks*, (Sophia-Antipolis, France), pp. 55–58, 3-5 March 2003.

[143] E. Crawley, R. Nair, B. Rajagopalan, and H. Sandick, *RFC2386 - A Framework for QoS-based Routing in the Internet.* Internet Engineering Task Force (IETF), August 1998. http://www.ietf.org/rfc/rfc2386.txt.

[144] D. D. Perkins and H. D. Hughes, "A Survey on Quality-of-Service Support for Mobile Ad Hoc Networks," *Wiley Journal on Wireless Communications and Mobile Computing*, vol. 2, pp. 503–513, August 2002.

[145] H. Xiao, W. Seah, A. Lo, and K. Chua, "A Flexible Quality of Service Model for Mobile Ad-Hoc Networks," in *IEEE Vehicular Technology Conference 2000-Spring*, vol. 1, (Tokyo), pp. 445–449, 15-18 May 2000.

[146] R. Braden, D. Clark, and S. Shenker, *RFC1633 - Integrated Services in the Internet Architecture: an Overview.* Internet Engineering Task Force (IETF), June 1994. http://www.ietf.org/rfc/rfc1633.txt.

[147] S. Blake, D. Black, M. Carlson, E. Davies, and Z. Wang, *RFC2475 - An Architecture for Differentiated Services.* Internet Engineering Task Force (IETF), December 1998. http://www.ietf.org/rfc/rfc2475.txt.

[148] R. Sivakumar, P. Sinha, and V. Bharghavan, "CEDAR: A Core-Extraction Distributed Ad Hoc Routing Algorithm," *IEEE Journal on Selected Areas in Communications*, vol. 17, pp. 1454–1465, August 1999.

[149] S. Chen and K. Nahrstedt, "Distributed Quality-of-Service Routing in Ad Hoc Networks," *IEEE Journal on Selected Areas in Communications*, vol. 17, pp. 1488–1505, August 1999.

[150] C. R. Lin and J.-S. Liu, "QoS Routing in Ad Hoc Wireless Networks," *IEEE Journal on Selected Areas in Communications*, vol. 17, pp. 1426–1438, August 1999.

[151] J. W. Lee, R. R. Mazumdar, and N. B. Shroff, "Joint Power and Data Rate Allocation for the Downlink in Multi-Class CDMA Wireless Networks," in *40th Annual Allerton Conference on Communications, Control, and Computing*, October 2002.

[152] M. Mirhakkak, N. Schult, and D. Thomson, "Dynamic Quality-of-Service for Mobile Ad Hoc Networks," in *The 1st IEEE Annual Workshop on Mobile and Ad Hoc Networking and Computing*, (Boston, MA, USA), pp. 137–138, 11 August 2000.

[153] R. Braden, L. Zhang, S. Berson, S. Herzog, and S. Jamin, *RFC2205 - Resource ReSerVation Protocol (RSVP) - Version 1 Functional Specification.* Internet Engineering Task Force (IETF), September 1997. http://www.ietf.org/rfc/rfc2205.txt.

[154] M. Barry, A. Campbell, and A. Veres, "Distributed Control Algorithms for Service Differentiation in Wireless Packet Networks," in *IEEE INFOCOM*, vol. 1, (Anchorage, AK, USA), pp. 582–590, 2001.

[155] S.-S. Kang and M. W. Mutka, "Provisioning Service Differentiation in Ad Hoc Networks by the Modification of Backoff Algorithm," in *The Internation Conference on Computer Communication and Network*, (Scottsdale, AZ, USK), October 2001.

[156] C. Lin and M. Gerla, "Asynchronous Multimedia Multihop Wireless Networks," in *IEEE INFOCOM*, vol. 1, (Kobe, Japan), pp. 118–125, 7-11 April 1997.

[157] C. Yu, B. Lee, and H. Y. Youn, "Energy Efficient Routing Protocols for Mobile Ad Hoc Networks," *Wiley Journal on Wireless Communications and Mobile Computing*, vol. 3, pp. 959–973, December 2003.

[158] S. Singh, M. Woo, and C. Raghavendra, "Power Aware Routing in Mobile Ad Hoc Networks," in *ACM/IEEE International Conference on Mobile Computing and Networking*, pp. 181–190, October 1998.

[159] J.-H. Chang and L. Tassiulas, "Energy Conserving Routing in Wireless Ad-Hoc Networks," in *IEEE INFOCOM*, vol. 1, (Tel Aviv, Israel), pp. 22–31, 26-30 March 2000.

[160] Q. Li, J. Aslam, and D. Rus, "Online Power-Aware Routing in Wireless Ad-Hoc Networks," in *The 7th ACM Annual International Conference on Mobile Computing and Networking*, (Rome, Italy), pp. 97–107, 2001.

[161] I. Stojmenovic and X. Lin, "Power-Aware Localized Routing in Wireless Networks," *IEEE Transactions on Parallel and Distributed Systems*, vol. 12, pp. 1122–1133, November 2001.

[162] K. Woo, C. Yu, D. Lee, H. Y. Youn, and B. Lee, "Non-Blocking, Localized Routing Algorithm for Balanced Energy Consumption in Mobile Ad Hoc Networks," in *The Ninth International Symposium in Modeling, Analysis and Simulation of Computer and Telecommunication Systems*, p. 117, 2001.

[163] C.-K. Toh, "Maximum Battery Life Routing to Support Ubiquitous Mobile Computing in Wireless Ad Hoc Networks," *IEEE Communications Magazine*, vol. 39, pp. 138–147, June 2001.

[164] B. Chen, K. Jamieson, H. Balakrishnan, and R. Morris, "Span: An Energy-Efficient Coordination Algorithm for Topology Maintenance in Ad Hoc Wireless Networks," *ACM Journal on Wireless Networks*, vol. 8, pp. 481–494, Septmeber 2002.

[165] Y. Xu, J. Heidemann, and D. Estrin, "Geography-Informed Energy Conservation for Ad Hoc Routing," in *The 7th ACM Annual International Conference on Mobile Computing and Networking*, (Rome, Italy), pp. 70–84, July 2001.

[166] Y. Xu, J. Heidemann, and D. Estrin, "Adaptive energy-conserving routing for multihop ad hoc networks," Tech. Rep. Technical Report 527, Information Science Institute, University of South California, May 2000.

[167] A. Boukerche and L. Bononi, "Simulation and Modeling of Wireless, Mobile, and Ad Hoc Networks," in *Mobile Ad Hoc Networking* (S. Basagni, M. Conti, S. Giordano, and I. Stojmenovic, eds.), ch. 14, pp. 373–409, Wiley-IEEE Press, 2004.

[168] C. Bettstetter, "Smooth is Better than Sharp: a Random Mobility Model for Simulation of Wireless Networks," in *ACM International Workshop on Modeling Analysis and Simulation of Wireless and Mobile Systems*, (Rome, Italy), pp. 19–27, 2001.

[169] C. Bettstetter, "Mobility Modeling in Wireless Networks: Categorization, Smooth Movement, and Border Effects," *ACM SIGMOBILE Mobile Computing and Communications Review*, vol. 5, pp. 55–66, July 2001.

[170] T. Camp, J. Boleng, and V. Davies, "A Survey of Mobility Models for Ad Hoc Network Research," *Wiley Journal on Wireless Communications and Mobile Computing*, vol. 2, pp. 483–502, August 2002.

[171] T. S. Rappaport, *Wireless Communications: Principles and Practice*. Upper Saddle River, NJ, USA: Prentice Hall PTR, 2 ed., December 2001.

[172] S. Shah, E. Hernandez, and A. Helal, "CAD-HOC: a CAD-Like Tool for Generating Mobility Benchmarks in Ad-Hoc Networks," in *IEEE Symposium on Applications and the Internet*, (Nara, Japan), pp. 270–279, 28 January-1 February 2002.

[173] J. Tian, J. Hahner, C. Becker, I. Stepanov, and K. Rothermel, "Graph-Based Mobility Model for Mobile Ad Hoc Network Simulation," in *The IEEE 35th Annual Simulation Symposium*, pp. 337–344, 14-18 April 2002.

[174] X. Hong, T. J. Kwon, M. Gerla, D. L. Gu, and G. Pei, "A Mobility Framework for Ad Hoc Wireless Networks," in *The 2nd ACM International Conference on Mobile Data Management*, pp. 185–196, 2001.

[175] C. Bettstetter, H. Hartenstein, and X. Perez-Costa, "Stochastic Properties of the Random Waypoint Mobility Model," *ACM Journal on Wireless Networks*, vol. 10, no. 5, pp. 555–567, 2004.

[176] J. Broch, D. A. Maltz, D. B. Johnson, Y.-C. Hu, and J. Jetcheva, "A Performance Comparison of Multi-Hop Wireless Ad Hoc Network Routing Protocols," in *The 4th Annual ACM/IEEE International Conference on Mobile Computing and Networking*, (Dallas, TX, USA), pp. 85–97, 1998.

[177] J. Yoon, M. Liu, and B. Noble, "Random Waypoint Considered Harmful," in *IEEE INFOCOM 2003*, vol. 2, pp. 1312–1321, 30 March-3 April 2003.

[178] E. Royer, P. Melliar-Smith, and L. Moser, "An Analysis of the Optimum Node Density for Ad Hoc Mobile Networks," in *IEEE International Conference on Communications*, vol. 3, (Helsinki, Finland), pp. 857–861, 11-14 June 2001.

[179] X. Hong, M. Gerla, G. Pei, and C.-C. Chiang, "A Group Mobility Model for Ad Hoc Wireless Networks," in *The 2nd ACM International Workshop on Modeling Analysis and Simulation of Wireless and Mobile Systems*, (Seattle, WA, USA), pp. 53–60, 1999.

[180] K. Wang and B. Li, "Group Mobility and Partition Prediction in Wireless Ad-Hoc Networks," in *IEEE International Conference on Communications*, vol. 2, pp. 1017–1021, 28 April-2 May 2002.

[181] J.-C. Cano and P. Manzoni, "Group Mobility Impact over TCP and CBR Traffic in Mobile Ad Hoc Networks," in *The 12th Euromicro Conference on Parallel, Distributed and Network-Based Processing*, pp. 382–389, 11-13 February 2004.

[182] G. Kondylis, S. Krishnamurthy, S. Dao, and G. Pottie, "Multicasting Sustained CBR and VBR Traffic in Wireless Ad-Hoc Networks," in *IEEE International Conference on Communications*, vol. 1, (New Orleans, LA, USA), pp. 543–549, 18-22 June 2000.

[183] D. Lucantoni, M. Neuts, and A. Reibman, "Methods for Performance Evaluation of VBR Video Traffic Models," *IEEE/ACM Transactions on Networking*, vol. 2, pp. 176–180, April 1994.

[184] Information Sciences Institute, University of Southern California, USA, "The Network Simulator *ns*-2." http://www.isi.edu/nsnam/ns/.

[185] OPNET Technologies, Inc., "OPNET - Making Networks and Applications Platform." http://www.opnet.com/.

[186] Omnest Global Inc., "OMNeT++ - Discrete Event Simulation System." http://www.omnetpp.org/.

[187] College of Computing, Georgia Institute of Technology, USA, "PDNS - Parallel/Distributed NS." http://www.cc.gatech.edu/computing/compass/pdns/.

[188] J. Panchal, O. Kelly, J. Lai, N. Mandayam, A. T. Ogielski, and R. Yates, "WiPPET, a Virtual Testbed for Parallel Simulations of Wireless Networks," *ACM SIGSIM Simulation Digest*, vol. 28, pp. 162–169, July 1998.

[189] X. Zeng, R. Bagrodia, and M. Gerla, "GloMoSim: a Library for Parallel Simulation of Large-Scale Wireless Networks," in *The 12th ACM Workshop on Parallel and Distributed Simulation*, (Banff, Alberta, Canada), pp. 154–161, 1998.

[190] D. Cavin, Y. Sasson, and A. Schiper, "On the Accuracy of MANET Simulators," in *The Second ACM International Workshop on Principles of Mobile Computing*, (Toulouse, France), pp. 38–43, October 2002.

[191] L.-L. Xie and P. Kumar, "A Network Information Theory for Wireless Communication: Scaling Laws and Optimal Operation," *IEEE Transactions on Information Theory*, vol. 50, pp. 748–767, May 2004.

[192] O. Leveque and I. E. Telatar, "Information-Theoretic Upper Bounds on the Capacity of Large Extended Ad Hoc Wireless Networks," *IEEE Transactions on Information Theory*, vol. 51, pp. 858–865, March 2005.

[193] P. Gupta and P. Kumar, "Towards an Information Theory of Large Networks: An Achievable Rate Region," *IEEE Transactions on Information Theory*, vol. 49, pp. 1877–1894, August 2003.

[194] A. Jovicic, P. Viswanath, and S. R. Kulkarni, "Upper Bounds to Transport Capacity of Wireless Networks," *IEEE Transactions on Information Theory*, vol. 50, pp. 2555–2565, November 2004.

[195] J. Hefferon, *Linear Algebra.* http://joshua.smcvt.edu/linearalgebra/, May 2003.

[196] M. Franceschetti, J. Bruck, and L. Schulman, "Microcellular Systems, Random Walks, and Wave Propagation," in *IEEE Antennas and Propagation Society International Symposium*, vol. 1, pp. 220–223, 16-21 June 2002.

[197] S. R. Kulkarni and P. Viswanath, "A Deterministic Approach to Throughput Scaling in Wireless Networks," *IEEE Transactions on Information Theory*, vol. 50, pp. 1041–1049, June 2004.

[198] F. Xue, L.-L. Xie, and P. Kumar, "The Transport Capacity of Wireless Networks Over Fading Channels," *IEEE Transactions on Information Theory*, vol. 51, pp. 834–847, March 2005.

[199] M. J. Neely and E. Modiano, "Capacity and Delay Tradeoffs for Ad Hoc Mobile Networks," *IEEE Transactions on Information Theory*, vol. 51, pp. 1917–1937, June 2005.

[200] A. Zemlianov and G. de Veciana, "Capacity of Ad Hoc Wireless Networks with Infrastructure Support," *IEEE Journal on Selected Areas in Communications*, vol. 23, pp. 657–667, March 2005.

[201] L. Hanzo, C. Wong, and M. Yee, *Adaptive Wireless Tranceivers.* John Wiley and Sons Ltd., 2002.

[202] L. Hanzo, L.-L. Yang, E.-L. Kuan, and K. Yen, *Single and Multi-Carrier DS-CDMA : Multi-User Detection, Space-Time Spreading, Synchronisation, Networking and Standards.* John Wiley and Sons Ltd., 2003.

[203] R. Steele, C.-C. Lee, and P. Gould, *GSM, cdmaOne and 3G Systems.* John Wiley and Sons Ltd., 2001.

[204] E. Biglieri, J. Proakis, and S. Shamai, "Fading Channels: Information-Theoretic and Communications Aspects," *IEEE Transactions on Information Theory*, vol. 44, pp. 2619–2692, October 1998.

[205] T. M. Cover and J. A. Thomas, *Elements of Information Theory*. John Wiley, 1991.

[206] P. Gupta and P. Kumar, "Critical Power for Asymptotic Connectivity in Wireless Networks," in *Stochastic Analysis, Control, Optimization and Applications : A Volume in Honor of W.H. Fleming* (W. McEneaney, G. Yin, and Q. Zhang, eds.), Boston: Birkhauser, 1 ed., November 1998.

[207] J. G. Proakis, *Digital Communications*. McGraw-Hill Companies, Inc., 4 ed., 2001.

[208] J. Cheng and N. Beaulieu, "Accurate DS-CDMA Bit-Error Probability Calculation in Rayleigh Fading," *IEEE Transactions on Wireless Communications*, vol. 1, pp. 3–15, January 2002.

[209] E. Lloyd, *Probability*, vol. II of *Handbook of Applicable Mathematics*. John Wiley and Sons Ltd., 1980.

[210] L. Hanzo, S. X. Ng, T. Keller, and W. Webb, *Quadrature Amplitude Modulation: From Basics to Adaptive Trellis-Coded, Turbo-Equalised and Space-Time Coded OFDM, CDMA and MC-CDMA Systemss*. John Wiley and Sons Ltd., 2 ed., November 2004.

[211] B. Choi and L. Hanzo, "Optimum Mode-Switching-Assisted Constant-Power Single- and Multicarrier Adaptive Modulation," *IEEE Transactions on Vehicular Technology*, vol. 52, pp. 536–560, May 2003.

[212] K. Cho and D. Yoon, "On the General BER Expression of One- and Two-Dimension Amplitude Modulations," *IEEE Transactions on Communications*, vol. 50, pp. 1074–1080, July 2002.

[213] K. Weltner, J. Grosjean, P. Schuster, and W. Weber, *Mathematics for Engineers and Scientists*. Stanley Thornes (Publishers) Ltd, 1986.

[214] P. Fan and M. Darnell, *Sequence Design for Communications Applications*. John Wiley, 1996.

[215] L. Hanzo, M. Münster, B. Choi, and T. Keller, *OFDM and MC-CDMA for Broadband Multi-User Communications, WLANs and Broadcasting*. John Wiley and Sons Ltd., 2003.

[216] W. C. Y. Lee, "Analysis and Realization of a Physical CDD System," *Wiley Journal on Wireless Communications and Mobile Computing*, vol. 3, pp. 571–583, August 2003.

[217] D. Li, "The Perspectives of Large Area Synchronous CDMA Technology for the Fourth-Generation Mobile Radio," *IEEE Communications Magazine*, vol. 41, pp. 114–118, March 2003.

[218] D. Li, "A High Spectrum Efficient Multiple Access Code," in *Fifth Asia-Pacific Conference on Communications and Fourth Optoelectronics and Communications Conference*, vol. 1, (Beijing, China), pp. 598–605, 18-22 October 1999.

[219] S. Stanczak, H. Boche, and M. Haardt, "Are LAS-codes a miracle ?," in *IEEE Global Telecommunications Conference*, vol. 1, (San Antonio, Texas, USA), pp. 589–593, 25-29 November 2001.

[220] B.-J. Choi and L. Hanzo, "On the Design of LAS Spreading Codes," in *IEEE 56th Vehicular Technology Conference 2002-Fall*, vol. 4, (Vancouver, British Columbia, Canada), pp. 2172–2176, 24-28 September 2002.

[221] S. Ni, H. Wei, J. S. Blogh, and L. Hanzo, "Network Performance of Asynchronous UTRA-like FDD/CDMA Systems using Loosely Synchronised Spreading Codes," in *IEEE 58th Vehicular Technology Conference 2003-Fall*, vol. 2, (Orlando, Florida, USA), pp. 1359–1363, 6-9 October 2003.

[222] H. Wei, L.-L. Yang, and L. Hanzo, "Interference-Free Broadband Single- and Multicarrier DS-CDMA," *IEEE Communications Magazine*, vol. 43, pp. 68–73, February 2005.

[223] J. A. Silvester and L. Kleinrock, "On the Capacity of Multihop Slotted ALOHA Networks with Regular Structure," *IEEE Transactions on Communications*, vol. 31, pp. 974–982, August 1983.

[224] R. Hekmat and P. V. Mieghem, "Interference in Wireless Multi-Hop Ad-Hoc Networks and Its Effect on Network Capacity," *Wireless Networks*, vol. 10, pp. 389–399, July 2004.

[225] G. L. Turin, F. D. Clapp, T. L. Johnston, S. B. Fine, and D. Lavry, "A Statistical Model of Urban Multipath Propagation," *IEEE Transactions on Vehicular Technology*, vol. 21, pp. 1–9, February 1972.

[226] T. Eng and L. B. Milstein, "Coherent DS-CDMA Performance in Nakagami Multipath Fading," *IEEE Transactions on Communications*, vol. 43, pp. 1134–1143, February/March/April 1995.

[227] E. Geraniotis and B. Ghaffari, "Performance of Binary and Quaternary Direct-Sequence Spread-Spectrum Multiple-Access Systems with Random Signature Sequences," *IEEE Transactions on Communications*, vol. 39, pp. 713–724, May 1991.

[228] J. S. Lehnert and M. B. Pursley, "Error Probabilities for Binary Direct-Sequence Spread-Spectrum Communications with Random Signature Sequences," *IEEE Transactions on Communications*, vol. 35, pp. 87–98, January 1987.

[229] M. B. Pursley, "Performance Evaluation for Phase-Coded Spread-Spectrum Multiple-Access Communication–Part I: System Analysis," *IEEE Transactions on Communications*, vol. 25, pp. 795–799, August 1977.

[230] M. K. Simon and M.-S. Alouini, "A Unified Approach to the Performance Analysis of Digital Communication over Generalized Fading Channels," *IEEE Proceedings*, vol. 86, pp. 1860–1877, September 1998.

[231] L.-L. Yang and L. Hanzo, "Performance of Generalized Multicarrier DS-CDMA Over Nakagami-m Fading Channels," *IEEE Transactions on Communications*, vol. 50, pp. 956–966, June 2002.

[232] V. Aalo, O. Ugweje, and R. Sudhakar, "Performance Analysis of a DS/CDMA System with Noncoherent M-ary Orthogonal Modulation in Nakagami Fading," *IEEE Transactions on Vehicular Technology*, vol. 47, pp. 20–29, February 1998.

[233] G. Efthymoglou, T. Piboongungon, and V. Aalo, "Performance of DS-CDMA Receivers with MRC in Makagami-m Fading Channels with Arbitrary Fading Parameters," *IEEE Transactions on Vehicular Technology*, vol. 55, pp. 104–114, January 2006.

[234] S. I. Park, S. R. Park, I. Song, and N. Suehiro, "Multiple-Access Interference Reduction for QS-CDMA Systems with a Novel Class of Polyphase Sequences," *IEEE Transactions on Information Theory*, vol. 46, pp. 1448–1458, July 2000.

[235] H. Wei, L.-L. Yang, and L. Hanzo, "Downlink SpaceCTime Spreading Using Interference Rejection Codes," *IEEE Transactions on Vehicular Technology*, vol. 55, pp. 1838–1847, November 2006.

[236] H. Wei, L.-L. Yang, and L. Hanzo, "On the Performance of Band-Limited Asynchronous DS-CDMA over Nakagami-*m* Channels," *IEEE Transactions on Wireless Communications*, vol. 5, pp. 1586–1593, July 2006.

[237] CWTS/China, *Physical Layer Specification for LAS-2000*, June 2000.

[238] J. Cheng and N. Beaulieu, "Precise Bit Error Rate Calculation for Asynchronous DS-CDMA in Nakagami Fading," in *IEEE Global Telecommunications Conference*, vol. 2, (San Francisco, CA), pp. 980–984, 27 September-1 December 2000.

[239] J. M. Holtzman, "A Simple, Accurate Method to Calculate Spread-Spectrum Multiple-Access Error Probabilities," *IEEE Transactions on Communications*, vol. 40, pp. 461–464, March 1992.

[240] J. S. Lehnert and M. B. Pursley, "Multipath Diversity Reception of Spread-Spectrum Multiple-Access Communications," *IEEE Transactions on Communications*, vol. 35, pp. 1189–1198, November 1987.

[241] T. M. Lok and J. S. Lehnert, "Error Probabilities for Generalized Quadriphase DS/SSMA Communication Systems with Random Signature Sequences," *IEEE Transactions on Communications*, vol. 44, pp. 876–885, July 1996.

[242] J. R. K. Morrow and J. S. Lehnert, "Bit-to-Bit Error Dependence in Slotted DS/SSMA Packet Systems with Random Signature Sequences," *IEEE Transactions on Communications*, vol. 37, pp. 1052–1061, October 1989.

[243] K. Sivanesan and N. C. Beaulieu, "Performance Analysis of Bandlimited DS-CDMA Systems in Nakagami Fading," in *IEEE International Conference on Communications*, vol. 1, (Paris, France), pp. 400–404, 20-24 June 2004.

[244] M. O. Sunay and P. J. McLane, "Calculating Error Probabilities for DS-CDMA Systems: When Not to Use the Gaussian Approximation," in *IEEE Global Telecommunications Conference*, vol. 3, (London, UK), pp. 1744–1749, 18-22 November 1996.

[245] M. O. Sunay and P. J. McLane, "Sensitivity of a DS CDMA System with Long PN Sequences to Synchronization Errors," in *IEEE International Conference on Communications*, vol. 2, (Seattle, WA, USA), pp. 1029–1035, 18-22 June 1995.

[246] C. Unger and G. P. Fettweis, "Analysis of the RAKE Receiver Performance in Low Spreading Gain DS/SS Systems," in *IEEE Global Telecommunications Conference 2002*, vol. 1, pp. 830–834, 17-21 November 2002.

[247] Y. C. Yoon, "Quadriphase DS-CDMA with Pulse Shaping and the Accuracy of the Gaussian Approximation for Matched Filter Receiver Performance Analysis," *IEEE Transactions on Wireless Communications*, vol. 1, pp. 761–768, October 2002.

[248] A. Mirbagheri and Y. C. Yoon, "Performance Analysis of a Linear MMSE Receiver for Bandlimited Random-CDMA Using Quadriphase Spreading over Multipath Channels," *IEEE Transactions on Wireless Communications*, vol. 3, pp. 1053–1066, July 2004.

[249] K. Sivanesan and N. C. Beaulieu, "Accurate BER Analysis of Bandlimited DS-CDMA System with EGC and SC Diversity over Nakagami Fading Channels," in *IEEE Wireless Communications and Networking Conference*, vol. 2, (New Orleans, Louisiana, USA), pp. 956–960, 13-17 March 2005.

[250] E. A. Geraniotis and M. B. Pursley, "Error Probability for Direct-Sequence Spread-Spectrum Multiple-Access Communications–Part II: Approximations," *IEEE Transactions on Communications*, vol. 30, pp. 985–995, May 1982.

[251] M. O. Sunay and P. J. McLane, "Comparison of Biphase Spreading to Quadriphase Spreading in DS CDMA Systems that Employ Long PN Sequences," in *Sixth IEEE International Symposium on Personal, Indoor and Mobile Radio Communications*, vol. 1, (Toronto, Canada), pp. 237–242, 27-29 September 1995.

[252] M. O. Sunay and P. J. McLane, "Effects of Carrier Phase and Chip Timing Errors on the Capacity of a Quadriphase Spread BPSK Modulated DS-CDMA System," in *IEEE Global Telecommunications Conference*, vol. 2, (Singapore), pp. 1114–1120, 13-17 November 1995.

[253] Q. Shi and M. Latva-Aho, "Accurate Bit-Error Rate Evaluation for Synchronous MC-CDMA over Nakagami-m-Fading Channels Using Moment Generating Functions," *IEEE Transactions on Wireless Communications*, vol. 4, pp. 422–433, March 2005.

[254] F. D. Garber and M. B. Pursley, "Performance of Offset Quadriphase Spread-Spectrum Multiple-Access Communications," *IEEE Transactions on Communications*, vol. 29, pp. 305–314, March 1981.

[255] R. T. Hsu and J. S. Lehnert, "A Characterization of Multiple-Access Interference in Generalized Quadriphase Spread-Spectrum Communications," *IEEE Transactions on Communications*, vol. 42, pp. 2001–2010, FEBRUARY/MARCH/APRIL 1994.

[256] D. Laforgia, A. Luvison, and V. Zingarelli, "Bit Error Rate Evaluation for Spread-Spectrum Multiple-Access Systems," *IEEE Transactions on Communications*, vol. 32, pp. 660–669, June 1984.

[257] M. B. Pursley, D. V. Sarwate, and W. E. Stark, "Error Probability for Direct-Sequence Spread-Spectrum Multiple-Access Communications–Part I: Upper and Lower Bounds," *IEEE Transactions on Communications*, vol. 30, pp. 975–984, May 1982.

[258] A. Annamalai, C. Tellambura, and V. K. Bhargava, "Equal-Gain Diversity Receiver Performance in Wireless Channels," *IEEE Transactions on Communications*, vol. 48, pp. 1732–1745, October 2000.

[259] I. S. Gradshteyn and I. M. Ryzhik, *Table of Integrals, Series, and Products.* Academic Press, 6 ed., 2000.

[260] A. Papoulis, *Probability, Random Variables, and Stochastic Processes.* McGraw-Hill, Inc., 3rd ed., 1991.

[261] S. O. Rice, "Mathematical Analysis of Random Noise," *Bell System Technical Journal*, vol. 23, pp. 282–332, July 1944.

[262] S. O. Rice, "Mathematical Analysis of Random Noise (Concluded)," *Bell System Technical Journal*, vol. 24, pp. 46–159, January 1945.

[263] M. Nakagami, "The m-Distribution – A General Formula of Intensity Distribution of Rapid Fading," in *Statistical Methods in Radio Wave Propagation* (W. C. Hoffman, ed.), pp. 3–36, London: Pergamon Press, 1960.

[264] S. O. Rice, "Statistical Properties of a Sine Wave Plus Random Noise," *Bell System Technical Journal*, vol. 27, pp. 109-157, January 1948.

[265] A. Erdelyi, W. Magnus, F. Oberhettinger, and F. G. Tricomi, *Higher Transcendental Functions*, vol. 1. New York, Toronto and London: McGraw-Hill Book Company, Inc., 1953.

[266] H. M. Srivastava and P. W. Karlsson, *Multiple Gaussian Hypergeometric Series.* Ellis Horwood, Ltd., 1985.

[267] R. S. Hoyt, "Probability Functions for the Modulus and Angle of the Normal Complex Variate," *Bell System Technical Journal*, vol. 26, pp. 318–359, April 1947.

[268] B. Chytil, "The Distribution of Amplitude Scintillation and the Conversion of Scintillation Indices," *Journal of Atmospheric and Terrestrial Physics*, vol. 29, pp. 1175–1777, September 1967.

[269] H. Exton, *Handbook of Hypergeometric Integrals – Theory, Applications, Tables, Computer Programs.* Chichester, New York, Brisbane, Toronto: Ellis Horwood Ltd., 1978.

[270] A. Annamalai, C. Tellambura, and V. K. Bhargava, "Exact Evaluation of Maximal-Ratio and Equal-Gain Diversity Receivers for M-ary QAM on Nakagami Fading Channels," *IEEE Transactions on Communications*, vol. 47, pp. 1335–1344, September 1999.

[271] A. Annamalai and C. Tellambura, "Error Rates for Nakagami-m Fading Multichannel Reception of Binary and M-ary Signals," *IEEE Transactions on Communications*, vol. 49, pp. 58–68, January 2001.

[272] X. Dong, N. C. Beaulieu, and P. H. Wittke, "Error Probabilities of Two-Dimensional M-ary Signaling in Fading," *IEEE Transactions on Communications*, vol. 47, pp. 352–355, March 1999.

[273] X. Dong and L. Xiao, "Symbol Error Probability of Two-Dimensional Signaling in Ricean Fading with Imperfect Channel Estimation," *IEEE Transactions on Vehicular Technology*, vol. 54, pp. 538–549, March 2005.

[274] J. Lu, K. B. Letaief, J.-I. Chuang, and M. L. Liou, "M-PSK and M-QAM BER Computation Using Signal-Space Concepts," *IEEE Transactions on Communications*, vol. 47, pp. 181–184, February 1999.

[275] L.-L. Yang and L. Hanzo, "A Recursive Algorithm for the Error Probability Evaluation of M-QAM," *IEEE Communications Letters*, vol. 4, pp. 304–306, October 2000.

[276] D. Yoon and K. Cho, "General Bit Error Probability of Rectangular Quadrature Amplitude Modulation," *Electronics Letters*, vol. 38, pp. 131–133, January 2002.

[277] K. Cho, D. Yoon, W. Jeong, and M. Kavehrad, "BER Analysis of Arbitrary Rectangular QAM," in *Thirty-Fifth Asilomar Conference on Signals, Systems and Computers*, vol. 2, (Pacific Grove, CA), pp. 1056–1059, 4-7 November 2001.

[278] J. S. Lim, K. Hyun, D. Yoon, and S. K. Park, "BER Performance of Rectangular QAM with MRC over Nakagami-n Fading Channels," *IEICE Transactions on Communications*, vol. E88-B, pp. 1697–1701, April 2005.

[279] L. Xiao and X. Dong, "The Exact Transition Probability and Bit Error Probability of Two-Dimensional Signaling," *IEEE Transactions on Wireless Communications*, vol. 4, pp. 2600–2609, September 2005.

[280] L. Habbab, M.Kavehrad, and C. Sundberg, "ALOHA with Capture over Slow and Fast Fading Radio Channels with Coding and Diversity," *IEEE Journal on Selected Areas in Commmunications*, vol. 7, pp. 79–88, January 1989.

[281] M. Chiani, "Performance of BPSK and GMSK with Multiple Cochannel Interferers," in *IEEE International Symposium on Personal, Indoor and Mobile Radio Communications*, vol. 3, (Taipei, Taiwan, R.O.C.), pp. 833–837, 15-18 October 1996.

[282] V. A. Aalo and J. Zhang, "On the Effect of Cochannel Interference on Average Error Rates in Nakagami-Fading Channels," *IEEE Communications Letters*, vol. 3, pp. 136–138, May 1999.

[283] A. Shah, A. M. Haimovich, M. K. Simon, and M.-S. Alouini, "Exact Bit-Error Probability for Optimum Combining with a Rayleigh Fading Gaussian Cochannel Interferer," *IEEE Transactions on Communications*, vol. 48, pp. 908–912, June 2000.

[284] K. A. Hamdi, "Exact Probability of Error of BPSK Communication Links Subjected to Asynchronous Interference in Rayleigh Fading Environment," *IEEE Transactions on Communications*, vol. 50, pp. 1577–1579, October 2002.

[285] J. Cheng and N. Beaulieu, "Error Rate of BPSK in Generalized Fading Channels with Co-Channel Interference," in *IEEE Vehicular Technology Conference Spring*, vol. 4, (Birmingham, Al, USA), pp. 1786–1790, 6-9 May 2002.

[286] N. Beaulieu and J. Cheng, "Precise Error-Rate Analysis of Bandwidth-Efficient BPSK in Nakagami Fading and Cochannel Interference," *IEEE Transactions on Communications*, vol. 52, pp. 149–158, January 2004.

[287] K. Sivanesan and N. C. Beaulieu, "Exact BER Analysis of Bandlimited BPSK with EGC and SC Diversity in Cochannel Interference and Nakagami Fading," *IEEE Communications Letters*, vol. 8, pp. 623–625, October 2004.

[288] Z. Du, J. Cheng, and N. C. Beaulieu, "BER Analysis of BPSK Signaling in Ricean-Faded Cochannel Interference," in *IEEE Global Telecommunications Conference*, (St. Louis, Missouri, USA), pp. 1211–1216, 28 November - 2 December 2005.

[289] A. Giorgetti and M. Chiani, "Influence of Fading on the Gaussian Approximation for BPSK and QPSK with Asynchronous Cochannel Interference," *IEEE Transactions on Wireless Communications*, vol. 4, pp. 384–389, March 2005.

[290] K. Sivanesan and N. C. Beaulieu, "Exact BER Analyses of Nakagami/Nakagami CCI BPSK and Nakagami/Rayleigh CCI QPSK Systems in Slow Fading," *IEEE Communications Letters*, vol. 8, pp. 45–47, January 2004.

[291] N. C. Beaulieu and A. A. Abu-Dayya, "Bandwidth Efficient QPSK in Cochannel Interference and Fading," *IEEE Transactions on Communications*, vol. 43, pp. 2464–2474, September 1995.

[292] J. Cheng, N. Beaulieu, and X. Zhang, "Precise BER Analysis of Dual-Channel Reception of QPSK in Nakagami Fading and Cochannel Interference," *IEEE Communications Letters*, vol. 9, pp. 316–318, April 2005.

[293] P. Moose, "A Technique for Orthogonal Frequency Division Multiplexing Frequency Offset Correction," *IEEE Transactions on Communications*, vol. 42, pp. 2908–2914, October 1994.

[294] T. Pollet, M. V. Bladel", and M. Moeneclaey, "BER Sensitivity of OFDM Systems to Carrier Frequency Offset and Wiener Phase Noise," *IEEE Transactions on Communications*, vol. 43, pp. 191–193, February/March/April 1995.

[295] J. Li and M. Kavehrad, "Effects of Time Selective Multipath Fading on OFDM Systems for Broadband Mobile Applications," *IEEE Communications Letters*, vol. 3, pp. 332–334, December 1999.

[296] B. Stantchev and G. Fettweis, "Time-Variant Distortions in OFDM," *IEEE Communications Letters*, vol. 4, pp. 312–314, October 2000.

[297] W. Hwang, H. Kang, and K. Kim, "Approximation of SNR Degradation Due to Carrier Frequency Offset for OFDM in Shadowed Multipath Channels," *IEEE Communications Letters*, vol. 7, pp. 581–583, December 2003.

[298] C. Athaudage and K. Sathananthan, "Probability of Error of Space-Time Coded OFDM Systems with Frequency Offset in Frequency-Selective Rayleigh Fading

Channels," in *IEEE International Conference on Communications*, vol. 4, (Seoul Korea), pp. 2593–2599, 16-20 May 2005.

[299] T. Keller and L. Hanzo, "Adaptive Multicarrier Modulation: a Convenient Framework for Time-Frequency Processing in Wireless Communications," *IEEE Proceedings*, vol. 88, pp. 611–640, May 2000.

[300] H. Cheon and D. Hong, "Effect of Channel Estimation Error in OFDM-Based WLAN," *IEEE Communications Letters*, vol. 6, pp. 190–192, May 2002.

[301] L. Rugini and P. Banelli, "BER of OFDM Systems Impaired by Carrier Frequency Offset in Multipath Fading Channels," *IEEE Transactions on Wireless Communications*, vol. 4, pp. 2279–2288, September 2005.

[302] K. Sathananthan and C. Tellambura, "Probability of Error Calculation of OFDM Systems with Frequency Offset," *IEEE Transactions on Communications*, vol. 49, pp. 1884–1889, November 2001.

[303] K. Sathananthan and C. Athaudage, "Exact Probability of Error of ST-Coded OFDM Systems with Frequency Offset in Flat Rayleigh Fading Channels," in *6th Australian Communications Theory Workshop*, (Brisbane, Australia), pp. 21–27, 2-4 February 2005.

[304] P. Tan and N. C. Beaulieu, "Improved BER Performance in OFDM Systems with Frequency Offset by Novel Pulse-Shaping," in *IEEE Global Telecommunications Conference*, vol. 1, (Dallas, Texas, USA), pp. 230–236, 29 November - 3 December 2004.

[305] P. Tan and N. Beaulieu, "Exact BER Analysis of a $\pi/4$-DQPSK OFDM System in the Presence of Carrier Frequency Offset over Frequency Selective Fast Rayleigh Fading Channels," in *IEEE International Conference on Communications*, vol. 1, (Seoul, Korea), pp. 488–494, 16-20 May 2005.

[306] Z. Kang, K. Yao, and F. Lorenzelli, "Nakagami-m Fading Modeling in the Frequency Domain for OFDM System Analysis," *IEEE Communications Letters*, vol. 7, pp. 484–486, October 2003.

[307] M. K. Simon and M.-S. Alouini, *Digital Communication over Fading Channels*. John Wiley & Sons, Inc., 2 ed., 2005.

[308] X. Liu and L. Hanzo, "Accurate BER Analysis of QPSK Modulated Asynchronous DS-CDMA Systems Communicating over Rayleigh Channels," in *IEEE Vehicular Technology Conference*, (Melbourne, Australia), 7-10 May 2006.

[309] X. Liu and L. Hanzo, "Exact BER Performance of Asynchronous DS-CDMA Systems Using Quadriphase Spreading and QPSK Modulation over Rayleigh Channels," in *IEEE Wireless Communications and Networking Conference*, (Las Vegas, NV, USA), 3-6 April 2006.

[310] Q. Shi and M. Latva-Aho, "Spreading Sequences for Asynchronous MC-CDMA Revisited: Accurate Bit Error Rate Analysis," *IEEE Transactions on Communications*, vol. 51, pp. 8–11, January 2003.

[311] D. G. Brennan, "Linear Diversity Combining Techniques," *Proceedings of the IEEE*, vol. 91, pp. 331–356, February 2003.

[312] R. M. Corless, G. H. Gonnet, D. E. G. Hare, D. J. Jeffrey, and D. E. Knuth, "On the Lambert W Function," *Advances in Computational Mathematics*, pp. 329–359, 1996.

[313] E. W. Weisstein, "Confluent Hypergeometric Function of the First Kind." MathWorld–A Wolfram Web Resource. http://mathworld.wolfram.com/ConfluentHypergeometricFunctionoftheFirstKind.html.

[314] S. Zhang and J. Jin, *Computation of Special Functions*. Wiley-Interscience, 1 ed., 1996.

[315] E. W. Weisstein, "Hypergeometric Function." MathWorld–A Wolfram Web Resource. http://mathworld.wolfram.com/HypergeometricFunction.html.

[316] E. W. Weisstein, "Generalized Hypergeometric Function." MathWorld–A Wolfram Web Resource. http://mathworld.wolfram.com/GeneralizedHypergeometricFunction.html.

[317] H. M. Srivastava and M. C. Daoust, "A Note on the Convergence of Kampé de Fériets Double Hypergeometric Series," *Math. Nachr.*, vol. 53, pp. 151–159, 1972.

Glossary

ABR	Associativity-Based Routing.
AMRIS	Ad hoc Multicast Routing protocol utilizing Increasing id numberS.
AMRoute	Ad hoc Multicast Routing.
AODV	Ad hoc On-Demand Distance Vector routing.
AQAM	Adaptive Quadrature Amplitude Modulation.
ARA	Ant-colony-based Routing Algorithm.
ARAN	Authenticated Routing for Ad-hoc Networks.
AWGN	Additive White Gaussian Noise.
BEP	Bit Error Probability.
BER	Bit Error Ratio.
BPS	Bits Per Symbol.
BPSK	Binary Phase Shift Keying.
BSS	Base Station Subsystem.
BTMA	Busy Tone Multiple Access.
BWA	Broadband Wireless Access.
CAMP	Core-Assisted Mesh Protocol.
CBR	Constant Bit Rate.
CBRP	Cluster-Based Routing Protocol.
CCI	Co-Channel Interference.

CDMA	Code Division Multiple Access.
CEDAR	Core-Extraction Distributed Ad hoc Routing.
CF	Characteristic Function.
CFO	Carrier Frequency Offset.
CGSR	Cluster-head Gateway Switch Routing.
CIR	Channel Impulse Response.
CLT	Central Limit Theorem.
CMMBR	Conditional Max-Min Battery Capacity Routing.
CSI	Channel State Information.
CSMA	Carrier Sense Multiple Access.
CSMA/CA	Carrier Sense Multiple Access with Collision Avoidance.
CTS	Clear To Send.
DAB	Digital Audio Broadcast.
DARPA	Defense Advanced Research Project Agency.
DDM	Differential Destination Multicast.
DDR	Distributed Dynamic Routing.
DiffServ	Differentiated Services.
DREAM	Distance Routing Effect Algorithm for Mobility.
dRSVP	dynamic Resource ReSerVation Protocol.
DS	Direct Sequence.
DSDV	Destination-Sequenced Distance Vector protocol.
DSR	Dynamic Source Routing.
DST	Distributed Spanning Trees-based routing.
DVB	Digital Video Broadcast.
DVMRP	Distance Vector Multicast Routing Protocol.

DYMO	Dynamic MANET On-demand routing.
ELBACTD	Extending the Littoral Battel-space Advance Concetp Technology Demonstration.
FAMA	Floor Acquisition Multiple Access.
FAR	Flow Augmentation Routing.
FD	Frequency-Domain.
FFT	Fast Fourier Transform.
FGMP	Forwarding Group Multicast Protocol.
FORP	Flow Oriented Routing Protocol.
FQMM	Flexible QoS Model designed for MANETs.
FSR	Fisheye State Routing.
GloMo	Global Mobile Information Systems.
GloMoSim	Global Mobile Information System Simulator.
GPS	Global Position System.
GSR	Global State Routing.
HSDPA	High Speed Downlink Packet Access.
HSR	Hierarchical State Routing.
ICI	Inter-Carrier Interference.
IETF	Internet Engineering Task Force.
IFW	Interference Free Window.
IGA	Improved Gaussian Approximation.
IHGA	Improved Holtzman Gaussian Approximation.
IntServ	Integrated Services.
ISI	Inter Symbol Interference.
LA	Large Area.

LAM	Lightweight Adaptive Multicast.
LAN	Local Area Network.
LAR	Location-Aided Routing.
LAS	Large Area Synchronous.
LEAR	Localized Energy-Aware Routing.
LGT	Location Guided Tree.
LMR	Light-weight Mobile Routing.
LOS	Line-Of-Sight.
LPR	Low-cost Packet Radio.
LS	Loosely Synchrnous.
LSA	Link State Advertisement.
MAC	Medium Access Control.
MACA	Multiple Access with Collision Avoidance.
MACA-CT	Common-Transmitter-based Multiple Access with Collision Avoidance.
MACA-RT	Receiver-Transmitter-based Multiple Access with Collision Avoidance.
MACAW	Multiple Access with Collision Avoidance for Wireless LANs.
MAI	Multiple Access Interference.
MAN	Metropolitan Area Network.
MANET	Mobile Ad hoc NETwork.
MAODV	Multicast Ad hoc On-demand Distance Vector protocol.
MBWR	Mobile Broadband Wireless Access.
MCEDAR	Multicast Core Extraction Distributed Ad hoc Rouging.
MGF	Moment Generating Functions.
MIP	Multipath Intensity Profile.
MMWN	Multimedia support in Mobile Wireless Network protocol.

MPI	Mulitpath Interference.
MRC	Maximal Ratio Combining.
MSC	Mobile Switching Centre.
MWMAN	Mobile Wireless Metropolitan Area Network.
NTDR	Near-Term Digital Radio.
ODMRP	On-Demand Multicast Routing Protocol.
OFDM	Orthogonal Frequency Division Multiplexing.
OG	Orthogonal Gold.
OLSR	Optimized Link State Routing.
OMM	Online MaxMin routing.
OMNet++	Objective Modular Network Testbed in C++.
OPNET	OPtimized Network Engineering Tool.
PAM	Pulse Amplitude Modulations.
PCMA	Power Controlled Multiple Access.
PDA	Personal Digital Assistant.
PDF	Probability Density Function.
PDNS	Parallel and Distributed *ns*.
PLR	Power aware Localized Routing.
PN	Pseudo Noise.
PRNET	Packet Radio Network.
QAM	Quadrature Amplitude Modulation.
QoS	Quality of Service.
R-QAM	Rectangular Quadrature Amplitude Modulation.
RDMAR	Relative Distance Micro-discovery Ad hoc Routing.
RFC	Request For Comments.

RICH-DP	Receiver Intiated Channel Hopping with Dual Polling.
ROAM	Routing On-demand Acyclic Multipath protocol.
RSVP	Resource ReSerVation Protocol.
RTS	Request To Send.
SER	Symbol Error Rate.
SGA	Standard Gaussian Approximation.
SIC	Successive Interference Cancellation.
SIGA	Simplified Improved Gaussian Approximation.
SINR	Signal-to-Interference-plus-Noise Ratio.
SLSP	Secure Link State routing Protocol.
SLURP	Scalable Location Update Routing Protocol.
SNR	Signal-to-Interference Ratio.
SSA	Signal Stability Adaptive protocol.
STAR	Source-Tree Adaptive Routing.
SURAN	Survivable Adaptive Network.
TBRPF	Topology Dissemination Based on Reverse-Path Forwarding.
TD	Time-Domain.
TI	Tactical Internet.
TORA	Temporally Ordered Routing Algorithm.
VBR	Variable Bit Rate.
WEP	Wired Equivalent Privacy.
WG	Working Group.
WH	Walsh-Hadamard.
WINGs	Wireless Internet Gateways.
Wippet	Wireless Propagation and Protocol Testbed.

WMAN Wireless Metropolitan Area Network.

WPAN Wireless Personal Area Network.

WRP Wireless Routing Protocol.

ZHLS Zone-based Hierarchical Link State.

ZRP Zone Routing Protocol.

ns-**2** Network Simulator version 2.

Author Index

C

H

I

L

M

N

S

T

Y

Z

Index

D

U

V

W

Z